

AD-A284 799



6



**DTIC**  
**ELECTE**  
**SEP. 28. 1994**  
**S B D**

DESIGN AND ANALYSIS OF CONSTRAINED LAYER  
DAMPING TREATMENTS FOR BENDING AND TORSION  
DISSERTATION  
Kimberly J. Balkema, Captain, USAF  
AFIT / DS / AA / 94-5  
Approved for public release; distribution unlimited

**DISTRIBUTION STATEMENT A**  
Approved for public release  
Distribution Unlimited

DEPARTMENT OF THE AIR FORCE  
AIR UNIVERSITY  
**AIR FORCE INSTITUTE OF TECHNOLOGY**

DTIC QUALITY INSPECTED 3

Wright-Patterson Air Force Base, Ohio

DESIGN AND ANALYSIS OF CONSTRAINED LAYER  
DAMPING TREATMENTS FOR BENDING AND TORSION  
DISSERTATION

Kimberly J. Balkema, Captain, USAF  
AFIT / DS / AA / 94-5

Approved for public release; distribution unlimited

*269 P8* **94-30534**  


DTIC QUALITY INSPECTED 3

**94 9 22 0 6 1**

The views expressed in this dissertation are those of the author and do not reflect the official policy or position of the Department of Defense or the U. S. Government.

Accession For	
NTIS GRA&I	<input checked="" type="checkbox"/>
DTIC TAB	<input type="checkbox"/>
Unannounced	<input type="checkbox"/>
Justification	
By _____	
Distribution/ _____	
Availability Codes	
Dist	Avail and/or Special
A-1	

AFIT / DS / AA / 94-5

DESIGN AND ANALYSIS OF CONSTRAINED LAYER  
DAMPING TREATMENTS FOR BENDING AND TORSION

DISSERTATION

Kimberly J. Balkema, Captain, USAF

AFIT / DS / AA / 94-5

Approved for public release; distribution unlimited

AFIT / DS / AA / 94-5

DESIGN AND ANALYSIS OF CONSTRAINED LAYER  
DAMPING TREATMENTS FOR BENDING AND TORSION

DISSERTATION

Presented to the Faculty of the School of Engineering  
of the Air Force Institute of Technology  
Air University

In Partial Fulfillment of the Requirements  
for the Degree of Doctor of Philosophy

Kimberly J. Balkema, B.S.M.E., M.S.

Captain, USAF

September 1994

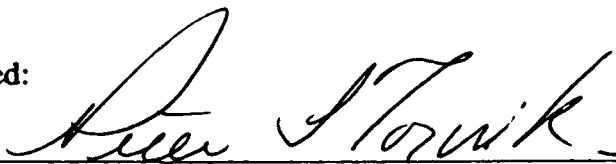
Approved for public release; distribution unlimited

AFTT / DS / AA / 94-5

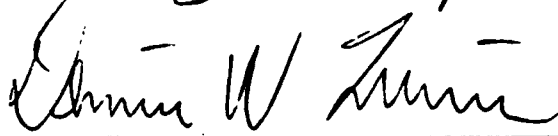
DESIGN AND ANALYSIS OF CONSTRAINED LAYER  
DAMPING TREATMENTS FOR BENDING AND TORSION

Kimberly J. Balkema, B.S., M.S.,  
Captain, USAF

Approved:

  
\_\_\_\_\_

  
\_\_\_\_\_

  
\_\_\_\_\_

Accepted:

  
\_\_\_\_\_

J. S. PRZEMIENIECKI  
Institute Senior Dean

## *Acknowledgements*

As soon as I was old enough to know what a PhD was, I knew I wanted one. (People are more tolerant of outrageous behavior if they think you are smart and you know what you are doing.) To attain this goal and write this dissertation, it took almost all the energy I had for three years (except for the energy used in scuba diving, skiing, and meeting my future husband). It also took a great deal of help from many people. I am deeply indebted to my advisor, Dr. Peter Torvik, for his support, assistance, and tolerance throughout the process. I feel lucky to have worked with him. My other committee members, Dr. Liebst and Dr. Quinn, were also very helpful, even though there were times where I wanted to strangle one of them. I would like to also thank my parents and my little sister Jill, who were nice enough to accept the fact that I didn't really care about all the details of my wedding as much as I cared about getting this degree completed. (The wedding occurs three days before graduation.) Most of all, I would like to thank Guy Demoret, my future husband, for his support throughout the process. He has helped me keep my perspective, and he has been patient with me when I have lost it. He has enriched my life in many ways, and I feel I am the luckiest woman in the world to be with him.

*Table of Contents:*

	<b>Page</b>
<b>Preface</b> .....	ii
<b>List of Figures</b> .....	vi
<b>Abstract</b> .....	viii
<b>I. Introduction</b> .....	1.1
<b>II. Literature Review: Analysis of Constrained Layer Damping</b> .....	2.1
<b>Early Constrained Layer Analysis of Rectangular Beams</b> .....	2.2
<b>Higher Order Effects</b> .....	2.3
Effect of Boundary Conditions .....	2.3
Higher Order Inertia and Shear Effects .....	2.4
Compressional Effects in the Viscoelastic Layer .....	2.5
Analysis of Isotropic Flat Plates .....	2.7
<b>Segmentation, Partial Coverage, and Optimal Design of Damping Treatments</b> .....	2.7
Segmentation of Constraining Layers .....	2.8
Partial Coverage .....	2.11
Other Optimal Design Efforts for Viscoelastic Damping Treatments	2.12
<b>Constrained Layers on Structural Elements with Generalized or Circular Cross-Sections</b> .....	2.13
Extension of Ross-Ungar-Kerwin Analysis: Ungar, 1962 .....	2.13
Applying Ungar's Analysis: Yin et. al., 1967 .....	2.14
Constraining Layer as a Hollow Concentric Beam: Di Taranto, 1974 .....	2.14
Longitudinal Cuts in the Constraining Layer: Vinogradov and Chernobrevskii, 1980 .....	2.15
Beam as a Thin Shell: Lu and others .....	2.16
Longitudinal and Circumferential Cuts: Sattinger, 1990 .....	2.17
Circular Shaft in Torsion: Chandrasekharan and Ghosh, 1974 .....	2.18
Spring in Torsion and Bending: Kishore and Ghosh, 1974 .....	2.18
<b>Constrained Layers Treatments with Composite Structural Elements</b> ..	2.20
<b>Chapter Summary</b> .....	2.22

<b>III. Optimal Length of Constrained Layer Damping Treatments . . . . .</b>	<b>3.1</b>
Description of the Optimal Length Effect . . . . .	3.1
The "Substrate Assumption" in Studies of Constrained Layer Damping Treatments . . . . .	3.3
Constraining Layer Equations of Motion . . . . .	3.4
Optimal Length Analysis of Plunkett and Lee: Uniform Substrate Strain . . . . .	3.7
Extension of the Plunkett and Lee Result: Linearly Varying Substrate Strain . . . . .	3.10
Linearly Varying Strain: Effect of Curvature on Loss Factor . . . . .	3.20
Chapter Summary . . . . .	3.28
<b>IV. Developing the Exact Equations of Motion for a Rectangular Beam with Segmented Constraining Layers . . . . .</b>	<b>4.1</b>
Equations of Motion of a Symmetric Five Layer Beam . . . . .	4.1
Adapting the Equations for Segmented Constraining Layers. . . . .	4.8
Sixth Order Equations of Motion . . . . .	4.12
Solving the Equations for the Segmented Damping Treatment . . . . .	4.15
Non-Dimensional Variables . . . . .	4.16
Form of the Assumed Solution . . . . .	4.19
Assembly of the Boundary Condition Matrix . . . . .	4.20
<b>V. The Complex Rayleigh Quotient . . . . .</b>	<b>5.1</b>
The Correspondence Principle . . . . .	5.2
Rayleigh's Quotient. . . . .	5.3
The Complex Rayleigh Quotient . . . . .	5.4
Using the Complex Rayleigh Quotient with Discrete Systems . . . . .	5.5
CRQ Form of Loss Factor: Compatibility with Ungar and Kerwin. . . . .	5.10
Example: 2 DOF System . . . . .	5.12
Complex Rayleigh Quotient with Continuous Systems . . . . .	5.17
Example of Complex Rayleigh Quotient: Constraining Layer on a Beam . . . . .	5.23
Segmented Constraining Layers on a Beam: Solutions for U and g . . . . .	5.25
Measures of Damping from the Complex Natural Frequency . . . . .	5.28
Comparison of Approximate Estimates with Exact Results . . . . .	5.32
Chapter Summary . . . . .	5.42

VI. Constrained Layer Damping on Beams of Circular Cross Section . . . . .	6.1
Beam and Damping Treatment Geometry . . . . .	6.3
Assumptions of Displacement and Shear . . . . .	6.5
Developing the Equations of Motion . . . . .	6.8
Special Case: Equations of Motion for Thin, Narrow Damping Strips	6.16
Chapter Summary . . . . .	6.20
VII. The Barberpole: Damping in Bending and Torsion . . . . .	7.1
Overview of the Bending and Torsion Problem . . . . .	7.2
Beam Geometry and Coordinate Systems . . . . .	7.5
Torsional Analysis . . . . .	7.7
Surface Displacements for Torsional Loading . . . . .	7.7
Equations of Motion for a Rigid Constraining Layer. . . . .	7.8
Observations on the Rigid Constraining Layer Results. . . . .	7.11
Equations of Motion for an Elastic Constraining Layer. . . . .	7.14
Observations on the Elastic Constraining Layer Results . . . . .	7.16
Solutions for Elastic Constraining Layer. . . . .	7.17
Bending Analysis . . . . .	7.19
Surface Displacements for the Bending Analysis. . . . .	7.19
Equations of Motion for Bending . . . . .	7.23
Bending Solutions: Pitch Angle $\alpha=0$ . . . . .	7.25
Bending Solutions: Arbitrary $\alpha$ . . . . .	7.28
Calculating Damping for the Fully Covered Barberpole Geometry . . . . .	7.30
Parametric Studies: Unsegmented Barberpole Strips in Bending. . . . .	7.35
Virtual Segmentation Effect . . . . .	7.35
Segmentation of the Barberpole Damping Strips . . . . .	7.35
Choice of Pitch Angle for the Unsegmented Barberpole in Bending.	7.43
Optimal Pitch Angle: Effects of Optimal Length . . . . .	7.43
Optimal Pitch Angle: Effects of Substrate Strain Amplitude. . .	7.47
Effectiveness of Unsegmented Barberpole Damping Treatment . . .	7.52
Segmentation of the Barberpole Damping Strips . . . . .	7.56
The Barberpole in Torsion . . . . .	7.57
The Segmented Barberpole in Bending . . . . .	7.60
Chapter Summary . . . . .	7.64

VIII. The Barberpole in Bending: Comparison of Theory and Experiment . . .	8.1
Experimental Apparatus . . . . .	8.1
Test Article . . . . .	8.1
Instrumentation . . . . .	8.2
Damping Treatment . . . . .	8.4
Barberpole Damping Configurations . . . . .	8.5
Experimental Procedure: Acquisition of Data. . . . .	8.6
Record Temperature and Prepare Instrumentation. . . . .	8.6
Create Initial Tip Displacement . . . . .	8.6
Initiate Test and Acquire Data . . . . .	8.6
Determining Damping from the Experimental Data. . . . .	8.7
Obtaining Damping Predictions from the Barberpole Analysis. . . . .	8.8
Experimental Results: Bare Beam . . . . .	8.9
Experimental Results: Unsegmented Barberpole . . . . .	8.15
Experimental Results: Segmented Barberpole . . . . .	8.18
Barberpole Loss Factors: Comparison of Theory and Experiment . . . . .	8.21
Chapter Summary . . . . .	8.23
IX. Summary and Conclusions . . . . .	9.1
Chapter 3 . . . . .	9.1
Chapter 4 . . . . .	9.3
Chapter 5 . . . . .	9.4
Chapter 6 . . . . .	9.5
Chapters 7 and 8 . . . . .	9.5
Closing Remarks . . . . .	9.7
Bibliography . . . . .	B.1
Vita . . . . .	V.1

*List of Figures*

Figure	Page
1.1 Viscoelastic Extensional Treatment . . . . .	1.3
1.2 Viscoelastic Constrained Layer Treatment . . . . .	1.3
3.1 Constrained Layer Treatment: Compliant Viscoelastic Layer . . . . .	3.2
3.2 Constrained Layer Treatment: Stiff Viscoelastic Layer . . . . .	3.2
3.3 Free Body Diagram of Constrained Layer Treatment . . . . .	3.5
3.4 Damping Effectiveness as a Function of Stiffness Parameter . . . . .	3.19
3.5 Values of $\sqrt{gL}$ that Maximize the Plunkett and Lee Loss Coefficient . .	3.19
3.6 Damping Effectiveness as a Function of Stiffness and Non-Uniformity Measures ( $\eta_v=1$ ; $C_1 \in [0,15]$ ; $C_2 \in [0,30]$ ) . . . . .	3.22
3.7 Damping Effectiveness as a Function of Stiffness and Non-Uniformity Measures ( $\eta_v=1$ ; $C_1 \in [0,10]$ ; $C_2 \in [0,5]$ ) . . . . .	3.22
3.8 Contour Plot of Damping Effectiveness ( $\eta_v=.1$ ; $C_1 \in [0,10]$ ; $C_2 \in [0,5]$ ) . . . . .	3.23
3.9 Contour Plot of Damping Effectiveness ( $\eta_v=.1$ ; $C_1 \in [0,15]$ ; $C_2 \in [0,30]$ ) . . . . .	3.23
3.10 Contour Plot of Damping Effectiveness ( $\eta_v=.5$ ; $C_1 \in [0,10]$ ; $C_2 \in [0,5]$ ) . . . . .	3.24
3.11 Contour Plot of Damping Effectiveness ( $\eta_v=.5$ ; $C_1 \in [0,15]$ ; $C_2 \in [0,30]$ ) . . . . .	3.24

3.12	Contour Plot of Damping Effectiveness ( $\eta_v=1$ ; $C_1 \in [0,10]$ ; $C_2 \in [0,5]$ ) .....	3.25
3.13	Contour Plot of Damping Effectiveness ( $\eta_v=1$ ; $C_1 \in [0,15]$ ; $C_2 \in [0,30]$ ) .....	3.25
3.14	Damping Effectiveness as a Function of Stiffness Parameter ( $C_2= 1$ )	3.27
3.15	Damping Effectiveness as a Function of Stiffness Parameter ( $C_2= 5$ )	3.27
3.16	Damping Effectiveness as a Function of Stiffness Parameter ( $C_2= 50$ )	3.28
4.1	Symmetric Five Layer Beam Geometries .....	4.2
4.2	Beam Displacements .....	4.3
4.3	Viscoelastic Shear Strain .....	4.5
5.1	Two Degree of Freedom System .....	5.12
5.2	Bar in Extension with Constraining Layer .....	5.19
6.1	Concentric Constraining Layer in Bending .....	6.2
6.2	Beam Coordinate System .....	6.4
6.3	Damping Strip Geometry .....	6.5

7.1	Barberpole Damping Treatment Configurations . . . . .	7.2
7.2	Barberpole Damping Strip Geometry . . . . .	7.5
7.3	Barberpole Coordinate System . . . . .	7.6
7.4	Torsional Displacement of Main Beam . . . . .	7.7
7.5	Torsional Rigid Body Analysis: Constraining Layer Deflections . . . . .	7.8
7.6	Coordinate Systems for Barberpole Bending Analysis . . . . .	7.21
7.7	Barberpole Damping Strips in Sets of Four Separated by $\pi/2$ Radians. . . . .	7.33
7.8	Surface Displacement of Barberpole in Bending . . . . .	7.37
7.9	Actual and Virtual Segment Configurations . . . . .	7.38
7.10	Barberpole Surface Displacement in s Direction . . . . .	7.39
7.11	Surface Displacement for Virtual Segment . . . . .	7.39
7.12	Unsegmented Barberpole Solution for Displacement u . . . . .	7.40
7.13	Displacement u for Virtual Segment Compared to Displacement u for Generator Segment at $\pi/2$ . . . . .	7.40
7.14	Unsegmented Barberpole Solution for Strain $u'$ . . . . .	7.41
7.15	Strain $u'$ for Virtual Segment Compared to Strain $u'$ for Generator Segment at $\pi/2$ . . . . .	7.41
7.16	Unsegmented Barberpole Solution for Shear Strain $\gamma_n$ . . . . .	7.42
7.17	Shear Strain $\gamma_n$ for Virtual Segment Compared to Shear Strain $\gamma_n$ for Generator Segment at $\pi/2$ . . . . .	7.42
7.18	Analogy Between Barberpole Displacements and Parfitt's Sinusoidal Displacement . . . . .	7.46

7.18	Analogy Between Barberpole Displacements and Parfitt's Sinusoidal Displacement . . . . .	7.46
7.19	Effect of Pitch Angle on Substrate Strain ( $E^2$ ) and Virtual Segment Optimal Length (H) . . . . .	7.49
7.20	Combined Effect of Substrate Strain and Pitch Angle on Loss Factor .	7.49
7.21	Effect of $\alpha$ on Bending Loss Factor . . . . .	7.50
7.22	Viscoelastic Shear Strain in Unsegmented Generator and Barberpole Strips. . . . .	7.55
7.23	Alternative Segmentation Pattern: Spiral Cuts . . . . .	7.57
7.24	Effects of Segment Length on Torsional Loss Factor . . . . .	7.58
7.25	Effect of $\alpha$ on Torsional Loss Factor . . . . .	7.59
7.26	Effect of $\alpha$ on Bending Loss Factor . . . . .	7.61
7.27	Effect of $\alpha$ on Bending and Torsional Loss Factors . . . . .	7.61
7.28	Effects of Strip Length on Bending Loss Factor . . . . .	7.63
8.1	Test Article and Root Support . . . . .	8.3
8.2	Properties of ISD-112 . . . . .	8.5
8.3	Undamped Beam: Tip Acceleration (Linear Scale) . . . . .	8.11
8.4	Undamped Beam: Tip Acceleration (Semi-Log Scale) . . . . .	8.12
8.5	Effect of Second Mode on Envelope of Vibration . . . . .	8.13
8.6	Unsegmented Barberpole: Tip Acceleration (Linear Scale) . . . . .	8.15
8.7	Unsegmented Barberpole: Tip Acceleration (Semi-Log Scale) . . . . .	8.16
8.8	Segmented Barberpole: Tip Acceleration (Semi-Log Scale) . . . . .	8.19

*Abstract*

In this dissertation, different aspects of constrained layer damping treatments on beams of various geometries are studied. First, the optimal length of a constrained layer damping treatment mounted on a surface in linear strain is identified as a function of the relative stiffnesses of the damping layers and the non-uniformity of the surface strain. The analysis extends previous work that considered the case of uniform surface strain.

Sixth order sandwich beam theory is then modified for use with a rectangular beam covered with a segmented constrained layer damping treatment. Non-dimensional variables are used to simplify the form of the problem. Also, equations are developed for a beam of circular cross section with thin narrow constrained layer strips placed parallel to the beam centerline, and it is shown the equations have the same form as the sixth order theory for the rectangular beam.

A new approximation method, the "Complex Rayleigh Quotient", is proposed to estimate the complex natural frequency and damping of structures. Complex mode shapes are used in a ratio similar in spirit to Rayleigh's Quotient to obtain an estimate for the complex frequency of the system. The method is defined for both discrete and continuous systems, and illustrated using a rectangular beam with a segmented damping treatment. The estimates of loss factor developed from the Complex Rayleigh Quotient were much closer to the exact solutions than those developed using the Modal Strain Energy method.

A new constrained layer configuration, the "barberpole", is presented for beams of circular cross section. An analysis is developed which show that the barberpole configuration can damp both bending and torsional vibrations. The barberpole also provides more damping than unsegmented strips for a beam in bending. An experiment was performed to gain confidence in the bending portion of the barberpole analysis.

# DESIGN AND ANALYSIS OF CONSTRAINED LAYER DAMPING TREATMENTS FOR BENDING AND TORSION

## *I. Introduction*

Modern designers of aerospace structures continually attempt to gain greater performance out of their hardware. For aircraft, reducing excess weight is often critical to better performance, and for space systems, reducing weight is a top priority because of the physical limitations of existing launch vehicles and the high cost per launch. Unfortunately, attempts to reduce weight can often result in structures with reduced stiffness and damping, making unwanted structural vibrations a major problem.

The problem of undesirable vibration has created extensive interest in the subject of vibration suppression. There are two general approaches to vibration suppression. Active damping or active control systems continually monitor the state of the structure, detect any deviation from the desired behavior, and then apply an appropriate force to correct the system motion. Passive damping methods attempt to augment the inherent damping of the structure through some design to increase the dissipation of kinetic energy into heat. Passive damping methods are attractive in many applications because of their relative simplicity, low cost, low weight, and inherent stability. Because an increase in the damping inherent in the structure may often make the task of active control easier, passive damping methods may also be considered a supplement to active control.

Viscoelastic coatings are often used as part of a passive damping treatment. A viscoelastic material converts kinetic energy into heat when it undergoes mechanical strain. There are two primary viscoelastic coating classifications. In the extensional or unconstrained layer treatment, a viscoelastic coating is added to one or more surfaces of an existing structure (Figure 1.1). Bending of the structure causes elongation or compression of the viscoelastic layer and the energy dissipated is proportional to the axial strain. The constrained layer treatment consists of one or more layers of viscoelastic material sandwiched between layers of high extensional stiffness. Damping comes from shear stress in the viscoelastic layers created by the relative deformation of the structural elements (Figure 1.2). Periodic cuts in the constraining layer have been shown to improve damping effectiveness (76:150, 46:41, 57:1678). From a mass optimization standpoint, a constrained layer damping treatment is more efficient than the extensional treatment, though the analysis is more complicated, especially if the constraining layer is cut into segments.

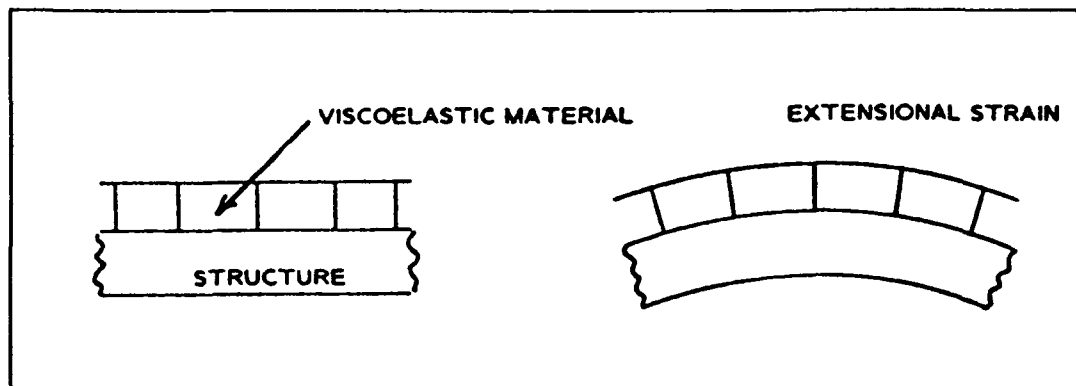


Figure 1.1. Viscoelastic Extensional Treatment

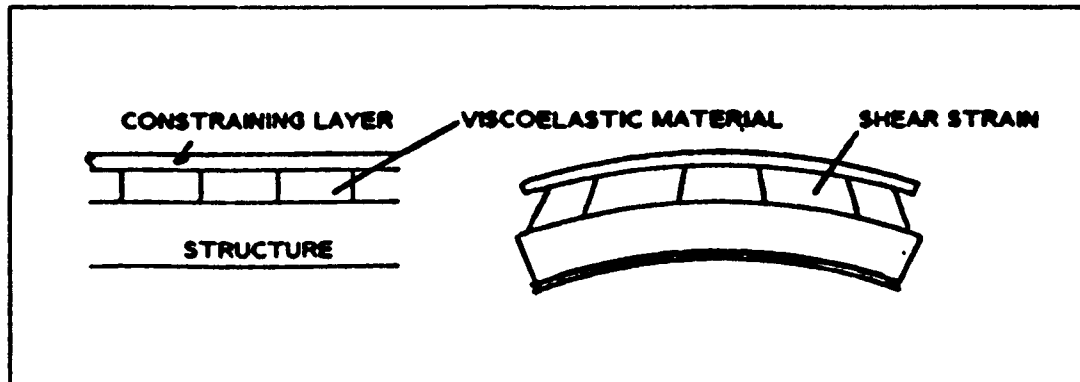


Figure 1.2. Viscoelastic Constrained Layer Treatment

The goal of this research is to investigate several different uses of constrained layer damping treatments in the damping of beams of various geometries. A review of existing literature is presented in Chapter 2. In Chapter 3, the impact of segmentation on the effectiveness of constrained layer damping treatment is discussed. The optimal length analysis of Plunkett and Lee is described, which identifies the optimal length of a segment mounted on a substrate with uniform surface strain (76:150). The analysis is extended for the case of linearly varying surface strain. The exact equations of motion for a continuous constrained layer damping treatment on a rectangular beam are developed in Chapter 4, then it is shown how these equations may be modified to include the effects of segmentation. In Chapter 5, a method based on Rayleigh's Quotient that uses complex mode shapes developed from the Correspondence Principle is used to predict the natural frequency and loss factor of structures. The results from the new method are compared with predictions from the Modal Strain Energy method and the exact solutions, and it is shown that the approximation using complex modes provides a much better estimate of the system damping than the Modal Strain Energy method. In

Chapter 6, a system of equations are developed for a beam of circular cross section with constrained layer strips parallel to the beam neutral axis. It is shown that, if the damping strips are thin and narrow, the equations collapse into a single 6th order equation similar in form to the flat beam problem described in Chapter 4. In Chapter 7, the equations of motion for both bending and torsion are developed for a beam of circular cross section with a damping treatment consisting of thin, narrow constrained layer strips oriented in a helical or "barberpole" configuration. The analysis shows that the barberpole configuration has the capability to damp both bending and torsional vibrations. In Chapter 8, results of an experiment performed to gain confidence in the bending portion of the barberpole theory are reported. Chapter 9 contains a summary of the dissertation research and the conclusions reached in the earlier chapters.

## *II. Literature Review: Analysis of Constrained Layer Damping*

A great deal of research has been published on the use of damping materials to control structural vibration. There are several reviews of various aspects of the field, including those by Nakra in 1977 (65:3) and 1981 (66:17), by Nelson in 1977 (69:3), by Torvik in 1980 (94:85), and by Yu in 1989 (106:1).

This chapter addresses previous work in constrained layer damping that is directly related to the goals of this research. These topics include some of the early work on constrained layer damping, the expansion of the theory to include higher order effects and non-pinned boundary conditions, the effects of partial coverage and segmentation, the application of constrained layer theory to generalized or circular cross sections, and the design of composites to use constrained layer concepts as an integral part of the structure. Because finite elements are not used in this research, papers that use this method for analysis have not been singled out as a special group, but it should be noted that finite element methods are being used extensively in the investigation of various viscoelastic problems (30:792, 33:203, 34:71, 35:1284, 47:199). Though most of the research described in this chapter involves constrained layer damping treatments, some relevant work associated with generalized damped systems is also discussed.

### *Early Constrained Layer Analysis of Rectangular Beams*

The analysis of the damping effects of constrained viscoelastic layers first blossomed in the late 1950's. Though some form of the problem was addressed by earlier researchers (72:48, 99), a series of papers by E. M. Kerwin, D. Ross, and E. F. Ungar served as a stimulus for research in the analysis, testing and application of constrained layer damping treatments. A review by Kerwin published in 1965 (37) describes much of the early work in this area. In general, the early work assumes the beam mode shapes are sinusoidal and considers forces in the damping treatment that act in a direction parallel to the neutral axis of the beam. These assumptions allowed the authors to develop closed form expressions for the loss factor.

In the 1959 paper "Damping of Flexural Waves by a Constrained Viscoelastic Layer" (36:952), Kerwin analyzed a constrained layer treatment on a plate and attributed the energy dissipation to shear induced in the viscoelastic layer. A complex shear modulus was assigned to the viscoelastic material, then an expression for the loss factor for the composite structure was developed from the structure's complex bending stiffness. A subsequent report by Ross, Ungar, and Kerwin (79:49) elaborated on the theory. The report included an analysis for multiple constraining layer configurations and the use of rigid spacers to improve the efficiency of damping treatments. In a later paper, Ungar and Kerwin defined expressions for a system loss factor using energy methods (97:954). Unlike some of the earlier work in the field, their definition for loss factor is valid for heavily damped systems with out of phase deformations.

### *Higher Order Effects*

*Effect of Boundary Conditions.* The Ross, Ungar, Kerwin analysis (and most of the papers that soon followed) assumed that all layers of the sandwich beam or plate moved with the same sinusoidal mode shape. DiTaranto developed a general 6th order equation in the longitudinal displacement that could be used with more general boundary conditions (17:881). He noted that the relationship between the loss factor and the frequency of vibration was independent of the boundary conditions as long as no energy is dissipated at the boundaries. Mead and Markus developed a 6th order equation in terms of the transverse displacement of the beam (59:163, 60:99). In the later paper, they considered the roots of the resulting characteristic equation and stated that the roots will be complex for other than simply supported boundary conditions. They reported that the frequency where the loss factor achieves its maximum is sensitive to boundary conditions, but the magnitude of this maximum does not vary significantly (60:111). These papers by DiTaranto and Mead and Markus retained the assumption that the relative spacing between beam and constraining layer is maintained throughout the deformation.

Lu and Douglas compared the Mead and Markus theory with experimental data (46:513). DiTaranto and Blasingame used DiTaranto's 6th order theory to investigate the influence of different boundary conditions and to identify some general design guidelines (18:633). D. K. Rao developed exact solutions for the 6th order theory for several boundary conditions (76:271). Cottle extended the 6th order theory to allow the individual elastic layers to have different boundary conditions (14).

*Higher Order Inertia and Shear Effects.* Other researchers have investigated higher order effects in sandwich beams. Yu developed equations using a variational approach for symmetric beams, including higher order inertial effects (105:790). Yan and Dowell developed an analysis for the sandwich beam which included longitudinal inertia, rotatory inertia, and shear strain in the beam and constraining layer (101:1041). In their analysis it was assumed that the shear stress in both the core and the face plates was uniform through their respective thicknesses, although not of the same value. They then considered a simplified form of their equation, neglecting several higher order effects. Their analysis results in a 4th order equation.

Mead (56:363) compared the 4th order equation from the Yan and Dowell analysis with the 6th order equation of DiTaranto (17:881), Mead and Markus (59:163) and others. Mead derived a more accurate analysis for a symmetric sandwich plate which includes higher order effects such as longitudinal inertia and face-plate shear deformation. He reported that the Yan and Dowell analysis agrees with the higher order analysis over a broad wavelength range for stiff, thick cores, but agrees over a narrower range for thin soft cores. Mead found that the 6th order analysis agrees with the higher order theory for all core thicknesses over a much wider wavelength range. For most viscoelastic damping applications, he concluded that the 6th order equations should be more accurate than the Yan and Dowell analysis as long as the flexural wavelengths are at least four times the thickness of the thickest face-plate.

Nakra and Grootenhuis developed equations that included the extensional effects of the viscoelastic layer in the longitudinal direction and stated that this effect is

significant for thick, stiff cores at low resonant frequencies (67:225). They used a correction factor in the formulation to account for the non-uniform shear stress through the thickness of the viscoelastic layer.

Y. V. K. S. Rao and Nakra included the effects of longitudinal inertia and shear deformation of the face plates of a sandwich beam (77:309). They stated that longitudinal inertia does not significantly affect the transverse displacement of the beam or plate, but can significantly affect the longitudinal strain response at higher frequencies. In a later paper, D. K. Rao performed an analysis of a short sandwich beam which included the inertia, shear, and extension of all layers (75:253). He compared the results of this higher order theory with earlier theories and then commented on the validity of these theories for different configurations. Markus (52:593) used D. K. Rao's analysis to show that incorporation of the higher order effects reduces the calculated loss factor from what is predicted by the Ross-Ungar-Kerwin theory.

*Compressional Effects in the Viscoelastic Layer.* In the previous research discussed, the authors assumed that the individual layers of the composite beam moved with the same transverse motion and neglected the effects of compressional deformation in the viscoelastic layer. The damping from such deformations may become significant in thick cores, and investigations of these effects began in the mid 1970's. Douglas and Yang modelled a constrained layer treatment as two separate beams coupled by a complex extensional spring (22:925). They concluded that compressional damping can provide significant vibration suppression at frequencies near the delamination frequency of the

composite beam, but provides little attenuation elsewhere. The delamination frequency is defined as the natural frequency of the composite beam at which the beam and constraining layer tend to separate from each other. Douglas later extended the compressional damping analysis to include rotatory inertia and shear deformation in the face plates of a short thick beam (21:343). Neither paper included the effects of shear damping in the viscoelastic layer.

In 1986 Miles and Reinhall extended the 6th order equations of DiTaranto and Mead and Markus to include the effects of longitudinal inertia and thickness deformation in the viscoelastic layer (63:56). Four coupled equations of motion in the transverse displacement and longitudinal displacement variables for the two face plates were developed using Hamilton's principle. These equations reduce to the earlier 6th order expression if longitudinal inertia is neglected and the transverse deformations of the two face plates are equated. One significant advantage of this extended formulation is that the actual end conditions of the constraining layer may be modelled. In practice, the constrained layer treatment is usually added on to an existing structure. The constraining layer often has free-free boundary conditions that do not firmly attach it to the primary beam, a situation which is not accurately modelled by the 6th order theory if the core is soft. Miles and Reinhall solved the equations numerically by using a Ritz method.

Other work has considered both compression and shear damping effects, including the analysis of sandwich beams by Sylwan (92:35), the investigation of an adhesive joint coupling two beams by Saito and Tani (81:229), and Yadagiri and others (100:445).

*Analysis of Isotropic Flat Layered Plates.* Though many of the early papers discussed damping of plates and beams, the "plate" analysis was limited to bending in one plane. Such plates can be considered beams that are wide enough to exhibit plane strain. Extensions of beam theory to the thin flat three-layer (i.e., "sandwich") plate with bending in two dimensions began in the late 1960's. In 1969 DiTaranto and McGraw developed the equations of motion for a freely vibrating three-layer plate, and solved the problem for simply supported boundary conditions (20:1081). Abdulhadi used the DiTaranto-McGraw analysis to determine the forced response of simply supported three-layer plates (1:93); and Durocher and Solecki extended the Yan and Dowell beam analysis to a plate (23:105). J. F. He and B. A. Ma (31:237) developed simplified equations for an unsymmetrical sandwich beam that neglects bending-extensional coupling, then solved them using an asymptotic approach. Several researchers have used finite element methods to analyze the viscoelastic sandwich plate configuration (30:792, 33:251, 34:71, 35:1284, 47:199, 48:63, 78: 467).

#### *Segmentation, Partial Coverage, and Optimal Design of Damping Treatments*

Several researchers have investigated the effects of using constrained layer damping treatments that only partially cover the beam or plate to be damped, including Nokes and Nelson (70:5), Markus (52:179), Grootenhuis (28:421), and Sylwan (107:219). Others have noted that the effectiveness of a constrained layer damping treatment can be improved by judicious segmentation of the constraining layer, including Plunkett and Lee (73:150), Kress (42:41), Alberts and others (3:274), Mantena and others (51:1678), and

Sattinger (84: HBA). Sandman considered the effects of segmenting the viscoelastic core of a sandwich beam (82:897).

*Segmentation of Constraining Layers.* One of the first analyses of the effects of segmentation of constrained layer damping treatments was presented by Parfitt at the Fourth International Congress on Acoustics in Copenhagen in 1962 (71:1). Parfitt's segmentation analysis was an extension of Kerwin's earlier work, with similar assumptions. In the analysis it was assumed that the base structure experiences sinusoidal bending and that the constrained layer damping treatment does not affect the strain configuration of the base structure. The loss factor of the viscoelastic layer is assumed to be small, and only the real part of the viscoelastic shear modulus is used when solving the Kerwin equation for shear in the viscoelastic layer. Parfitt showed that segmentation of the damping treatment improved its effectiveness, and that there exists an optimum length that produces a maximum loss factor:

$$L_{optimal} = \frac{3.28}{\sqrt{g}}, \quad g = \frac{Re[G_v^*]}{(2h_v)(2h_c)E_c} \quad (2.1)$$

In Equation (2.1)  $2h_v$  and  $2h_c$  are the thicknesses of the viscoelastic and constraining layer,  $Re[G_v^*]$  is the real part of the complex viscoelastic shear modulus, and  $E_c$  is the constraining layer elastic modulus.

In the same year Parfitt presented his work, a paper on the effectiveness of partial coverage was presented by Pulgrano at the 64th Meeting of the Acoustical Society of America (74:1976). Only an abstract of Pulgrano's work is currently available. In a later

paper, Zeinetdinova and others experimentally confirmed that segmentation of the constraining layer significantly improved the system loss factor even when Parfitt's assumptions of a thin damping treatment and small viscoelastic loss factor were not satisfied (107:347). They reported that for the thick cores tested with loss factors of .5, the multiplier for optimal segment length is somewhere between three and four, which is consistent with the value of 3.28 identified by Parfitt.

Parfitt's work was later cited and expanded upon by Plunkett and Lee in a 1970 paper published in the Journal of the Acoustical Society of America (73:150). Plunkett and Lee analyzed a constraining layer mounted on a substrate experiencing uniform strain, and developed an expression for optimal length similar to that of Parfitt:

$$L_{optimal} \approx \frac{3.28}{\sqrt{g}}, \quad g = \frac{|G_v^*|}{(2h_v)(2h_c)E_c} \quad (2.2)$$

Unlike Parfitt, Plunkett and Lee did not limit their analysis to the case where the viscoelastic loss factor is small, and their expression contains the absolute value of the shear modulus. Plunkett and Lee also considered the case of multiple layers of constrained layer damping treatment on a beam. This work was extended by Torvik and Strickland in their analysis of multiple segmented layer damping treatments for plates (95: 985).

Alberts, Chen, and Xia used the optimal length defined by Plunkett and Lee to investigate segmentation of constrained layer damping treatments (3:274). They used Equation (2.2) to design optimal damping treatments for the first and fourth modes, then used the Modal Strain Energy approach with the MSC/NASTRAN finite element package to find the resulting response for beams with the optimal damping treatments. Their

analysis indicated that the loss factor from a properly segmented constraining layer could be as much as seventeen times larger than the loss factor from the same constraining layer without cuts. They also stated that the most significant factor in the predictive accuracy of any optimal length analysis that assumes linear material properties is correct viscoelastic material data. Because higher strains are developed in the layer using an optimal length treatment, it is critical that the viscoelastic properties used in the linear analysis are determined in tests performed at similar strain amplitudes.

In 1987 Kress investigated the segmentation problem and produced an optimal length "handformula" similar to that developed by Parfitt and Plunkett and Lee, but including the extensional stiffness of the base layer (42:41). Kress also developed a more accurate implicit formula for optimal length which must be solved using an iterative approach. He compared these different approaches with the results of a transfer matrix analysis which modelled the main beam and constraining layer as Bernoulli-Euler beams, and assumed the viscoelastic layer was in a state of plane stress. Kress reported that the predictions of optimal length obtained from the implicit formula agreed with the those from the transfer matrix analysis. Kress' handformula showed an +11 percent discrepancy, and the Plunkett and Lee equation showed a -13% to +17% discrepancy, depending on the value of  $G_v$  used in the formula.

Kerwin and Smith considered the effects of segmentation on damping treatments for extensional waves ( 38:KK<sup>1</sup> ). They noted that the optimal segment length for

---

<sup>1</sup>This reference is from a collection of papers; the letter designator "KK" is used instead of a page number to identify the reference.

extensional treatments was essentially the same as for the bending problem, but the loss factors for extensional treatments were in general three times less than similar flexural treatments because of the higher percentage of strain energy seen in the main beam during extensional deformation.

*Partial Coverage.* In 1968, Nokes and Nelson showed that partial coverage of constrained layers gives a better system loss factor than full coverage (70:5) for some constrained layer configurations. This effect had been observed earlier in experiments by Yoos and Nelson (104:1). The Nokes and Nelson analysis was based on the Ross, Ungar and Kerwin assumptions, including that the mode shapes of the beam are unaffected by the damping treatment. Their development assumes that the constrained layer is centered on the beam and their results may be applied for any symmetric beam mode. The authors identified a parameter  $R$  as a measure of the coupling between structure and constraining layer:

$$R = \frac{G_v^* L^2}{2h_v} \left[ \left( \frac{1}{2h_c E_c} + \frac{1}{2h_b E_b} \right) \right] \quad (2.3)$$

where  $2h_v$ ,  $2h_c$ , and  $2h_b$  are the thicknesses of the viscoelastic layer, constraining layer, and beam. If the beam to be damped is much thicker than the constraining layer,  $R$  is equivalent to the term  $gL^2$  used in the Plunkett and Lee analysis. For small  $R$ , the damping decreases continuously as coverage is decreased. For larger  $R$ , the stiff viscoelastic layer extends the compliant constraining layer and the shear strain in the viscoelastic layer is concentrated at the edges of the damping treatment. This is clearly

a suboptimal application of viscoelastic material, and the authors found that as  $R$  increases, the loss factor is maximized with a treatment that covers a decreasing percentage of the beam.

Mantena, Gibson, and Hwang experimented with partial constrained layer coverage of composite cantilever beams and compared their results with predictions from a finite element model (51:1678). They reported increases in loss factor with partial coverage and explored the effects of different boundary conditions on the loss factor.

Lall, Asnani, and Nakra compared three formulations of the partial beam problem (43:247). In the first method the modal loss factor is assumed proportional to the ratio of the energy dissipated to the maximum strain energy during a cycle of harmonic motion, where the modes are assumed to be those of the undamped beam. The second method was based on a Rayleigh-Ritz approach, which yields natural frequencies as well as loss factors. The third formulation was based on a classical-cum-search method, where the exact equations of the Bernoulli-Euler beam and sandwich beam theory are solved with continuity conditions for displacement, slope, moment, and shear force at the beam interfaces. For an arbitrarily located constraining layer patch, the continuity conditions provide a 14th order system of linear homogeneous equations from which the complex natural frequency and resulting loss factor can be found.

*Other Optimal Design Efforts for Viscoelastic Damping Treatments:* Several researchers have sought an optimal design for constrained layer damping treatments by tailoring the material properties and thicknesses of elastic and viscoelastic layers, but leaving them

unsegmented. Mead and DiTaranto considered the optimal design of a simply supported three layer beam, and reported that displacement, velocity, acceleration, and stress were minimized for the sandwich beam with elastic plates of approximately equal magnitude (58:174). Classical optimal design methods have been used to design constrained layer damping treatments. Lifshitz and Leibowitz (44:1027) developed an optimization program using 6th order beam theory that includes design inequality constraints similar to those seen in standard structural design problems. Hajela and Lin (29:S96) used both a nonlinear programming approach and a genetic search method to get an optimal segmented layer solution. Farkas and Jarmai (25:47) used optimal design methods with inequality constraints to design a minimum cost sandwich beam whose outer layers have a box beam cross section. Kodiyalam and Molnar (41:1) considered the optimization of constrained layer damping treatments where both the constraining layer and the primary structure are made of an aluminum honeycomb material.

*Constrained Layers on Structural Elements with Generalized or Circular Cross-Sections*  
*Extension of Ross-Kerwin-Ungar Analysis: Ungar, 1962.* In 1962, Ungar published "Loss Factors of Viscoelastically Damped Beam Structures" (96:1082), which extended the work by Ross, Kerwin, and Ungar on layered rectangular beams to axially uniform beams with a more general cross-section. He first derived an expression for the loss factor of a composite structure in strain energy terms, then developed equations for a structure of arbitrary but uniform cross-section consisting of either two or three different materials. These equations were then simplified by making assumptions about the relative

properties of the viscoelastic material and structure. The loss factor for the generalized beam cross section has the same form as the loss factor developed for the rectangular beam.

*Applying Ungar's analysis: Yin et. al., 1967.* The validity of Ungar's analysis for a broad range of cross-sections was investigated in 1967 by Yin, Kelly and Barry (103:773). The researchers applied the expressions developed by Ungar to various cross-sections, then compared the theoretical predictions to experimental results. One of the configurations tested was a hollow circular beam consisting of concentric elastic-viscoelastic- elastic layers. Both Ungar's theory and the authors' experiments indicated that the viscoelastic material in this configuration provides far less damping than an equivalent amount of material used in a flat constrained layer treatment on a rectangular beam. Ungar had identified the separation distance between the neutral plane of the beam and the centroid of the constraining layer as being critical to the performance of the damping treatment, and this quantity is zero for the concentric circular configuration. The authors' experiment confirmed that damping was negligible. To show the poor damping was not some peculiarity of a circular cross section, a box beam with a concentric constrained layer was tested; again both the experiment and the Ungar analysis indicated negligible damping.

*Constraining Layer as a Hollow Concentric Beam: DiTaranto, 1974.* R. A. DiTaranto investigated the vibration of a beam with a hollow circular cross-section damped by a

concentric constrained layer (16:845). He modelled both the constraining layer and the inner structure as two distinct concentric beams with circular cross-sections coupled by the viscoelastic layer, which was assumed incompressible. The two resulting fourth-order partial differential equations were solved by assuming a sinusoidal mode shape and harmonic time dependence. The problem reduces to a complex set of algebraic equations involving the natural frequency and eigenvalues. He solved these equations numerically and discussed the effect of varying some of the equation parameters.

To illustrate the results, he compared the problem to a two degree of freedom spring-mass-damper system. At the fundamental frequency the two masses move in phase, and the damper between them does not effectively dissipate energy because of the small relative motions involved. At a higher frequency, the two masses move out of phase and considerable damping is obtained. Similar results were seen in the more complex concentric beam problem, where the fundamental frequency of the composite beam has negligible damping. Because the beam and constraining layer move together, minimal shear is induced in the viscoelastic layer. The results for the fundamental frequency are comparable with the earlier investigations of concentric damping treatments for beams of circular cross section (96:1082, 103:773)

*Longitudinal Cuts in the Constraining Layer: Vinogradov and Chernobrevskii, 1980.*

In 1980, Vinogradov and Chernobrevskii reported that the loss factors of a constrained layer damping treatment on a tubular beam were significantly increased when

the treatment was cut along the generator lines<sup>2</sup> of the beam (98:328). They analyzed and tested configurations with one, two, and four cuts in the concentric constraining layer along the surface generator lines. The damping treatments in the two-cut and four-cut geometries consist of strips parallel to the beam axis. In their analysis, the researchers assumed that the shear strain in the viscoelastic layer was uniform throughout the width of the strip. Both theory and experiment showed that the loss factor increases with an increase in the number of cuts in the damping treatment.

*Beam as a Thin Shell: Lu and others.* Several researchers have investigated the use of constrained layer or other viscoelastic treatments to suppress vibrations in thin cylindrical shells and rings. Several papers consider only "breathing" or lobar modes, while others also consider beam bending modes. Two general configurations are considered. The first configuration is a system of concentric shells consisting of alternating elastic and viscoelastic materials (2:803, 4:121, 15:748). The second configuration consists of a single shell with a discontinuous damping treatment such as small lumped mass vibration isolators positioned around the shell circumference (24:902, 45:513), or a series of small beams attached with viscoelastic layers running parallel to the axis of the shell (19:74, 49:395, 50:1).

In a recent paper, Lu, Roscoe, and Douglas used shell theory to describe the motion of a simply supported cylindrical beam covered with strips of constrained layer

---

<sup>2</sup> A *generator line* or *generatrix* is a line whose motion generates a surface, and in this context it refers to lines parallel to the beam centerline that define the cylindrical surface of the beam.

damping treatment running parallel to the cylindrical beam axis (49:395). The inhomogeneous shell equations developed by Flugge (27:219) are used to describe the main beam. The constraining layers are modelled as rectangular beams, the viscoelastic layer is modelled as a massless spring, and the stresses from the damping strips are modelled as surface forces on the main beam. The authors performed experiments which were compared with the theory. In the analysis, the small beams acting as constraining layers are assumed to be uniform along the length of the beam and simply supported. In their experiment, the constraining layers were free-free and segmented into five pieces along the beam axis. Although the analysis could not match the boundary conditions of the experiment, the agreement between prediction and experiment for the tested configuration was reasonable.

Because boundary conditions are difficult to handle in shell theory, finite elements are often used for structures with circular cross section. Lu and Everstine used a finite element approach to model a constrained layer damping treatment on a beam of circular cross section, as well as lumped mass dampers mounted on rings (47:199). Fowler and others used finite elements in an optimal design program to find the optimal material properties and thicknesses for damping treatments mounted on panels and cylindrical beams (26).

*Longitudinal and Circumferential Cuts: Sattinger, 1990.* Sattinger reported that a segmented constrained layer treatment applied to a tubular structure can be effective in

simultaneously damping global bending, torsion, and axial vibrations (84:HBA<sup>3</sup>). The interest in axial vibrations was tied to the use of tubular structures in large truss assemblies, where the lowest frequencies of the entire structure, called "global modes", involve axial vibrations of the individual struts at very low frequencies. Because the frequencies of concern were much lower than the natural frequencies of the tubular structure itself, a quasistatic approach was used in the analysis.

Sattinger used two different approaches to predict the loss factor for the configurations considered. One approach was based on new interpretations of the quasistatic closed form solutions generated by Torvik (94:85), and another approach used finite elements with the strain energy principle of Ungar and Kerwin. The finite element approach used offset beam elements for the viscoelastic layer. Because Sattinger was unable to find any existing closed form solution for the torsion problem, he used finite elements for the torsion problem and for those configurations that could not be evaluated using the closed form analysis. He reported that the closed form analysis of the bending and axial loss factors showed reasonable agreement with an experiment on a tubular structure with hollow rectangular cross-sections.

*Circular Shaft in Torsion: Chandrasekharan and Ghosh, 1974.* In 1974, Chandrasekharan and Ghosh investigated the damping characteristics of a fixed-free composite circular shaft in torsion with an elastic-viscoelastic core (11:1). A quasistatic

---

<sup>3</sup>This reference is from a collection of papers; the letter designator "HBA" identifies the reference instead of a page number.

analysis was performed, then the shaft was modelled as a lumped parameter system using equivalent quantities for inertia and stiffness. The authors concluded that a hollow elastic shaft with a solid viscoelastic core was not an effective design for damping torsional vibrations. If an elastic inner core is added, the annular viscoelastic layer yields a much higher damping factor. They reported that there exists an optimum thickness of the viscoelastic layer which maximizes the overall damping factor, and that a better damping factor results if the inner elastic core is stiffer than the outer hollow shaft.

*Spring in Torsion and Bending: Kishore and Ghosh 1975.* Kishore and Ghosh performed a static analysis of a bar with constant curvature under a combination of torsion and bending (40:621). The bar had a circular cross-section with concentric elastic-viscoelastic-elastic layers. In the configuration studied, the curved bar was clamped at one boundary, and a lever lying in the plane of the beam and passing through the center of curvature was fixed to the outer tube at the other end of the bar. A force perpendicular to the plane of the beam was applied to the lever at the center of curvature, which in turn transmitted a combined torque and an out of plane force to the outer tube. This loading is equivalent to that seen by a helical spring. The authors reported that if the cross section of the bar is fixed, the damping is maximized for a certain length of bar. If all the layers are continuous, the loss factor drops sharply as the length of the bar increases, but if the elastic core of the bar is cut into segments, loss factors equal to the optimal value were obtained for longer bars. They also reported that the overall damping factor increases as the radius of curvature increases, and ultimately reaches the value for a

straight composite bar. As in the pure torsion problem, their analysis showed that there exists an optimum thickness of the viscoelastic layer for a given set of geometric parameters.

### *Constrained Layer Treatments with Composite Structural Elements*

Recently several researchers have used constrained layer concepts to design composite materials with integral damping. An early paper addressed stress coupling in flat plates (64:347), while later papers addressed the phenomenon in circular tubes (12:1, 8:HAC, 5:HCB).

Sattinger and Sanjana used the analysis developed by Sattinger (84:HBA) to predict the loss factor of a circular composite tube containing an embedded, encapsulated constraining layer (86:1). The encapsulated layer concept consists of a constraining layer sandwiched between two viscoelastic layers, which are in turn sealed between two load bearing layers of composite material. The viscoelastic material is not in the load path.

Bronowicki and Diaz in 1989 reported a form of embedding in a hollow composite tube called the "Alternating Ply Concept" for damping in extension and bending (10:GCA). This concept increases damping by allowing the viscoelastic material to carry some of the axial load. The walls of the tube consist of a viscoelastic layer sandwiched between two angle ply composite layers. The angle plies are stiffened by alternating segments of stiff uniaxial composites. The authors developed a finite element based upon the closed form solution of membrane cylindrical shells to analyze this configuration.

Chen and Wada (13:1) attempted to use axial/twist coupling in a constrained layer treatment on an aluminum tube to induce additional shear in the viscoelastic layer. Their analysis indicated that the additional tangential shear developed by the non-symmetrical constraining layer was not enough to overcome the reduction in axial stiffness that the off-axis ply generated, though the authors noted that the performance of such a treatment on a tailored composite strut may be improved.

Belknap and Kosmatka constructed a circular composite tube which takes advantage of the axial/twist coupling generated in non-symmetric composite layups (7:HAC). The tube consists of a viscoelastic layer sandwiched between two composite concentric layers which, when subjected to bending or axial extension, twist in opposite directions and induce shear in the viscoelastic layer.

Barrett also investigated the use of stress coupling to reduce vibrations (5:HCB) and developed a theory for constrained layer treatments on anisotropic laminated plates (6:453). In Reference 5, the general analytical equations are developed for a composite tube experiencing axial vibration with several alternating elastic and viscoelastic layers. He applied this development to a three-layer problem similar to that of Belknap and Kosmatka, and observed the existence of an optimal off-axis ply layup for his choice of materials and geometry. He noted some of the advantages and disadvantages of incorporating such an anisotropic ply configuration, including the advantage that such a configuration will damp torsion, axial, and bending vibrations. A serious disadvantage of this configuration is that the inner and outer composite layers must be allowed to rotate relative to each other.

Chen and Dolgin recently suggested an alternative use of composite stress coupling in axial members that avoids the need for a rotational degree of freedom between the two elastic layers. They proposed having the fiber orientation of the inner and outer composite walls vary continuously along the length of the beam in the form of a sine function, where the inner and outer walls are out of phase with respect to each other (12:239). Along the length of the tube shear is induced in the viscoelastic material by opposing rotations of the layers. Because these effects cancel at the ends, the edges of the inner and outer tubes may be fixed to each other.

### *Summary*

There has been an extensive amount of research in constrained layer damping treatments. Several of the issues identified in this chapter will be discussed and extended in later chapters. The issue of an optimal length for constrained layer damping treatment surfaced in much of the research that was discussed, and it will be heavily stressed in Chapters 3, 4, 5, and 7. In Chapters 4 and 6, damped beams are analyzed whose equations of motion have the same form as those developed by Mead and Markus for a three layer sandwich beam (59:163). The ineffectiveness of a hollow concentric constrained layer damping treatment for damping a beam of circular cross section will motivate the work in Chapters 6 and 7.

### *III. Optimal Length of Constrained Layer Damping Treatments*

The performance of a constrained layer damping treatment is greatly affected by its length. In this chapter, the optimal length effect is described. It is shown that segmentation of the constraining layer improves damping performance if the viscoelastic layer is relatively stiff or the surface to be damped is relatively long. Equations are developed that describe a constraining layer mounted on a substrate with an arbitrarily surface displacement. Plunkett and Lee analyzed this problem for the special case of uniform strain in the substrate (73:150), and their conclusions about the optimal length of the constraining layer are presented. Their analysis is extended for the case of linearly varying strain in the substrate, and the impact of constraining layer length on the loss factor will be discussed.

#### *Description of the Optimal Length Effect*

In an effective constrained layer damping treatment, there is a balance between the length of the damping treatment and the relative stiffness of the viscoelastic layer and constraining layer. First consider an idealized constrained layer damping treatment, where the viscoelastic layer is relatively compliant compared to the constraining layer (Figure 3.1). The forces transferred to the constraining layer are relatively small, and so the strain

in the constraining layer is negligible. As a result, the longer the damping treatment, the greater the viscoelastic shear and the greater the damping.

Now consider the case where the viscoelastic layer is relatively stiff compared with the constraining layer. As the overall length of the strip increases, the stress in the viscoelastic layer increases, and eventually the constraining layer begins to stretch. In this situation, most of the viscoelastic layer is in a state of extensional strain, and the shear strain is concentrated at the ends (Figure 3.2).

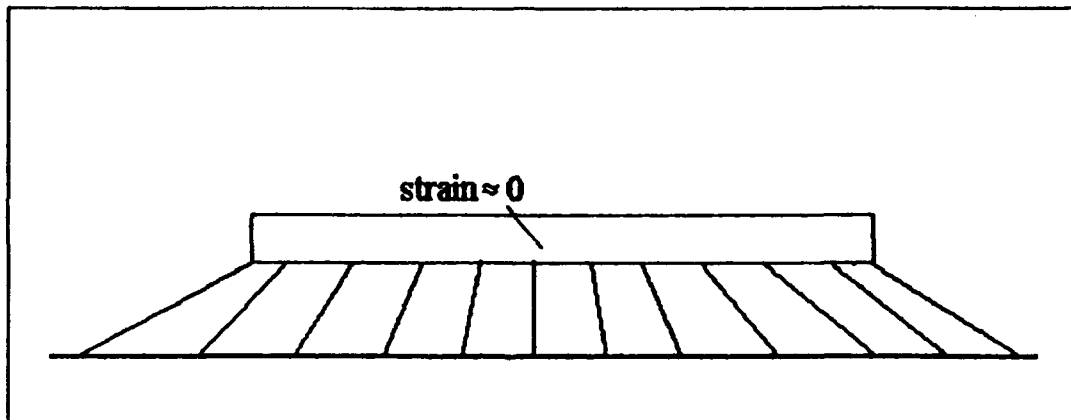


Figure 3.1. Constrained Layer Treatment: Compliant Viscoelastic Layer

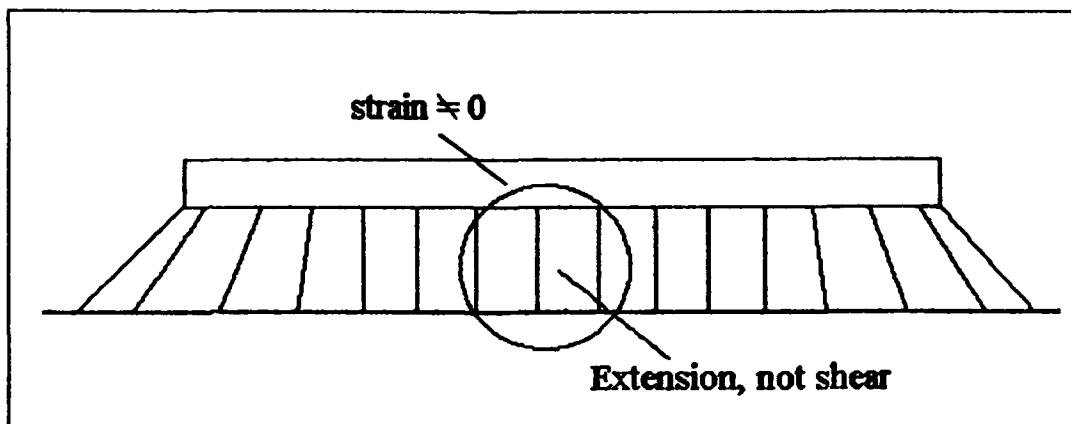


Figure 3.2. Constrained Layer Treatment: Stiff Viscoelastic Layer

### *The "Substrate Assumption" in Studies of Constrained Layer Damping Treatments*

The exact equations of motion for a beam with segmented constraining layers are difficult to solve, so previous researchers sought ways to evaluate the optimal length effect without dealing with the exact equations. One approach taken was to analyze the constraining layer by assuming the main beam displacements are specified and are unchange the forces in the damping treatment. In this dissertation, this will be referred to as the "substrate approach".

When using the substrate approach, it is often assumed that either the surface to be damped is in a state of uniform strain, or that the strain distribution of the surface is known a priori, e.g., approximated by the strain distribution of the undamped structure. The uniform strain assumption is attractive when general conclusions are sought about the damping treatment that are independent of the base structure deflections, while the latter approach is useful when the damping of a specific structure is sought. Damping treatments are often added to existing structures that are much stiffer than the constraining layer, and the assumption that the structure vibrates in its undamped mode shape is a reasonable approximation for such structures.

### *Constraining Layer Equations of Motion*

In this section, equations are developed that describe the displacement of a constraining layer mounted on a substrate with an arbitrary specified displacement. The analysis is consistent with the approach and assumptions made by Plunkett and Lee

(73:150). Their results for the special case of uniform substrate strain will be described in the next section.

The damping within the system is modelled using the Correspondence Principle as described in Chapter 5. The equilibrium equation for the constraining layer displacement and its solution are developed as if the system is purely elastic and the viscoelastic shear modulus is a real number. Once the corresponding elastic problem is solved, a complex form of the modulus is substituted into the solution to calculate the various energy terms required to identify the system damping. The following complex form for the viscoelastic shear modulus  $G_v^*$  will be used throughout this chapter:

$$G_v^* = G_v' (1 + i\eta_v) = G_v' (\cos\theta + i\sin\theta), \quad \theta = \tan^{-1}\eta_v \quad (3.1)$$

The elastic modulus  $G_v'$  and the loss factor  $\eta_v$  are experimentally obtained properties of the viscoelastic material. In using the complex modulus, it is tacitly assumed that the motion is sinusoidal in time. For a stress  $\sigma(t) = \text{Re}\{\sigma^* e^{i\Omega t}\}$  and strain  $\gamma(t) = \text{Re}\{\gamma^* e^{i\Omega t}\}$ , the complex modulus is defined by the ratio of the two amplitudes, i.e.,  $G_v^* = \sigma^*/\gamma^*$ . In this chapter, however, the frequency is assumed to be low enough that all inertia terms may be neglected.

In the analysis, it is assumed that the damping treatment is thin and Poisson effects are negligible. The damping treatment has length  $L$ , and the constraining and viscoelastic layers have thicknesses  $2h_c$  and  $2h_v$  (Figure 3.3). Both the damping treatment and the substrate have unit width. The extensional modulus for the constraining layer,

$E_c$ , is much larger than the viscoelastic extensional modulus. Normal stresses are neglected in the viscoelastic layer, and the viscoelastic shear strain is assumed to be uniform through the thickness of the viscoelastic layer. The constraining layer experiences uniform normal stresses through its thickness. The coordinate system is positioned so  $x = 0$  is at the midpoint of the constraining layer.

If a free body diagram is drawn for a portion of the constraining layer (Figure 3.3), the following equilibrium equation may be formulated:

$$2h_c \frac{d\sigma_c}{dx} = \tau_v \quad (3.2)$$

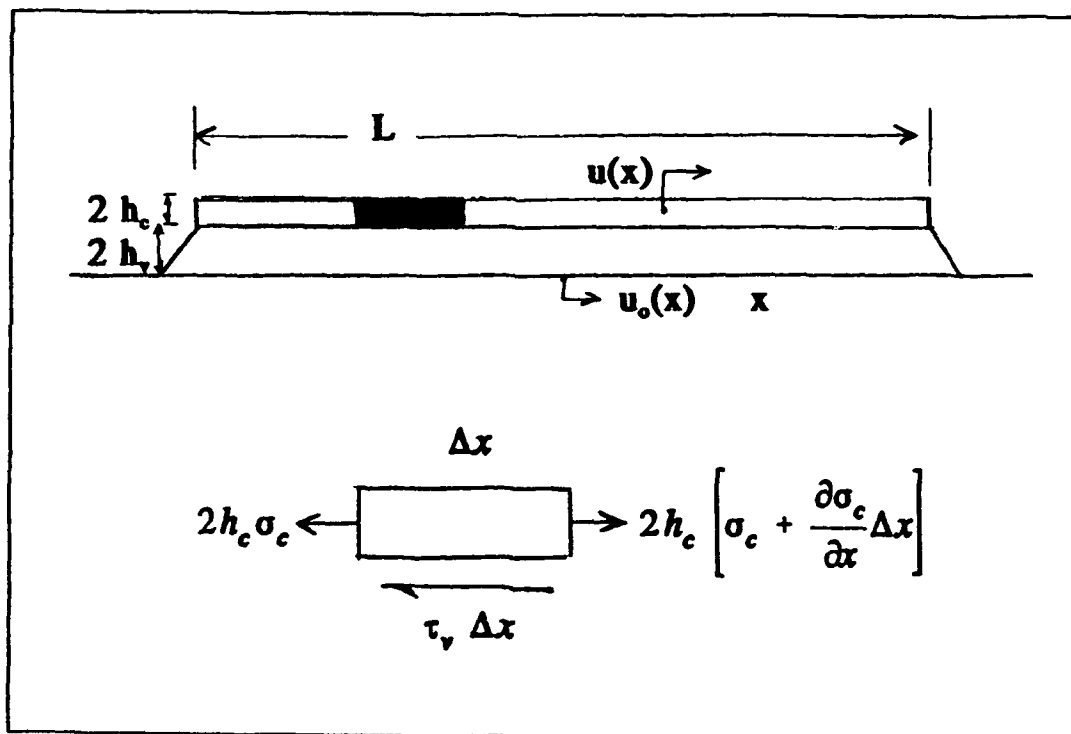


Figure 3.3. Free Body Diagram of Constrained Layer Treatment

Let the constraining layer displacement in the x direction be identified as  $u = u(x)$ , and the substrate displacement in the x direction as  $u_o(x)$ . The extensional stress in the viscoelastic layer may be written in terms of u:

$$\sigma_c = E_c \frac{du}{dx} \quad (3.3)$$

If it is assumed that the viscoelastic shear strain is uniform through the thickness of the layer, the shear stress may be defined as:

$$\tau_v = G_v \gamma_v = G_v \frac{u - u_o(x)}{2h_v} \quad (3.4)$$

The appropriate boundary conditions are developed by noting that the ends of the constraining layer must be free of stress. By substituting Equations (3.2) and (3.3) into Equation (3.4) and substituting in the complex form of the shear modulus, the equilibrium equation and its boundary conditions have the following form:

$$\frac{d^2u}{dx^2} - g^* u = -g^* u_o(x), \quad \left. \frac{du}{dx} \right|_{s=\pm \frac{l}{2}} = 0 \quad (3.5)$$

where

$$g^* = \frac{G_v^*}{(2h_c)(2h_v)E_c} = g (\cos\theta + i \sin\theta), \quad g = \frac{G_v}{(2h_c)(2h_v)E_c}$$

### *Optimal Length Analysis of Plunkett and Lee: Uniform Substrate Strain*

Plunkett and Lee analyzed Equation (3.5) for the case where the substrate displacement has the form  $u_0(x) = \epsilon_0 x$ , where  $\epsilon_0$  is the uniform extensional strain in the substrate. With these assumptions, the solution to the equation and boundary conditions becomes:

$$u = \epsilon_0 \left[ x - \frac{\sinh(\sqrt{g^*}x)}{\sqrt{g^*} \cosh\left(\frac{\sqrt{g^*}L}{2}\right)} \right] \quad (3.7)$$

By substituting the solution into Equation (3.4), the viscoelastic shear strain becomes:

$$\gamma^* = \frac{u - u_0(x)}{2h_v} = \left[ \frac{-\epsilon_0 \sinh(\sqrt{g^*}x)}{2h_v \sqrt{g^*} \cosh\left(\frac{\sqrt{g^*}L}{2}\right)} \right] \quad (3.8)$$

To provide a measure of the effectiveness of the damping treatment, Plunkett and Lee defined a non-dimensional loss coefficient proportional to the system loss factor. Their loss coefficient is equal to the energy dissipated over one cycle of vibration in the entire strip, divided by a nominal energy term. The nominal energy term is equal to the strain energy that would exist in the constraining layer if the constraining layer was in a state of uniform strain of magnitude  $\epsilon_0$ :

$$W_{nominal} = \frac{1}{2} \epsilon_0^2 (2h_c) E_c L_c \quad (3.9)$$

Consider the energy dissipated over one cycle of vibration in an element of viscoelastic material with complex modulus  $G_v^* = G_v(\cos\theta + i \sin\theta)$ . Let the shear strain  $\gamma^*$  and the strain rate  $\dot{\gamma}^*$  be represented by the following expressions:

$$\begin{aligned}\gamma^* &= \gamma_o e^{i\Omega t} = \gamma_o (\cos\Omega t + i \sin\Omega t) \\ \dot{\gamma}^* &= \frac{\partial \gamma^*}{\partial t} = \Omega \gamma_o (-\sin\Omega t + i \cos\Omega t)\end{aligned}\tag{3.10}$$

Use has been made of the fact that a complex magnitude of strain  $\gamma^*$  can be replaced by its real magnitude  $\gamma_o$  through redefinition of the origin of time. The stress in the material resulting from a strain  $\gamma^*$  becomes:

$$\begin{aligned}\sigma^* &= G_v \gamma_o [\cos\theta \cos\Omega t - \sin\theta \sin\Omega t \\ &\quad + i (\cos\theta \sin\Omega t + \sin\theta \cos\Omega t)]\end{aligned}\tag{3.11}$$

The energy dissipated per unit volume is the real part of the stress multiplied by the real part of the strain rate  $\dot{\gamma}$  integrated over the period of the vibration:

$$\Delta w_o = \int_t^{t+\frac{2\pi}{\Omega}} \text{Re}[\sigma^*] \text{Re}[\dot{\gamma}^*] dt = \pi G_v \sin\theta \gamma_o^2\tag{3.12}$$

Plunkett and Lee used an expression similar to Equation 3.12 integrated over the volume of the viscoelastic layer to define the total energy dissipated in the damping treatment (assuming the strip has unit width):

$$\Delta W = \pi G_v(2h_v) \sin\theta \int_{-\frac{L}{2}}^{\frac{L}{2}} |\gamma'|^2 dx \quad (3.13)$$

By calculating  $\Delta W$ , applying various trigonometric identities, then dividing  $\Delta W$  by the nominal energy term in Equation (3.9), Plunkett and Lee presented the following form for their loss coefficient (73:153):

$$\frac{\Delta W}{W_{nominal}} = \frac{4 \pi}{\sqrt{g} L} \left[ \frac{\sinh(A) \sin(\frac{\theta}{2}) - \sin(B) \cos(\frac{\theta}{2})}{\cosh(A) + \cos(B)} \right] \quad (3.14)$$

$$A = \sqrt{g} L \cos(\frac{\theta}{2}), \quad B = \sqrt{g} L \sin(\frac{\theta}{2})$$

Equation (3.14) will be shown to be a special case of the linearly varying strain problem that will be derived in the next section. It should be noted that the system loss coefficient appears in this relatively simple form because of the nominal energy chosen. Equation (3.14) does not produce an actual system loss factor, which is defined as the energy dissipated over one radian of a cycle of vibration divided by the maximum strain energy,  $U$ , stored in the system. The system loss factor would have the form  $\Delta W/(2\pi U)$ . The strain energy of the substrate is not readily defined because the substrate is considered arbitrarily large. The use of the nominal strain energy in Equation (3.14) produces a loss coefficient that is independent of the substrate characteristics, yet can be used to obtain the true loss factor once the strain energy of the substrate is defined.

The loss coefficient defined in Equation (3.14) is a function of only two parameters: the viscoelastic loss modulus  $\theta = \tan^{-1}(\eta_v)$  and the non-dimensional stiffness

parameter  $\sqrt{g} L$ . When Plunkett and Lee plotted the loss coefficient as a function of  $\sqrt{g}L$  with  $\eta_v$  held fixed, they noted that the function was maximized for a value of  $\sqrt{g}L$  near 3.28, regardless of the choice of  $\eta_v$ . This relation identifies an optimal length for the strip if the material properties and thicknesses of the damping layers (and therefore  $g$ ) are specified:

$$L_{optimal} = \frac{3.28}{\sqrt{g}} \quad (3.15)$$

Because of its simplicity, this result has been widely applied in the design of damping treatments for cases which do not reflect the conditions in which the result was derived.

#### *Extension of the Plunkett and Lee Result: Linearly Varying Substrate Strain*

In this section, the Plunkett and Lee analysis is extended to consider a damping strip on a substrate with linearly varying strain. This extension of the existing analysis allows conclusions to be drawn about the optimal length of constrained layer damping treatments for a broader class of problems.

A substrate with linearly varying strain will have a quadratic surface displacement.

If  $u_0(x) = 1/2 ax^2+bx+c$ , Equation (3.5) will have the following form:

$$\frac{d^2u}{dx^2} - g \cdot u = -g \cdot \left[ \frac{1}{2} ax^2 + bx + c \right], \quad \left. \frac{du}{dx} \right|_{x=\pm \frac{L}{2}} = 0 \quad (3.16)$$

This problem reduces to the case considered by Plunkett and Lee when  $b = \epsilon_0$  and  $a =$

$c = 0$ . The solution to the equation has the following form:

$$u = \frac{1}{2}ax^2 + bx + c + \frac{a}{g^*} + P \cosh\sqrt{g^*}x + Q \sinh\sqrt{g^*}x \quad (3.17)$$

where

$$P = \frac{-aL}{2\sqrt{g^*} \sinh(\frac{\sqrt{g^*}L}{2})}, \quad Q = \frac{-b}{\sqrt{g^*} \cosh(\frac{\sqrt{g^*}L}{2})} \quad (3.18)$$

The solution for  $u$  may be used to define the viscoelastic shear strain:

$$\gamma^* = \frac{u - u_0(x)}{2h_v} = \frac{1}{2h_v} \left[ \frac{a}{g^*} - \frac{aL \cosh\sqrt{g^*}x}{2\sqrt{g^*} \sinh(\frac{\sqrt{g^*}L}{2})} - \frac{b \sinh\sqrt{g^*}x}{\sqrt{g^*} \cosh(\frac{\sqrt{g^*}L}{2})} \right] \quad (3.19)$$

To simplify the expression for viscoelastic shear strain, define the non-dimensional parameters  $C_1^* = \sqrt{g^*}L$  and  $C_2 = aL/b$ . From the definition of  $g^*$  and the definition of the root of a complex number (89:10), the complex parameter  $C_1^*$  may be written as  $C_1^* = C_1 (\cos(\theta/2) + i \sin(\theta/2))$ , where  $C_1 = \sqrt{g}L$ . When these terms are substituted into Equation (3.19), it can be written in the following form:

$$\gamma^* = \frac{bL}{2h_v} \left[ \frac{C_2}{C_1^{*2}} - \frac{C_2 \cosh\sqrt{g^*}x}{2C_1^* \sinh(\frac{C_1^*}{2})} - \frac{\sinh\sqrt{g^*}x}{C_1^* \cosh(\frac{C_1^*}{2})} \right] \quad (3.20)$$

A loss coefficient similar in nature to that defined by Plunkett and Lee may be calculated. Define a loss coefficient  $H$  (capital eta) to be equal to the energy dissipated

over one cycle of the viscoelastic layer divided by  $2\pi U_{nominal}$ , where the nominal energy equals the total strain energy that would exist in the constraining layer if its strain were equal to the substrate strain below it:

$$U_{nominal} = \frac{1}{2} \int E_c (ax+b)^2 dVol = \frac{1}{2} E_c (2h_c) b^2 L \left[ 1 + \frac{1}{12} \left( \frac{aL}{b} \right)^2 \right] \quad (3.21)$$

The loss coefficient H has the following form:

$$\begin{aligned} H &= \frac{\Delta W}{2\pi U_{nominal}} = \frac{G_v (2h_v) \sin\theta \int |\gamma^*|^2 dx}{E_c (2h_c) b^2 L \left[ 1 + \frac{1}{12} \left( \frac{aL}{b} \right)^2 \right]} \\ &= \frac{C_1^2 \sin\theta}{\left( 1 + \frac{1}{12} C_2^2 \right) L} \left[ \int_{-\frac{1}{2}}^{\frac{1}{2}} \left| A_1^* - A_2^* \cosh\sqrt{g^*} x - A_3^* \sinh\sqrt{g^*} x \right|^2 dx \right] \end{aligned} \quad (3.22)$$

where

$$A_1^* = \frac{C_2}{C_1^{*2}}, \quad A_2^* = \frac{C_2}{2C_1^* \sinh\left(\frac{1}{2}C_1^*\right)}, \quad A_3^* = \frac{1}{C_1^* \cosh\left(\frac{1}{2}C_1^*\right)} \quad (3.23)$$

Some manipulation of the integrand in Equation (3.22) is desirable before integration. In this dissertation, an overline identifies the conjugate of a complex number, and  $\text{Re}[z^*]$  and  $\text{Im}[z^*]$  identify the real and imaginary parts of the complex number  $z^*$ . Consider the following properties of complex numbers:

$$|z^*|^2 = z^* \overline{z^*} \quad (3.24)$$

$$\overline{x+y} = \overline{x} + \overline{y}, \quad \overline{xy} = \overline{x} \overline{y}, \quad \overline{\left(\frac{x}{y}\right)} = \frac{\overline{x}}{\overline{y}} \quad (3.25)$$

$$x \overline{y} + \overline{x} y = 2 \operatorname{Re}[x \overline{y}] = 2 \operatorname{Re}[\overline{x} y] \quad (3.26)$$

$$\sinh(a \pm ib) = \sinh(a) \cos(b) \pm i \cosh(a) \sin(b) \quad (3.27)$$

$$\cosh(a \pm ib) = \cosh(a) \cos(b) \pm i \sinh(a) \sin(b)$$

By using Equations (3.24)-(3.27), the integrand in Equation (3.22) can be written in the following form:

$$\begin{aligned} & \left| A_1 - A_2 \cosh \sqrt{g} x - A_3 \sinh \sqrt{g} x \right|^2 \\ &= |A_1|^2 + |A_2|^2 |\cosh \sqrt{g} x|^2 + |A_3|^2 |\sinh \sqrt{g} x|^2 - 2 \operatorname{Re}[A_1 \overline{A_2} \cosh \sqrt{g} x] \\ & \quad - 2 \operatorname{Re}[A_1 \overline{A_3} \sinh \sqrt{g} x] + 2 \operatorname{Re}[A_2 \overline{A_3} \cosh \sqrt{g} x \overline{\sinh \sqrt{g} x}] \end{aligned} \quad (3.28)$$

The last two terms in Equation (3.28) are odd functions in  $x$ , and their integrals over the strip length are zero. The loss coefficient may therefore be written as the sum of four integrals:

$$H = \frac{C_1^2 \sin \theta}{1 + \frac{1}{12} C_2^2} [I_1 + I_2 + I_3 + I_4] \quad (3.29)$$

where

$$\begin{aligned}
I_1 &= |A_1^*|^2 \\
I_2 &= |A_2^*|^2 \frac{1}{L} \int_{-\frac{L}{2}}^{\frac{L}{2}} |\cosh\sqrt{g^*}x|^2 dx \\
I_3 &= |A_3^*|^2 \frac{1}{L} \int_{-\frac{L}{2}}^{\frac{L}{2}} |\sinh\sqrt{g^*}x|^2 dx \\
I_4 &= -\frac{2}{L} \int_{-\frac{L}{2}}^{\frac{L}{2}} \text{Re} \left[ \overline{A_1^*} A_2^* \cosh\sqrt{g^*}x \right] dx
\end{aligned} \tag{3.30}$$

Define the following relations:

$$\alpha = \sqrt{g} \cos \frac{\theta}{2}, \quad \beta = \sqrt{g} \sin \frac{\theta}{2}, \quad \alpha^2 + \beta^2 = g \tag{3.31}$$

The expression  $\sqrt{g^*}x = \sqrt{gx} [\cos(\theta/2) + i \sin(\theta/2)]$  may be used with the identities in Equation (3.27) to manipulate the integrands listed in Equation (3.30):

$$\begin{aligned}
|\cosh\sqrt{g^*}x|^2 &= \cosh^2(\alpha x) \cos^2(\beta x) + \sinh^2(\alpha x) \sin^2(\beta x) \\
&= \frac{1}{2} [ \cosh(2\alpha x) + \cos(2\beta x) ]
\end{aligned} \tag{3.32}$$

$$\begin{aligned}
|\sinh\sqrt{g^*}x|^2 &= \sinh^2(\alpha x) \cos^2(\beta x) + \cosh^2(\alpha x) \sin^2(\beta x) \\
&= \frac{1}{2} [ \cosh(2\alpha x) - \cos(2\beta x) ]
\end{aligned} \tag{3.33}$$

$$\begin{aligned}
&\text{Re} \left[ \overline{A_1^*} A_2^* \cosh\sqrt{g^*}x \right] \\
&= \text{Re} \left[ \overline{A_1^*} A_2^* \right] \text{Re} [\cosh\sqrt{g^*}x] - \text{Im} \left[ \overline{A_1^*} A_2^* \right] \text{Im} [\cosh\sqrt{g^*}x] \\
&= \text{Re} \left[ \overline{A_1^*} A_2^* \right] \cosh(\alpha x) \cos(\beta x) - \text{Im} \left[ \overline{A_1^*} A_2^* \right] \sinh(\alpha x) \sin(\beta x)
\end{aligned} \tag{3.34}$$

The integral of Equation (3.32) is:

$$\int_{-\frac{L}{2}}^{\frac{L}{2}} |\cosh\sqrt{g} \cdot x|^2 dx = \frac{\sinh(\alpha L)}{2\alpha} + \frac{\sin(\beta L)}{2\beta} \quad (3.35)$$

The integral of Equation (3.33) becomes:

$$\int_{-\frac{L}{2}}^{\frac{L}{2}} |\sinh\sqrt{g} \cdot x|^2 dx = \frac{\sinh(\alpha L)}{2\alpha} - \frac{\sin(\beta L)}{2\beta} \quad (3.36)$$

The integrals of the components of Equation (3.34) are:

$$\int_{-\frac{L}{2}}^{\frac{L}{2}} \cosh(\alpha x) \cos(\beta x) dx = \frac{2\alpha \sinh(\frac{\alpha L}{2}) \cos(\frac{\beta L}{2}) + 2\beta \cosh(\frac{\alpha L}{2}) \sin(\frac{\beta L}{2})}{\alpha^2 + \beta^2} \quad (3.37)$$

$$\int_{-\frac{L}{2}}^{\frac{L}{2}} \sinh(\alpha x) \sin(\beta x) dx = \frac{2\alpha \cosh(\frac{\alpha L}{2}) \sin(\frac{\beta L}{2}) - 2\beta \sinh(\frac{\alpha L}{2}) \cos(\frac{\beta L}{2})}{\alpha^2 + \beta^2} \quad (3.38)$$

Integrals  $I_1$ ,  $I_2$ ,  $I_3$ , and  $I_4$  can be formed by the proper combination of these integrals with the appropriate coefficients. The square of the moduli of  $A_1^*$ ,  $A_2^*$ , and  $A_3^*$  may be written as functions of  $C_1$ ,  $C_2$ , and  $\theta$ :

$$|A_1^*|^2 = \frac{C_2^2}{C_1^4} \quad (3.39)$$

$$|A_2^*|^2 = \frac{C_2^2}{2C_1^2 [\cosh(\alpha L) - \cos(\beta L)]} \quad (3.40)$$

$$|A_3|^2 = \frac{2}{C_1^2 [\cosh(\alpha L) + \cos(\beta L)]} \quad (3.41)$$

The term  $\bar{A}_1 A_2$  may be written as:

$$\bar{A}_1 A_2 = \frac{C_2^2}{2C_1^3 \left( \cos\left(\frac{\theta}{2}\right) - i \sin\left(\frac{\theta}{2}\right) \right) \sinh\left(\frac{C_1}{2}\right)} = \frac{C_2^2 (Re_{den} - i Im_{den})}{2 C_1^3 (Re_{den}^2 + Im_{den}^2)} \quad (3.42)$$

where

$$\begin{aligned} Re_{den} &= Re \left[ \left( \cos\left(\frac{\theta}{2}\right) - i \sin\left(\frac{\theta}{2}\right) \right) \sinh\left(\frac{C_1}{2}\right) \right] \\ &= \cos\left(\frac{\theta}{2}\right) \sinh\left(\frac{\alpha L}{2}\right) \cos\left(\frac{\beta L}{2}\right) + \left(\sin\left(\frac{\theta}{2}\right)\right) \cosh\left(\frac{\alpha L}{2}\right) \sin\left(\frac{\beta L}{2}\right) \end{aligned} \quad (3.43)$$

$$\begin{aligned} Im_{den} &= Im \left[ \left( \cos\left(\frac{\theta}{2}\right) - i \sin\left(\frac{\theta}{2}\right) \right) \sinh\left(\frac{C_1}{2}\right) \right] \\ &= \cos\left(\frac{\theta}{2}\right) \cosh\left(\frac{\alpha L}{2}\right) \sin\left(\frac{\beta L}{2}\right) - \sin\left(\frac{\theta}{2}\right) \sinh\left(\frac{\alpha L}{2}\right) \cos\left(\frac{\beta L}{2}\right) \end{aligned} \quad (3.44)$$

With the components of  $I_1$ ,  $I_2$ ,  $I_3$ , and  $I_4$  defined, the loss coefficient  $H$  can be formulated from Equation (3.29). The loss coefficient is a function of  $C_1$ ,  $C_2$ , and  $\theta$  (or  $\eta_v$ , since  $\eta_v = \tan\theta$ ). In the next section, contour plots will be used to show the effect of changes in the three parameters on the loss coefficient.

It can be shown that the loss coefficient of the uniform strain problem developed by Plunkett and Lee is a special case of the development above. The Plunkett and Lee configuration is modelled by setting  $a = c = 0$  and  $b = \epsilon_0$  in the definition of  $u_0(x)$ . If  $a = 0$ , then  $C_2 = 0$ , and  $I_1 = I_2 = I_4 = 0$ . By combining the terms from Equations (3.33) and

(3.41) above, it can be seen that  $I_3$  has the following form:

$$I_3 = |A_3|^2 \frac{1}{L} \int_{-\frac{L}{2}}^{\frac{L}{2}} |\sinh \sqrt{g} x|^2 dx = \frac{\frac{\sinh(\alpha L)}{\cos(\frac{\theta}{2})} - \frac{\sin(\beta L)}{\sin(\frac{\theta}{2})}}{C_1^3 [\cosh(\alpha L) + \cos(\beta L)]} \quad (3.45)$$

There is a relationship between the variables  $\alpha$  and  $\beta$  defined in Equation (3.31) and the variables  $A$  and  $B$  defined in Equation (3.14) that were used by Plunkett and Lee:

$$A = \alpha L = \sqrt{g} L \cos(\frac{\theta}{2}), \quad B = \beta L = \sqrt{g} L \sin(\frac{\theta}{2}) \quad (3.46)$$

By substituting  $A$  and  $B$  into Equation (3.45), replacing  $C_1$  by  $\sqrt{g}L$ , substituting  $I_3$  into Equation (3.29), noting that  $C_2 = 0$ , and invoking some trigonometric identities, the loss coefficient becomes:

$$H = C_1^2 \sin \theta I_3 = \frac{2}{\sqrt{g}L} \frac{\sinh(A) \sin(\frac{\theta}{2}) - \sin(B) \cos(\frac{\theta}{2})}{[\cosh(A) + \cos(B)]} \quad (3.47)$$

The Plunkett and Lee loss coefficient defined in Equation (3.14) is equal to  $2\pi H$ , where the factor of  $2\pi$  is accounted for in the definition of  $H$ . As a result, the Plunkett and Lee result may be considered a special case of the linearly varying strain analysis presented in this section.

The function  $H/\theta$  provides a measure of the ability of a damping treatment to utilize the inherent damping of the viscoelastic material. Figure 3.4 contains a plot of  $H/\theta$  for the uniform strain problem for various values of  $\theta = \tan^{-1}\eta_v$ , where  $H$  is defined

in Equation (3.46). The value of  $\sqrt{gL}$  that provides the maximum loss factor for a given value of  $\theta$  is plotted in Figure 3.5. The value of  $\sqrt{gL}$  is relatively consistent over a large range of  $\eta_v$ , approaching 3.278 as  $\eta_v$  drops to zero, equal to 3.25 at  $\eta_v = 1$ , and dropping to 3.195 for  $\eta_v = 10$ .

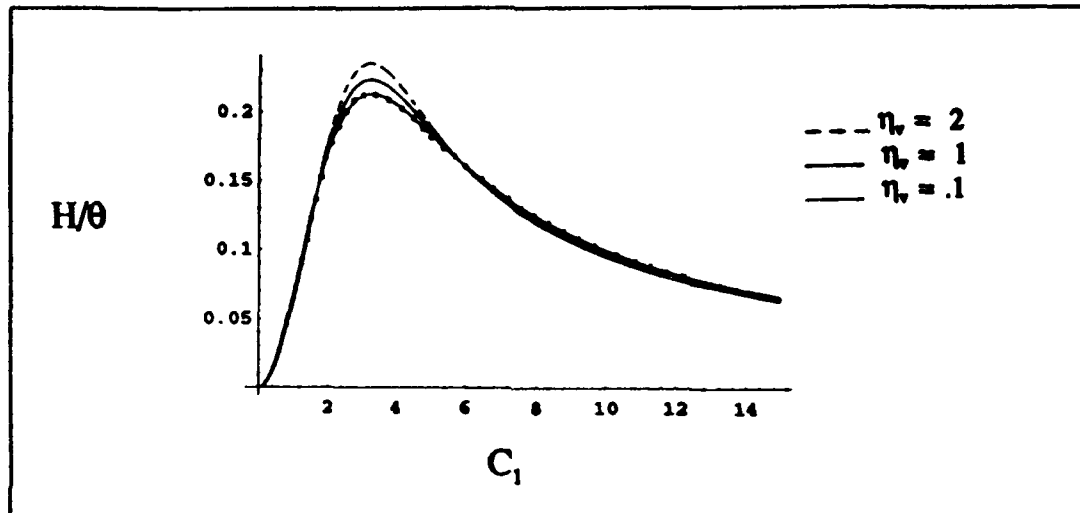


Figure 3.4. Damping Effectiveness as a Function of Stiffness Parameter ( uniform substrate strain )

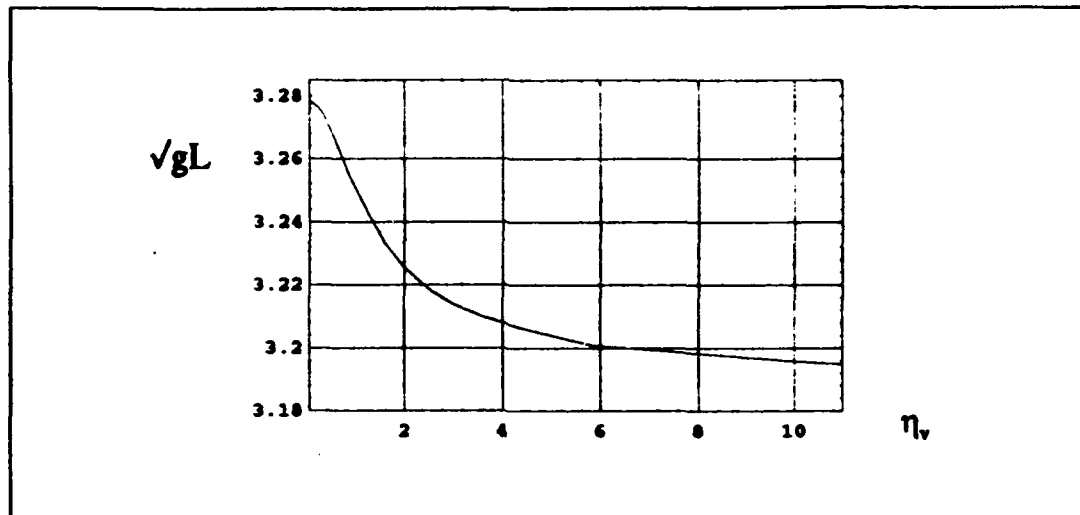


Figure 3.5. Values of  $\sqrt{gL}$  that Maximize Plunkett and Lee Loss Coefficient ( uniform substrate strain )

### *Linearly Varying Strain: Effect of Curvature on Loss Factor*

The analysis described in the previous section may be used to show how the optimal length of the constrained layer damping treatment is affected by the parameter  $C_2$ , a measure of the non-uniformity of the substrate strain. Recall that the substrate displacement  $u_0(x) = 1/2 a x^2 + b x + c$ , where  $x = 0$  at the midpoint of the constraining layer. The substrate strain is equal to  $\epsilon(x) = ax + b$ , and for a segment of length  $L$ , the change in substrate strain across the strip length is  $\Delta\epsilon = aL$ . The nonuniformity parameter  $C_2 = aL/b$  is therefore equal to the change in strain over the strip length divided by the mean value of the strain.  $C_2$  may take on any real value. For a state of uniform strain,  $u_0(x) = bx + c$  and  $C_2 = 0$ . The parameter  $C_2$  increases as the linear component of strain is increased, and if the mean of the substrate strain is zero, then  $C_2$  is infinite.

Surface and contour plots of the function  $H/\theta$  as functions of  $C_1 = \sqrt{gL}$  and  $C_2 = aL/b$  were plotted to evaluate the effects of substrate strain nonuniformity on the effectiveness of the damping treatment. One group of plots has the domain  $C_1 \in [0,15]$  and  $C_2 \in [0,30]$ , while the second set of plots has the domain  $C_1 \in [0,10]$  and  $C_2 \in [0,5]$ . Representative surface plots for both groups are seen in Figures 3.6 and 3.7. Figures 3.8 through 3.13 show contour plots for  $\eta_v = .1$  ( $\theta = .0997$ ),  $\eta_v = .5$  ( $\theta = .463$ ), and  $\eta_v = 1$  ( $\theta = .785$ ) over the two domains.

The contour plots illustrate that the value of  $C_1$  that provides a maximum value of  $H/\theta$  will increase with an increase in  $C_2$ , then approach a limit as  $C_2$  becomes large. The limiting value will vary with the value of the viscoelastic loss factor  $\eta_v$ . If  $C_{1\text{opt}}$  is

the value of  $C_1$  that provides a maximum value of  $H/\theta$ , then the optimal length of the damping strip is equal to  $C_1_{opt}$  divided by the square root of  $g$ . The trends shown in the contour plots indicate that the optimal strip length for a case of linearly varying strain in the substrate is longer than the optimal length for the case of uniform strain.

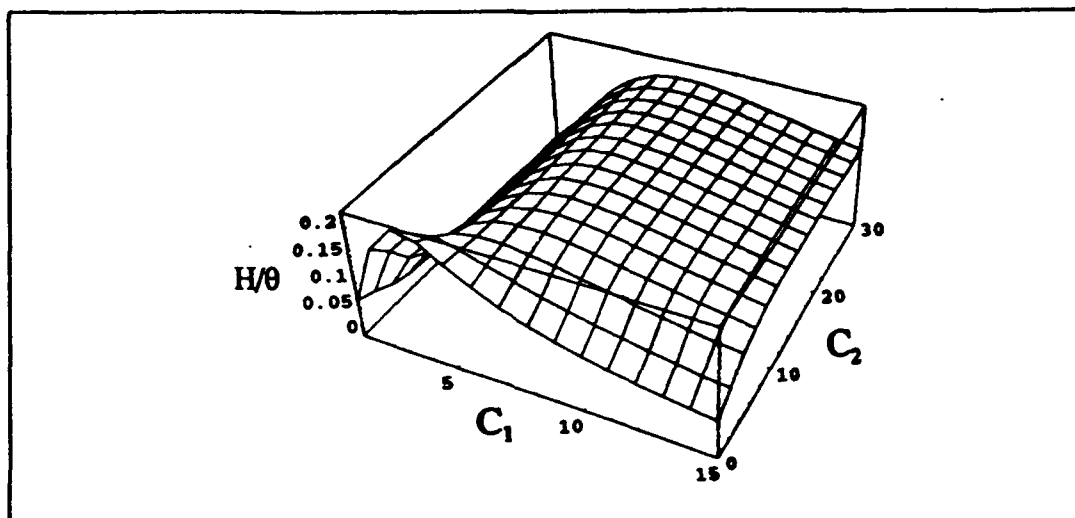


Figure 3.6. Damping Effectiveness as a Function of Stiffness ( $C_1$ ) and Nonuniformity ( $C_2$ ) Measures;  $\eta_v = 1$ ;  $C_1 \in [0,15]$ ,  $C_2 \in [0,30]$

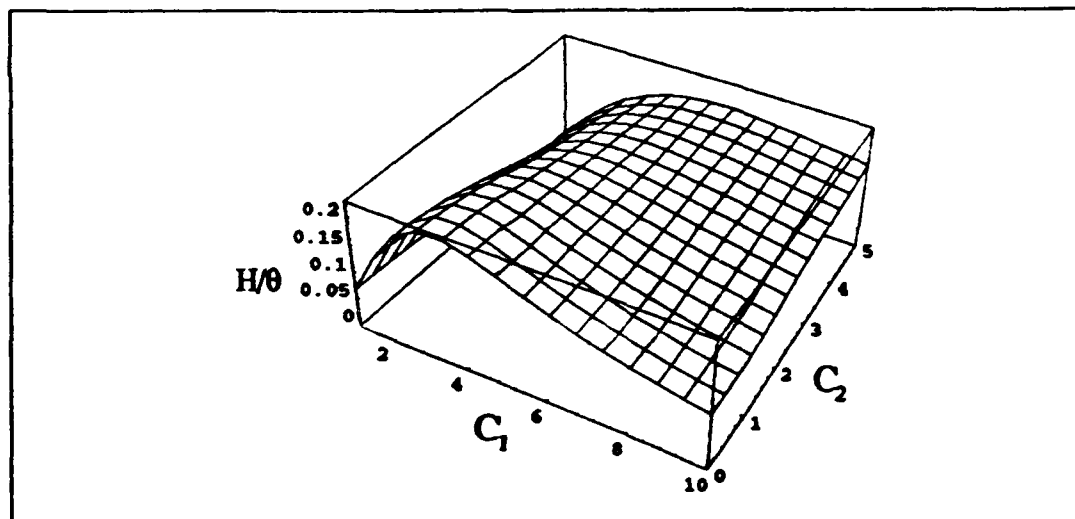


Figure 3.7. Damping Effectiveness as a Function of Stiffness ( $C_1$ ) and Nonuniformity ( $C_2$ ) Measures;  $\eta_v = 1$ ;  $C_1 \in [0,10]$ ,  $C_2 \in [0,5]$

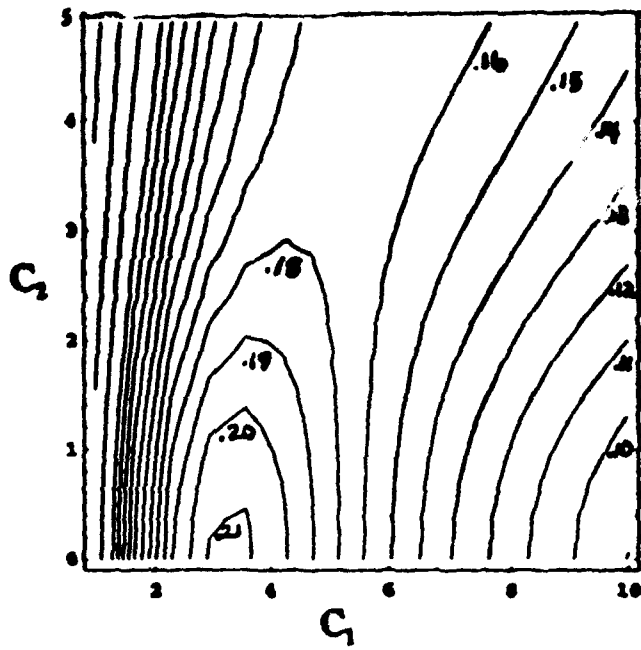


Figure 3.8. Contour Plot of Damping Effectiveness;  
 $\eta_v = .1$  ( $\theta = .0997$ );  $C_1 \in [0,10]$ ,  $C_2 \in [0,5]$

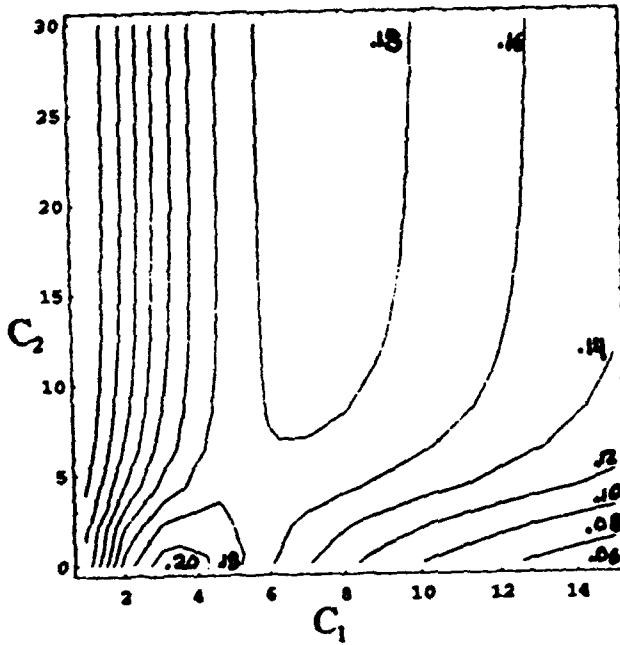


Figure 3.9. Contour Plot of Damping Effectiveness;  
 $\eta_v = .1$  ( $\theta = .0997$ );  $C_1 \in [0,15]$ ,  $C_2 \in [0,30]$

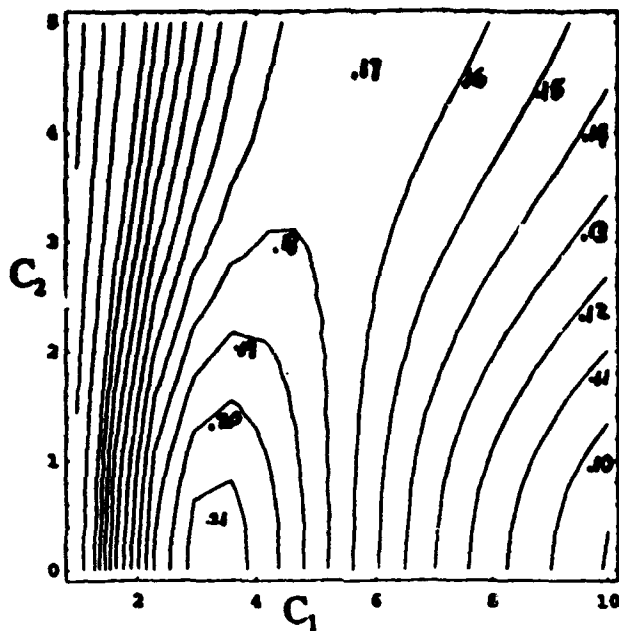


Figure 3.10. Contour Plot of Damping Effectiveness;  
 $\eta_v = .5$  ( $\theta = .464$ );  $C_1 \in [0,10]$ ,  $C_2 \in [0,5]$

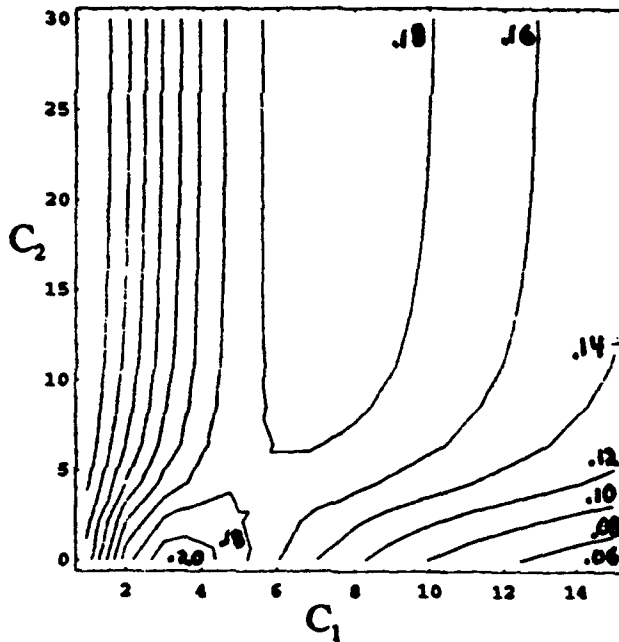


Figure 3.11. Contour Plot of Damping Effectiveness;  
 $\eta_v = .5$  ( $\theta = .464$ );  $C_1 \in [0,15]$ ,  $C_2 \in [0,30]$

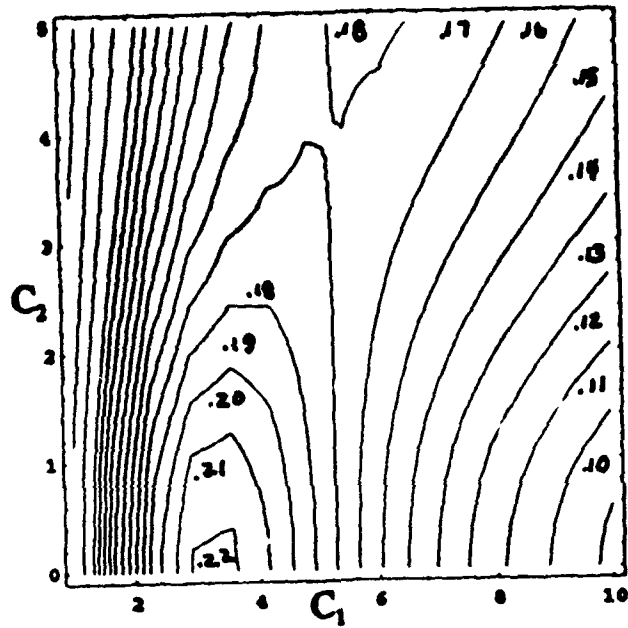


Figure 3.12. Contour Plot of Damping Effectiveness;  
 $\eta_v = 1$  ( $\theta = .785$ );  $C_1 \in [0,10]$ ,  $C_2 \in [0,5]$

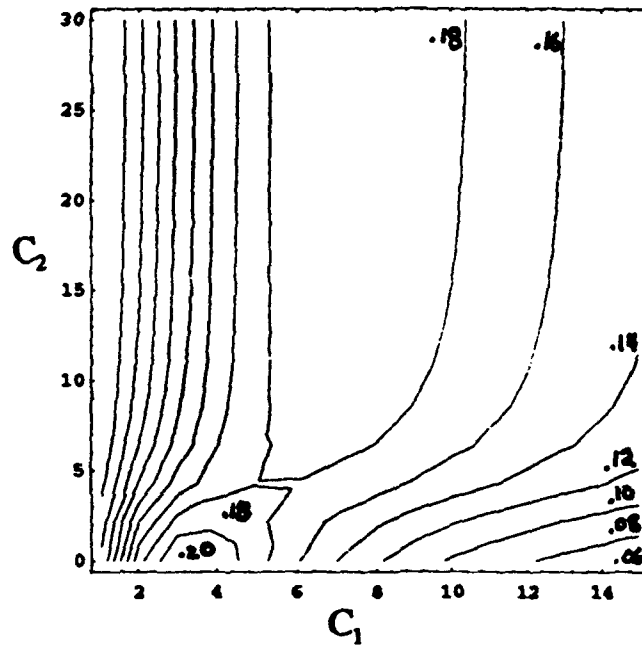


Figure 3.13. Contour Plot of Damping Effectiveness;  
 $\eta_v = 1$  ( $\theta = 785$ );  $C_1 \in [0,15]$ ,  $C_2 \in [0,30]$

Figures 3.14 through 3.16 contain plots that show the dependence of  $H/\theta$  on  $C_1$  for  $C_2 = 0$ ,  $C_2 = 5$ , and  $C_2 = 50$  for various values of  $\eta_v$ . Though the value of  $C_1$  at the maximum value of the function varies with the value of  $C_2$ , it can be seen that the optimal value of  $C_1$  is relatively insensitive to variations of  $\eta_v$  if  $C_2$  is fixed. Table 3.1 provides the values of  $C_1$  that provide a maximum value of the function  $H/\theta$  for specified values of  $C_2$  and  $\eta_v$ . From Table 3.1 it can be seen that the use of the Plunkett and Lee optimal design criteria of  $C_{1\text{ opt}} = 3.28$  provides an error of less than 10% for values of  $\eta_v \leq 1.6$  and  $C_2 \leq 2$ , but the discrepancy increases with the value of  $C_2$ . The Plunkett and Lee analysis underpredicts the optimal length if the change in substrate strain over the length of the damping strip is large compared to the average value of the strain.

*Table 3.1 Values of  $C_1$  that Maximize Loss Coefficient for Specified  $\theta$  and  $C_2$*

$C_2$ :	0	1	2	3	4	5	10	50
$\eta_v$ ( $\theta$ )								
.20 (.20)	3.28	3.38	3.72	4.38	5.24	5.91	7.02	7.41
.50 (.46)	3.27	3.36	3.69	4.34	5.23	5.90	6.98	7.36
1.0 (.78)	3.25	3.34	3.64	4.28	5.20	5.89	6.91	7.26
1.6 (1.0)	3.23	3.31	3.59	4.20	5.19	5.89	6.85	7.16
10 (1.5)	3.20	3.25	3.44	3.93	5.23	5.93	5.89	6.87

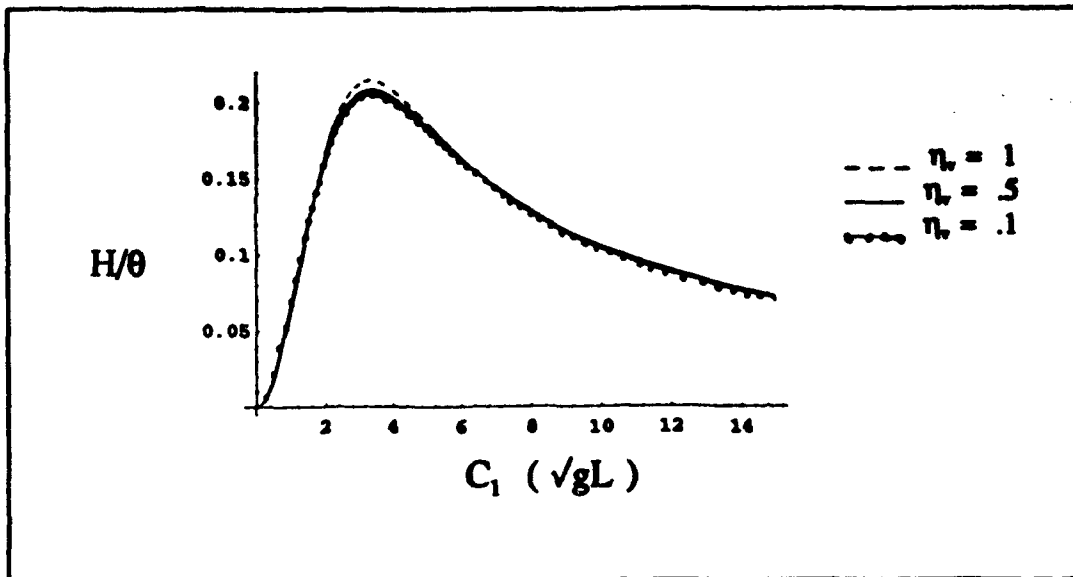


Figure 3.14. Damping Effectiveness as a Function of Stiffness Parameter ( $C_1$ ); ( $C_2 = 1$ )

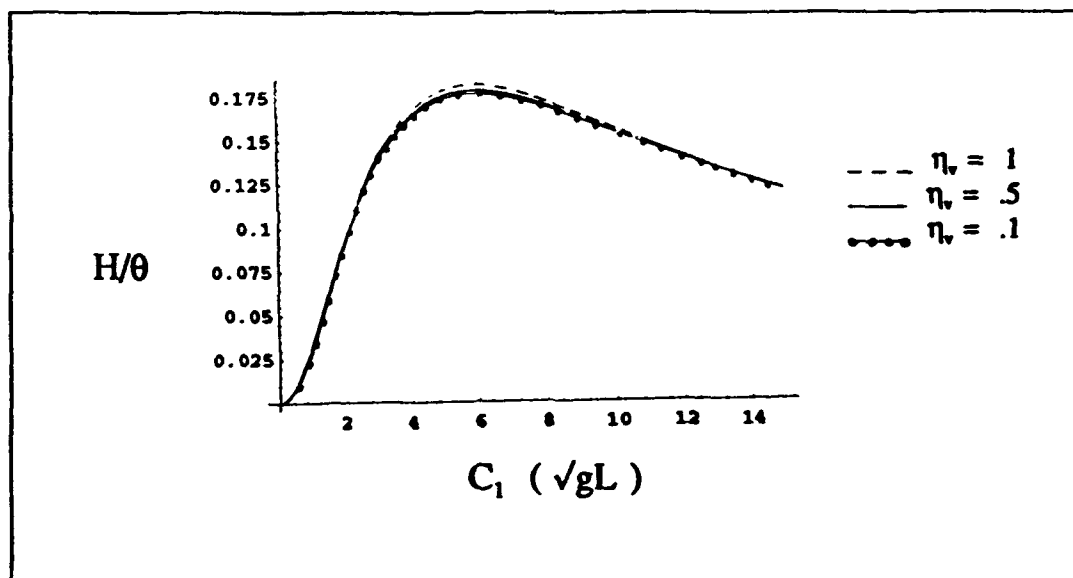


Figure 3.15. Damping Effectiveness as a Function of Stiffness Parameter ( $C_1$ ); ( $C_2 = 5$ )

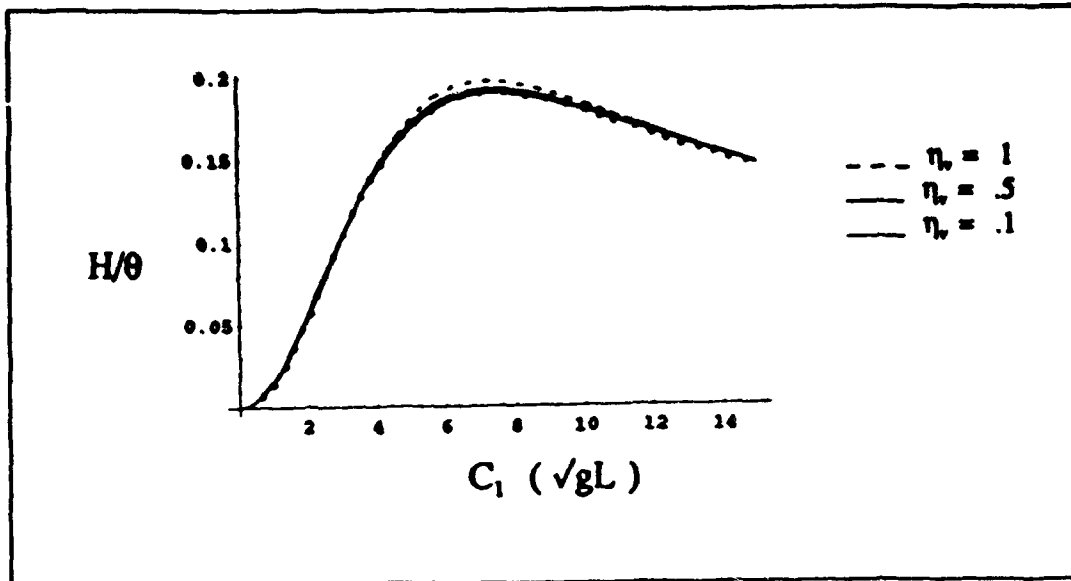


Figure 3.16. Damping Effectiveness as a Function of Stiffness Parameter ( $C_1$ ); ( $C_2 = 50$ )

### Chapter Summary

In this chapter, the impact of length on the effectiveness of a constrained layer damping treatment was discussed, and it was shown that damping effectiveness could be optimized by choosing a damping treatment length appropriate to the geometry and material properties of the viscoelastic layer and constraining layer. The equilibrium equation and boundary conditions were formulated for a constraining layer on a substrate with a specified displacement. The work of Plunkett and Lee, who considered this problem for the special case of uniform strain in the substrate (76:150), is discussed. They showed that a loss coefficient for this configuration depends only on the parameters  $\sqrt{gL}$  and  $\theta$ , where  $\theta = \tan^{-1}\eta_v$ , and  $\sqrt{gL}$  is a stiffness parameter that is a function of the

material properties and thickness of the damping layers. Plunkett and Lee identified an optimal length for the constraining layer strip equal to  $3.28/\sqrt{g}$ . Numerical results given here (Figure 3.5 and Table 3.1) show how the maximum of the loss coefficient varies with changes in  $\eta_v$  for the uniform substrate strain problem. Table 3.1 shows that the optimal length drops slightly with an increase in  $\eta_v$ , but the effect is less than 2.5% for  $\eta_v < 10$ .

In this chapter the Plunkett and Lee analysis was extended for the case of a linearly varying substrate strain of the form  $ax+b$ , where  $a$  and  $b$  are arbitrary constants. The corresponding loss coefficient was shown to be a function of parameters  $\theta$  and  $C_1 = \sqrt{g}L$ , plus an additional parameter that accounts for the degree of non-uniformity of the substrate strain,  $C_2 = aL/b$ . The value of the optimal length of the damping strip is obtained by identifying the value of  $C_1$  that maximizes the loss coefficient for a specified value of  $\theta$  and  $C_2$ , then dividing by  $\sqrt{g}$ . It was shown that an increase in  $C_2$  results in an increase in the value of  $C_1$  that provides optimal damping, but that the shift in optimal length is not rapid. The difference between the optimal length from the linearly varying analysis and the value identified by Plunkett and Lee in the uniform strain problem is less than 10% for values of  $\eta_v \leq 1.6$  and  $C_2 \leq 2$ , but the discrepancy increases with the value of  $C_2$ . As a result, if the strain is "almost uniform", designs may be based on the original result. If the strain has a significant variation across the length of the strip, interpolation functions may be used to get a quadratic curve fit for the substrate displacements, and the parameter  $C_2$  may be calculated.

#### *IV. Developing the Exact Equations of Motion for a Rectangular Beam with Segmented Constraining Layers*

In Chapter 3 it was shown that a constrained layer damping treatment provides better damping if its length is properly chosen. In this chapter, the exact equations of motion are developed for a rectangular beam with a damping treatment applied to both sides of the beam. First, the equations of motion are developed assuming the damping treatment is continuous over the full length of the beam. Equations are then developed for the case where the constraining layer is periodically cut into segments of equal length. The equations are non-dimensionalized and the approach used to solve the equations is described. In Chapter 5, the solutions obtained by using this approach are compared with various approximate methods.

##### *Equations of Motion of a Symmetric Five Layer Beam*

In this section, the equations of motion are developed for a beam damped with continuous constraining layers. The Correspondence Principle is used in the development of the equations of motion. In this approach, equations of motion are formulated and solved as if the viscoelastic material were an elastic material whose shear modulus  $G_v$  were a real number. Once a solution is found, the shear modulus of the viscoelastic material is replaced by a complex number,  $G_v(1+i\eta_v)$  to model the effects of damping in the viscoelastic layer.

The beam that is analyzed has a uniform rectangular cross section and two symmetric strips of constrained layer damping treatment parallel to the beam neutral plane (Figure 4.1). The equations of motion are formulated in terms of the mode shapes  $w$  and  $u$ , which correspond to the transverse displacement of the main beam and the axial displacement of the midplane of the upper constraining layer (Figure 4.2). The mode shapes  $w$  and  $u$  are functions of  $z$ , and their corresponding displacements  $\bar{w}$  and  $\bar{u}$  are functions of  $z$  and time  $t$ .

The  $z$  axis is coincident with the centerline of the beam. Because of the symmetry of the constraining layers, their axial displacements are equal in magnitude and opposite in direction. It is assumed that the damping treatment moves with the same transverse displacement as the main beam, and that the main beam is much stiffer than the constraining layers. Note that there is no axial displacement of the beam midplane due to the equal and opposite loadings that the damping strips exert on the main beam in the axial direction.

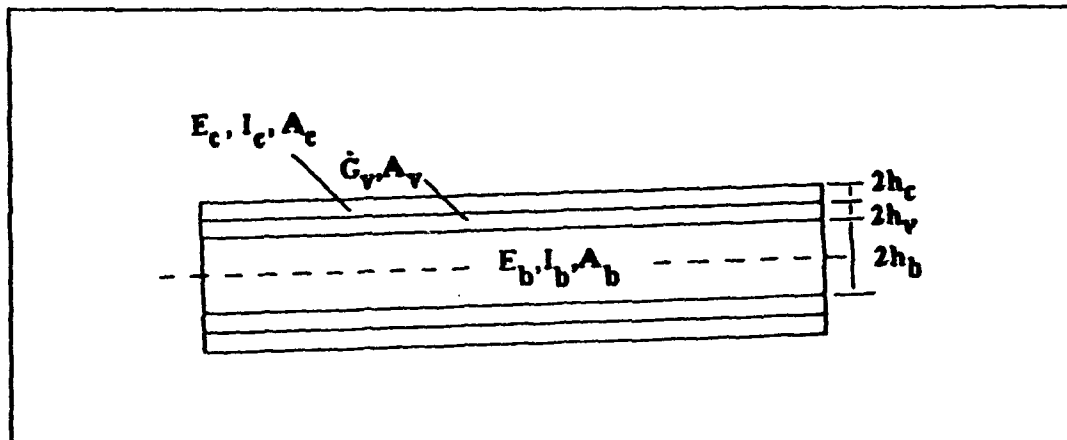


Figure 4.1. Symmetric Five Layer Beam Geometry

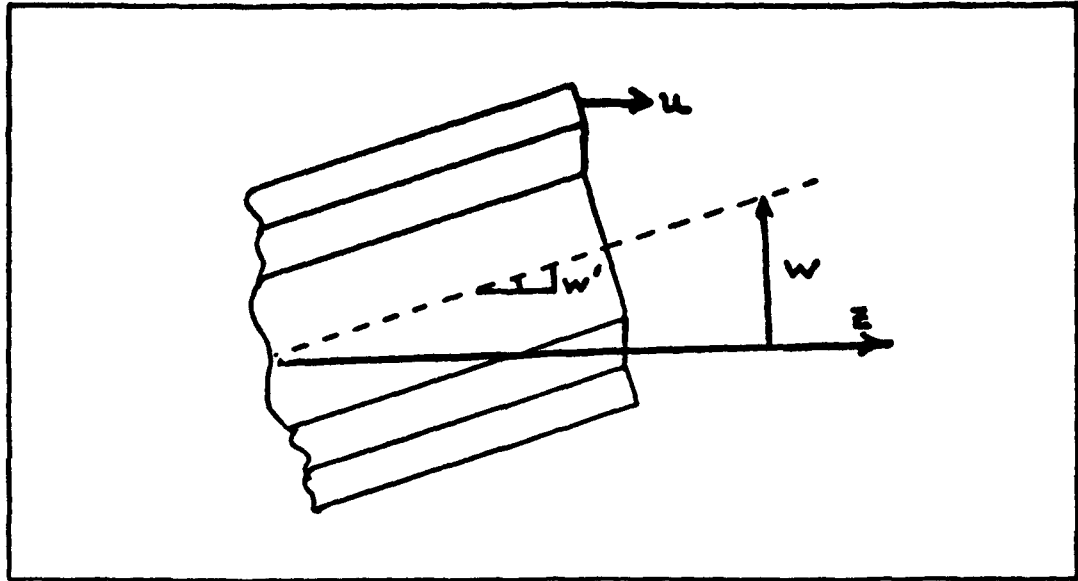


Figure 4.2. Beam Displacements

The equations of motion are developed using Hamilton's principle. The kinetic and potential energy terms included in the formulation are the same as those considered by DiTaranto (17:881) and Mead and Markus (59:163). Rotatory kinetic energy and shear deformation are ignored because the beam length is large compared to beam height. The potential energy due to extension of the viscoelastic layer in both axial and transverse directions is also neglected because the viscoelastic extensional modulus is much smaller than the extensional moduli of the constraining layer and main beam.

The total kinetic energy of the main beam, constraining layers, and viscoelastic layers due to the transverse displacement becomes:

$$T = \frac{1}{2} \int_0^L m_r \left[ \frac{\partial \bar{w}}{\partial t} \right]^2 dz \quad (4.1)$$

where

$$m_t = \rho_b A_b + 2[\rho_c A_c + \rho_v A_v] \quad (4.2)$$

$$A_b = 2h_b b, \quad A_c = 2h_c b, \quad A_v = 2h_v b$$

It is assumed that the time dependence of the displacement  $\bar{w}$  is of the form  $e^{i\Omega t}$ , where  $\Omega$  represents the natural frequency of the system. The variation of the kinetic energy becomes:

$$\delta T = - \int_0^L \Omega^2 m_t w \delta w dz \quad (4.3)$$

where  $w$ , the mode shape, is solely a function of  $z$ .

The strain energy of the main beam and the constraining layers due to bending and its variation have the following form:

$$U_b = \frac{1}{2} \int_0^L D_t w''^2 dz, \quad \delta U_b = \int_0^L D_t w'' \delta w'' dz \quad (4.4)$$

where

$$(\cdot)' = \frac{d(\cdot)}{dz}, \quad D_t = E_b I_b + 2E_c I_c \quad (4.5)$$

After integrating by parts, the variation of the bending strain energy becomes:

$$\delta U_b = \int_0^L D_t w'''' \delta w dz + D_t w'' \delta w' \Big|_0^L - D_t w'''' \delta w \Big|_0^L \quad (4.6)$$

The axial strain in each of the constraining layers is equal to  $u'$ , and the resulting strain energy for the two strips becomes:

$$U_c = \frac{1}{2} \int_0^L 2E_c A_c (u')^2 dz \quad (4.7)$$

After taking the variation of Equation (4.7) and integrating by parts:

$$\delta U_c = - \int_0^L 2E_c A_c u'' \delta u dz + 2E_c A_c u' \delta u \Big|_0^L \quad (4.8)$$

The relative axial motion between the upper and lower surfaces of the main beam and constraining layers creates shear in the viscoelastic layer (Figure 4.3):

$$\gamma_v = \frac{u_A - u_B}{2h_v} + w' = \frac{1}{2h_v} (u + y_o w') \quad (4.9)$$

where

$$u_A = u + h_c w' , \quad u_B = -h_b w' , \quad y_o = h_b + 2h_v + h_c \quad (4.10)$$

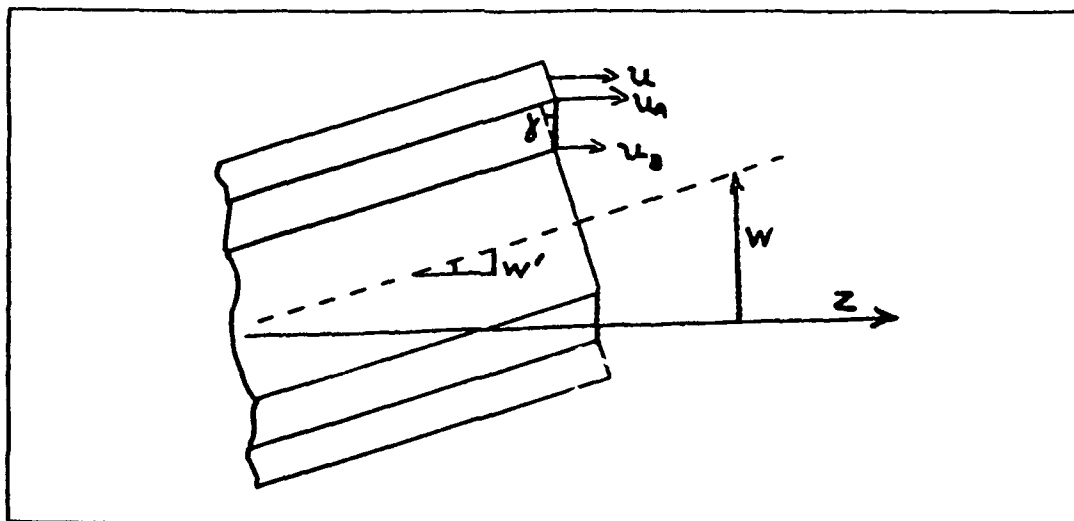


Figure 4.3. Viscoelastic Shear Strain

The potential energy of the two viscoelastic layers becomes:

$$U_v = \frac{1}{2} \int_0^L \frac{2G_v A_v}{(2h_v)^2} [u + y_o w']^2 dz \quad (4.11)$$

After integrating by parts, the variation of the viscoelastic potential energy becomes:

$$\begin{aligned} \delta U_v = \int_0^L \frac{2G_v A_v}{(2h_v)^2} \{ (u + y_o w') \delta u - (u' + y_o w'') y_o \delta w \} dz \\ + \frac{2 G_v A_v y_o}{(2h_v)^2} (u + y_o w') \delta w \Big|_0^L \end{aligned} \quad (4.12)$$

Hamilton's principle may be written in the following form for the problem:

$$\begin{aligned} \int_{t_1}^{t_2} [\sum \delta T - \sum \delta U] dt = 0 \\ = \int_{t_1}^{t_2} \int_0^L \{ [ \dots ] \delta u + [ \dots ] \delta w \} dz dt \\ + \int_{t_1}^{t_2} \{ [ \dots ] \delta u + [ \dots ] \delta w + [ \dots ] \delta w' \} \Big|_0^L dt \end{aligned} \quad (4.13)$$

Equation (4.13) consists of a combination of terms within an integral over  $z$  and a set of boundary terms. The terms used in Equation (4.13) are defined in Equations (4.3), (4.6), (4.8), and (4.12).

By setting the arguments of  $\delta w$  and  $\delta u$  within the integral over  $z$  to zero, and dividing each by  $D_i$  and  $2 E_c A_c$  respectively, the equations of motion are identified:

$$w'''' - \frac{2 G_v A_v y_o}{(2h_v)^2 D_t} [u' + y_o w''] - \Omega^2 \frac{m_t}{D_t} w = 0 \quad (4.14)$$

$$u'' - g u = g y_o w' \quad (4.15)$$

where

$$g = \frac{G_v}{E_c 2h_v 2h_c}, \quad y_o = h_b + 2h_v + h_c \quad (4.16)$$

$$D_t = E_b I_b + 2E_c I_c, \quad m_t = \rho_b A_b + 2\rho_v A_v + 2\rho_c A_c$$

When the boundary terms are set to zero, the following relations are obtained:

$$\left[ D_t w'''' - \frac{2G_v A_v y_o}{(2h_v)^2} (u' + y_o w'') \right] \delta w \Big|_0^L = 0 \quad (4.17)$$

$$D_t w'' \delta w' \Big|_0^L = 0 \quad (4.18)$$

$$2 E_c A_c u' \delta u \Big|_0^L = 0 \quad (4.19)$$

Equations (4.17) through (4.19) identify boundary conditions that must be satisfied at the free ends of the beam. Equation (4.17) specifies that at the ends of the beam either the total applied shear (i.e., the term in square brackets) must equal zero or the  $w$  displacement must be specified (i.e.,  $\delta w=0$ ). Equation (4.18) specifies that either the applied moment  $D_t w''$  must be zero or that the rotation  $w'$  must be specified. Equation (4.19) specifies that either the extensional stresses at the free ends of the constraining

layers must be zero or that the  $u$  displacements must be specified. The appropriate boundary conditions to use for a given problem will depend on the nature of the constraints at the ends of the beam and constraining layers.

### *Adapting the Equations for Segmented Constraining Layers*

In this section, the equations of motion and the boundary conditions for the continuous damping treatment are modified to represent a configuration with  $M$  damping segments, each with length  $2L_c$ . The effect of segmentation on the equations of motion may be understood by considering the approach used to derive the equations. Both the continuous and the segmented constraining layer configurations have the same general definitions for the strain energy terms at an arbitrary position on the beam. Each energy term for the continuous constraining layer formulation is defined over an integral from  $z=0$  to  $z=L$ . Because  $u$  is not continuous across the cuts in the constraining layer for the segmented configuration, each of the energies in the segmented problem must be defined piecewise over each segment:

$$T, U = \int_0^{2L_c} (\dots) dz + \int_{2L_c}^{4L_c} (\dots) dz + \dots + \int_{2(M-1)L_c}^{2ML_c} (\dots) dz \quad (4.20)$$

When these individual integrals are integrated by parts, the resulting boundary terms are defined at the cuts in each segment:

$$(\dots)|_0^{2L_c} + (\dots)|_{2L_c}^{4L_c} + \dots + (\dots)|_{2(M-1)L_c}^L \quad (4.21)$$

When Hamilton's principle is applied, the results are in the following form:

$$\begin{aligned}
 & \sum [\delta T - \delta U] = 0 \\
 & = \int_0^{2L_c} [(\dots)\delta u_1 + (\dots)\delta w_1] dz + \int_{2L_c}^{4L_c} [(\dots)\delta u_2 + (\dots)\delta w_2] dz + \\
 & \quad \dots + \int_{2(M-1)L_c}^{2ML_c} [(\dots)\delta u_M + (\dots)\delta w_M] dz \\
 & + [(\dots)\delta u_1 + (\dots)\delta w_1 + (\dots)\delta w_1'] \Big|_0^{2L_c} + \dots + [(\dots)\delta u_M + (\dots)\delta w_M + (\dots)\delta w_M'] \Big|_{2(M-1)L_c}^{2ML_c}
 \end{aligned} \tag{4.22}$$

To identify values of  $u$  and  $w$  over the "mth segment", the subscript  $m$  is used. When the coefficients of the  $\delta u_m$  and  $\delta w_m$  terms within the integral are set equal to zero, coupled differential equations are generated for each of the  $M$  segments. The differential equations defined over the  $m$ th segment are identical to those for the unsegmented configuration:

$$w_m'''' - \frac{2 G_v A_v y_o}{(2h_v)^2 D_t} [u_m' + y_o w_m''] - \Omega^2 \frac{m_t}{D_t} w_m = 0 \tag{4.23}$$

$$u_m'' - g u_m = g y_o w_m' \tag{4.24}$$

When the boundary terms associated with  $\delta u_m$  are set equal to zero, boundary conditions are obtained that specify that both ends of the  $m$ th constraining layer segment must be free of extensional stresses:

$$E_c A_c u_m' \Big|_{2(m-1)L_c} = 0, \quad E_c A_c u_m' \Big|_{2mL_c} = 0 \tag{4.25}$$

Continuity conditions specify that the beam must have a single displacement  $w$  and slope

$w'$  at each cut in the constraining layer:

$$w_m \Big|_{z=2mL_c} = w_{m+1} \Big|_{z=2mL_c}, \quad w'_m \Big|_{z=2mL_c} = w'_{m+1} \Big|_{z=2mL_c} \quad (4.26)$$

Finally, the boundary terms that contain  $\delta w'_m$  and  $\delta w_m$  must be addressed.

Consider the form of the  $\delta w_m$  terms from Hamilton's Principle:

$$(\dots) \delta w_1 \Big|_0^{2L_c} + (\dots) \delta w_2 \Big|_{2L_c}^{4L_c} + \dots + (\dots) \delta w_M \Big|_{2(M-1)L_c}^L = 0 \quad (4.27)$$

This condition is satisfied if the terms at  $z=0$  and  $z=L$  are set equal to zero and if the terms at the inter-segment boundaries are set equal to each other:

$$(\dots) \delta w_1 \Big|_0 = 0, \quad (\dots) \delta w_M \Big|_L = 0 \quad (4.28)$$

$$(\dots) \delta w_1 \Big|_{2L_c} = (\dots) \delta w_2 \Big|_{2L_c}, \quad (\dots) \delta w_2 \Big|_{4L_c} = (\dots) \delta w_3 \Big|_{4L_c}, \quad \dots$$

Since  $\delta w_m$  and  $\delta w_{m+1}$  must have the same value at the same point, the inter-segment boundary conditions may be satisfied by setting their arguments equal to each other. The same approach can be used for the boundary conditions that contain  $\delta w'_m$ . The inter-segment boundary terms from Hamilton's Principle containing  $\delta w'_m$  and  $\delta w_m$  yield continuity conditions for total moment and shear at the segment boundaries:

$$D_t w''_m \Big|_{z=2mL_c} = D_t w''_{m+1} \Big|_{z=2mL_c} \quad (4.29)$$

$$\left[ D_t w_m''' - \frac{2G_v A_c y_o}{(2h_v)^2} (u_m + y_o w_m') \right] \Big|_{z=2mL_c} = \left[ D_t w_{m+1}''' - \frac{2G_v A_c y_o}{(2h_v)^2} (u_{m+1} + y_o w_{m+1}') \right] \Big|_{z=2mL_c} \quad (4.30)$$

The remaining boundary conditions at  $z=0$  and  $z=L$  are applied to the solutions of segment 1 and M respectively:

$$\left[ D_t w_1''' - \frac{2G_v A_c y_o}{(2h_v)^2} (u_1 + y_o w_1') \right] \delta w_1 \Big|_{z=0} = 0 \quad (4.31)$$

$$\left[ D_t w_M''' - \frac{2G_v A_c y_o}{(2h_v)^2} (u_M + y_o w_M') \right] \delta w_M \Big|_{z=L} = 0 \quad (4.32)$$

$$D_t w_1'' \delta w_1' \Big|_{z=0} = 0, \quad D_t w_M'' \delta w_M' \Big|_{z=L} = 0 \quad (4.33)$$

To summarize, the equations that define a beam with M constraining layer segments consist of M pairs of differential equations identical in form to the coupled equations of the beam with continuous constraining layers. For the segmented problem, there exist a total of 6M boundary and continuity conditions that couple the M pairs of equations together. There are three boundary conditions at each end of the main beam that are identical to the unsegmented problem. There are also six conditions at the internal

segment boundaries that specify that the displacement, slope, shear, and moment of the main beam are continuous across the cut and that  $u'_{m-}$  and  $u'_{m+}$  are equal to zero.

### *Sixth Order Equations of Motion*

For the damped beam with continuous constraining layers, the equations of motion consist of a pair of linear coupled equations in the variable  $w$  and  $u$  (Equations (4.14) and (4.15)). These equations can be combined into a single 6th order equation in  $w$ :

$$w^{(6)} - g(1+Y)w^{(4)} - \frac{\Omega^2 m_t}{D_t}(w'' - gw) = 0 \quad (4.34)$$

where

$$g = \frac{G_v}{(2h_b)(2h_c)E_c}, \quad Y = \frac{2y_o^2 b(2h_c)E_c}{D_t} \quad (4.35)$$

The  $u$  variable may also be eliminated from the boundary conditions. The requirement that the extensional strains are zero at both ends of the constraining layer may be written in the following form:

$$u'|_{z=0,L} = 0 \quad \rightarrow \quad w'''' - gY w'' - \frac{\Omega^2 m_t}{D_t} w \Big|_{z=0,L} = 0 \quad (4.36)$$

The total bending moment  $M_T$  at any position of the beam is proportional to the following expression:

$$M_T = w'''' - g(1+Y)w'' - \frac{\Omega^2 m_t}{D_t} w \quad (4.37)$$

If one of the ends of the main beam is free of applied moment, the expression in Equation (4.37) is set equal to zero at  $z=0$  or  $z=L$ . (If one or both ends of the main beam are restricted from rotation, then  $w'$  is set equal to zero at those positions.) For end conditions where both  $u'$  and the total moment  $M_T$  is zero, Equations (4.36) and Equation (4.37) can be combined to produce the condition  $w''=0$ .

Because rotatory inertia is neglected, moment equilibrium on an element of the beam requires that the total shear force  $V_T$  is equal to the first derivative with respect to  $z$  of the total moment. The total shear force is therefore proportional to the derivative of Equation (4.37):

$$V_T = w^{(5)} - g(1+Y)w''' - \frac{\Omega^2 m_t}{D_t} w' \quad (4.38)$$

As with the total moment, the expression in Equation (4.38) is set equal to zero at  $z=0$  or  $z=L$  if one of the ends of the beam is free of applied shear force. If displacement is restricted at one of the boundaries, then  $z$  is set equal to zero at that position.

It is interesting to note that both the equations and the boundary conditions described above for the symmetric five layer beam have the same form as the "sixth order beam theory" identified by Mead and Markus for an unsegmented three layer beam (59:163), except for slight differences in the constants  $g$  and  $Y$ . The Mead and Markus

expression for  $g$  reduces to the form identified in Equation (4.35) if it is assumed that  $2 h_b E_b \rightarrow \infty$ . Because the balanced loads of the five layer configuration produce no axial elongation of the neutral axis of the main beam, the main beam behaves as if its extensional stiffness is infinitely large, but its bending stiffness is finite. The value of  $Y$  defined in Equation (4.35) is equal to two times the Mead and Markus expression for  $Y$ . The doubling of  $Y$  occurs because  $Y$  provides a measure of the relative stiffness of the constraining layer as compared to the main beam, and the five layer configuration has two constraining layers instead of one.

The same substitution of variables described above can be used for the segmented problem. The sixth order differential equation defined over the  $m$ th segment becomes:

$$w_m^{(6)} - g(1+Y)w_m^{(4)} - \frac{\Omega^2 m_t}{D_t}(w_m'' - gw_m) = 0, \quad m = 1, \dots, M \quad (4.39)$$

The requirement that  $u_m' = 0$  at both ends of each segment generates  $2M$  boundary conditions:

$$w_m'''' - gY w_m'' - \frac{\Omega^2 m_t}{D_t} w_m \Big|_{z=2L_c(m-1)} = 0 \quad (4.40)$$

$$w_m'''' - gY w_m'' - \frac{\Omega^2 m_t}{D_t} w_m \Big|_{2L_c m} = 0 \quad m = 1 \dots M$$

The expressions in Equations (4.37) and (4.38) that are proportional to  $M_T$  and  $V_T$  are used to enforce continuity of moment and shear at the inter-segment boundaries. They

are also set equal to zero at  $z=0$  or  $z=L$  if the beam has a boundary condition that is free of moment or shear. These boundary conditions are described in the next section for the case of a cantilever beam.

*Solving the Equations for the Segmented Damping Treatment:*

To obtain an exact solution for the segmented system of equations, the differential equation must be solved over the length of each segment using the appropriate boundary conditions. In this section, the approach is illustrated for the case of a cantilever beam with  $M$  pairs of identical constraining layer segments with free ends. Each of the damping segments has length  $2 L_c$ .

The  $M$  differential equations defined in Equation (4.39) must be solved over each of the beam segments. The general solution over the  $m$ th segment may be written in the following form:

$$w_m = \sum_{j=1}^6 A_{mj} \exp[p_j z] \quad (4.41)$$

The  $p_j$  eigenvalues are obtained from the roots of the characteristic equation of Equation (4.39). The six distinct eigenvalues are identical for all segments.

The general solution to the equation is substituted into the appropriate boundary and continuity conditions for each segment. The total set of boundary conditions for a beam with  $M$  segments produces a homogeneous matrix equation with  $6 M$  unknown  $A_{mj}$  coefficients. The individual entries of the  $6M \times 6M$  matrix are functions of the  $p_j$

eigenvalues, and the eigenvalues are functions of the unknown natural frequency of the system:

$$\begin{bmatrix} f_{11}[p_j(\Omega)] & f_{12}[p_j(\Omega)] & \cdot & \cdot & \cdot \\ f_{21}[p_j(\Omega)] & f_{22}[p_j(\Omega)] & \cdot & \cdot & \cdot \\ \cdot & \cdot & \cdot & \cdot & \cdot \\ \cdot & \cdot & \cdot & \cdot & \cdot \\ \cdot & \cdot & \cdot & \cdot & f_{6M}[p_j(\Omega)] \end{bmatrix} \begin{Bmatrix} A_{11} \\ A_{12} \\ \cdot \\ \cdot \\ A_{M6} \end{Bmatrix} = \begin{Bmatrix} 0 \\ 0 \\ \cdot \\ \cdot \\ 0 \end{Bmatrix} \quad (4.42)$$

(The form of the individual functions within the matrix will be described later in the chapter.) The natural frequency may be found by setting the determinant of the matrix equal to zero. Once  $\Omega$  is identified for a particular mode, all terms in the boundary condition matrix are specified and the equation may be solved for the  $A_{mj}$  coefficients.

Though this approach is straightforward and often used in structural vibration problems, the implementation for this particular problem is challenging. It will be seen in the next section that the matrix in Equation (4.42) contains a mixture of very large and very small terms that make the use of standard numerical methods difficult. As a result, any configuration that is more complicated than the single segment case is customarily approached with finite element methods.

*Non-Dimensional Variables.* When the main beam is covered with damping segments of equal length, the use of non-dimensional spatial and temporal variables can simplify the problem. If both the variables and the form of the assumed solution are chosen

properly, the magnitudes of the numbers in the boundary condition matrix are smaller. Furthermore, the boundary condition matrix can be assembled from a set of submatrices that have the same form for each segment.

The greatest improvement from non-dimensionalization results from the transformation of the spatial coordinate. The non-dimensional spatial variable zeta ( $\zeta$ ) is defined as  $\zeta = x/(2L_c)$ , where  $2L_c$  is the segment length. With this choice of variable, the boundary conditions are applied at  $\zeta = \{0, 1, 2, \dots, M\}$  for a  $M$  segment case. The variable transformation requires a change in the differential operators used in the equations and boundary conditions:

$$\frac{d(\cdot)}{dx} = \frac{d(\cdot)}{d\zeta} \frac{d\zeta}{dx} = \frac{1}{2L_c} \frac{d(\cdot)}{d\zeta} \tag{4.43}$$

$$\frac{d^n(\cdot)}{dx^n} = \frac{1}{(2L_c)^n} \frac{d^n(\cdot)}{d\zeta^n}$$

Though the time coordinate plays a relatively minor role in this problem because a sinusoidal solution is assumed, a non-dimensional form may be used. The non-dimensional time changes the size of the natural frequency that appears in the characteristic equation, which changes the spacing of the  $p_j$  eigenvalues. The non-dimensional time coordinate tau ( $\tau$ ) is defined by the following expression:

$$\tau = k \Omega_o t, \quad \Omega_o = \sqrt{\frac{D_t}{m_t L^4}} = \sqrt{\frac{D_t}{m_t (2 L_c M)^4}} \quad (4.44)$$

Note that  $\Omega_o$  is a parameter with units of frequency and  $k$  is an arbitrary constant that may be used to vary the spacing of the eigenvalues. The use of non-dimensional time  $\tau$  in the assumed form of the solution generates a scaled frequency  $\Omega_s$ :

$$\exp(i \Omega t) = \exp\left[i \Omega \frac{\tau}{k \Omega_o}\right] = \exp(i \Omega_s \tau) \quad (4.45)$$

where

$$\Omega_s = \frac{\Omega}{k \Omega_o} = \frac{\Omega M^2}{k} (2 L_c)^2 \sqrt{\frac{m_t}{D_t}} \quad (4.46)$$

When written in terms of non-dimensional spatial and temporal variables, the differential equation for the  $m$ th segment has the following form :

$$w_m^{(6)} - g(2 L_c)^2 (1+Y) w_m^{(4)} - \left[\frac{k \Omega_s}{M^2}\right]^2 w_m'' + \left[\frac{k \Omega_s}{M^2}\right]^2 (2 L_c)^2 g w_m = 0 \quad (4.47)$$

The boundary conditions may also be written in terms of the non-dimensional variables. The non-dimensional expressions that are proportional to total moment  $M_T$  and total shear  $V_T$  are:

$$M_T \sim w'''' - g(2L_c)^2(1+Y) w'' - \left[ \frac{k\Omega_s}{M^2} \right]^2 w \quad (4.48)$$

$$V_T \sim w^{(5)} - g(2L_c)^2(1+Y) w''' - \left[ \frac{k\Omega_s}{M^2} \right]^2 w' \quad (4.49)$$

Equations (4.48) and (4.49) are used to enforce continuity of the beam at the inter-segment boundaries. They are also used to identify a beam end condition that is free of applied moment or shear stress. The non-dimensional form of the equation that specifies that  $u'$  must be zero at the free ends of the constraining layer has the following form:

$$w'''' - gY(2L_c)^2 w'' - \left[ \frac{k\Omega_s}{M^2} \right]^2 w = 0 \quad (4.50)$$

Now that the differential equation and the boundary conditions have been identified in their non-dimensional form, the form of the solution can be assumed and the boundary condition matrix can be assembled.

*Form of the Assumed Solution.* A good choice of assumed solution simplifies the assembly of the boundary condition matrix. Recall that the value of  $\zeta$  on the left hand side (LHS) of the  $m$ th segment is  $\zeta=m-1$ , while the value of  $\zeta$  on the right hand side

(RHS) of the segment  $\zeta=m$ . Consider a solution over the  $m$ th segment that has the following form:

$$w_m = \sum_{j=1}^6 A_{j+6(m-1)} \exp[p_j (\zeta - m + 1)] \quad (4.51)$$

Note that the index of the A coefficients range from 1 to  $6M$  in this form of the solution.

At the two end points of the segment, the assumed solution for the  $m$ th segment reduces to a particularly simple form:

$$LHS : \quad w_m = \sum_{j=1}^6 A_{j-6m+1} \quad (4.52)$$

$$RHS : \quad w_m = \sum_{j=1}^6 A_{j-6m+1} \exp(p_j)$$

By substituting Equation (4.51) into the non-dimensionalized differential equation, the following result is obtained:

$$\begin{aligned} & \sum_{j=1}^6 A_{j+6(m-1)} \exp[p_j (\zeta - m + 1)] \\ & \times \left[ p_j^6 - g(2L_c)^2(1+Y) p_j^4 - \left[ \frac{k \Omega_s}{M^2} \right]^2 p_j^2 + \left[ \frac{k \Omega_s}{M^2} \right]^2 (2L_c)^2 g \right] = 0 \end{aligned} \quad (4.53)$$

Because the characteristic equation (the large expression in brackets) is identical for all segments, the same six  $p_j$  eigenvalues are used in the solution for all segments.

*Assembly of the Boundary Condition Matrix.* Now consider the form of the boundary conditions for a beam with cantilever end conditions and  $M$  segments. The fixed root of the beam is located at  $\zeta=0$ , and the boundary conditions may be written as:

$$w_1(\zeta=0) = \sum_{j=1}^6 A_j = 0 \quad (4.54)$$

$$w_1'(\zeta=0) = \sum_{j=1}^6 p_j A_j = 0$$

These may be written in matrix form as  $[BCroot] \{A_1\} = \{0\}$ , defined as:

$$\begin{bmatrix} 1 & 1 & 1 & 1 & 1 & 1 \\ p_1 & p_2 & p_3 & p_4 & p_5 & p_6 \end{bmatrix} \begin{Bmatrix} A_1 \\ A_2 \\ A_3 \\ A_4 \\ A_5 \\ A_6 \end{Bmatrix} = \begin{Bmatrix} 0 \\ 0 \end{Bmatrix} \quad (4.55)$$

At the free end of the cantilever beam,  $\zeta=M$  and both the total moment and shear equal zero. The appropriate boundary conditions can be found by substituting the assumed solution into the expressions for  $M_T$  and  $V_T$  in Equations (4.48) and (4.49), then setting them equal to zero. The equations can be written in matrix form as  $[BCtip]\{A_M\}=\{0\}$ :

$$\begin{bmatrix} \phi_1 & \phi_2 & \phi_3 & \phi_4 & \phi_5 & \phi_6 \\ p_1\phi_1 & p_2\phi_2 & p_3\phi_3 & p_4\phi_4 & p_5\phi_5 & p_6\phi_6 \end{bmatrix} \begin{Bmatrix} A_{6M-5} \\ A_{6M-4} \\ A_{6M-3} \\ A_{6M-2} \\ A_{6M-1} \\ A_{6M} \end{Bmatrix} = \begin{Bmatrix} 0 \\ 0 \end{Bmatrix} \quad (4.56)$$

where

$$\phi_j = \left[ p_j^4 - g(2L_c)^2 (1+\gamma)p_j^2 - \left[ \frac{k\Omega_s}{M^2} \right]^2 \right] \exp(p_j) \quad (4.57)$$

Because both the moment and  $u'$  are zero at the tip for this problem, the moment free boundary condition can be written as  $w'' = 0$ . For this case, the matrix in Equation (4.56) becomes:

$$\begin{bmatrix} p_1^2 e^{p_1} & p_2^2 e^{p_2} & p_3^2 e^{p_3} & p_4^2 e^{p_4} & p_5^2 e^{p_5} & p_6^2 e^{p_6} \\ p_1 \phi_1 & p_2 \phi_2 & p_3 \phi_3 & p_4 \phi_4 & p_5 \phi_5 & p_6 \phi_6 \end{bmatrix} \quad (4.58)$$

For each segment, conditions of continuity must be enforced, as well as the requirement that  $u'=0$ . Consider the position  $\zeta=m$ , which defines the interface between segments  $m$  and  $m+1$ . The expressions defining the continuity of the displacement  $w$ , the slope  $w'$  and the moment  $w''$  have the following form:

$$w_{m \text{ RHS}} = w_{m+1 \text{ LHS}} \quad \rightarrow \quad \sum_{j=1}^6 A_{j+6(m-1)} e^{p_j} = \sum_{j=1}^6 A_{j+6m} \quad (4.59)$$

$$w'_{m \text{ RHS}} = w'_{m+1 \text{ LHS}} \quad \rightarrow \quad \sum_{j=1}^6 p_j A_{j+6(m-1)} e^{p_j} = \sum_{j=1}^6 p_j A_{j+6m} \quad (4.60)$$

$$w''_{m \text{ RHS}} = w''_{m+1 \text{ LHS}} \quad \rightarrow \quad \sum_{j=1}^6 p_j^2 A_{j+6(m-1)} e^{p_j} = \sum_{j=1}^6 p_j^2 A_{j+6m} \quad (4.61)$$

Recall that the expression representing total shear in the beam is :

$$V_T \sim w^{(5)} - g(2L_c)^2(1+Y) w''' - \left[ \frac{k\Omega_s}{M^2} \right]^2 w' \quad (4.62)$$

Shear continuity must be enforced, but because the requirement that  $w'$  must be continuous across the cut has already been imposed in Equation (4.60),  $w'$  and its argument may be dropped when using Equation (4.62) to impose continuity. When the assumed solution is substituted into the remainder of Equation (4.62), the shear continuity boundary condition becomes:

$$\begin{aligned} V_{T_{m \text{ RHS}}} &= V_{T_{m+1 \text{ LHS}}} \quad \rightarrow \\ \sum_{j=1}^6 \left[ p_j^5 - g(2L_c)^2 (1+Y)p_j^3 \right] A_{j+6(m-1)} e^{p_j} & \quad (4.63) \\ &= \sum_{j=1}^6 \left[ p_j^5 - g(2L_c)^2 (1+Y)p_j^3 \right] A_{j+6m} \end{aligned}$$

This may be written in a more compact form as :

$$\sum_{j=1}^6 \Psi_j e^{p_j} A_{j+6(m-1)} = \sum_{j=1}^6 \Psi_j A_{j+6m} \quad (4.64)$$

where

$$\Psi_j = \left[ p_j^5 - g(2L_c)^2 (1+Y)p_j^3 \right] \quad (4.65)$$

The four boundary conditions may be written as  $[Continuity]\{A_m, A_{m+1}\}^T = \{0\}$ :

$$\begin{bmatrix}
 e^{p_1} & e^{p_2} & e^{p_3} & \dots & e^{p_6} & | & -1 & -1 & \dots & -1 \\
 p_1 e^{p_1} & p_2 e^{p_2} & p_3 e^{p_3} & \dots & p_6 e^{p_6} & | & -p_1 & -p_2 & \dots & -p_6 \\
 p_1^2 e^{p_1} & p_2^2 e^{p_2} & p_3^2 e^{p_3} & \dots & p_6^2 e^{p_6} & | & -p_1^2 & -p_2^2 & \dots & -p_6^2 \\
 \psi_1 e^{p_1} & \psi_2 e^{p_2} & \psi_3 e^{p_3} & \dots & \psi_6 e^{p_6} & | & -\psi_1 & -\psi_2 & \dots & -\psi_6
 \end{bmatrix}
 \begin{bmatrix}
 A_{6m-5} \\
 A_{6m-4} \\
 A_{6m-3} \\
 \cdot \\
 A_{6m} \\
 \dots \\
 A_{6m+1} \\
 A_{6m+2} \\
 \cdot \\
 \cdot \\
 \cdot \\
 A_{6m+6}
 \end{bmatrix}
 =
 \begin{bmatrix}
 0 \\
 0 \\
 0 \\
 0
 \end{bmatrix}
 \quad (4.66)$$

Note that the matrix portion of this condition contains no dependence on  $m$ , the segment being considered.

Now consider the equation that specifies that  $u'=0$  at the cut ends of the constraining layers. By substituting the assumed solution into Equation (4.50), the following matrix equation  $[u \text{ prime}] \{A_m\} = \{0\}$  may be found for the  $m$ th segment:

$$\begin{bmatrix}
 \chi_1 & \chi_2 & \chi_3 & \chi_4 & \chi_5 & \chi_6 \\
 e^{p_1} \chi_1 & e^{p_2} \chi_2 & e^{p_3} \chi_3 & e^{p_4} \chi_4 & e^{p_5} \chi_5 & e^{p_6} \chi_6
 \end{bmatrix}
 \begin{bmatrix}
 A_{6m-5} \\
 A_{6m-4} \\
 A_{6m-3} \\
 A_{6m-2} \\
 A_{6m-1} \\
 A_{6m}
 \end{bmatrix}
 =
 \begin{bmatrix}
 0 \\
 0
 \end{bmatrix}
 \quad (4.67)$$

where

$$\chi_j = \left[ p_j^4 - gY(2Lc)^2 p_j^2 - \left[ \frac{k\Omega_s}{M^2} \right]^2 \right] \quad (4.68)$$

The matrices defined in Equations (4.66) and (4.67) are identical for all segments, which simplifies the assembly of the boundary condition matrix for the full system. The full set of boundary conditions may be written as  $[BC_{matrix}]\{A_{total}\}=\{0\}$ , where  $\{A_{total}\}=\{A_1, A_2, A_3, \dots, A_{6M}\}$  and  $[BC_{matrix}]$  has the following form:

$$\left[ \begin{array}{cccccccc} [BCroot] & 0 & 0 & 0 & \cdot & \cdot & \cdot & 0 & 0 \\ [u_{prime}] & 0 & 0 & 0 & \cdot & \cdot & \cdot & 0 & 0 \\ [-Continuity-] & 0 & 0 & 0 & \cdot & \cdot & \cdot & 0 & 0 \\ 0 & [u_{prime}] & 0 & 0 & \cdot & \cdot & \cdot & 0 & 0 \\ 0 & [-Continuity-] & 0 & 0 & \cdot & \cdot & \cdot & 0 & 0 \\ \cdot & \cdot \\ \cdot & \cdot \\ \cdot & [u_{prime}] & 0 \\ 0 & 0 & 0 & 0 & \cdot & \cdot & \cdot & [-Continuity-] & \\ 0 & 0 & 0 & 0 & \cdot & \cdot & \cdot & 0 & [u_{prime}] \\ 0 & 0 & 0 & 0 & \cdot & \cdot & \cdot & 0 & [BCtip] \end{array} \right] \quad (4.69)$$

Note that matrices  $[BCroot]$ ,  $[BCtip]$ ,  $[Continuity]$ , and  $[u_{prime}]$  were defined in Equations (4.55), (4.56), (4.58), and (4.66) respectively.

At this point the formulation of the problem is complete. The complex form of  $G_v$  is substituted into the boundary condition matrix, resulting in a matrix with a complex determinant. The eigenvalues within the matrix are functions of the parameter  $\Omega^*$ . The

unknown complex natural frequency is found by identifying the value of  $\Omega^*$  that produces a matrix whose complex determinant has a modulus equal to zero.

The formulation developed in this chapter was used to find the complex natural frequencies of a beam with six pairs of damping segments. A complete description of the geometries that were considered and the results that were obtained is presented in the next chapter, where they are compared with two approximate methods. The MatLab software package (53) was used to process the problem. An initial estimate of the complex natural frequency was obtained from the approximate methods discussed in the next chapter, then the estimate was refined by iteratively seeking a minimum value of the modulus of the determinant in the vicinity of the initial guess for  $\Omega^*$ . The final value for  $\Omega^*$  was found using the existing Matlab minimization algorithms, which would diverge unless the initial guesses provided were very accurate.

It should be noted that obtaining a solution for the six segment problem was not a trivial matter. Previous researchers such as Rao (76:271) and Cottle (14) reported difficulties with obtaining a solution for the single segment configuration. The boundary condition matrix is numerically ill-conditioned; i.e., it contains both very large and very small terms in combinations that can not be corrected by standard matrix operations. Many general purpose computer algorithms are ineffective when applied to a problem of this nature. The author believes that there were three aspects of the problem formulation that may have helped made it possible to obtain a solution. The size of the terms in the boundary condition matrix was reduced by proper scaling of the non-dimensional

temporal and spatial variables. The boundary condition matrix was a banded matrix consisting of repeating submatrices due to the choice of assumed solution. Finally, a very good initial guess for the complex natural frequency was used as the starting point for the iterative process. This initial guess was obtained from the Complex Rayleigh Quotient method, which is described in the next chapter.

## *V. The Complex Rayleigh Quotient*

In this chapter, approximate methods that predict natural frequencies and damping in structures are described, and the Complex Rayleigh Quotient (CRQ) is introduced. The Complex Rayleigh Quotient is used in the analysis of structures whose components have out of phase displacements. The approach produces an estimate of the complex natural frequency for the system from a ratio of terms that are similar in form to Rayleigh's Quotient. The terms in this ratio are developed using approximations to the complex modes of the system. The system damping may be estimated from the ratio of imaginary to real parts of the complex frequency.

The form of the Complex Rayleigh Quotient is first developed for general discrete linear viscoelastic systems, and a two degree of freedom system is used to illustrate the method. The form of the Complex Rayleigh Quotient is then considered for continuous systems, and is illustrated using constrained layer damping treatments of various configurations. For the case of segmented constrained layer damping treatments mounted on a beam, the approximate mode shapes are developed using the "substrate assumption". In this approach, the exact equations of the constraining layer are solved by approximating the deflections of the damped structure by its corresponding undamped mode shapes. The constraining layer solutions produce complex mode shapes when the Correspondence Principle is invoked. The results using this approach are compared with

the exact solution, which was obtained by following the procedure outlined in Chapter 4.

It is shown that for the configurations examined, the Complex Rayleigh Quotient produces a better estimate of the loss factor for the first three modes than does the Modal Strain Energy approach.

### *The Correspondence Principle*

The development of the Complex Rayleigh Quotient requires use of the Correspondence Principle, which identifies a correspondence between viscoelastic and elastic problems. The principle as stated by Bland states:

"If the elastic solution for any dependent variable in a particular problem is of the form  $f = \text{Real}[f_e e^{i\Omega t}]$ , and if the elastic moduli in  $f_e$  are replaced by the corresponding complex moduli to give  $f_{ve}$ , then the viscoelastic solution for that variable in the corresponding problem is given by  $f = \text{Real}[f_{ve} e^{i\Omega t}]$ ."(9:67)

The Correspondence Principle allows tools developed for conservative systems to be used in the analysis of damped systems. The corresponding elastic problem is formulated and solved by using a real number to represent the modulus of a viscoelastic component. Once the elastic solution is found, damping inherent in the viscoelastic material is accounted for by using a complex modulus, which identifies the phase difference between stress and strain in a material. Caution must be exercised, however, in the computation of energies. Work must be computed using the product of a real force and a real displacement, where the real force is the real part of the product of a complex modulus and a complex strain.

### *Rayleigh's Quotient*

In classical undamped vibration analysis, a method used to find estimates of a system's fundamental frequency is known as Rayleigh's Quotient. Rayleigh's Quotient is based on Rayleigh's Principle, which states that for a conservative system vibrating at a natural frequency, the maximum system kinetic energy is equal to the maximum potential energy. For a more detailed treatment of this topic, see Reference (61:207).

Rayleigh's Quotient is obtained by setting expressions for maximum kinetic and maximum strain energy equal to each other, then solving for the natural frequency,  $\Omega$ . To formulate Rayleigh's Quotient for a general system consisting of  $N$  individual components, estimates of the mode shape are used to identify the maximum kinetic energies  $\Omega^2 T_n$  and maximum strain energies  $U_n$  of each part of the system. For this configuration, the form of Rayleigh's Quotient becomes:

$$\Omega^2 = \frac{\sum_{n=1}^N U_n}{\sum_{n=1}^N T_n} \quad (5.1)$$

The particular form of the kinetic and strain energies for both discrete and continuous systems will be described in later sections. Rayleigh's Quotient is often used when an estimate of fundamental frequency is desired and only a coarse estimate of the mode shape is available. In such cases, the approximation to the frequency produced by Rayleigh's Quotient provides an upper bound to the true fundamental frequency (61:207).

### *The Complex Rayleigh Quotient (CRQ)*

In this section, the Complex Rayleigh Quotient (CRQ) is introduced for the analysis of damped discrete or continuous structures with complex mode shapes. Complex mode shapes provide information on out of phase displacements for damped systems. The resulting terms that correspond to the maximum kinetic and strain energies in Rayleigh's Quotient for an elastic system are complex. In this chapter the Complex Rayleigh Quotient is defined using complex mode shapes for both discrete and continuous systems.

The idea of using Rayleigh's Quotient with damped systems was first proposed by McIntyre and Woodhouse for orthotropic plates (54:209). In this work, McIntyre and Woodhouse assumed that the imaginary portion of the complex modulus was much smaller than its real part. They considered the strain energy terms within Rayleigh's Quotient, and argued that the influence of the complex viscoelastic modulus on the mode shapes was much smaller than the direct effect of the modulus in the expression for strain energy. As a result, they used Rayleigh's Quotient to obtain a complex frequency by using real mode shapes and the complex viscoelastic modulus in the expressions for strain energy. The real mode shapes were found by replacing the complex viscoelastic modulus by its real part. Others have used the approach for the analysis of plates and other damped systems (55:1397, 62:K3-3, 102:187). These researchers have all used real mode shapes in their formulation of Rayleigh's Quotient.

The use of real mode shapes in a complex form of Rayleigh's Quotient was justified by the assertion that the imaginary portion of the complex viscoelastic modulus is much smaller than its real part. Though this may have been a good assumption for the problem considered by McIntyre and Woodhouse (the analysis of the wooden top plates of violins), this assumption is not appropriate for the case of structures with applied viscoelastic damping treatments. For several viscoelastic materials used in damping treatments, the real and imaginary portions of the complex modulus are equal in magnitude (87).

For the case of a viscoelastic system with complex mode shapes, the maximum kinetic and strain energies in the individual components will occur at different times in the cycle of vibration. As a result, the proper definition of strain energy and kinetic energy that should be used in Rayleigh's Quotient is not immediately obvious. In the next few sections, the appropriate expression will be developed for both discrete and continuous systems through manipulation of the system equations of motion.

*Using the Complex Rayleigh Quotient with Discrete Systems:*

The form of the Complex Rayleigh Quotient for a discrete system may be developed from the equations of motion. Before viscoelastic systems are considered, consider a N degree of freedom linear elastic system represented by the following matrix equation:

$$M \{\ddot{\bar{x}}\} + K\{\bar{x}\} = 0 \quad (5.2)$$

Here  $\{\bar{x}\}$  is a vector of unknown real displacements that are functions of time, M is a

diagonal real mass matrix, and  $K$  is a symmetric real stiffness matrix. A broad class of elastic systems have equations of this form if the system coordinates are used to identify displacements of masses in an inertial reference frame. If a solution is sought that has the form  $\{\bar{x}\} = \{x\} \exp[i\Omega t]$ , where  $\{x\}$  is a vector that is independent of time, the matrix equation becomes:

$$\Omega^2 M \{x\} = K \{x\} \quad (5.3)$$

Expressions for kinetic and strain energy can be obtained from the equations of motion by multiplying both sides by  $1/2 \{x\}^T$ :

$$\Omega^2 \frac{1}{2} \{x\}^T M \{x\} = \frac{1}{2} \{x\}^T K \{x\} \quad (5.4)$$

The left hand side of Equation (5.4) equals the maximum kinetic energy of the system, while the right hand side equals the maximum strain energy of the system. Rayleigh's Quotient is formulated by dividing both sides of Equation (5.4) by  $1/2 \{x\}^T M \{x\}$ :

$$\Omega^2 = \frac{\{x\}^T K \{x\}}{\{x\}^T M \{x\}} \quad (5.5)$$

Now consider how the problem changes for the corresponding linear viscoelastic problem. For the linear viscoelastic problem,  $\{x\}$  is a vector of complex displacements, some elements of the  $K$  matrix are complex, and the natural frequency is complex. By using asterisks to denote the complex quantities, Equation (5.3) may be written in the following form for the viscoelastic system:

$$\Omega^2 M \{x^*\} = K^* \{x^*\} \quad (5.6)$$

It is desirable to obtain an equation for the viscoelastic problem similar to the energy balance in Equation (5.4) by multiplying Equation (5.6) by some factor. If both sides of Equation (5.6) are multiplied by one-half the conjugate of  $\{x^*\}^T$ , a term similar in spirit to the maximum kinetic energy appears on the left hand side:

$$\Omega^2 \frac{1}{2} \{\bar{x}^*\}^T M \{x^*\} = \frac{1}{2} \{\bar{x}^*\}^T K^* \{x^*\} \quad (5.7)$$

It should be stressed that the left hand side of Equation (5.7) is not precisely the kinetic energy of the system. An expression for kinetic energy must be a positive real quantity, but the left hand side of Equation (5.7) is complex due to the presence of  $\Omega^2$ . The expression  $\{\bar{x}^*\}^T [M] \{x^*\}$  is a positive real quantity, but it is associated with the sum of the maximum kinetic energies of each displacement  $x_n$ , which do not occur simultaneously because of phase differences in the individual displacements. Despite the fact that Equation (5.7) does not simply equate maximum kinetic and potential energies, it can be manipulated into a form defined to be the Complex Rayleigh Quotient for discrete systems:

$$\Omega^2 = \frac{\{\bar{x}^*\}^T K^* \{x^*\}}{\{\bar{x}^*\}^T M \{x^*\}} \quad (5.8)$$

If the exact value for  $\{x^*\}$  is used in Equation (5.8), it provides the exact value for the complex natural frequency. If an approximation to the vector  $\{x^*\}$  is used in Equation

(5.8), it may also be used to find an estimate of the complex natural frequency in the same way Rayleigh's Quotient is used in elastic systems.

The complex frequency obtained from the Complex Rayleigh Quotient can be used to determine the damping of the system. The time dependence of the system has the form  $\exp[i\Omega^*t]$ , so a complex frequency of the form  $\Omega^* = \Omega_R + i \Omega_I$  implies an oscillatory component of the form  $\exp[i \Omega_R t]$  and a decaying component of the form  $\exp[- \Omega_I t]$ . This decaying component is often written as  $\exp[-\zeta \Omega_n t]$ , where  $\zeta$  is defined as the fraction of critical damping and  $\Omega_n$  is the undamped natural frequency of the system. This provides the relation  $\Omega_I = \zeta \Omega_n$ . The relation between the damped natural frequency and the undamped natural frequency for a system with linear viscous damping is  $\Omega_R = \Omega_n(1-\zeta^2)$ .

By manipulating these terms, relationships between the complex natural frequency and damping may be found:

$$\frac{\Omega_I}{\Omega_R} = \frac{\zeta}{\sqrt{1-\zeta^2}}, \quad \frac{Im[\Omega^{*2}]}{Re[\Omega^{*2}]} = \frac{2\zeta(1-\zeta^2)}{1-2\zeta^2} \quad (5.9)$$

The second expression in Equation (5.9) can be used to identify the damping from the complex frequency once the real and imaginary parts of  $\Omega^{*2}$  are defined from the Complex Rayleigh Quotient.

To define the real and imaginary parts of  $\Omega^{*2}$ , it is helpful to break the complex stiffness matrix  $K^*$  into its real and imaginary parts by defining  $K^* = K_R + i K_I$ , where  $K_R$  and  $K_I$  are symmetric real matrices. It is also helpful to show that if  $[A]$  is a symmetric

real  $N \times N$  matrix and  $\{x^*\}$  is a complex  $N \times 1$  vector, then  $\{\bar{x}^*\}^T [A] \{x^*\}$  is a real number.

Because  $[A]$  is symmetric,  $A_{ij} = A_{ji}$  and the product  $[A] \{x^*\}$  may be written in the following form:

$$[A] \{x^*\} = A_{ij} x_j^* = \begin{Bmatrix} A_{11} x_1^* + A_{12} x_2^* + \dots + A_{1N} x_N^* \\ A_{21} x_1^* + A_{22} x_2^* + \dots + A_{2N} x_N^* \\ \vdots \\ A_{N1} x_1^* + A_{N2} x_2^* + \dots + A_{NN} x_N^* \end{Bmatrix} \quad (5.10)$$

The product  $\{\bar{x}^*\}^T [A] \{x^*\}$  becomes:

$$\begin{aligned} \{\bar{x}^*\} [A] \{x^*\} &= \bar{x}_i^* A_{ij} x_j^* \\ &= \bar{x}_1^* (A_{11} x_1^* + A_{12} x_2^* + \dots + A_{1N} x_N^*) \\ &+ \bar{x}_2^* (A_{21} x_1^* + A_{22} x_2^* + \dots + A_{2N} x_N^*) \\ &+ \dots \\ &+ \bar{x}_N^* (A_{N1} x_1^* + A_{N2} x_2^* + \dots + A_{NN} x_N^*) \end{aligned} \quad (5.11)$$

Because  $[A]$  is symmetric with real elements, it may be seen from Equation (5.11) that  $\{\bar{x}^*\}^T [A] \{x^*\}$  is the sum of individual terms that are real numbers. Let  $x_n^* = a + ib$  and  $x_m^* = c + id$ . The following terms are real numbers:

$$x_n^* \bar{x}_n^* = a^2 + b^2, \quad x_n^* \bar{x}_m^* + \bar{x}_n^* x_m^* = 2ac + 2bd \quad (5.12)$$

Each term in Equation (5.11) has one of these forms, so the quantity  $\{\bar{x}^*\}^T [A] \{x^*\}$  is a real number. This result can be used to manipulate the numerator of the right hand side of Equation (5.8). The real and imaginary parts of the numerator are easily separated:

$$\begin{aligned} \{\bar{x}^*\}^T K^* \{x^*\} &= \{\bar{x}^*\}^T [K_R + i K_I] \{x^*\} \\ &= \{\bar{x}^*\}^T K_R \{x^*\} + i \{\bar{x}^*\}^T K_I \{x^*\} \end{aligned} \quad (5.13)$$

The denominator of the right hand side of Equation (5.8) is real since M is a diagonal real matrix. The ratio of imaginary to real parts of the square of the complex frequency becomes:

$$\frac{Im[\Omega^{*2}]}{Re[\Omega^{*2}]} = \frac{2\zeta(1-\zeta^2)}{1-2\zeta^2} = \frac{\{\bar{x}^*\}^T K_I \{x^*\}}{\{\bar{x}^*\}^T K_R \{x^*\}} \quad (5.14)$$

If the overall damping of the system is small, then the loss factor becomes:

$$\eta \approx 2\zeta \approx \frac{Im[\Omega^{*2}]}{Re[\Omega^{*2}]} = \frac{\{\bar{x}^*\}^T K_I \{x^*\}}{\{\bar{x}^*\}^T K_R \{x^*\}} \quad (5.15)$$

The real part of the complex natural frequency is equal to the frequency of vibration for the damped system, so both frequency and damping predictions are provided by the Complex Rayleigh Quotient.

#### *CRQ Form of Loss Factor: Compatibility with Ungar and Kerwin*

In this section, it is shown that the loss factor produced by the Complex Rayleigh Quotient has the same form as the loss factor developed by Ungar and Kerwin for a system of N viscoelastic springs (97:954). Suppose the complex stiffness of the nth spring is defined as  $K_n^* = K_{R_n} + i K_{I_n}$  and the complex elongation of the nth spring is defined as

$\Delta X_n^*$ . As with complex displacements, the complex nature of the elongation is an artifice that captures phase information. The actual elongation is the real part of the complex quantity.

For this system, Ungar and Kerwin identified the following form for the loss factor:

$$\eta = \frac{\sum D_n}{2\pi \sum W_n} \quad (5.16)$$

where  $D_n$  is the energy dissipated by the  $n$ th spring and  $W_n$  is the energy stored in an elastic spring with stiffness  $K_{Rn}$  with elongation  $|\Delta X_n^*|$ :

$$D_n = \pi K_{In} |\Delta X_n^*|^2 \quad (5.17)$$

$$W_n = \frac{1}{2} K_{Rn} |\Delta X_n^*|^2 \quad (5.18)$$

By substituting the expression for  $D_n$  and  $W_n$  into Equation (5.16), the system loss factor may be written as:

$$\eta = \frac{\sum K_{In} |\Delta X_n^*|^2}{\sum K_{Rn} |\Delta X_n^*|^2} \quad (5.19)$$

One notable aspect of this result is that the  $W_n$  terms are defined in terms of their individual amplitudes  $|\Delta X_n^*|$ , though in general the different values of  $\Delta X_n^*$  will not be in phase with each other. This expression for loss factor is equivalent to Equation (5.15), which was developed from the Complex Rayleigh Quotient analysis for small damping. The terms

$(\bar{x}')^T [K_r] (x')$  and  $(\bar{x}')^T [K_i] (x')$  in Equation (5.15) are equal to the magnitudes of the spring elongation multiplied by either the real or the imaginary part of the spring stiffnesses. This will be illustrated later in the chapter using a two degree-of-freedom system.

*Example: 2 Degree of Freedom System*

A simple example using the Complex Rayleigh Quotient with a discrete system should prove helpful in illustrating the concepts before continuous systems are considered. Consider the two degree of system illustrated in Figure 5.1, which consists of a one degree of freedom elastic system with mass  $m$  and spring stiffness  $k_1$  with a secondary mass  $m$  attached by a viscoelastic spring with stiffness  $k_2 = k_r + i k_i$ . (For this example, the asterisks will be dropped from complex numbers for convenience).

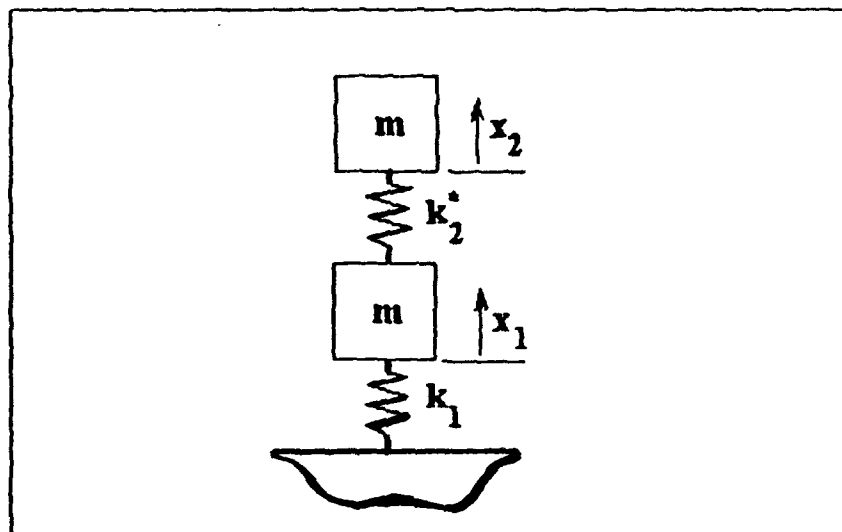


Figure 5.1. Two Degree of Freedom System

The solutions to the equations are developed using the Correspondence Principle. If harmonic time dependence is assumed, the equations of motion for the system may be written in the following form:

$$\begin{bmatrix} k_1+k_2 & -k_2 \\ -k_2 & k_2 \end{bmatrix} \begin{Bmatrix} X_1 \\ X_2 \end{Bmatrix} = \Omega^2 \begin{bmatrix} m & 0 \\ 0 & m \end{bmatrix} \begin{Bmatrix} X_1 \\ X_2 \end{Bmatrix} \quad (5.20)$$

A non-trivial solution to the eigenvalue problem exists only for values of  $\Omega^2$  that satisfy the characteristic equation:

$$\Omega^4 - \Omega^2 \frac{k_1+2k_2}{m} + \frac{k_1 k_2}{m^2} = 0 \quad (5.21)$$

The roots of the characteristic equation yield the two natural frequencies of the system:

$$\Omega_1^2 = \frac{k_1+2k_2}{2m} - \sqrt{\left(\frac{k_1+2k_2}{2m}\right)^2 - \frac{k_1 k_2}{m^2}}, \quad \Omega_2^2 = \frac{k_1+2k_2}{2m} + \sqrt{\left(\frac{k_1+2k_2}{2m}\right)^2 - \frac{k_1 k_2}{m^2}} \quad (5.22)$$

The scale of the mode shapes is arbitrary. Define the displacement of the primary mass as  $X_1=1$  for both frequencies. The displacement of the second mass corresponding to frequencies  $\Omega_1$  and  $\Omega_2$  may be found by substituting  $X_1=1$  and the natural frequency into Equation (5.20). If the complex mode shape corresponding to the  $j$ th frequency is defined as  $\{X_1, X_2\} = \{1, X_{2j}\}$ , the  $X_{2j}$  terms have the following form:

$$X_{21} = \frac{k_1}{2k_2} + \sqrt{\left(1 + \frac{k_1}{2k_2}\right)^2 - \frac{k_1}{k_2}}, \quad X_{22} = \frac{k_1}{2k_2} - \sqrt{\left(1 + \frac{k_1}{2k_2}\right)^2 - \frac{k_1}{k_2}} \quad (5.23)$$

Now that the formulation of the exact solution is complete, consider the form that the Complex Rayleigh Quotient as defined in Equation (5.8) would take for this problem. Let the mode shape (or an approximation to the mode shape) be defined as  $X = \{X_1, X_2\}$ . The Complex Rayleigh Quotient becomes:

$$\begin{aligned} \Omega^2 &= \frac{\overline{X}^T K X}{\overline{X}^T M X} = \frac{(k_1 + k_2)|X_1|^2 - k_2(X_1 \overline{X_2} + \overline{X_1} X_2) + k_2|X_2|^2}{m(|X_1|^2 + |X_2|^2)} \\ &= \frac{k_1|X_1|^2 + k_2|X_1 - X_2|^2}{m(|X_1|^2 + |X_2|^2)} \end{aligned} \quad (5.24)$$

For the viscoelastic problem, the spring constant  $k_2$  in Equation (5.24) is complex. If the true mode shapes are used in Equation (5.24), the square of the natural frequency that results is identical to the expression defined in Equation (5.22). If an approximation to the true mode shape is substituted into Equation (5.24), then the expression produces an approximation to the natural frequency.

For a lightly damped system, the loss factor may be calculated by using Equation (5.15):

$$\eta_{system} = \frac{Im[k_2^*]|X_1 - X_2|^2}{k_1|X_1|^2 + Re[k_2^*]|X_1 - X_2|^2} \quad (5.25)$$

The equations above were used in a case study that examined the relative effectiveness of using real and complex mode shapes in Equation (5.24) to predict the fundamental frequency of the system. Equation (5.23) was used to obtain two real approximations to the actual complex mode shape. The first real mode shape was obtained by replacing the complex stiffness  $k_2$  by its real part, an approach analogous to the method used by McIntyre and Woodhouse in their complex form of Rayleigh's Quotient. The second real mode shape was obtained by replacing the complex stiffness  $k_2$  by its modulus. The predicted frequencies that resulted from substituting the real mode shapes into Equation (5.24) were compared with the results from substituting the true complex mode shapes calculated from Equation (5.23). Loss factors were obtained from the frequencies by using small damping approximations (Equation (5.15) ).

Three configurations were considered, all with spring constant  $k_1 = 1$  and varying values of the complex portion of the spring constant  $k_2$ . The three configurations had increasing amounts of damping, with  $k_2$  equal to  $1+.1i$ ,  $1+.5i$ , and  $1+1i$  for the three cases. A comparison of the natural frequencies for the three configurations may be seen in Table 5.1.

TABLE 5.1. 2 Degree of Freedom System: Fundamental Frequency and Mode Shape

CONFIGURATION 1: $k_2=1+.1i$			
	mode shape using $k_2^*$	mode shape using $ k_2^* $	mode shape using $\text{Re}[k_2^*]$
mode shape	{1.00, 1.61-.0715 i }	{1, 1.61}	{1, 1.62}
$\Omega_1$	.619+.00847 i	.619+.00847 i	.618+.00854 i
$\eta_1$	.0274	.0274	.0276
error in $\eta_1$	n. a.	.06%	.7%
CONFIGURATION 2: $k_2=1+.5 i$			
	mode shape using $k_2^*$	mode shape using $ k_2^* $	mode shape using $\text{Re}[k_2^*]$
mode shape	{1.00, 1.46 -.275 i }	{1.00, 1.54}	{1.00, 1.62}
$\Omega_1$	.634+.0354 i	.620+.0351 i	.620+.0426 i
$\eta_1$	.112	.114	.138
error in $\eta_1$	n. a.	1.6%	23%
CONFIGURATION 3: $k_2=1+1i$			
	mode shape using $k_2^*$	mode shape using $ k_2^* $	mode shape using $\text{Re}[k_2^*]$
mode shape	{1, 1.25 - .312 i }	{ 1, 1.41}	{ 1, 1.62}
$\Omega_1$	.662+.0457 i	.627+.0457i	.624+.00846 i
$\eta_1$	.139	.146	.276
error in $\eta_1$	n.a.	5.6%	99%

It may be seen from Table 5.1 that the damping predictions obtained from the real mode shapes become worse as the complex portion of the stiffness of  $k_2$  increases. It is interesting to note that when the viscoelastic spring has a significant imaginary component, the predictions may be improved significantly by using the modulus of the complex spring stiffness instead of the real part of the stiffness.

### *Complex Rayleigh Quotient with Continuous Systems*

The Complex Rayleigh Quotient can be developed for one-dimensional continuous systems using an approach similar to that used for discrete systems. Although the mode shapes for continuous systems consist of one or more complex valued functions instead of complex vectors, the two types of problems have some common aspects. In this section a general approach to using the Complex Rayleigh Quotient for continuous linear systems will be described, then illustrated using the example of a constraining layer on a bar.

The general form of the Complex Rayleigh Quotient for continuous systems is most easily derived if the system of equations are presented in matrix operator format. Before a viscoelastic system is examined, consider its corresponding elastic system. Suppose the equations of motion have the following form:

$$\Omega^2 M\{u\} = L\{u\} \quad (5.26)$$

The form of the equations of motion for the continuous system (Equation (5.26)) and the equations of motion for the discrete system (Equation (5.6)) are similar. The vector  $\{u\}$

contains the system mode shapes, which are functions of the independent variable  $x$ . The matrices  $M$  and  $L$  are symmetric linear operators. For the elastic system of equations written in operator format, energy terms are formed by multiplying both sides of Equation (5.26) by  $1/2 u^T$  and integrating over the length of the beam:

$$\frac{1}{2} \Omega^2 \int_0^L \{u\}^T M \{u\} dx = \frac{1}{2} \int_0^L \{u\}^T L \{u\} dx \quad (5.27)$$

The left hand side of Equation (5.27) is equal to the maximum kinetic energy of the system and the right hand side is equal to the maximum potential energy of the system. Rayleigh's Quotient is found by solving for  $\Omega^2$ .

In the viscoelastic problem,  $\Omega^2$ ,  $u$ , and the elements of the linear operator  $L$  are complex. To obtain the complex terms that correspond to the maximum kinetic and potential energies, both sides of the equations of motion are multiplied by  $1/2 \bar{u}^T$  and integrated over the length of the structure:

$$\frac{1}{2} \Omega^2 \int_0^L \{\bar{u}\}^T M \{u\} dx = \frac{1}{2} \int_0^L \{\bar{u}\}^T L \{u\} dx \quad (5.28)$$

As in the discrete problem, the left hand side of Equation (5.28) is not the maximum kinetic energy of the system because  $\Omega^2$  is a complex number and the maximum displacements associated with each value of  $x$  do not occur at the same moment in time. By manipulating Equation (5.28), the general expression for the Complex Rayleigh Quotient may be obtained for continuous systems:

$$\Omega^2 = \frac{\int_0^L \langle \bar{u} \rangle^T L(u) dx}{\int_0^L \langle \bar{u} \rangle^T M(u) dx} \quad (5.29)$$

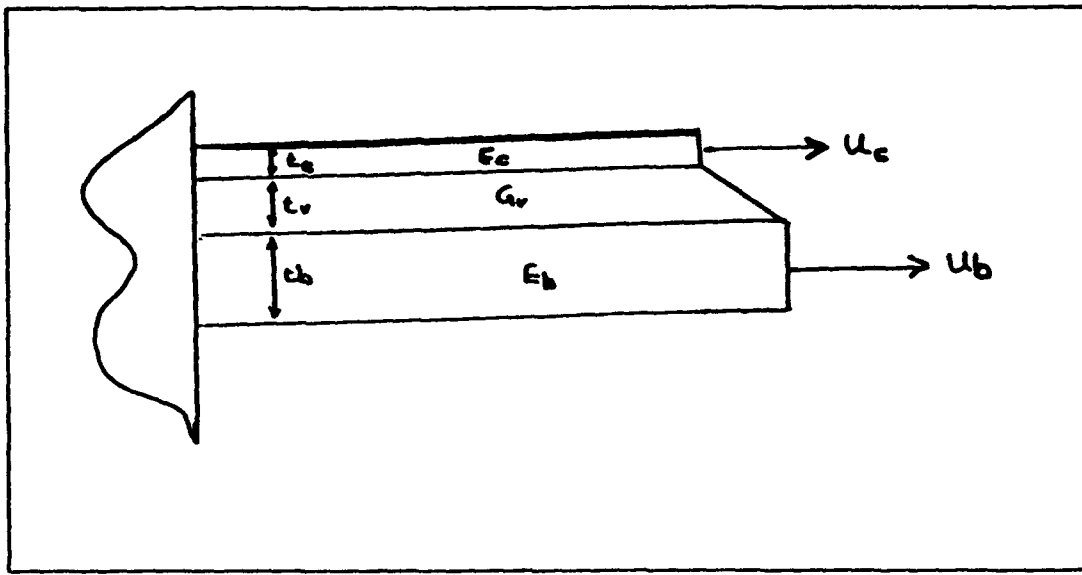


Figure 5.2. Bar in Extension with Constraining Layer

The development for a general continuous system can be illustrated for the case of a rectangular bar covered with a constrained layer damping treatment (Figure 5.2). Let  $\bar{u}_b$  be the extensional displacement of the bar and let  $\bar{u}_e$  be the extensional displacement of the constraining layer, where both displacements are functions of  $x$  and  $t$ . After the separation of variables has been accomplished, let  $u_b$  and  $u_e$  denote the corresponding mode shapes, which are functions of  $x$ . Let both the bar and the damping layers have unit width. The equations of motion for the system are developed using the Correspondence Principle. For the corresponding elastic system, the potential energy in the bar, constraining layer, and

viscoelastic layer may be written as:

$$U_b = \frac{1}{2} \int_0^L E_b t_b \left[ \frac{\partial \bar{u}_b}{\partial x} \right]^2 dx \quad (5.30)$$

$$U_c = \frac{1}{2} \int_0^L E_c t_c \left[ \frac{\partial \bar{u}_c}{\partial x} \right]^2 dx \quad (5.31)$$

$$U_v = \frac{1}{2} \int_0^L \frac{G_v}{t_v} (\bar{u}_c - \bar{u}_b)^2 dx \quad (5.32)$$

If the mass of the viscoelastic layer is negligible compared to the bar and constraining layers, the total kinetic energy of the system may be written as:

$$T = \frac{1}{2} \int_0^L \rho_b t_b \left( \frac{\partial \bar{u}_b}{\partial t} \right)^2 dx + \frac{1}{2} \int_0^L \rho_c t_c \left( \frac{\partial \bar{u}_c}{\partial t} \right)^2 dx \quad (5.33)$$

By invoking Hamilton's Principle, the kinetic and potential energies may be used to develop the following coupled equations of motion:

$$\begin{aligned} E_b t_b \frac{\partial^2 \bar{u}_b}{\partial x^2} - \frac{G_v}{t_v} (\bar{u}_b - \bar{u}_c) &= \rho_b t_b \frac{\partial^2 \bar{u}_b}{\partial t^2} \\ E_c t_c \frac{\partial^2 \bar{u}_c}{\partial x^2} + \frac{G_v}{t_v} (\bar{u}_b - \bar{u}_c) &= \rho_c t_c \frac{\partial^2 \bar{u}_c}{\partial t^2} \end{aligned} \quad (5.34)$$

For  $\bar{u}_c = u_c \exp[i \Omega t]$  and  $\bar{u}_b = u_b \exp[i \Omega t]$ , these equations become:

$$E_b t_b \frac{d^2 u_b}{dx^2} - \frac{G_v}{t_v} (u_b - u_c) = - \Omega^2 \rho_b t_b u_b \quad (5.35)$$

$$E_c t_c \frac{d^2 u_c}{dx^2} + \frac{G_v}{t_v} (u_b - u_c) = - \Omega^2 \rho_c t_c u_c$$

These equations may be written in operator matrix form :

$$\Omega^2 M\{u\} = L\{u\} \quad (5.36)$$

where  $u = \{ u_b , u_c \}^T$  is a vector of functions, and M and L represent linear operators written in matrix form:

$$M = \begin{bmatrix} \rho_b t_b & 0 \\ 0 & \rho_c t_c \end{bmatrix}, \quad L = - \begin{bmatrix} \rho_b t_b D^2 - \frac{G_v}{t_v} & \frac{G_v}{t_v} \\ \frac{G_v}{t_v} & \rho_c t_c D^2 - \frac{G_v}{t_v} \end{bmatrix} \quad (5.37)$$

In the L operator matrix, D denotes a derivative with respect to x. The boundary conditions of the problem have the following form:

$$u(0) = \begin{Bmatrix} u_b \\ u_c \end{Bmatrix} \Big|_{x=0} = 0, \quad \frac{du(L)}{dx} = \begin{Bmatrix} \frac{du_b}{dx} \\ \frac{du_c}{dx} \end{Bmatrix} \Big|_{x=L} = 0 \quad (5.38)$$

Now consider the corresponding viscoelastic problem, where  $G_v$ ,  $u$ , and  $\Omega$  are complex. If an estimate of  $u$  is available, the complex terms that correspond to the potential and kinetic energies of the system may be calculated. At first glance, the numerator of the Complex Rayleigh Quotient does not look like the familiar expression for

potential energy, but the original form of the potential energy can be retrieved by integrating by parts. Consider the numerator of the Complex Rayleigh Quotient for the constraining layer in axial extension:

$$\begin{aligned} \int \bar{u}^T L u \, dx = & - \int \bar{u}_b \left[ E_b t_b \frac{d^2 u_b}{dx^2} - \frac{G_v^*}{t_v} (u_b - u_c) \right] dx \\ & - \int \bar{u}_c \left[ E_c t_c \frac{d^2 u_c}{dx^2} + \frac{G_v^*}{t_v} (u_b - u_c) \right] dx \end{aligned} \quad (5.39)$$

By integrating by parts and using the boundary conditions provided in Equation (5.38) to set the boundary terms equal to zero, the following expressions result:

$$\begin{aligned} \int \bar{u}^T L u \, dx = & \int E_b t_b \frac{du_b}{dx} \frac{d\bar{u}_b}{dx} \, dx + \int E_c t_c \frac{du_c}{dx} \frac{d\bar{u}_c}{dx} \, dx \\ & + \int \frac{G_v^*}{t_v} (u_b - u_c) \overline{(u_b - u_c)} \, dx \end{aligned} \quad (5.40)$$

Recall that if  $f(x)$  is an arbitrary complex valued function, the function  $g(x) = f(x)\bar{f}(x)$  is equal to the square of the magnitude of  $f$  at each value of  $x$ . From Equation (5.40) it can be seen that the terms used for strain energy in the Complex Rayleigh Quotient have the same form as the strain energy expressions of the corresponding elastic problem, except that the real quadratic strain terms in the elastic problem are replaced by the square of the magnitude of the complex strains obtained by using complex mode shapes.

The denominator of the Complex Rayleigh Quotient has the following form for the bar:

$$\int \overline{u}^T M u \, dx = \int [ \rho_b t_b \overline{u}_b u_b + \rho_c t_c \overline{u}_c u_c ] \, dx \quad (5.41)$$

By substituting Equations (5.40) and (5.41) into Equation (5.29), the Complex Rayleigh Quotient is formed for the damped bar. Equation (5.29) produces the exact value of the complex frequency if the exact mode shapes are used in Equations (5.40) and (5.41); if an approximation to the mode shapes are used, Equation (5.29) produces an approximation of the complex frequency.

Notice that both the kinetic energy and potential energy terms used to form the Complex Rayleigh Quotient have the same form as the corresponding elastic problem, except that the real quadratic strain and displacement terms in the elastic problem are replaced by the square of the magnitudes of the complex strains and displacements. This was also true for the discrete problems discussed in the previous section.

*Example of Complex Rayleigh Quotient: Constraining Layer on a Beam.*

In this section the Complex Rayleigh Quotient is used to obtain an estimate for the complex natural frequency of the damped rectangular beam described in Chapter 4. In Chapter 4, equations of motion were developed for both continuous and segmented constraining layers. In this section, the form of the strain energies are developed for use in the Complex Rayleigh Quotient, then the solutions are identified for use in the strain

energy expressions. Similarities between the loss factors obtained from the Complex Rayleigh Quotient and the Modal Strain Energy method will also be identified. Some of the definitions and equations identified in Chapter 4 will be repeated in this section to assist the reader.

*Form of Displacements and Strain Energies.* The two displacements identified in the problem are the transverse displacement  $w$  of the beam and constraining layers, and the axial displacement  $u$  of the constraining layers. In the exact solution developed in Chapter 4, both  $u$  and  $w$  are complex valued functions. In the approximate solution used in the Complex Rayleigh Quotient, it will be assumed that the displacement  $w$  can be approximated by the undamped mode shapes of the beam. As a result, a real valued function for  $w$  is used in the kinetic and strain energies, while the function for  $u$  is complex.

The complex solution for the displacement  $u$  results in a complex extensional strain,  $u''$ , and a complex viscoelastic shear strain,  $\gamma'$ . The strain energies used in the Complex Rayleigh associated with the damping layers are defined using the square of the moduli of the complex strains:

$$U_c = \frac{1}{2} \iiint E_c (u')^* \overline{(u')^*} dvol, \quad U_\gamma^* = \frac{1}{2} \iiint G_v^* \gamma'^* \overline{\gamma'^*} dvol \quad (5.42)$$

If the viscoelastic shear modulus is defined as  $G_v^* = G_v' (1+i \eta_v)$ , the strain energy associated with the viscoelastic shear strain is complex and has the form  $U_\gamma^* = U_\gamma' (1+i \eta_v)$ .

The combined strain energy of the beam and the constraining layers due to bending depend on  $w''$ , which is a real function:

$$U_b = \frac{1}{2} \int_0^L D_t (w'')^2 dz, \quad D_t = E_b I_b + 2E_c I_c \quad (5.43)$$

The equivalent system kinetic energy has the following form:

$$T^* = (\Omega^*)^2 \frac{1}{2} \int_0^L m_t w^2 dz, \quad m_t = \rho_b A_b + 2\rho_v A_v + 2\rho_c A_c \quad (5.44)$$

The form of the Complex Rayleigh Quotient for the damped beam becomes:

$$\Omega_{CRQ}^{*2} = \frac{U_b + U_c + U_\gamma^*}{\frac{1}{2} \int_0^L m_t w^2 dz} \quad (5.45)$$

*Solutions for  $u$  and  $\gamma$  for Segmented Constraining Layers.* An approximate solution for the segmented constraining layer geometry described in Chapter 4 is found by assuming that the transverse displacement  $w$  of the damped beam may be approximated by its undamped mode shape. Consider the case of a beam covered with  $M$  pairs of segments, each of length  $2L_c$ . Let  $z_m = (2m-1)L_c$  identify the  $z$  coordinate at the center of the  $m$ th segment, and let  $z = z_m L_c$  identify its boundaries. Define  $\hat{w}$  to be the undamped mode shape that is used to approximate the actual deflection of the beam. For a Bernoulli-Euler beam,  $\hat{w}$  has the following form:

$$\hat{w} = A \cos(pz) + B \sin(pz) + C \cosh(pz) + D \sinh(pz) \quad (5.46)$$

The constraining layer equation has the same form for each segment, and the boundary conditions specify that the strain in the constraining layer is zero at the cut ends of each segment:

$$u_m'' - g^* u_m = g^* y_o w', \quad u_m' \delta u_m \Big|_{z=0, L_c} = 0 \quad (5.47)$$

where

$$g^* = \frac{G_v^*}{4h_v h_c E_c}, \quad y_o = h_b + 2h_v + h_c \quad (5.48)$$

The "m" subscript on u in Equation (5.47) identifies the displacement defined over the mth segment. Note that Equation (5.47) has the same form as the differential equation that describes a constraining layer mounted on a substrate (Equation (3.5)).

By substituting  $\hat{w}$  into Equation (5.47), the particular solution for u may be found:

$$u_{p_m} = a \sin(pz) + b \cos(pz) + c \sinh(pz) + d \cosh(pz) \quad (5.49)$$

$$a = \frac{g y_o p A}{p^2 + g}, \quad b = \frac{-g y_o p B}{p^2 + g}, \quad c = \frac{g y_o p C}{p^2 - g}, \quad d = \frac{g y_o p D}{p^2 - g} \quad (5.50)$$

The first derivative of the particular solution is:

$$u_{p_m}' = a_1 \cos(pz) + b_1 \sin(pz) + c_1 \cosh(pz) + d_1 \sinh(pz) \quad (5.51)$$

where

$$a_1 = \frac{8\gamma_0 p^2 A}{p^2 + g}, \quad b_1 = \frac{8\gamma_0 p^2 B}{p^2 + g}, \quad c_1 = \frac{8\gamma_0 p^2 C}{p^2 - g}, \quad d_1 = \frac{8\gamma_0 p^2 D}{p^2 - g} \quad (5.52)$$

The homogeneous solution for the  $m$ th segment may be written as:

$$u_{h_m} = P_m \cosh(\sqrt{g}(z - z_m)) + Q_m \sinh(\sqrt{g}(z - z_m)), \quad z \in (z_m - L_c, z_m + L_c) \quad (5.53)$$

where

$$P_m = \frac{\sin(pL_c)(-a_1 \sin(pz_m) + b_1 \cos(pz_m)) + \sinh(pL_c)(c_1 \sinh(pz_m) + d_1 \cosh(pz_m))}{\sqrt{g} \sinh(\sqrt{g}L_c)} \quad (5.54)$$

$$Q_m = \frac{\cos(pL_c)(a_1 \cos(pz_m) + b_1 \sin(pz_m)) + \cosh(pL_c)(c_1 \cosh(pz_m) + d_1 \sinh(pz_m))}{\sqrt{g} \cosh(\sqrt{g}L_c)}$$

The solution for  $u$  is the sum of homogeneous and particular solutions defined over each segment:

$$u = \sum_{m=1}^M u_m \quad (5.55)$$

where

$$u_m = \begin{cases} u_{h_m} + u_{p_m}, & z \in (z_m - L_c, z_m + L_c) \\ 0, & \text{otherwise} \end{cases} \quad (5.56)$$

The shear strain  $\gamma$  in the viscoelastic layer must be defined piecewise over each segment:

$$\gamma_m = \begin{cases} \frac{u_m + y_o \dot{w}'}{2h_v}, & z \in (z_m - L_c, z_m + L_c) \\ 0, & \text{otherwise} \end{cases} \quad (5.58)$$

Now that the solution is known, it may be used to obtain both real and complex mode shapes, depending on whether a real or complex  $G_v$  is used in the solution. The complex mode shapes can be used in the Complex Rayleigh Quotient defined in Equation (5.45).

*Measures of Damping from the Complex Natural Frequency:*

The system damping can be obtained from the complex frequency defined by the Complex Rayleigh Quotient. For a lightly damped system, Equation (5.15) may be used to identify the loss factor:

$$\eta_{CRQ} = \frac{Im[\Omega_{CRQ}^{*2}]}{Re[\Omega_{CRQ}^{*2}]} \quad (5.59)$$

The real and imaginary parts of  $\Omega_{CRQ}^{*2}$  may be identified by using the expression  $U_\gamma^* = U_\gamma'(1+i\eta_v)$  with Equation (5.45):

$$\begin{aligned}
\operatorname{Re}\left[\Omega_{CRQ}^2\right] &= \frac{U_b + U_c + \operatorname{Re}\left[U_\gamma^*\right]}{\frac{1}{2} \int_0^L m_i w^2 dz} = \frac{U_b + U_c + U_\gamma'}{\frac{1}{2} \int_0^L m_i w^2 dz} \\
\operatorname{Im}\left[\Omega_{CRQ}^2\right] &= \frac{\operatorname{Im}\left[U_\gamma^*\right]}{\frac{1}{2} \int_0^L m_i w^2 dz} = \frac{\eta_\nu U_\gamma'}{\frac{1}{2} \int_0^L m_i w^2 dz}
\end{aligned}
\tag{5.60}$$

The loss factor can be written as:

$$\eta_{CRQ} = \frac{\eta_\nu U_\gamma'}{U_\gamma' + U_b + U_c}
\tag{5.61}$$

It is interesting to note that if real mode shapes instead of complex mode shapes are used in the Complex Rayleigh Quotient, the loss factor defined in Equation (5.61) is equivalent to that obtained by the Modal Strain Energy (MSE) method, a well known approximation approach (39:71, 40:1284). The Modal Strain Energy method was presented for use with structures that contain viscoelastic materials, including applied viscoelastic damping treatments. In this method, the mode shapes of a structure are found as if all parts of the system are purely elastic, an approach which produces mode shapes that are real valued functions. These real mode shapes are used to calculate a value for the corresponding damped system. Suppose the system has J elastic components and K viscoelastic components, and  $\eta_k$  represents the loss factor of the kth viscoelastic material. If  $U_j$  and  $U_k$  are the strain energies calculated from the real mode shapes for the elastic and viscoelastic portions of the structure, then an estimate of the structural damping for the

corresponding damped mode may be found from the following expression:

$$\eta_{MSE} = \frac{\sum_{k=1}^K \eta_k U_k}{\sum_{k=1}^K U_k + \sum_{j=1}^J U_j} \quad (5.62)$$

For the beam with a segmented damping treatment, the Modal Strain Energy approach would predict a loss factor of the following form:

$$\eta_{MSE} = \frac{\eta_v U_{\gamma R}}{U_{\gamma R} + U_{c_r} + U_b} \quad (5.63)$$

where  $U_b$  is defined in Equation (5.43) and the strain energies of the constraining layer and viscoelastic layer are defined using the real mode shapes:

$$U_{c_r} = \frac{1}{2} \iiint E_c (u')^2 dvol, \quad U_{\gamma R} = \frac{1}{2} \iiint G_v' \gamma^2 dvol \quad (5.64)$$

The values for  $u'$  and  $\gamma$  in Equation (5.64) are obtained from Equations (5.55) and (5.58) if a real value is used for  $G_v$  in those expressions.

Note that the loss factors from the Complex Rayleigh Quotient (Equation (5.61)) and the Modal Strain Energy approach (Equation (5.63)) have the same form. The difference in the two methods is that the strain energy terms  $U_{\gamma'}$  and  $U_c$  used in the Complex Rayleigh Quotient method are derived from complex solutions for  $u$  and contain integrals of the square of the magnitudes of complex strains. The strain energy terms contained in the Modal Strain Energy method contain the square of the real strains. If real mode shapes

are used in the Complex Rayleigh Quotient and the damping is small, the analysis produces a loss factor identical to that obtained using the Modal Strain Energy method.

The real strain energy expressions used in the Modal Strain Energy method may also be used to get a real estimate of the natural frequency using Rayleigh's Quotient:

$$\Omega_{RQ}^2 = \frac{U_b + U_{c_r} + U_{Y_R}}{\frac{1}{2} \int_0^L m_i w^2 dz} \quad (5.65)$$

Estimates of damping and natural frequency using Equations (5.63) and (5.65) will be compared with estimates using the complex modes later in this chapter.

In summary, the Complex Rayleigh Quotient was used in the analysis of a beam with a segmented constrained layer damping treatment. Approximations to the displacements and strains of the damping layers were found by approximating the displacement of the main structure by its undamped mode shape, then solving the exact constraining layer equations of motion. The only approximation associated with this solution is that the constraining layer will have some effect on the mode shapes of the main beam that is not taken into account using this approach. The complex strains and displacements are used in expressions for strain energy and kinetic energy that are substituted into the Complex Rayleigh Quotient. The system loss factor may be obtained from the ratio of imaginary to real parts of the ratio, and may be written in a form similar to that obtained by the Modal Strain Energy approach.

### *Comparison of Approximate Estimates with Exact Results.*

In this section the Complex Rayleigh Quotient is used to predict the natural frequencies and loss factors of a thin 91.44 cm (36") steel cantilever beam with six 15.24 cm (6") damping segments of equal length applied to both faces of the beam. Both the beam and the damping layers have unit width. The strain energies are formulated using the complex mode shapes obtained by substituting the complex viscoelastic modulus into the solutions developed in the previous section. These results are compared with the exact solutions, which are obtained by using the approach described in Chapter 4. The Complex Rayleigh Quotient results are also compared with estimates of natural frequency and loss factor obtained by using real mode shapes with the Modal Strain Energy method and the Rayleigh's Quotient. Two different approaches are used to obtain real mode shapes from the solutions identified in the previous section. One set of mode shapes is developed by substituting the real part of  $G_v^*$  into the solutions defined in the previous section, while the other set is obtained by substituting the modulus of  $G_v^*$  in the same solutions.

Predictions were obtained for three beam geometries of different thicknesses. The thicknesses of the beam layers for the three configurations are identified in Table 5.2. (Recall that the thicknesses of the beam, constraining layer, and viscoelastic layer are  $2h_b$ ,  $2h_c$ , and  $2h_v$ , respectively.) The percent of the cross sectional area of the composite beam that consists of the main beam is 78% for configuration 1, 58% for configuration 2 and 42% for configuration 3, so the effect of the damping treatment increases with configuration number. The beam extensional modulus is  $E_b = 20.7 \times 10^{10}$  pascals (30,000,000 lb/in<sup>2</sup>) and

the beam density is  $\rho_b = 7.01 \times 10^3 \text{ kg/m}^3$  (.000735 lb-sec<sup>2</sup>/in<sup>4</sup>). The constraining layer has an extensional modulus of  $E_c = 6.89 \times 10^{10}$  pascals (10,000,000 lb/in<sup>2</sup>) and a density of  $\rho_c = 2.34 \times 10^3 \text{ kg/m}^3$  (.000245 lb-sec<sup>2</sup>/in<sup>4</sup>). The viscoelastic layer has a density of  $\rho_v = 982 \text{ kg/m}^3$  (.000103 lb-sec<sup>2</sup>/in<sup>4</sup>) and a shear modulus of  $G_v^* = G_v'(1+.5i)$  where  $G_v' = 2.41 \times 10^5$  pascals (35 lb/in<sup>2</sup>). For the cases studied,  $G_v$  and  $\eta_v$  are held constant with frequency. The damping treatment geometry is similar to some of the prefabricated damping treatments made by 3M that consist of a layer of aluminum with a thin self-adhesive viscoelastic layer. The ISD-112 viscoelastic material manufactured by 3M has similar viscoelastic properties for frequencies below 10 hertz at room temperature, although the properties have a temperature and frequency dependence that is not modelled in this study. The natural frequencies and damping predicted for the three configurations are seen in Tables 5.3, 5.4, and 5.5. Quantities calculated using the Rayleigh's Quotient, the Complex Rayleigh Quotient, and the Modal Strain Energy method are denoted by "RQ", "CRQ", and "MSE" respectively. The loss factors obtained from the Complex Rayleigh Quotient were calculated using small damping approximations (Equation (5.15)).

*Table 5.2. Segmented Beam Thicknesses for Configurations 1, 2, and 3*

	Beam ( $2h_b$ )	Constraining Layer ( $2h_c$ )	Viscoelastic Layer ( $2h_v$ )
Configuration 1	1.3 mm (.050")	.13 mm (.005")	.051 mm (.002")
Configuration 2	0.50 mm (.020")	.13 mm (.005")	.051 mm (.002")
Configuration 3	0.25 mm (.010")	.13 mm (.005")	.051 mm (.002")

*Table 5.3 Predicted Frequencies and Loss Factors for Configuration 1*

Quantity	Method	Mode 1	Mode 2	Mode 3
frequency	exact	8.1155+.09416 i	50.763+.5820 i	141.776+1.6042 i
loss factor	exact	.02321	.02293	.02263
frequency	RQ (Re[G <sub>v</sub> *)	8.1002	50.675	141.56
loss factor	MSE (Re[G <sub>v</sub> *)	.02595	.02562	.02522
frequency	RQ ( G <sub>v</sub> *)	8.124	50.82	141.96
loss factor	MSE ( G <sub>v</sub> *)	.02555	.025620	.02498
frequency	CRQ	8.1267+.09759 i	50.836 +.6040 i	141.99+1.6664 i
loss factor	CRQ	.02402	.02376	.02347

*Table 5.4 Predicted Frequencies and Loss Factors for Configuration 2*

<u>Quantity</u>	<u>Method</u>	<u>Mode 1</u>	<u>Mode 2</u>	<u>Mode 3</u>
frequency	exact	3.5316 +.1085 i	22.003 +.672 i	61.14+1.86 i
loss factor	exact	.06145	.06109	.06092
frequency	RQ (Re[G <sub>v</sub> *])	3.544	22.102	61.47
loss factor	MSE (Re[G <sub>v</sub> *])	.07387	.07339	.07289
frequency	RQ ( G <sub>v</sub> * )	3.573	22.28	61.97
loss factor	MSE ( G <sub>v</sub> * )	.07196	.07167	.07144
frequency	CRQ	3.5785 +.1208 i	22.3105 +.7499 i	62.03 +2.079 i
loss factor	CRQ	.06750	.06723	.0670

*Table 5.5 Predicted Frequencies and Loss Factors for Configuration 3*

<u>Quantity</u>	<u>Method</u>	<u>Mode 1</u>	<u>Mode 2</u>	<u>Mode 3</u>
frequency	exact	2.133+.113 i	13.205+.7053 i	36.43+1.973 i
loss factor	exact	.106	.1068	.1083
frequency	RQ (Re[G <sub>v</sub> *])	2.230	13.85	38.28
loss factor	MSE (Re[G <sub>v</sub> *])	.1378	.1380	.1384
frequency	RQ ( G <sub>v</sub> * )	2.264	14.06	38.87
loss factor	MSE ( G <sub>v</sub> * )	.1320	.1329	.1340
frequency	CRQ	2.272+.1404 i	14.10 +.8757 i	38.98+2.442 i
loss factor	CRQ	.1236	.1241	.1253

In Table 5.6, the undamped frequencies  $\Omega_u$  of the bare cantilever beam for the three configurations are given for the first three modes, and the percent shift in the natural frequency caused by the damping treatment is shown. The undamped frequencies have the following form:

$$\Omega_u = k^2 \sqrt{\frac{E_b I_b}{\rho_b A_b L^4}}$$

where  $k = 1.875, 4.694, 7.855$  for modes 1, 2, and 3 respectively. The shift in natural frequency between the undamped beam and the exact solution becomes:

$$\Delta \% = \frac{Re[\Omega_e^*] - \Omega_u}{\Omega_u} \times 100\%$$

where  $\Omega_e^*$  denotes the complex natural frequency from the exact formulation.

*Table 5.6 Frequency Shifts Due to Addition of the Segmented Damping Treatment.*

Configuration	quantity	Mode 1	Mode 2	Mode 3
Configuration 1	$\Omega_u$	7.91	49.6	138.8
Configuration 1	$\Delta\%$	2.5%	2.3%	2.1%
Configuration 2	$\Omega_u$	3.16	19.8	55.5
Configuration 2	$\Delta\%$	10.4%	9.9%	9.2%
Configuration 3	$\Omega_u$	1.58	19.91	27.8
Configuration 3	$\Delta\%$	25.8%	24.9%	23.8%

### *Discussion of Results*

From Tables 5.3 through 5.5, it may be seen that the approximate methods provide better estimates of natural frequency and damping as the stiffness of the beam increases relative to the damping treatment. This result is expected because the approximate mode shapes for the damped system were derived by assuming that the main beam displacements are approximated by the undamped beam mode shapes.

*Natural Frequency.* For the first three modes examined, the approximate methods produced accurate estimates of the natural frequencies of the system. The frequency errors associated with the approximate methods are seen in Table 5.7. The percent error is defined as follows:

$$\% e = \frac{Re[\Omega_e^*] - Re[\Omega_{approximate}]}{Re[\Omega_e^*]} \times 100\%$$

where the notation  $\Omega_e^*$  denotes the complex natural frequency obtained from the exact formulation in Chapter 4. For almost all configurations, the size of the errors increase a few tenths of a percent as the mode numbers increase. The errors increase significantly with configuration number (i.e., errors associated with configuration 2 are larger than configuration 1, and errors associated with configuration 3 are larger than configuration 2) because the undamped mode shape become a less accurate estimate of the beam deflection. The Complex Rayleigh Quotient frequency errors for configurations 1, 2, and 3 are less

than .15%, 1.5% and 7.0% respectively for all modes considered. When real mode shapes are formed by replacing the complex modulus  $G_v^*$  with its real part, and these mode shapes are used with Rayleigh's Quotient, the resulting frequency errors are less than -.19%, .54% and 5.1% for configurations 1, 2, and 3. The Rayleigh Quotient frequency errors associated with real mode shapes formed by replacing  $G_v^*$  with its magnitude are less than .13%, 1.4% and 6.7% respectively for all modes. The magnitude for the errors using all the methods are relatively closely spaced.

*Table 5.7 Errors in Natural Frequency using Approximate Methods:*

Configuration 1			
	Mode 1	Mode 2	Mode 3
RQ ( $\text{Re}[ G_v^* ]$ )	-.19%	-.17%	-.15%
RQ ( $  G_v^*  $ )	.10%	.11%	.13%
CRQ	.14%	.14%	.15%
Configuration 2			
RQ ( $\text{Re}[ G_v^* ]$ )	.36%	.45%	.54%
RQ ( $  G_v^*  $ )	1.2%	1.3%	1.4%
CRQ	1.3%	1.4%	1.5%
Configuration 3			
RQ ( $\text{Re}[ G_v^* ]$ )	4.6%	4.9%	5.1%
RQ ( $  G_v^*  $ )	6.2%	6.5%	6.7%
CRQ	6.5%	6.8%	7.0%

*Loss Factor:* The loss factor calculations for the three configurations (Table 5.8) show trends similar to the natural frequency calculations. The loss factor errors increase with configuration number because the undamped mode shape becomes a less accurate estimate of the beam deflection of the beam. For all the methods, the values of system loss factor, and the errors associated with them, do not increase significantly with mode number. In this study, the viscoelastic material's loss factor and shear modulus were held constant with frequency, since the purpose was to compare the predictions of various methods. In an actual structure, the loss factors would vary with mode number due to the frequency dependence of the material properties. The errors corresponding to the loss factors obtained from the Complex Rayleigh Quotient for configurations 1, 2, and 3 are less than 3.7%, 10.0% and 16.4 % respectively for all modes considered. These values are a significant improvement over the corresponding Modal Strain Energy results. When the real mode shapes are formulated using the real part of  $G_v^*$ , the Modal Strain Energy errors are less than 11.8%, 20.2%, and 29.7% for configurations 1, 2, and 3. When the real mode shapes formed by using the magnitude of  $G_v^*$ , the Modal Strain Energy errors are 10.4%, 17.3%, and 24.6% respectively. Note that use of the magnitude of  $G_v^*$  when formulating the real mode shapes provides a better estimate for loss factor than using the real part of  $G_v^*$ .

*Table 5.8 Errors in Loss Factors using Approximate Methods:*

Configuration 1

	Mode 1	Mode 2	Mode 3
MSE ( $\text{Re}[G_v^*]$ )	11.8%	11.7%	11.5%
MSE ( $ G_v^* $ )	10.1%	10.3%	10.4%
CRQ	3.5%	3.6%	3.7%

Configuration 2

MSE ( $\text{Re}[G_v^*]$ )	20.2%	20.1%	19.7%
MSE ( $ G_v^* $ )	17.1%	17.3%	17.3%
CRQ	9.8%	10.0%	10.0%

Configuration 3

MSE ( $\text{Re}[G_v^*]$ )	29.7%	29.2%	28.1%
MSE ( $ G_v^* $ )	24.6%	24.4%	23.8%
CRQ	16.4%	16.2%	15.7%

*Chapter Summary*

In this chapter it was shown that complex mode shapes derived from the Correspondence Principle and used in a complex form of Rayleigh's Quotient may be used to estimate the system complex natural frequency. The form of the "Complex Rayleigh Quotient" was derived for both discrete and continuous systems. An expression for loss factor was found from the ratio of imaginary to real parts of the square of the complex

natural frequency. It was shown for the discrete system that this loss factor has a form similar to that identified by Ungar and Kerwin (97:954). It was also shown that if real mode shapes are used to form the strain energies, the loss factor formed from the Complex Rayleigh Quotient has the same form as the loss factor obtained from the Modal Strain Energy method. The use of the Complex Rayleigh Quotient was illustrated using a two degree of freedom system and a bar in extension covered with a constrained layer damping treatment.

Natural frequencies and loss factors of a beam with a segmented constraining layer were also considered. The exact solutions developed in Chapter 4 were compared with estimates from the Complex Rayleigh Quotient and the Modal Strain Energy method. It was shown that the errors of the loss factors produced from the Complex Rayleigh Quotient were much smaller than those obtained from the Modal Strain Energy method. The natural frequency errors from the Complex Rayleigh Quotient were slightly worse than the errors obtained using real mode shapes in Rayleigh's Quotient, but the difference in the frequency errors of the two methods was less than 2%.

## *VI. Constrained Layer Damping on Beams of Circular Cross Section*

Although much has been published on the use of constrained layer damping treatments on beams and plates, most papers have addressed beams of rectangular cross section. While beams with circular cross sections have advantages in situations where the direction of loading is uncertain or a possibility of torsional loading exists, the journal publications that discuss the damping of such beams with constrained layer damping treatments are limited.

Both theory and experiment indicate that a uniform concentric constrained layer on a beam with a circular cross section is not an effective damping treatment for bending vibration (98:328, 103:780). When the circular beam bends, the concentric constraining layer surrounding is also forced to bend due to the near incompressibility of the viscoelastic layer. Thus the concentric constraining layer bends with the same curvature about the same neutral axis. If the standard Bernoulli-Euler assumptions are made regarding the displacements of the main beam and constraining layer, this configuration provides negligible relative motion between beam and constraining layer and thus no shear in the viscoelastic layer (Figure 6.1). The extensional strain in the viscoelastic layer is equivalent to that seen in an extensional damping treatment, a geometry with no constraining layer.

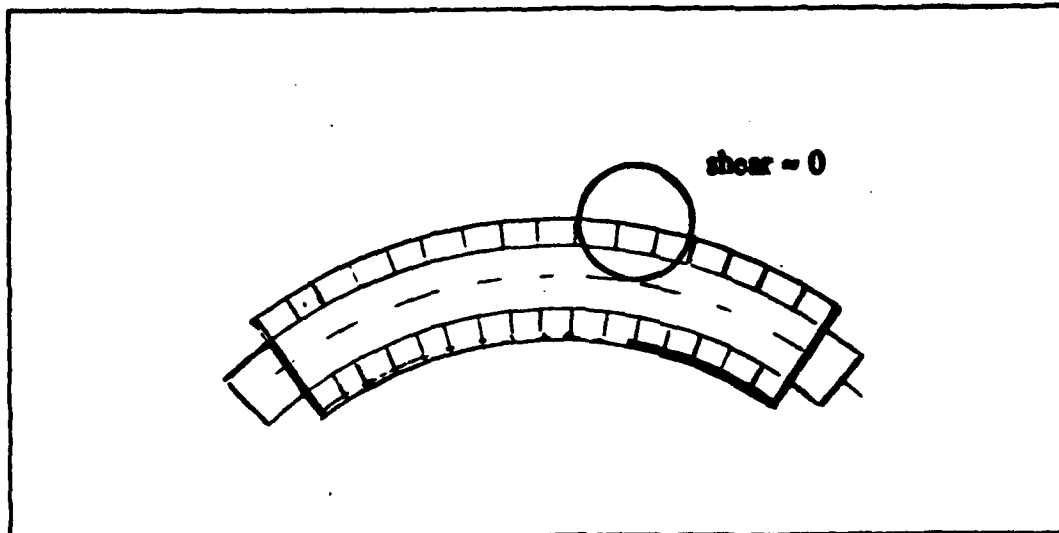


Figure 6.1. Concentric Constraining Layer in Bending

Previous work has indicated that the performance of a concentric constrained layer damping treatment on beams of circular cross section may be improved by cuts parallel to the beam generator lines<sup>1</sup> (98:328). Other articles on the damping of tubular structures have emphasized the importance of segmenting the constraining layer strips to insure their length is near optimal (83:53, 84:10). This previous work suggests that the optimal geometry of damping treatment for a beam of circular cross section consists of narrow strips cut to optimal length that run parallel to the main beam generator lines. The most shear will occur in the damping strips furthest from the neutral axis once the plane of

---

<sup>1</sup> A *generator line* or *generatrix* is a line whose motion generates a surface. The term is used in this chapter to refer to lines parallel to the beam centerline that define the cylindrical surface of the beam. The term "generator strip" is used to identify damping strips whose longest axis is parallel to the generator lines.

bending is established. Since the circular cross-section is axisymmetric and bending may occur in any orientation, all strips are equally important.

In this chapter the equations of motion are developed for a beam with a circular cross section with a constrained layer damping treatment consisting of strips parallel to the beam generator lines. For the case where the strips are narrow and thin, and all strips have identical material properties and dimensions, it is shown that the equations have the same form as the system of equations that describe a rectangular beam with a constrained layer damping treatment. The effects of segmentation of the constraining layer along the beam length are not addressed in this chapter, but once the system of equations is reduced to a form similar to the rectangular beam problem, the methods described in Chapter 5 may be applied.

#### *Beam and Damping Treatment Geometry*

The beam to be analyzed has a circular cross-section and is covered with strips of constrained layer damping treatment running parallel to the generator lines of the cylindrical surface. A cylindrical coordinate system is used in the analysis. The  $z$  axis is coincident with the centerline of the undeformed beam, and the beam neutral plane is identified by values of  $\theta$  equal to  $0$  and  $\pi$ . The transverse beam displacement is in the  $r$  direction at  $\theta = \pi/2$  radians (Figure 6.2). The constraining layer strips are arranged in  $J$  symmetric pairs, and each pair is identified by an index  $j$ . If one of the strips is identified by a central angle  $\theta_j$ , then an identical strip is located at an angle  $\theta_j + \pi$  radians.

Each strip covers an angle  $2\Delta\theta$ . Because of beam symmetry, the displacements of the two constraining layers are equal in magnitude and opposite in direction, and the centroid of the main beam experiences no displacement in the  $z$  direction. The analysis is further simplified by assuming that each pair of constraining layer strips has a matching pair of strips separated by an angle of  $\pi/2$  radians (Figure 6.3). For each strip at angle  $\theta_j$ , there will be an identical strip at angles  $\theta_j+\pi/2$ ,  $\theta_j+\pi$ , and  $\theta_j+3\pi/2$ . It is also assumed that all strips of the constraining layer have the same cross section and material properties, though in some situations the use of different materials for individual strips may help extend the effectiveness of the damping treatment over different temperatures or frequencies.

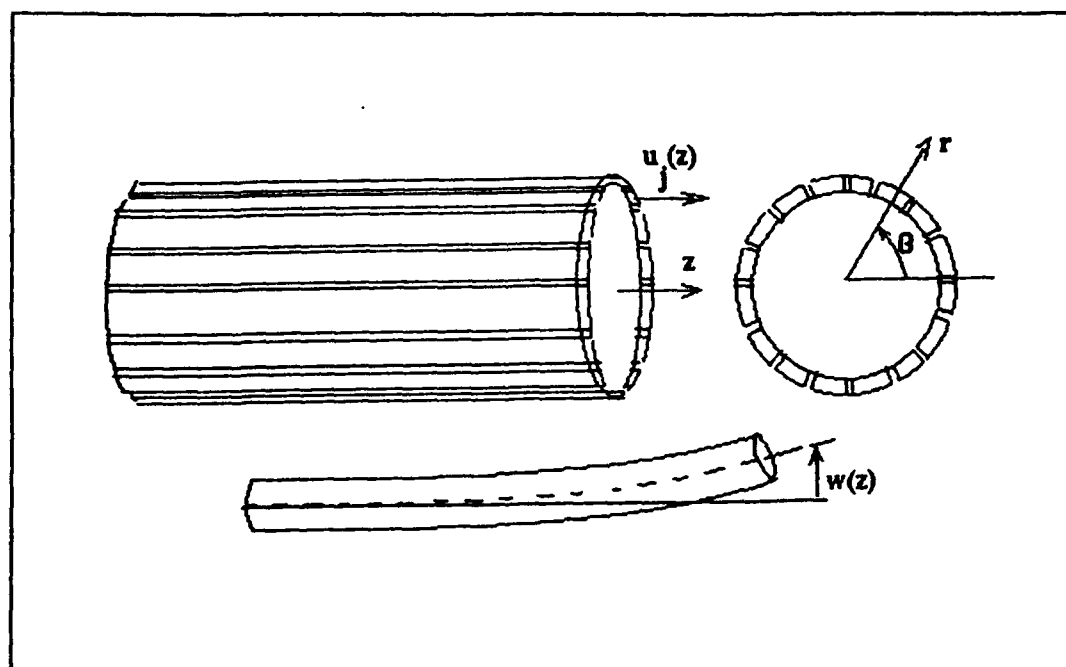


Figure 6.2. Beam Coordinate System

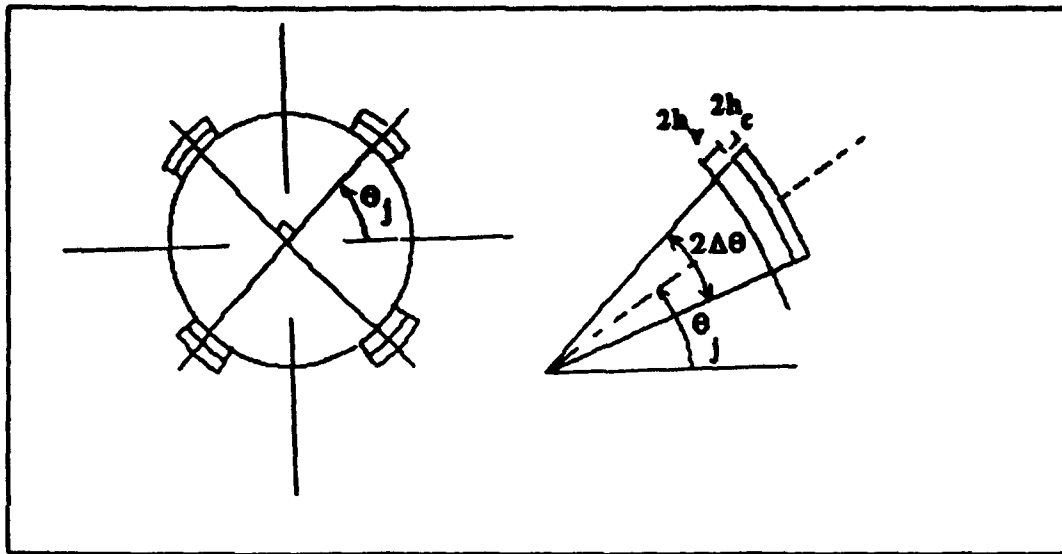


Figure 6.3. Damping Strip Geometry

Throughout the analysis, the subscripts "v" and "c" are used to identify quantities that pertain to the viscoelastic layers and constraining layers of the damping treatment. The viscoelastic layer thickness is  $2h_v$ , and its shear modulus is identified as  $G_v$ , while the constraining layer thickness is  $2h_c$  and its elastic modulus is identified as  $E_c$ .

#### *Assumptions of Displacement and Shear*

The equations of motion will be written in terms of the mode shapes  $w$  and  $u_j$ , which are associated with the transverse displacement of the beam neutral plane and the  $z$  direction displacements of the constraining layer centroid (Figure 6.2). It is assumed that the centroids of the damping treatment move with the same transverse displacement as the main beam. Prior to the separation of spatial and temporal variables, the symbols

functions of the  $z$  coordinate. It is assumed that the centroids of the damping treatment move with the same transverse displacement as the main beam.

To properly define the strain energies in the damping layers, the  $z$  direction displacement of an arbitrary point of the constraining layer must be defined in terms of the variables  $w$  and  $u_j$ . The total displacement of an arbitrary point of the  $j$ th constraining layer at coordinates  $(r, \theta, z)$  may be defined as the sum of the centroid displacement  $u_j$  and the relative displacement:

$$u_{j \text{ total}} = u_j + u_{j \text{ relative}} \quad (6.1)$$

To find  $u_{j \text{ relative}}$ , suppose for a moment that the viscoelastic layer acts as a perfect spacer and resists shear. In this situation, the constraining layer would be forced to flex about the main beam's neutral axis, and the  $z$  direction displacement of an arbitrary point of the constraining layer at location  $(r, \theta, z)$  due to beam flexure would be:

$$u_{\text{flexure}} = - r \sin \theta w' , \quad w' = \frac{dw}{dz} \quad (6.2)$$

Note that  $r \sin \theta$  is the distance of the point from the neutral plane, and Equation (6.2) arises from Bernoulli-Euler beam assumptions. The  $(r, \theta)$  coordinates of the  $j$ th constraining layer centroid are  $r=R+2h_v+h_c$  and  $\theta=\theta_j$ . If the distance between the centerlines of the beam and the constraining layer is defined as  $y_o=R+2h_v+h_c$ , Equation (6.2) may be used to identify the displacement of the constraining layer centroid due to flexure:

$\bar{w} = \bar{w}(z,t)$  and  $\bar{u}_j = \bar{u}_j(z,t)$  will be used. It will be assumed that the solutions have the form  $\bar{w} = w(z) \exp(i\Omega t)$  and  $\bar{u}_j = u_j(z) \exp(i\Omega t)$ .

To properly define the strain energies in the damping layers, the  $z$  direction displacement of an arbitrary point of the constraining layer must be defined in terms of the variables  $w$  and  $u_j$ . The total displacement of an arbitrary point of the  $j$ th constraining layer at coordinates  $(r,\theta,z)$  may be defined as the sum of the centroid displacement  $u_j$  and the relative displacement:

$$u_{j \text{ total}} = u_j + u_{j \text{ relative}} \quad (6.1)$$

To find  $u_{j \text{ relative}}$ , suppose for a moment that the viscoelastic layer acts as a perfect spacer and resists shear. In this situation, the constraining layer would be forced to flex about the main beam's neutral axis, and the  $z$  direction displacement of an arbitrary point of the constraining layer at location  $(r,\theta,z)$  due to beam flexure would be:

$$u_{\text{flexure}} = -r \sin\theta w', \quad w' = \frac{dw}{dz} \quad (6.2)$$

Note that  $r \sin\theta$  is the distance of the point from the neutral plane, and Equation (6.2) arises from Bernoulli-Euler beam assumptions. The  $(r,\theta)$  coordinates of the  $j$ th constraining layer centroid are  $r=R+2h_v+h_c$  and  $\theta=\theta_j$ . If the distance between the centerlines of the beam and the constraining layer is defined as  $y_o=R+2h_v+h_c$ , Equation (6.2) may be used to identify the displacement of the constraining layer centroid due to flexure:

$$u_{j \text{ centroid flexure}} = -y_o \sin \theta_j w' \quad (6.3)$$

By using Equations (6.2) and (6.3), the z direction displacement of an arbitrary point of the constraining layer at (r,θ,z) relative to the centroid may be written as:

$$\begin{aligned} u_{j \text{ relative}} &= u_{\text{flexure}} - u_{j \text{ centroid flexure}} \\ &= (-r \sin \theta + y_o \sin \theta_j) w' \end{aligned} \quad (6.4)$$

Now that the relative displacement is identified, allow the possibility of shear in the viscoelastic layer. The total z direction displacement of an arbitrary point of the constraining layer at coordinates (r,θ,z) may be defined from Equations (6.1) and (6.4):

$$u_{j \text{ total}} = u_j + u_{j \text{ relative}} = u_j + (y_o \sin \theta_j - r \sin \theta) w' \quad (6.5)$$

The resulting z direction extensional strain in the constraining layer at position (r,θ,z) is therefore:

$$\epsilon_{zz_j} = \frac{d(u_{j \text{ total}})}{dz} = u_j' + (y_o \sin \theta_j - r \sin \theta) w'' \quad (6.6)$$

The expression for constraining layer displacement in Equation (6.5) may also be used to find the shear strain in the viscoelastic layer. From Bernoulli-Euler beam assumptions, the main beam surface deflection at position θ is  $u_{\text{substrate}} = -R \sin \theta w'$ . If it is assumed that the shear strain is constant through the thickness of the viscoelastic layer, the viscoelastic shear at any position θ may be written as:

$$\begin{aligned}
\gamma_{rz} &= \frac{u_j \cos(r=R+2h_v) - u_{substrate}}{2h_v} + \sin\theta w' \\
&= \frac{u_j + [y_o \sin\theta_j - (R+2h_v) \sin\theta] w' + R \sin\theta w'}{2h_v} + \sin\theta w' \quad (6.7) \\
&= \frac{u_j + y_o \sin\theta_j w'}{2h_v}
\end{aligned}$$

Notice that the expression for shear is independent of the  $\theta$  coordinate. This indicates that the viscoelastic shear strain is constant over the cross sectional area of a single strip, though the strain will vary with the distance of the strip centroid from the neutral plane.

#### *Developing the Equations of Motion*

In this section, expressions for kinetic and strain energies of the beam and damping strips are developed, the variations of these energies are obtained, then the equations of motion are developed using Hamilton's Principle. The strain energies from the flexure of the main beam, the shear in the individual viscoelastic layers, and the extension and flexure of the constraining layers are included in the formulation, as well as the kinetic energy resulting from the transverse displacement of the beam and the damping layers. The energies due to rotatory inertia and shear deformation in the main beam are ignored because the beam modal length is large compared to beam height. The potential energy from the extension of the viscoelastic layer is also neglected since its modulus is much smaller than those of the constraining layer and main beam. The energy

modulus is much smaller than those of the constraining layer and main beam. The energy terms used in the analysis are similar to those considered by DiTaranto (17:881) and Mead and Markus (59:163) in their evaluations of rectangular beams with an added constraining layer.

It is assumed that the beam and the  $J$  pairs of damping strips all move with the same transverse displacement. All the strips have the same cross sectional area and material properties, so the total kinetic energy of the system is:

$$T_{total} = \frac{1}{2} \int_0^L m_t \left[ \frac{\partial \tilde{w}}{\partial t} \right]^2 dz \quad (6.8)$$

$$m_t = \sum \rho A = \rho_b A_b + 2J [\rho_c A_c + \rho_v A_v]$$

With the assumption that  $\tilde{w}(z,t) = w(z) \exp(i\Omega t)$ , the variation of the kinetic energy becomes:

$$\delta T_{total} = - \int_0^L \Omega^2 m_t w \delta w dz \quad (6.9)$$

The strain energy of the main beam due to bending, and the variation of that energy, has the following form:

$$U_b = \frac{1}{2} \int_0^L E_b I_b w''^2 dz, \quad \delta U_b = \int_0^L E_b I_b w'' \delta w'' dz \quad (6.10)$$

After integrating by parts, the variation of the beam strain energy becomes:

$$\delta U_b = \int_0^L E_b I_b w'''' \delta w dz + E_b I_b w'' \delta w' \Big|_{z=0,L} - E_b I_b w''' \delta w \Big|_{z=0,L} \quad (6.11)$$

Consider the  $j$ th constraining layer, identified by its central angle  $\theta_j$ . The extensional strain identified in Equation (6.6) yields a strain energy of the following form:

$$U_{c_j} = \frac{1}{2} \iiint E_c \epsilon_{z_j}^2 dV_c \quad (6.12)$$

$$= \frac{1}{2} \int_0^L \int_{y_o-h_c}^{y_o+h_c} \int_{\theta_j-\Delta\theta}^{\theta_j+\Delta\theta} E_c [u_j' + y_o \sin\theta_j w'' - r \sin\theta w'']^2 r d\theta dr dz$$

The variation of this strain energy becomes:

$$\delta U_{c_j} = \iiint \left\{ E_c [ (u_j' + y_o \sin\theta_j w'') - r \sin\theta w'' ] \delta u_j' \right. \\ \left. + E_c [ y_o \sin\theta_j (u_j' + y_o \sin\theta_j w'') - r \sin\theta (u_j' + y_o \sin\theta_j w'') \right. \\ \left. + (r^2 \sin^2\theta - r \sin\theta y_o \sin\theta_j) w'' \right] \delta w'' \} dV_c \quad (6.13)$$

The variables  $u_j$  and  $w$  and the constants  $y_o$ ,  $\theta_j$ , and  $E_c$  do not vary across the cross section, so Equation (6.13) may be integrated over the constraining layer cross sectional area. To simplify the resulting expression, define the following terms:

$$A_c = \iint dA_c = 4 h_c \Delta\theta y_o \quad (6.14)$$

$$I_j = \iint r^2 \sin^2\theta dA_c = 2 y_o h_c (y_o^2 + h_c^2) \left[ \Delta\theta - \frac{1}{2} \cos(2\theta_j) \sin(2\Delta\theta) \right] \quad (6.15)$$

$$\underline{A}y = 4 h_c \sin(\Delta\theta) (y_o^2 + \frac{1}{3} h_c^2), \quad \iint r \sin\theta dA_c = \underline{A}y \sin\theta_j \quad (6.16)$$

Note that if the damping strips are narrow and thin, then  $\sin(\Delta\theta) \approx \Delta\theta$ ,  $y_o^2 + 1/3 h_c^2 \approx y_o^2$ , and  $\underline{A}y$  is approximately equal to  $A_c y_o$ . By integrating Equation (6.13) and using

Equations (6.14) through (6.16), the variation of the strain energy may be written in the following form:

$$\begin{aligned} \delta U_{c_j} = \int_0^L \{ & E_c [ A_c u_j' + \sin\theta_j (A_c y_o - \Delta y) w'' ] \delta u_j' \\ & + E_c [ (A_c y_o - \Delta y) \sin\theta_j (u_j' + y_o \sin\theta_j w'') + (I_j - y_o \sin^2\theta_j \Delta y) w'' ] \delta w'' \} dz \end{aligned} \quad (6.17)$$

Define the following geometrical parameters to simplify the expression for  $\delta U_{c_j}$ :

$$\Delta(Ay) = (A_c y_o - \Delta y) = 4h_c \left( \Delta\theta y_o^2 - \sin(\Delta\theta) \left( y_o^2 + \frac{1}{3} h_c^2 \right) \right) \quad (6.18)$$

$$I_{t_j} = (I_j - y_o \sin^2\theta_j \Delta y) \quad (6.19)$$

After substituting these parameters into Equation (6.17) and integrating by parts, the  $\delta u_j$  and  $\delta w$  terms may be collected:

$$\begin{aligned} \delta U_{c_j} = \int_0^L \{ & [ -E_c A_c u_j'' - E_c \Delta(Ay) \sin\theta_j w''' ] \delta u_j \\ & + [ E_c I_{t_j} w'''' + E_c \Delta(Ay) \sin\theta_j (u_j''' + y_o \sin\theta_j w'''' ) ] \delta w \} dz \\ & + [ E_c A_c u_j' + E_c \Delta(Ay) \sin\theta_j w'' ] \delta u_j |_{z=0,L} \\ & + [ E_c I_{t_j} w'' + E_c \Delta(Ay) \sin\theta_j (u_j' + y_o \sin\theta_j w'') ] \delta w' |_{z=0,L} \\ & - [ E_c I_{t_j} w''' + E_c \Delta(Ay) \sin\theta_j (u_j'' + y_o \sin\theta_j w''') ] \delta w |_{z=0,L} \end{aligned} \quad (6.20)$$

Consider the strip of identical cross section located opposite the  $j$ th strip, with center angle equal to  $\underline{\theta}_j = \theta_j + \pi$  radians. The  $z$  direction displacement of the opposing strip,  $\underline{u}_j$ , will be equal in magnitude and opposite in direction to the  $z$  direction

displacement of the original strip. The parameters  $A_y$ ,  $\Delta(Ay)$ ,  $I_y$ , and  $y_o$  are unchanged for the opposing strip, while  $\sin \theta_j = -\sin\theta_j$ ,  $u_j = -u_j$ , and  $\delta u_j = -\delta u_j$ . As a result, the variation of the strain energy of the opposing strip is identical to Equation (6.20), and the variation of the pair of strips may be written as  $2 \delta U_{e,j}$ .

The strain energy in the viscoelastic layer of the  $j$ th strip due to shear is uniform across the cross section:

$$U_{v_j} = \frac{1}{2} \int_0^L G_v A_v \gamma_{\tau z_j}^2 dz = \frac{1}{2} \int_0^L \frac{G_v A_v}{(2h_v)^2} [u_j + y_o \sin\theta_j w']^2 dz \quad (6.21)$$

where  $A_v$  is the area of the cross-section of the viscoelastic layer:

$$A_v = 4h_v(R+h_v)\Delta\theta \quad (6.22)$$

After integrating by parts and collecting terms, the variation of the viscoelastic strain energy has the following form:

$$\begin{aligned} \delta U_{v_j} = & \int \frac{G_v A_v}{(2h_v)^2} [(u_j + y_o \sin\theta_j w') \delta u_j - y_o \sin\theta_j (u_j' + y_o \sin\theta_j w'') \delta w] dz \\ & + \frac{G_v A_v}{(2h_v)^2} y_o \sin\theta_j [u_j + y_o \sin\theta_j w'] \delta w \Big|_{z=0,L} \end{aligned} \quad (6.23)$$

Because the viscoelastic layers of the  $\theta_j$  and  $\theta_j + \pi$  strips have the same strain energies, the variation of the strain energy for the pair of strips is  $2 \delta U_{v,j}$ .

To develop the equations of motion for a beam with  $J$  pairs of strips, the variation of the energies for all the strips is required. Because  $w$ ,  $G_v$ ,  $A_v$ ,  $h_v$ , and  $y_o$  do not vary

with the strip number, the total strain energy in the viscoelastic layers of J pairs of strips may be written as:

$$\begin{aligned}
 \delta U_{v_{total}} &= 2 \sum_{j=1}^J \delta U_{v_j} \\
 &= \int \frac{2G_v A_v}{(2h_v)^2} \left\{ \sum_{j=1}^J [(u_j + y_o \sin\theta_j w') \delta u_j] - \sum_{j=1}^J [y_o \sin\theta_j (u_j' + y_o \sin\theta_j w'')] \delta w \right\} dz \\
 &\quad + \frac{2G_v A_v y_o}{(2h_v)^2} \sum_{j=1}^J [\sin\theta_j (u_j + y_o \sin\theta_j w')] \delta w \Big|_{z=0,L}
 \end{aligned} \tag{6.24}$$

The variation of the constraining layer energy for the J pairs of strips may be adapted from Equation (6.20):

$$\begin{aligned}
 \delta U_{c_{total}} &= \int \left\{ \sum_{j=1}^J [(-2E_c A_c u_j'' - 2E_c \Delta(Ay) \sin\theta_j w''')] \delta u_j \right\} \\
 &\quad + \sum_{j=1}^J [2E_c I_{t_j} w'''' + 2E_c \Delta(Ay) \sin\theta_j (u_j''' + y_o \sin\theta_j w''')] \delta w \Big| dz + B.T.
 \end{aligned} \tag{6.25}$$

where B.T. designates the boundary terms in  $\delta U_{c_{total}}$  :

$$\begin{aligned}
 B.T. &= \sum_{j=1}^J [ [2E_c A_c u_j' + 2E_c \Delta(Ay) \sin\theta_j w'' ] \delta u_j \Big|_{z=0,L} ] \\
 &\quad + \left\{ \sum_{j=1}^J [2E_c I_{t_j} w'' + \sum_{j=1}^J [2E_c \Delta(Ay) \sin\theta_j (u_j' + y_o \sin\theta_j w'')] \right\} \delta w' \Big|_{z=0,L} \\
 &\quad - \left\{ \sum_{j=1}^J [2E_c I_{t_j} w''' + \sum_{j=1}^J [2E_c \Delta(Ay) \sin\theta_j (u_j'' + y_o \sin\theta_j w''')] \right\} \delta w \Big|_{z=0,L}
 \end{aligned} \tag{6.26}$$

The variational energies identified in Equations (6.9), (6.10), (6.24) and (6.25) can be used in Hamilton's Principle, which will have the following form:

$$\begin{aligned}
& \delta U_b + \delta U_{v_{total}} + \delta U_{c_{total}} - \delta T_{total} = 0 \\
& = \int_0^L \left\{ \sum_{j=1}^J [ \dots ] \delta u_j \right\} + [ \dots ] \delta w \} dz \quad (6.27) \\
& + ( \dots ) \delta w |_{0,L} + ( \dots ) \delta w' |_{0,L} + ( \dots ) \delta u |_{0,L}
\end{aligned}$$

The variational energies consist of a combination of terms within an integral over  $z$ , as well as a set of boundary terms. Hamilton's principle is satisfied by setting the arguments of the  $\delta w$  and  $\delta u_j$  terms equal to zero in Equation (6.27). By setting the bracketed terms within the integrand of Equation (6.27) equal to zero, the equations of motion are identified:

$$u_j'' - g_r u_j = g_r y_o \sin \theta_j w' - \frac{\Delta(Ay)}{A_c} \sin \theta_j w''', \quad j = 1 \dots J \quad (6.28)$$

$$\begin{aligned}
EI_{total} w'''' - \frac{2 G_v A_v}{(2h_v)^2} \sum_{j=1}^J [ y_o \sin \theta_j (u_j' + y_o \sin \theta_j w'') ] - \Omega^2 m_t w \\
= 2 E_c \Delta(Ay) \sum_{j=1}^J \sin \theta_j (u_j''' + y_o \sin \theta_j w'''' )
\end{aligned} \quad (6.29)$$

where

$$\begin{aligned}
g_r = \frac{G_v A_v}{(2h_v)^2 A_c E_c} = \frac{G_v (R+h_2)}{4h_v h_c E_c (R+2h_2+h_3)} \quad (6.30) \\
EI_{total} = E_b I_b + 2 \sum_{j=1}^J [ E_c I_t ]
\end{aligned}$$

The boundary terms from Equation (6.27) provide the following boundary conditions:

$$\left[ E_c A_c u_j' + E_c \Delta(Ay) \sin\theta_j w'' \right] \delta u_j \Big|_{x=0, L} = 0, \quad j = 1 \dots J \quad (6.31)$$

$$\left[ EI_{total} w'' + 2 E_c \Delta(Ay) \sum_{j=1}^J \sin\theta_j (u_j' + y_o \sin\theta_j w'') \right] \delta w' \Big|_{x=0, L} = 0 \quad (6.32)$$

$$\left[ EI_{total} w''' - \frac{2 G_v A_v y_o}{(2h_v)^2} \sum_{j=1}^J [\sin\theta_j (u_j + y_o \sin\theta_j w')] \right. \\ \left. + 2 E_c \Delta(Ay) \sum_{j=1}^J \sin\theta_j (u_j'' + y_o \sin\theta_j w''') \right] \delta w \Big|_{x=0, L} = 0 \quad (6.33)$$

Because the strips are applied to the beam in sets of four, where each pair of strips has a complementary pair  $\pi/2$  radians away, the summations of the  $\sin^2\theta_j$  terms may be written in a simple form:

$$\sum_{j=1}^J \sin^2\theta_j = \sum_{j=1}^{\frac{J}{2}} [\sin^2\theta_j + \sin^2(\theta_j + \pi/2)] = \frac{J}{2} \quad (6.34)$$

With this substitution, the differential equations become:

$$u_j'' - g_r u_j = g_r y_o \sin\theta_j w' - \frac{\Delta(Ay)}{A_c} \sin\theta_j w''', \quad j = 1 \dots J \quad (6.35)$$

$$EI_{total} w'''' - \frac{G_v A_v y_o}{(2h_v)^2} [2 \sum_{j=1}^J (\sin\theta_j u_j') + J y_o w''] - \Omega^2 m_t w \\ = E_c \Delta(Ay) [2 \sum_{j=1}^J (\sin\theta_j u_j''') + J y_o w''''] \quad (6.36)$$

*Special Case: Equations of Motion for Thin Narrow Damping Strips.*

In this section, the case where the damping strips are thin and narrow will be considered. For this configuration, the parameter  $\Delta(Ay)$  defined in Equation (6.18) is small compared to the value of  $A_c y_o$  or  $\underline{Ay}$ :

$$\Delta(Ay) = (A_c y_o - \underline{Ay}) = 4h_c \left( \Delta\theta y_o^2 - \sin(\Delta\theta) \left( y_o^2 + \frac{1}{3}h_c^2 \right) \right) \quad (6.37)$$

In the equations of motion (Equations (6.35)-(6.36)) and boundary conditions (Equations (6.31)-(6.33)),  $\Delta(Ay)$  appears with higher order derivatives of  $u$  and  $w$ . For most configurations of interest, the magnitude of these derivatives decrease with order. (As an example, consider the derivatives of a pinned-pinned beam whose mode shape is  $w = \sin(n\pi z/L)$ .) For the case of thin, narrow strips, the terms containing  $\Delta(Ay)$  can be disregarded, and the equations of motion and boundary conditions may be simplified:

$$u_j'' - g_r u_j = g_r y_o \sin\theta_j w', \quad u_j' \delta u_j |_{z=0,L} = 0, \quad j=1 \dots J \quad (6.38)$$

$$EI_{total} w'''' - \frac{G_v A_v y_o}{(2h_v)^2} \left[ 2 \sum_{j=1}^J (\sin\theta_j u_j) + J y_o w' \right] - \Omega^2 m_t w = 0 \quad (6.39)$$

$$\left[ EI_{total} w'''' - \frac{G_v A_v y_o}{(2h_v)^2} \left( 2 \sum_{j=1}^J (\sin\theta_j u_j) + J y_o w' \right) \right] \delta w \Big|_{z=0,L} = 0 \quad (6.40)$$

$$EI_{total} w'' \delta w' \Big|_{z=0,L} = 0 \quad (6.41)$$

Consider Equation (6.38), the second order differential equation in  $u_j$ . If somehow the function  $w'$  was known, then a solution for  $u_j$  could easily be found for a strip located at  $\theta_j = \pi/2$ . If such a solution was identified as  $u_1$ , the defining equation for  $u_1$  and its corresponding boundary condition could be written in terms of a linear operator,  $L$ :

$$L [ u_1 ] = g_r y_o w' , \quad u_1' \delta u_1 |_{z=0,L} = 0 \quad (6.42)$$

where

$$L = \left[ \frac{d^2}{dz^2} - g_r \right] \quad (6.43)$$

If both sides of Equation (6.42) are multiplied by  $\sin \theta_j$ , the term can be brought within the linear operator:

$$\sin \theta_j L [ u_1 ] = L [ \sin \theta_j u_1 ] = g_r y_o \sin \theta_j w' \quad (6.44)$$

The boundary conditions associated with  $u_1$  may also be manipulated to contain the term  $u_1 \sin \theta_j$  :

$$u_1' \delta u_1 |_{z=0,L} = 0 \quad \rightarrow \quad (u_1 \sin \theta_j)' \delta (u_1 \sin \theta_j) |_{z=0,L} = 0 \quad (6.45)$$

By comparing Equations (6.44) and (6.45) with Equation (6.38), it can be seen that the expression  $u_1 \sin \theta_j$  satisfies the equations and boundary conditions that define  $u_j$ . When the substitution  $u_j = u_1 \sin \theta_j$  is made in Equations (6.38) through (6.41), and the relation  $\sum \sin^2 \theta_j = J/\Omega$  is applied, the equations may be written as:

$$u_j = \sin\theta_j u_1, \quad j = 1 \dots J \quad (6.46)$$

$$u_1'' - g_r u_1 = g_r y_o w', \quad u_1' \delta u_1 \Big|_{z=0,L} = 0 \quad (6.47)$$

$$EI_{total} w'''' - \frac{G_v A_v y_o J}{(2h_v)^2} [u_1' + y_o w''] - \Omega^2 m_v w = 0 \quad (6.48)$$

$$EI_{total} w'' \delta w' \Big|_{z=0,L} = 0, \quad EI_{total} w'''' - \frac{G_v A_v y_o J}{(2h_v)^2} [u_1' + y_o w''] \delta w \Big|_{z=0,L} = 0 \quad (6.49)$$

The equations in  $u_1$  and  $w$  have the same form as the coupled system of equations developed in Chapter 4 for the rectangular beam, though the definitions of the constants are different for the two configurations. The rectangular beam equations have been solved in the literature for various boundary conditions (76:271). After proper interpretation of the constants in the equation, the rectangular beam results may be applied to the problem of a beam of circular cross section covered with thin narrow strips.

Once  $u_1$  and  $w$  are known for a given set of boundary conditions, the relationship  $u_j = u_1 \sin\theta_j$  may be used to determine the contributions of the other strips to the damping of the entire beam. By combining this relationship with Equation (6.7), the viscoelastic shear strain for the  $j$ th strip can be written in terms of the shear strain of the strip with  $\theta_j = \pi/2$ :

$$\gamma_{rz_j} = \frac{u_j + y_o \sin \theta_j w'}{2h_v} = \sin \theta_j \gamma_{rz_1} \quad (6.50)$$

This expression can be used to develop a relationship between the viscoelastic strain energies of the two strips:

$$U_{v_j} = \sin^2 \theta_j U_{v_1} \quad (6.51)$$

For systems where the beam strain energy is large compared to the energies of the damping strips, and the damping of the constraining layer and beam is negligible, the Modal Strain Energy method provides the following approximation to the system loss factor:

$$\eta_{\text{system}} = \frac{2 \sum_{j=1}^J \eta_v U_{v_j}}{U_b + 2 \sum_{j=1}^J U_{v_j} + 2 \sum_{j=1}^J U_{c_j}} \approx \frac{2 \sum_{j=1}^J \eta_v U_{v_j}}{U_b} \quad (6.52)$$

where

$$U_{v_j} = \frac{1}{2} \int_0^L G_v A_v \gamma_{rz_j}^2 dz \quad (6.53)$$

By using the relationships between the  $j$ th strip and the strip at  $\theta_j = \pi/2$ , the loss factor may be written as:

$$\eta_{\text{system}} \approx 2 \sum_{j=1}^J \sin^2 \theta_j \frac{\eta_v U_{v_1}}{U_b} = \frac{J \eta_v U_{v_1}}{U_b} \quad (6.54)$$

Because there are a total of  $2J$  strips on the beam, this result indicates that the energy dissipated by a full set of strips on the beam of circular cross section is equivalent to the energy that would be dissipated by half the total number of strips at a distance  $R$  from the neutral axis. Loss factors are a function of both the energy dissipated and the total strain energy of the beam, so a comparison of loss factors for damped beams with rectangular and circular cross sections will depend on the cross sections considered. The loss factor of a damped beam with a solid circular cross section is .65 times the size of the loss factor of a beam with a solid square cross section that has the same bending stiffness and the same coverage of constrained layer damping treatment.

#### *Chapter Summary*

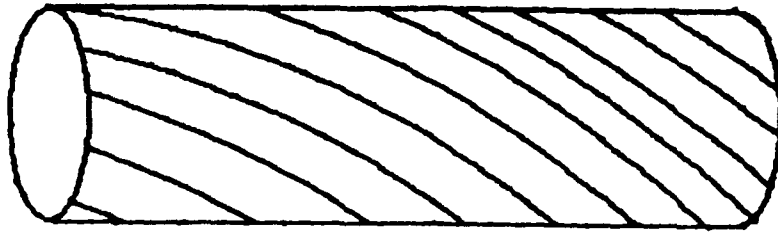
In this chapter, the equations of motion were developed for a beam of circular cross section damped with a constrained layer damping treatment. The damping treatment consisted of constrained layer damping strips placed parallel to the beam generator lines. It was shown that the equations simplify for configurations where the strips are placed in sets of 4, where each strip within the set is separated by an angle of  $\pi/2$  radians. For the special case of thin narrow damping strips, it was shown that the equations of motion have the same form as the equations derived in Chapter 4 for the damped rectangular beam. This result enables the approaches developed for the rectangular beam to be applied directly to beams of circular cross section.

## VII. *The Barberpole: Damping in Bending and Torsion*

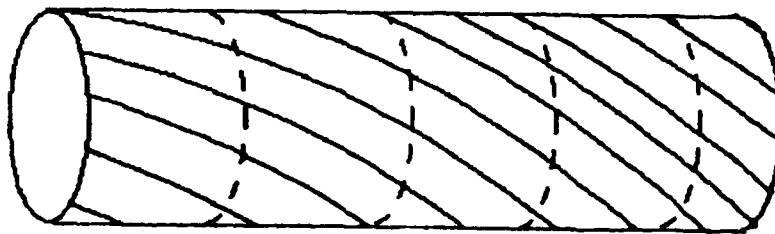
In this chapter, a new constrained layer damping configuration is proposed for beams of circular cross section that may experience both bending and torsional vibrations. The "barberpole" configuration consists of narrow strips of damping treatment oriented at an angle with respect to the generators<sup>1</sup> of the beam's cylindrical surface. The individual damping strips may be continuous over the length of the beam, or periodically segmented along the strip length (Figure 7.1). A quasistatic analysis is developed to evaluate the effectiveness of the barberpole configuration for damping bending and torsional vibrations. It is shown that damping for both bending and torsion is attainable with the same damping treatment if the constraining layer strips are periodically segmented. It is also shown that for the pure bending problem, the unsegmented barberpole geometry provides an improvement in damping over unsegmented straight strips. At each crossing of the beam neutral plane, the constraining layer is free of extensional stress, which provides a "virtual segmentation" effect. This virtual segmentation provides an alternative to conventional segmentation of the damping layer when the more conventional approach is undesirable due to environmental or operational reasons.

---

<sup>1</sup> A *generator line* or *generatrix* is a line whose motion generates a surface. The term is used in this chapter to refer to lines parallel to the beam neutral axis that define the cylindrical surface of the beam. The term "generator strip" is used to identify damping strips whose longest axis is parallel to the generator lines.



7.1a. Unsegmented Barberpole



7.1b. Segmented Barberpole

Figure 7.1. Barberpole Configurations

### *Overview of the Bending and Torsion Problem*

In Chapter 6 it was noted that previous research on constrained layer damping treatments for cylindrical beams in bending (84:HBA, 98:328) has shown that the optimal constrained layer configuration consists of series of narrow strips segmented to optimal length that are placed along the beam generator lines. One's intuition would suggest that narrow generator strips are not an effective configuration for damping torsional vibrations, and this is confirmed by the analysis presented in this chapter. For the damping treatment to be effective, the constraining layer must resist the motion of the beam surface to induce strain in the viscoelastic layer. When the beam is in torsion, the beam surface is in pure shear, and narrow constraining layer strips parallel to the generator lines do not effectively resist this shear. Narrow strips applied along the principal axes of strain at an angle of  $\pi/4$  radians relative to the beam generator lines provide maximum resistance to this deformation, and the relative displacements of the beam surface and the constraining layer induce shear in the viscoelastic layer. Strips aligned at a angle other than  $\pi/4$  radians will also produce some resistance to surface deformations caused by torsion.

If a structural element is to be subjected to both bending and torsional vibrations, damping for both can be accomplished by the proposed barberpole configuration. The analysis in this chapter confirms that the optimal constrained layer treatment for bending vibrations consists of circumferentially narrow constrained layer strips aligned parallel to the beam axis that are cut to an optimal length, while the optimal pitch angle of such strips on a beam subjected to torsion is  $\pi/4$  radians. The optimal treatment for a mixture

of vibrations is some angle between these two extremes, and depends on the relative importance of torsional damping in the problem. The choice of pitch angle in the mixed-vibration problem is analogous to determining the "optimal" ply configuration of a composite material; the optimal pitch angle depends upon the combination of bending and torsion loads expected.

The segmented length of the constraining layer strip is also a design variable. It will be shown that the optimal length analysis of Plunkett and Lee can be applied directly to the torsional problem for any choice of pitch angle. The analysis may also be applied directly to the bending problem when the pitch angle is zero, and the strips are parallel to the beam surface generator lines. A nonzero pitch angle produces non-uniform strain in the surface, and the effects of such non-uniformity on optimal length were examined in Chapter 3.

It should be noted that if the beam to be damped is part of a larger structural assembly, the frequencies of concern are often associated with mode shapes of the structure, and not the beam itself. In such a situation, the damping should be optimized at the natural frequencies of the "global modes" of the assembly (84:HBA). Because in such cases the frequencies are very low, a quasistatic analysis would better model the behavior of the damping treatment in the frequency range of concern than an analysis at the natural frequency of the damped beam.

### Beam Geometry and Coordinate Systems

The beam to be analyzed has a circular cross section of radius  $R$ . The  $(r, \theta, z)$  coordinate system may be used to describe the beam and constraining layers, where the  $z$  axis is coincident with the axis of the undeformed beam and the  $\theta=0$  line is aligned with the beam neutral plane. Consider a narrow rectangular damping strip with its longest dimension oriented at an angle  $\alpha$  relative to the beam  $z$  axis (Figures 7.2 and 7.3). The length of the damping strip is  $2l$ , its width is  $2b$ , and the viscoelastic layer and constraining layer thicknesses are  $2h_v$  and  $2h_c$  respectively. The beam's cross section is assumed to be much larger than that of the constraining layer, thus, for this analysis, a "substrate approach" is appropriate. It is assumed that the beam surface displacements are specified and are unaffected by the damping treatment. This assumption has been used in previous analyses of constraining layers on flat plates (73:150).

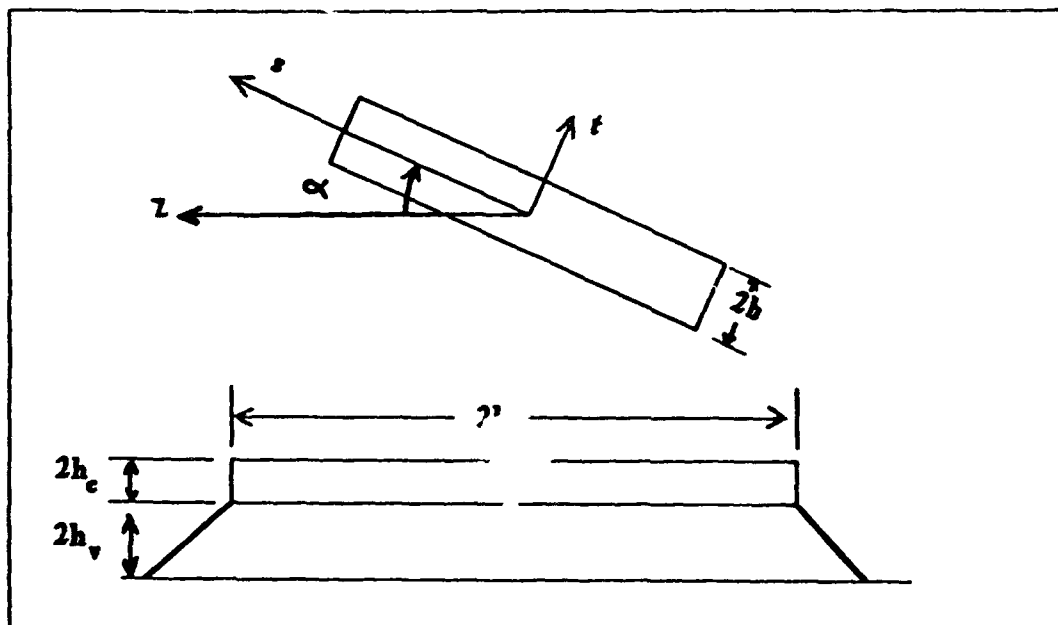


Figure 7.2. Barberpole Damping Strip Geometry

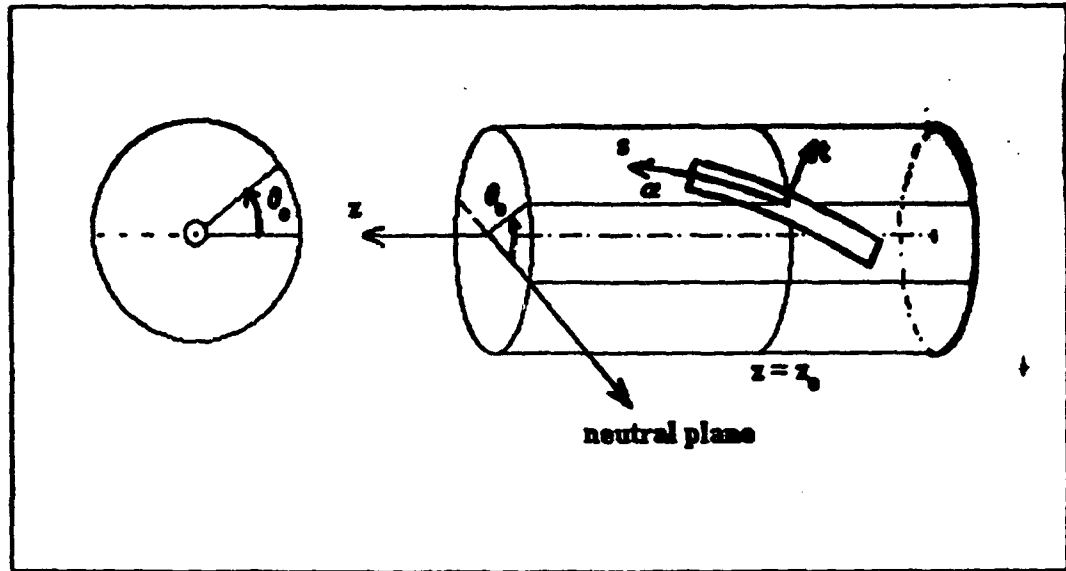


Figure 7.3. Barberpole Coordinate Systems

A local coordinate system may be developed that is better suited to developing the constraining layer equations of motion. With the beam in its undeformed position, define a local  $s$ - $t$  coordinate system centered on the beam surface under the constraining layer centroid, and oriented in the principal directions of the damping treatment (Figure 7.3). Define the  $s$ - $t$  axes in the direction of the  $z$ - $\theta$  axes after a clockwise rotation of angle  $\alpha$ , where it is assumed that  $-\pi/2 < \alpha < \pi/2$ . The  $s$  coordinate is aligned with the damping strip's longest dimension, and  $s$  is positive in the direction of increasing  $z$ . The pitch angle  $\alpha$  is positive when an increase in  $s$  results in an increase in the  $\theta$  coordinate. Let  $(\theta_0, z_0)$  identify the  $(\theta, z)$  coordinate of the origin of the  $s$ - $t$  coordinate system. The transformation between the two systems is:

$$z = z_0 + s \cos \alpha + t \sin \alpha \quad \theta = \theta_0 + \frac{s \sin \alpha + t \cos \alpha}{R} \quad (7.1)$$

but the equations of motion for both the torsional and bending analysis will be written in the  $s-t$  coordinate system.

### Torsional Analysis

**Surface Displacements for Torsional Loading.** The displacements of the beam surface are found for the torsional problem by assuming a uniform twisting moment through the beam. Consider a cantilever beam or bar with a twisting moment applied to its free end. Each cross section of the beam experiences a rotation proportional to its distance from the fixed end that may be written as  $\Theta(z) = C_T z$ , where  $C_T$  is the twist per unit length (Figure 7.4). This is equivalent to a quasistatic loading assumption.

Because the bar has a circular cross section, there is no warping. The surface displacement in the  $z$  direction is zero, and the surface displacement in the  $\theta$  direction is  $RC_T z$ . The surface displacements in the  $s$  and  $t$  directions are defined as  $w_s$  and  $w_t$ :

$$\begin{aligned} w_s &= RC_T \sin\alpha (z_0 + s \cos\alpha - t \sin\alpha) \\ w_t &= RC_T \cos\alpha (z_0 + s \cos\alpha - t \sin\alpha) \end{aligned} \quad (7.2)$$

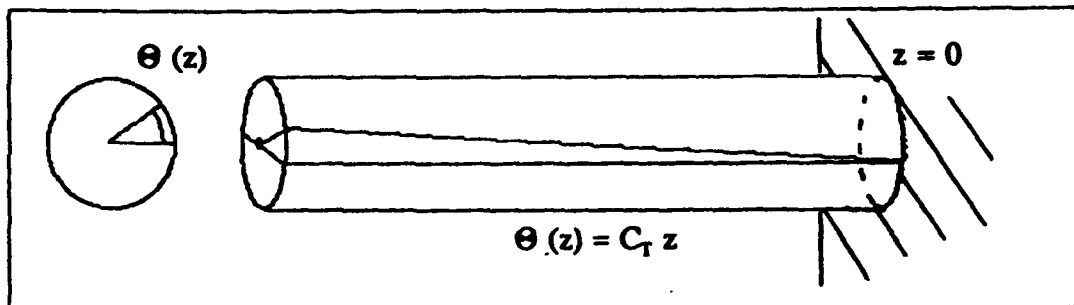


Figure 7.4. Torsional Displacement

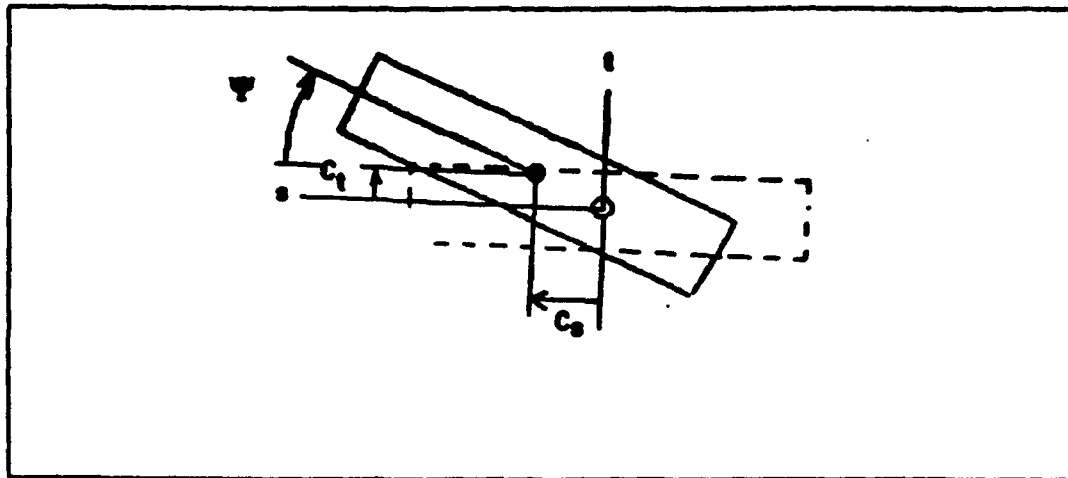


Figure 7.5. Torsional Rigid Body Analysis: Constraining Layer Deflections

*Equations of Motion for a Rigid Constraining Layer.* In this section, a set of equations are developed for the constraining layer using principles of equilibrium. The Correspondence Principle is invoked, and the viscoelastic shear modulus  $G_v$  is treated as a real constant while the equations are formulated and solved for the corresponding elastic problem. For all loads in the  $s$ - $t$  directions, it is assumed that the constraining layer acts like a rigid body, resisting both shear and extensional deformations. To satisfy equilibrium, the total moment and forces in the  $s$ - $t$  plane applied by the viscoelastic layer to the constraining layer must equal zero.

In the rigid constraining layer formulation, the centroid of the constraining layer undergoes a displacement  $C_t$  and  $C_s$  in the  $s$  and  $t$  directions, and the strip also undergoes a small rigid body rotation  $\psi$  ( $\Psi$ ) (Figure 7.5). Each point on the constraining layer moves from its original position on the beam surface. The displacement of an arbitrary

point may be written in terms of the three rigid body displacements. Let  $u_s$  and  $u_t$  be the displacements in the  $s$  and  $t$  directions of an arbitrary point on the constraining layer originally located at coordinates  $(s,t)$ :

$$u_s = C_s - t \Psi, \quad u_t = C_t + s \Psi \quad (7.3)$$

The shear strains in the viscoelastic layer are assumed uniform through the thickness, and are defined as the differences in the constraining layer and substrate displacements divided by the viscoelastic layer thickness:

$$\gamma_{rs} = \frac{u_s - w_s}{2h_v} = \frac{C_s - t\Psi - w_s}{2h_v}, \quad \gamma_{rt} = \frac{u_t - w_t}{2h_v} = \frac{C_t + s\Psi - w_t}{2h_v} \quad (7.4)$$

It is assumed that the viscoelastic material is homogeneous throughout the volume and  $G_v$  is a constant. The equations of equilibrium may be written as:

$$\begin{aligned} \sum F_s &= \iint G_v \gamma_{rs} ds dt = 0, & \sum F_t &= \iint G_v \gamma_{rt} ds dt = 0 \\ \sum M_r &= \iint G_v (\gamma_{rs} t - \gamma_{rt} s) ds dt = 0 \end{aligned} \quad (7.5)$$

The integrals in Equation (7.5) are integrated over the entire area of the constraining layer, from  $s=0$  and from  $t=0$ , and the resulting equations provide solutions for  $C_s$ ,  $C_t$ , and  $\Psi$  in terms of the specified surface displacements  $w_s$  and  $w_t$ :

$$C_s = \frac{1}{4bt} \iint w_s ds dt = RC_T \sin \alpha z_0 \quad (7.6)$$

$$C_t = \frac{1}{4bl} \iint w_t \, ds \, dt = RC_T \cos \alpha \, z_0 \quad (7.7)$$

$$\Psi = \frac{RC_T (b^2 \sin^2 \alpha + l^2 \cos^2 \alpha)}{(b^2 + l^2)} \quad (7.8)$$

Note that the expressions for  $C_s$  and  $C_t$  are equal to the displacements of the beam surface under the centroid of the constraining layer, indicating that the constraining layer behaves as if it were pinned at its centroid.

With this knowledge of the constraining layer displacements  $C_s$ ,  $C_t$ , and  $\Psi$ , a sense of the relative magnitudes of the shear terms for the quasistatic case can be obtained.  $C_s$  and  $C_t$  from Equations (7.6) and (7.7) may be substituted into Equation (7.4) to simplify the expressions for  $\gamma_{rs}$  and  $\gamma_{rt}$ :

$$\gamma_{rs} = \frac{-t\Psi - RC_T \sin \alpha (s \cos \alpha - t \sin \alpha)}{2h_v} \quad (7.9)$$

$$\gamma_{rt} = \frac{s\Psi - RC_T \cos \alpha (s \cos \alpha - t \sin \alpha)}{2h_v} \quad (7.10)$$

Because it is assumed the constraining layer undergoes no shear, the average value for the  $\gamma_{rs}$  strain in the viscoelastic layer is equal to one-half the value of the  $\gamma_{rs}$  strain in the substrate:

$$\begin{aligned} \gamma_{st \text{ visco}} &= \frac{1}{2} \gamma_{st \text{ substrate}} = \frac{1}{2} \left[ \frac{\partial w_s}{\partial t} + \frac{\partial w_t}{\partial s} \right] \\ &= \frac{1}{2} RC (\cos^2 \alpha - \sin^2 \alpha) \end{aligned} \quad (7.11)$$

The strain energies resulting from these shears may be integrated over the area of the damping strip, and their magnitudes may be compared:

$$U_{\gamma_n} = \frac{blG_v}{3h_v} [b^2(\Psi - RC_T \sin^2\alpha)^2 + l^2(RC_T \sin\alpha \cos\alpha)^2] \quad (7.12)$$

$$U_{\gamma_n} = \frac{blG_v}{3h_v} [l^2 (\Psi R C_T \cos^2\alpha)^2 + b^2 (R C_T \cos\alpha \sin\alpha)^2] \quad (7.13)$$

$$U_{\gamma_n} = bl h_v G_v R^2 C_T^2 (\cos 2\alpha)^2 \quad (7.14)$$

For the case where  $b^2 \ll l^2$  and  $\Psi = RC_T \cos^2\alpha$ , the expressions for the  $\gamma_n$  and  $\gamma_n$  shear and their corresponding potential energies simplify further:

$$\gamma_{rs} \approx \frac{RC_T [-t \cos 2\alpha - s \sin\alpha \cos\alpha]}{2h_v} \quad (7.15)$$

$$\gamma_n \approx \frac{RC_T t \cos\alpha \sin\alpha}{2h_v} \quad (7.16)$$

$$U_{\gamma_n} \approx \frac{bl G_v R^2 C_T^2}{3h_v} [b^2(\cos 2\alpha)^2 + l^2(\sin\alpha \cos\alpha)^2] \quad (7.17)$$

$$U_{\gamma_n} \approx \frac{b^3 l G_v}{3 h_v} (RC_T \cos\alpha \sin\alpha)^2 \quad (7.18)$$

*Observations on the Rigid Constraining Layer Results.* The relative sizes of the strains and strain energies in the rigid constraining layer analysis can be used to identify which

terms dominate the problem, and how the analysis might be extended to include an elastic constraining layer. Consider the case where  $\alpha$  is not zero. Note that for  $b^2 \ll l^2$  the ratio of  $U_{\gamma_{rs}}$  over  $U_{\gamma_{rs}}$  is approximately equal to the ratio  $(b/l)^2$  and the ratio of the  $\gamma_{rs}$  and  $\gamma_{rs}$  shear terms at any point  $(s,t)$  on the surface is approximately equal to  $t/s$ :

$$\frac{\gamma_{rs}}{\gamma_{rs}} \approx \frac{t \cos \alpha \sin \alpha}{-t \cos 2\alpha - s \sin \alpha \cos \alpha} \approx \frac{t}{s} \quad \text{for } t \ll s \quad (7.19)$$

$$\frac{U_{\gamma_{rs}}}{U_{\gamma_{rs}}} \approx \frac{b^2 (\cos \alpha \sin \alpha)^2}{b^2 (\cos 2\alpha)^2 + l^2 (\sin \alpha \cos \alpha)^2} \approx \frac{b^2}{l^2} \quad \text{for } b^2 \ll l^2 \quad (7.20)$$

$U_{\gamma_{rs}}$  is also much smaller than  $U_{\gamma_{rs}}$  for the typical case where  $h_v$  is small compared to  $b$  and  $l$ :

$$\frac{U_{\gamma_{rs}}}{U_{\gamma_{rs}}} \approx \frac{3h_v^2 (\cos 2\alpha)^2}{b^2 (\cos 2\alpha)^2 + l^2 (\sin \alpha \cos \alpha)^2} \quad (7.21)$$

Thus it can be seen that for thin narrow strips the viscoelastic strain energy resulting from the  $\gamma_{rs}$  strain dominates the problem.

When the strips are aligned with the beam generator lines (i.e.,  $\alpha=0$ ), the solution for the rigid body displacements and angular rotation reduce to the following:

$$C_s = 0, \quad C_t = RC_T z_o, \quad \Psi = \frac{RC_T l^2}{b^2 + l^2} \approx RC_T \quad (7.22)$$

The viscoelastic shear terms for any point  $(s,t)$  on the damping strip become:

$$\gamma_n = -\frac{t\Psi}{2h_v} = -\frac{t R C_T}{2h_v} \quad (7.23)$$

$$\gamma_n = \frac{s(\Psi - RC_T)}{2h_v} = \frac{s RC_T}{2h_v} \left[ \frac{b^2}{b^2+l^2} \right] \quad (7.24)$$

$$\gamma_n = \frac{1}{2} RC_T \quad (7.25)$$

The viscoelastic strain energies integrated over the area of the segment become:

$$U_{\gamma_n} = \frac{b^3 l G_v (RC_T)^2}{3h_v} \left[ \frac{l^2}{b^2+l^2} \right]^2 \quad (7.26)$$

$$U_{\gamma_n} = \frac{bl^3 G_v (RC_T)^2}{3h_v} \left[ \frac{b^2}{b^2+l^2} \right]^2 \quad (7.27)$$

$$U_{\gamma_n} = 4 bl h_v G_v (RC_T)^2 \quad (7.28)$$

Although it would be incorrect to say that thin strips parallel to the generator lines provide no damping in torsion, all the terms are small. The strain energies associated with  $\gamma_n$  and  $\gamma_n$  are small because  $b \ll l$  for narrow strips. The strain energy associated with  $\gamma_n$  is small because  $2h_v$  is small for thin viscoelastic layers. In general, the shear in the viscoelastic layer of a constrained layer damping treatment is inversely proportional to its thickness, and so increasing the  $2h_v$  dimension would be counterproductive.

*Equations of Motion for an Elastic Constraining Layer.* The torsional analysis will now be modified to include elastic extension in the constraining layer. For the case of long, narrow strips, the rigid body analysis showed that the  $\gamma_n$  viscoelastic shear stresses are much larger than all others. These stresses tend to stretch the constraining layer in the s direction. To model this behavior, define  $u=u(s)$  to be the s direction displacement of the constraining layer averaged across the width of the strip. The displacement  $u$  includes the displacements due to the stretching of the constraining layer as well as the rigid body displacement identified as  $C_1$  in the earlier analysis. The variables  $\Psi$  and  $C_1$  are used to define the rigid body rotation and the rigid body displacement in the t direction.

This analysis uses quasistatic assumptions. The defining equations for the constraining layer are developed using the Principle of Minimum Potential Energy, which specifies that the strain energy within a system attains an absolute minimum when the elements of the system are in equilibrium (61:448). The standard variational notation is used, where  $\delta u$ ,  $\delta C_1$ , and  $\delta \Psi$  denotes the variations of  $u$ ,  $C_1$ , and  $\Psi$  in the problem.

The strain energy from the elastic extension in the constraining layer has the following form:

$$U_c = \frac{1}{2} \int E_c A_c (u')^2 ds \qquad (\cdot)' = \frac{d(\cdot)}{ds} \qquad (7.29)$$

The viscoelastic shear strains and the resulting strain energies become:

$$\gamma_{rs} = \frac{u - t\Psi - RC_T \sin\alpha(z_0 + s \cos\alpha - t \sin\alpha)}{2h_v} \quad (7.30)$$

$$\gamma_{rn} = \frac{C_i + s\Psi - RC_T \cos\alpha(z_0 + s \cos\alpha - t \sin\alpha)}{2h_v}$$

$$U_{\gamma_{rs}} = \frac{1}{2} \int \frac{G_v}{2h_v} \left[ 2b(u - RC_T \sin\alpha(z_0 + s \cos\alpha))^2 + \frac{2b^3}{3} (RC_T \sin^2\alpha - \Psi)^2 \right] ds \quad (7.31)$$

$$U_{\gamma_{rn}} = \frac{1}{2} \int \frac{G_v}{2h_v} \left[ 2b(C_i + s\Psi - RC_T \cos\alpha(z_0 + s \cos\alpha))^2 + \frac{2b^3}{3} (RC_T \cos\alpha \sin\alpha)^2 \right] ds$$

The Principle of Minimum Potential Energy may be written as:

$$\begin{aligned} \sum \delta U = & \int_{-l}^l \left[ \delta u \left[ -E_c A_c u'' + \frac{G_v 2b}{2h_v} (u - RC_T \sin\alpha(z_0 + s \cos\alpha)) \right] \right. \\ & \left. + \delta C_i \left[ \frac{G_v 2b}{2h_v} [C_i + s\Psi - RC_T \cos\alpha(z_0 + s \cos\alpha)] \right] + \right. \quad (7.32) \\ & \left. \delta \Psi \left[ \frac{-2b^3}{3} (RC_T \sin^2\alpha - \Psi) + 2bs (C_i + s\Psi - RC_T \cos\alpha(z_0 + s \cos\alpha)) \right] \right] ds \\ & + E_c A_c u' \delta u \Big|_{-l}^l = 0 \end{aligned}$$

Equations are developed by setting the arguments of the variational terms in Equation (7.32) equal to zero. The  $\delta C_i$  and  $\delta \Psi$  terms are independent of  $s$  and therefore the integral over  $s$  may be brought inside the bracketed expression:

$$\int_{-l}^l \delta u \left[ -E_c A_c u'' + \frac{G_v 2b}{2h_v} (u - RC_T \sin\alpha(z_0 + s \cos\alpha)) \right] ds = 0 \quad (7.33)$$

$$\delta C_i \int_{-l}^l \frac{G_v 2b}{2h_v} \{C_i + s\Psi - RC_T \cos\alpha (z_o + s \cos\alpha)\} ds = 0 \quad (7.34)$$

$$\delta \Psi \int_{-l}^l \left\{ \frac{-2b^3}{3} (RC_T \sin^2\alpha - \Psi) \right. \quad (7.35)$$

$$\left. + 2bs (C_i + s\Psi - RC_T \cos\alpha (z_o + s \cos\alpha)) \right\} ds = 0$$

$$E_c A_c u' \delta u |_{-l}^l = 0 \quad (7.36)$$

The values of  $C_i$  and  $\Psi$  developed from Equations (7.34) and (7.35) are identical to those found in Equations (7.6) and (7.7) in the rigid body configuration. The differential equation in  $u$  and its boundary condition are obtained from Equation (7.33) and (7.36):

$$u'' - g u = -g RC_T \sin\alpha (z_o + s \cos\alpha), \quad u' |_{s=l} = 0 \quad (7.37)$$

where

$$g = \frac{G_v}{(2h_v)(2h_c) E_c} \quad (7.38)$$

*Observations on the Elastic Constraining Layer Results.* The solution to Equation (7.37), the torsional differential equation, has the following form:

$$u = RC_T \sin\alpha \left[ z_o + s \cos\alpha - \frac{\cos\alpha \sinh(\sqrt{g} s)}{\sqrt{g} \cosh(\sqrt{g} l)} \right] \quad (7.39)$$

The constant term in the solution,  $RC \sin\alpha z_0$ , identifies a rigid body displacement equal to the  $C_s$  term from the previous section (Equation (7.6)). By substituting Equation (7.39) into Equation (7.30), the expression for the  $\gamma_{rs}$  shear in the viscoelastic layer becomes:

$$\gamma_{rs} = \frac{-RC_T \cos\alpha \sin\alpha \sinh\sqrt{g}s}{2h_v \sqrt{g} \cosh\sqrt{g}l} \quad (7.40)$$

It can be seen from Equation (7.40) that the rigid body displacement does not affect the strain in the viscoelastic layer.

The viscoelastic shear strain identified in Equation (7.40) has a form similar to the viscoelastic shear strain in a constrained layer mounted on a substrate in a state of uniform strain  $\epsilon_0$ , which was discussed in Chapter 3 (Equation (3.8)). In the barberpole configuration, the "effective strain", is  $\epsilon_0 = RC_T \sin\alpha \cos\alpha$ . Because Plunkett and Lee developed their conclusions about optimal length from a loss coefficient derived from the expression for the viscoelastic shear strain, their conclusions can be applied directly to the barberpole torsional problem.

Equations (7.39) and (7.40) show that  $u'$  and the shear strain in the viscoelastic layer are proportional to the effective strain,  $RC_T \cos\alpha \sin\alpha$ . An optimal choice of pitch angle increases the shear strain in the viscoelastic layer and improves the performance of the damping treatment. This formulation exhibits an expected result: the effective substrate strain is largest when the function  $\cos\alpha \sin\alpha$  is maximized, i.e., at  $\alpha = \pi/4$  radians. This is expected because this angle identifies the principal axes of strain for the

beam surface, and the displacement of the substrate in the  $s$  direction is maximized. If the damping treatment is designed primarily to eliminate torsional vibration, then the pitch angle should be chosen to maximize the effective substrate strain and the individual strips should be segmented to optimal length.

The torsional differential equation (Equation (7.37)) reduces to its homogeneous form for  $\alpha=0$ . This indicates that there are no strains induced by the  $u$  displacement which must be added to the small viscoelastic shear strains calculated in the rigid body case.

The general methods used to calculate a loss factor for the barberpole configuration are discussed after the bending analysis. To obtain values of loss factor, the strain energies of the individual components of the system must be calculated. For the torsional problem, the strains  $u'$  and  $\gamma$  are the same for all strips on a fully coated barberpole, a fact which allows the loss factor of a barberpole with  $N$  strips to be formulated using one set of strain energies  $N$  times.

### *Bending Analysis*

In this section, equations of motion for the constraining layer are developed that characterize the barberpole geometry in bending. A quasistatic approach is taken in the analysis, and therefore kinetic energies are not considered. The equations are formulated using the Principle of Minimum Potential Energy.

*Surface Displacements for Bending Analysis.* The surface displacements of the beam in bending are much more complicated than those of the torsion problem. In this analysis, a definition of displacements for the beam surface is used that eliminates any rigid body displacement that does not induce strain in the viscoelastic layer. Strains are calculated for the surface after deformation, and the displacements are defined by integrating the strains over the interval  $(0,s)$ . With this definition, the displacement of the beam surface at the origin of the  $s$ - $t$  system is always zero. This approach simplifies the analysis considerably, yet allows the shear in the viscoelastic layer to be properly identified.

The surface displacements used in the analysis are developed from the elasticity solution for a prismatic beam in pure bending. In the elasticity solution, the cross section of the main beam is assumed solid, which is clearly not the case for many cylindrical beams used in practical applications. Despite this, the choice was made to use the elasticity solution to characterize the beam surface strains because it is a well known result that allows a relatively straightforward analysis of the barberpole geometry.

Saada (80:355-359) identifies the solution of the elasticity problem for pure bending in terms of an  $(x_1, x_2, x_3)$  cartesian reference system identified in Figure (7.6). In such a coordinate system, the displacements of the beam subjected to an applied moment  $M$  in the  $x_1 x_2$  plane are:

$$u_1 = C_B x_1 x_2 \quad u_2 = -\frac{1}{2} C_B (x_1^2 - \nu x_3^2 + \nu x_2^2) \quad u_3 = -\nu C_B x_2 x_3 \quad (7.41)$$

where

$$C_B = \frac{M}{EI_{beam}} \quad (7.42)$$

and  $\nu$  is Poisson's ratio.  $C_B$  is a constant equal to the applied beam moment divided by the beam bending stiffness, and is a measure of the curvature of the beam. As seen in Figure 7.6, the transformation of the beam surface from  $x_1, x_2, x_3$  coordinates into the  $r, \theta, z$  system is  $x_1 = z$ ,  $x_2 = -r \sin \theta$ , and  $x_3 = r \cos \theta$ . The beam surface displacements in the  $r, \theta, z$  directions become:

$$\begin{aligned} u_r &= u_3 \cos \theta - u_2 \sin \theta \\ &= \nu R^2 C_B \sin \theta \cos^2 \theta + \frac{1}{2} C_B \sin \theta (z^2 + \nu R^2 (\sin^2 \theta - \cos^2 \theta)) \end{aligned} \quad (7.43)$$

$$\begin{aligned} u_\theta &= -u_2 \cos \theta - u_3 \sin \theta \\ &= -\nu R^2 C_B \sin^2 \theta \cos \theta + \frac{1}{2} C_B \cos \theta (z^2 + \nu R^2 (\sin^2 \theta - \cos^2 \theta)) \end{aligned} \quad (7.44)$$

$$u_z = \nu R^2 C_B \sin \theta \cos \theta \quad (7.45)$$

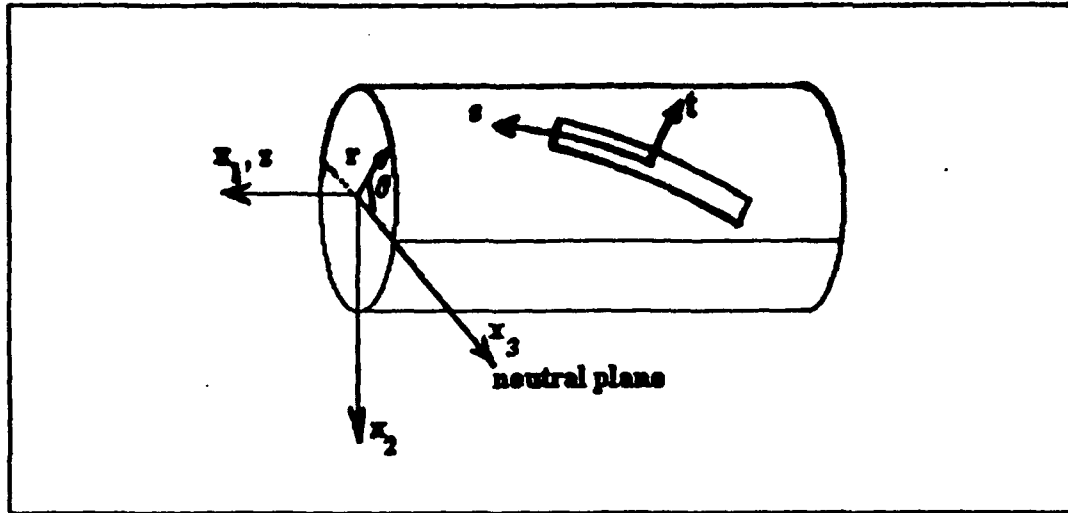


Figure 7.6. Coordinate Systems for the Barberpole Bending Analysis

These displacements may be used to calculate  $\epsilon_{\theta\theta}$  and  $\epsilon_{zz}$  strains using the standard assumptions of linear theory (80: 138):

$$\epsilon_{\theta\theta} = \frac{1}{r} \frac{\partial u_{\theta}}{\partial \theta} + \frac{u_r}{r} = \nu RC_B \sin\theta \quad (7.46)$$

$$\epsilon_{zz} = \frac{\partial u_z}{\partial z} = -RC_B \sin\theta$$

The extensional strains in the s-t system may be found through an appropriate transformation (80: 78):

$$e_{ss} = \cos^2\alpha e_{zz} + \sin^2\alpha e_{\theta\theta} = -RC_B (\cos^2\alpha - \nu \sin^2\alpha) \sin\theta \quad (7.47)$$

$$e_{tt} = \sin^2\alpha e_{zz} + \cos^2\alpha e_{\theta\theta} = -RC_B (\sin^2\alpha - \nu \cos^2\alpha) \sin\theta$$

All  $\gamma_{st}$  strains on the beam surface are ignored in this analysis. The surface displacements in the s and t directions may be found by substituting in the coordinate transformation for

$\theta$ , then integrating the strains over their respective arclengths:

$$\theta = \theta_0 + \frac{s \sin \alpha + t \cos \alpha}{R}$$

$$\int_0^s e_{ss} ds = \frac{R^2 C_B (\cos^2 \alpha - \nu \sin^2 \alpha)}{\sin \alpha} \left[ \cos \left( \theta_0 + \frac{s \sin \alpha + t \cos \alpha}{R} \right) - \cos \left( \theta_0 + \frac{t \cos \alpha}{R} \right) \right]$$

$$\int_0^t e_{tt} dt = \frac{R^2 C_B (\sin^2 \alpha - \nu \cos^2 \alpha)}{\cos \alpha} \left[ \cos \left( \theta_0 + \frac{s \sin \alpha + t \cos \alpha}{R} \right) - \cos \left( \theta_0 + \frac{s \sin \alpha}{R} \right) \right]$$

(7.48)

The surface displacements  $w_s$  and  $w_t$  used in the analysis are the integrals in Equation (7.48) averaged over the strip width  $2b$ :

$$w_s = \frac{1}{2b} \int_{-b}^b \left[ \int_0^s e_{ss} ds \right] dt = W_s(\alpha) \left[ \cos \left( \theta_0 + s \frac{\sin \alpha}{R} \right) - \cos(\theta_0) \right] \quad (7.49)$$

$$w_t = \frac{1}{2b} \int_{-b}^b \left[ \int_0^t e_{tt} dt \right] ds = -W_t(\alpha) \cos \left( \theta_0 + s \frac{\sin \alpha}{R} \right) \quad (7.50)$$

where

$$W_s(\alpha) = \frac{R^2 C_B (\cos^2 \alpha - \nu \sin^2 \alpha)}{\sin \alpha} \operatorname{sinc} \left( \frac{b \cos \alpha}{R} \right) \quad (7.51)$$

$$W_t(\alpha) = \frac{-R^2 C_B (\sin^2 \alpha - \nu \cos^2 \alpha)}{\cos \alpha} \left[ 1 - \operatorname{sinc} \left( \frac{b \cos \alpha}{R} \right) \right] \quad (7.52)$$

$$\operatorname{sinc}(x) = \frac{\sin(x)}{x} \quad (7.53)$$

Note that the expression for  $w_t$  is well defined as  $\alpha$  approaches zero:

$$\begin{aligned} \lim_{\alpha \rightarrow 0} w_s &= R^2 C_B \operatorname{sinc}\left(\frac{b}{R}\right) \frac{\lim_{\alpha \rightarrow 0} \left[ \cos\left(\theta_0 + s \frac{\sin \alpha}{R}\right) - \cos \theta_0 \right]}{\lim_{\alpha \rightarrow 0} [\sin \alpha]} \\ &= -RC_B \operatorname{sinc}\left(\frac{b}{R}\right) \sin \theta_0 s \end{aligned} \quad (7.54)$$

For narrow strips,  $\operatorname{sinc}(b \cos \alpha/R) \approx 1$  and the  $w_s$  term becomes small when compared to  $w_t$ . This indicates that the displacements in the  $s$  direction, and the resulting  $\gamma_n$  shears, are the dominant effects for the barberpole geometry in bending.

*Developing Equations of Motion for Barberpole in Bending.* As in the torsion problem, the bending equations of motion are developed using the Principle of Minimum Potential Energy. Define two constraining layer displacements that are functions of  $s$ : let  $u$  define the displacement in the  $s$  direction and let  $u_t$  define the displacement in the  $t$  direction. The displacements are allowed to vary with the  $s$  coordinate but not the  $t$  coordinate, defining an average value across the width of the strip. Because the constraining layer is much longer in the  $s$  direction than it is wide in the  $t$  direction, the effect of viscoelastic shear and constraining layer extension is more significant in the  $s$  direction than in the  $t$  direction. The choice of  $u$  and  $u_t$  as displacements allows the strain in the viscoelastic layer to be adequately modelled, but totally ignores any lateral displacement in the constraining layer due to Poisson effects.

The  $\gamma_n$  and  $\gamma_n$  viscoelastic shear strains are assumed uniform through the thickness of the layer, and they are defined as the difference between constraining layer and

substrate displacement divided by the viscoelastic layer thickness :

$$\gamma_{rs} = \frac{1}{2h_v} (u - w_s), \quad \gamma_{rt} = \frac{1}{2h_v} (u_t - w_t) \quad (7.55)$$

The constraining layer experiences an axial strain  $\epsilon_x$  and a shearing strain  $\epsilon_{xy}$  :

$$\epsilon_{xx} = \frac{du}{ds} = u', \quad \epsilon_{xy} = \frac{du_t}{ds} = u_t' \quad (7.56)$$

Equations (7.55) and (7.56) may be used to write the strain energies in terms of the unknown displacements  $u$  and  $u_t$ . The strain energies resulting from the viscoelastic shear strains are:

$$U_{\gamma_{rs}} = \frac{1}{2} \int G_v A_v \gamma_{rs}^2 ds = \frac{1}{2} \int \frac{G_v A_v}{(2h_v)^2} (u - w_s)^2 ds \quad (7.57)$$

$$U_{\gamma_{rt}} = \frac{1}{2} \int G_v A_v \gamma_{rt}^2 ds = \frac{1}{2} \int \frac{G_v A_v}{(2h_v)^2} (u_t - w_t)^2 ds$$

The variation of these strain energies are:

$$\delta U_{\gamma_{rs}} = \int \frac{G_v A_v}{(2h_v)^2} (u - w_s) \delta u ds, \quad \delta U_{\gamma_{rt}} = \int \frac{G_v A_v}{(2h_v)^2} (u_t - w_t) \delta u_t ds \quad (7.58)$$

The strain energies associated with the constraining layer are:

$$U_{c \gamma_{xy}} = \frac{1}{2} \int G_c A_c \epsilon_{xy}^2 ds = \frac{1}{2} \int G_c A_c u_t'^2 ds \quad (7.59)$$

$$U_{c \sigma_{xx}} = \frac{1}{2} \int E_c A_c \epsilon_{xx}^2 ds = \frac{1}{2} \int E_c A_c u'^2 ds$$

After taking the variation of the strain energies and integrating by parts:

$$\delta U_{c \gamma_n} = \int -G_c A_c u'' \delta u ds + u' \delta u|_{s=1} \quad (7.60)$$

$$U_{c \sigma_n} = \int -E_c A_c u_t'' \delta u_t ds + u_t' \delta u_t|_{s=1}$$

The Principle of Minimum Potential Energy has the following form for this problem:

$$\begin{aligned} \sum \delta U &= \delta U_{v \gamma_n} + \delta U_{v \gamma_n} + \delta U_{c \gamma_n} + \delta U_{c \sigma_n} \\ &= \int_{-1}^1 [(\dots)\delta u + (\dots)\delta u_t] ds + [(\dots)\delta u + (\dots)\delta u_t]|_{-1}^1 = 0 \end{aligned} \quad (7.61)$$

By collecting terms and setting the arguments of  $\delta u$  and  $\delta v$  equal to zero, the equations of motion are obtained:

$$\frac{d^2 u}{ds^2} - g u = -g w_s, \quad u'|_{s=1} = 0, \quad g = \frac{G_v}{4h_v h_c E_c} \quad (7.62)$$

$$\frac{d^2 u_t}{ds^2} - g_v u_t = -g_v w_t, \quad u_t'|_{s=1} = 0, \quad g_v = \frac{G_v}{4h_v h_c G_c} \quad (7.63)$$

Note that Equation (7.62) is identical to Equation (3.5) in Chapter 3, which describes a constraining layer on a flat substrate with an effective surface displacement equal to  $w_s$ .

*Special Case: Pitch Angle  $\alpha = 0$ .* An interesting special case of the generalized barberpole problem occurs when the damping strips are parallel to the  $z$  axis of the beam. The analysis provides a baseline by which the barberpole treatment may be judged, and allows a comparison between damping beams of circular and rectangular cross section.

When the pitch angle  $\alpha$  is zero,  $w_1$  is independent of  $s$  (Equation (7.50)) and  $\gamma_n=0$ . Equation (7.54) defines the form of  $w_n$ , and Equation (7.62) may be written as:

$$\frac{d^2 u}{ds^2} - gu = gRC_B \sin\theta_0 \operatorname{sinc}\left(\frac{b}{R}\right) s \quad u'|_{s=0} = 0 \quad (7.64)$$

where the sinc function is defined in Equation (7.53). Note that the right hand side of Equation (7.64) is linear in  $s$ , with all other terms fixed by the geometry of the beam and constraining layer. Like the torsional problem, this analysis produces a differential equation identical to one that describes a constraining layer on a flat substrate experiencing uniform strain (Equation (3.5)), so the optimal length results of Plunkett and Lee can be applied directly to the problem.

From the right hand side of Equation (7.64) it can be seen that the effective substrate strain amplitude is equal to  $RC_B \sin\theta_0 \operatorname{sinc}(b/R)$ . As expected, the strain amplitude increases with beam radius  $R$ , curvature  $C_B$ , and increasing distance from the neutral axis (which is proportional to  $\sin\theta_0$ ). What is interesting is that the strain amplitude per unit area also increases with the decrease of ratio  $b/R$ . This indicates that for a strip at a specified  $\theta_0$  location, the narrower the strip, the greater the effective strain and the more effective the damping treatment. The function  $\operatorname{sinc}(b/R)$  approaches zero as  $b/R$  approaches  $\pi$ . This indicates that the effective strain experienced by the constraining layer approaches zero when the strip width  $2b$  is equal to the circumference of the main beam. While this result is in agreement with the previous work which indicates that concentric damping treatments do not effectively damp circular beams

(101:328, 106:773), this may be a serendipitous result. The approach taken to develop these equations assumes the constraining layer is in the form of a strip, and some of the effects that were neglected might become significant long before the strip approaches the full width of the beam circumference.

The ODE in Equation (7.64) has the following solution:

$$u = - RC_B \operatorname{sinc}\left(\frac{b}{R}\right) \sin\theta_o \left[ s - \frac{\sinh\sqrt{g} s}{\sqrt{g} \cosh\sqrt{g} l} \right] \quad (7.65)$$

From this solution, the shear strain in the viscoelastic layer may be calculated:

$$\gamma_{rs} = \frac{RC_B \operatorname{sinc}\left(\frac{b}{R}\right) \sin\theta_o \sinh\sqrt{g} s}{2h_v \sqrt{g} \cosh\sqrt{g} l} \quad (7.66)$$

To summarize, the solution of the barberpole equations for the special case of  $\alpha=0$  produces several expected results. A narrow strip (i.e., a small  $b/R$  ratio) provides the most shear in the viscoelastic layer, and a concentric constraining layer configuration (where  $b/R=\pi$ ) yields zero viscoelastic shear. The amount of shear in the strip increases with its distance from the neutral plane. For a given strip geometry, the optimal length result of Plunkett and Lee may be used to determine the optimal segment length. The results of this analysis will be compared with the case of  $\alpha \neq 0$  to assess the relative effectiveness of the barberpole in bending.

**Solving the Bending Equations for Arbitrary  $\alpha$ :** For the case where  $\alpha$  is nonzero, the expression for  $w_s$  and  $w_t$  identified in Equations (7.49) and (7.50) may be substituted into the general differential equations (Equations (7.62) and (7.63)):

$$\frac{d^2 u}{ds^2} - g u = -g W_s(\alpha) \left[ \cos\left(\theta_o + s \frac{\sin \alpha}{R}\right) - \cos(\theta_o) \right] \quad (7.67)$$

$$\frac{d^2 u_t}{ds^2} - g_v u_t = g_v W_t(\alpha) \cos\left(\theta_o + s \frac{\sin \alpha}{R}\right) \quad (7.68)$$

$$W_s(\alpha) = \frac{R^2 C_B (\cos^2 \alpha - \nu \sin^2 \alpha)}{\sin \alpha} \operatorname{sinc}\left(\frac{b \cos \alpha}{R}\right) \quad (7.69)$$

$$W_t(\alpha) = \frac{-R^2 C_B (\sin^2 \alpha - \nu \cos^2 \alpha)}{\cos \alpha} \left[ 1 - \operatorname{sinc}\left(\frac{b \cos \alpha}{R}\right) \right] \quad (7.70)$$

The solution for  $u$  is:

$$u = W_s(\alpha) \left[ \frac{g \cos\left(\theta_o + s \frac{\sin \alpha}{R}\right)}{g + \left(\frac{\sin \alpha}{R}\right)^2} - \cos(\theta_o) + P \cosh(\sqrt{g} s) + Q \sinh(\sqrt{g} s) \right] \quad (7.71)$$

where

$$P = \frac{\sqrt{g} \sin \alpha \cos \theta_o \sin\left(\frac{l \sin \alpha}{R}\right)}{R \sinh(\sqrt{g} l) \left[ g + \left(\frac{\sin \alpha}{R}\right)^2 \right]} \quad Q = \frac{\sqrt{g} \sin \alpha \sin \theta_o \cos\left(\frac{l \sin \alpha}{R}\right)}{R \cosh(\sqrt{g} l) \left[ g + \left(\frac{\sin \alpha}{R}\right)^2 \right]} \quad (7.72)$$

The viscoelastic shear strain  $\gamma_{xx}$  is:

$$\gamma_{\pi} = -\frac{W_s(\alpha)}{2h_v} \left[ \left( 1 + \frac{s}{s + \left(\frac{\sin\alpha}{R}\right)^2} \right) \cos\left(\theta_o + s \frac{\sin\alpha}{R}\right) + P \cosh(\sqrt{g}s) + Q \sinh(\sqrt{g}s) \right] \quad (7.73)$$

The solution for  $u_x$  becomes:

$$u_x = W_s(\alpha) \left[ \frac{-g_v \cos\left(\theta_o + s \frac{\sin\alpha}{R}\right)}{g_v + \left(\frac{\sin\alpha}{R}\right)^2} + P_s \cosh(\sqrt{g_v} s) + Q_s \sinh(\sqrt{g_v} s) \right] \quad (7.74)$$

where

$$P_s = \frac{-\sqrt{g_v} \sin\alpha \cos\theta_o \sin\left(\frac{l \sin\alpha}{R}\right)}{R \sinh(\sqrt{g_v} l) \left[ g_v + \left(\frac{\sin\alpha}{R}\right)^2 \right]} \quad Q_s = \frac{-\sqrt{g_v} \sin\alpha \sin\theta_o \cos\left(\frac{l \sin\alpha}{R}\right)}{R \cosh(\sqrt{g_v} l) \left[ g_v + \left(\frac{\sin\alpha}{R}\right)^2 \right]} \quad (7.75)$$

The viscoelastic strain  $\gamma_{\pi}$  is:

$$\gamma_{\pi} = \frac{W_s(\alpha)}{2h_v} \left[ \left( 1 - \frac{P_s}{s + \left(\frac{\sin\alpha}{R}\right)^2} \right) \cos\left(\theta_o + s \frac{\sin\alpha}{R}\right) + P \cosh(\sqrt{g_v} s) + Q \sinh(\sqrt{g_v} s) \right] \quad (7.76)$$

For long, narrow strips,  $W_s(\alpha)$  is much larger than  $W_l(\alpha)$ . Since the  $\gamma_{\pi}$  and  $\gamma_n$  strains are proportional to the two terms, the  $\gamma_{\pi}$  strain provides most of the damping in the problem.

The implications of these solutions are discussed for both the unsegmented and segmented barberpole geometry in later sections.

### *Calculating Damping for the Fully Covered Barberpole Geometry*

The torsional and bending solutions for a single damping strip on a beam can be used to calculate the loss factor for the fully covered barberpole geometry. For the parametric studies in this chapter, the Modal Strain Energy method is used to calculate the beam loss factors. Both the Modal Strain Energy method and the Complex Rayleigh Quotient method are used to obtain damping values that will be compared with the experimental results in Chapter 8. The Modal Strain Energy method was used for the parametric studies because the computation of loss factor was simplified by the use of real mode shapes. The approximation was acceptable because the studies were used to illustrate the qualitative effects of the barberpole design on the loss factor, not to obtain the best possible estimate of loss factor for a single configuration.

To calculate loss factors, expressions for strain energy must be developed for the individual components of the system. For a barberpole treatment with  $N$  strips, the Modal Strain Energy method provides the following expression for the system loss factor:

$$\eta_{system} = \frac{\sum_{n=1}^N \eta_{v_n} U_{Y_n}}{U_b + \sum_{n=1}^N U_{Y_n} + \sum_{n=1}^N U_{c_n}} \quad (7.77)$$

In Equation (7.77)  $U_b$  is the strain energy in the beam,  $\eta_{v_n}$  is the loss factor of the viscoelastic material, and  $U_{Y_n}$  and  $U_{c_n}$  are the strain energies associated with constraining layer and the viscoelastic layer of the  $n$ th strip. Equation (7.77) may be used for both

bending and torsion by substituting in the appropriate definitions of  $U_b$ ,  $U_\gamma$ , and  $U_c$  which will be described shortly.

For the barberpole in torsion, it can be seen from Equations (7.39) and (7.40) that  $u'$  and  $\gamma_{rs}$  are independent of strip position, so if all strips have the same geometry and material properties, their strain energies are equal. This may be used to simplify the expression for loss factor in Equation (7.77):

$$\eta_{system} = \frac{\eta_v N U_\gamma}{U_b + N U_\gamma + N U_c} \quad (7.78)$$

For the torsion problem, the damping layer strain energies have the following form:

$$U_c = \frac{1}{2} \int_{-l}^l E_c A_c u'^2 ds \quad (7.79)$$

$$U_\gamma = \frac{1}{2} \int_{-l}^l Re[G_v^*] A_v \gamma_{rs}^2 ds$$

where  $u'$  and  $\gamma_{rs}$  are developed from Equations (7.39) and (7.40). Recall that in the torsional analysis, the cross section of the main beam undergoes a rotation equal to  $\Theta(z) = C_T z$ . If the beam has length  $L$  and a polar area moment of inertia equal to  $J_b$ , then the strain energy in the main beam from torsion is defined as:

$$U_b = \frac{1}{2} \int_0^L G_b J_b \left[ \frac{d\Theta(z)}{dz} \right]^2 dz = \frac{1}{2} G_b J_b L C_T^2 \quad (7.80)$$

By substituting these relations into Equation (7.78), the loss factor for the barberpole in torsion can be calculated.

Calculating the loss factor for the bending problem is not as straightforward as the torsional problem. When the barberpole is in bending, the solutions for  $u'$  and  $\gamma$  are not the same for each strip because of the presence of  $\theta_0$  in the solution for  $u$  (Equation (7.71)). The large number of individual strips on a fully coated barberpole leads to a very tedious computation. This may be avoided if all the damping strips have the same cross section and material properties, and they are placed in sets of four, where the strips in each set are separated by an angular interval of  $\pi/2$  radians (Figure 7.7). For such a configuration, it is shown in Appendix 7A that the damping strip whose position is defined by  $\theta_0=\pi/4$  has strain energies that are equal to the average value of the strain energies for the fully covered barberpole configuration. With this result, the bending loss factor for the beam has the same form as Equation (7.78). The damping layer strain energies used in Equation (7.78) will have the same form as Equation (7.79), but with  $u'$  and  $\gamma$  defined by setting  $\theta_0=\pi/4$  in Equations (7.71) and (7.73). In the bending analysis, the main beam has a neutral axis displacement of  $h(z)=1/2 C_B z^2$ . The strain energy  $U_b$  is written as:

$$U_b = \frac{1}{2} \int_0^L E_b I_b \left[ \frac{d^2 h(z)}{dz^2} \right]^2 dz = \frac{1}{2} E_b I_b L C_B^2 \quad (7.81)$$

Using these terms in Equation (7.78) produces the bending loss factor as predicted by the Modal Strain Energy Method.

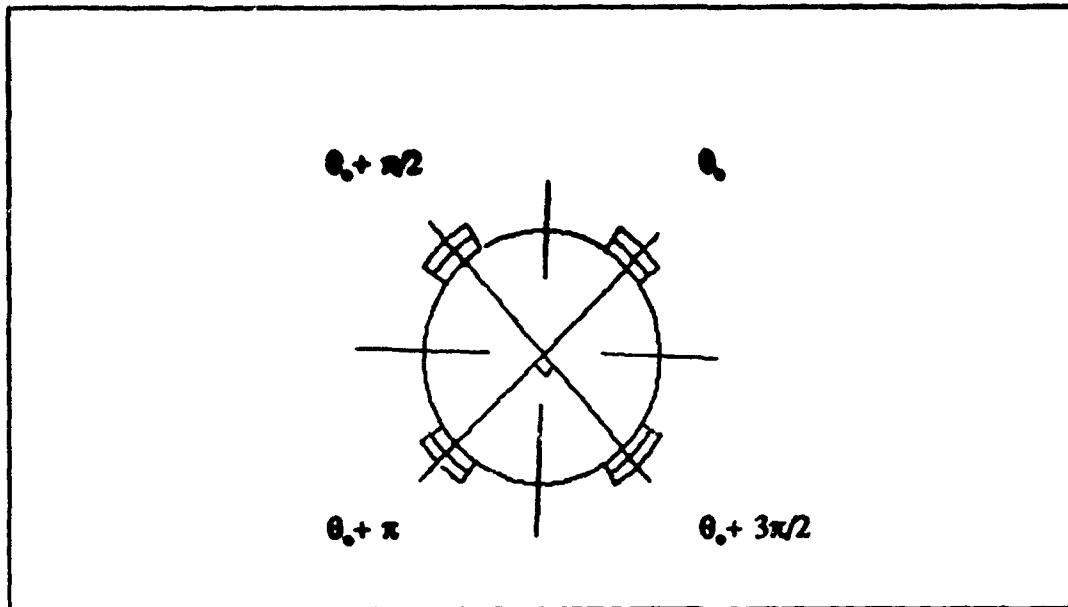


Figure 7.7. Barberpole Damping Strips in Sets of Four Separated by  $\pi/2$  Radians

It was shown in Chapter 4 that for small damping, the loss factor predicted by the Complex Rayleigh Quotient could be manipulated into a form identical to that of the Modal Strain Energy method. The difference between the two forms is that the square of the magnitudes of the complex strains are used in the strain energy expressions for the Complex Rayleigh Quotient, while the square of the real strains are used with the Modal Strain Energy method. For the barberpole problem, the loss factor predicted by the Complex Rayleigh Quotient for both bending and torsion has the following form:

$$\eta_{CRQ} = \frac{N \eta_v U_{\gamma CRQ}}{U_b + N U_{\gamma CRQ} + N U_{c CRQ}} \quad (7.82)$$

where

$$U_{c CRQ} = \frac{1}{2} \int_{-l}^l E_c A_c u'' \overline{u''} ds \quad (7.83)$$

$$U_{\gamma CRQ} = \frac{1}{2} \int_{-l}^l G_v A_v \gamma' \overline{\gamma'} ds$$

For the torsion problem,  $U_b$  is given by Equation (7.80), and  $u''$  and  $\gamma'_n$  are found by using a complex value for  $G_v$  and  $g$  in Equations (7.39) and (7.40). For the bending problem,  $U_b$  is defined in Equation (7.81), and  $u''$  and  $\gamma'_n$  are found by using a complex value for  $G_v$  and  $g$  in Equations (7.71) and (7.73).

*Parametric Studies: Unsegmented Barberpole Strips in Bending.*

In the next few sections, the relative effectiveness of various barberpole geometries are considered. Unless otherwise noted, the beam radius is  $R = 38 \text{ mm}$  (1.5"), the beam wall thickness is  $\Delta t = .71 \text{ mm}$  (.028"), the beam and constraining layer elastic moduli are  $E_b = E_c = 6.89 \times 10^{10} \text{ pascals}$  ( $10 \times 10^6 \text{ lbs/in}^2$ ), the constraining layer thickness is  $2h_c = .13 \text{ mm}$  (.005"), the viscoelastic layer thickness is  $2h_v = .05 \text{ mm}$  (.002"), the damping strip width is  $2b = .56 \text{ mm}$  (.22"), and the viscoelastic shear modulus is  $G_v^* = G_v(1+i\eta_v)$  where  $G_v = 331 \times 10^3 \text{ pascals}$  (48  $\text{lbs/in}^2$ ) and  $\eta_v = 1$ . The viscoelastic material properties correspond to ISD-112 at 25°C at 20 hertz, which is a damping material produced by 3M (87). For the parametric studies, it was assumed that there was 95% total coverage of the beam by the damping treatment, where the missing 5% results from gaps between adjacent damping strips. These properties, when combined with a pitch angle of .615 radians, correspond to the experimental configuration that is discussed in Chapter 8.

*Virtual Segmentation Effect.* For the bending problem, consider the solution for  $u$  and  $\gamma_n$  for a very long strip that crosses the neutral plane of the beam several times. The solutions for  $u$  and  $\gamma_n$  are proportional to  $w_s$ , except at the free ends of the strip. Recall that  $w_s$  and  $W_s(\alpha)$  have the following form:

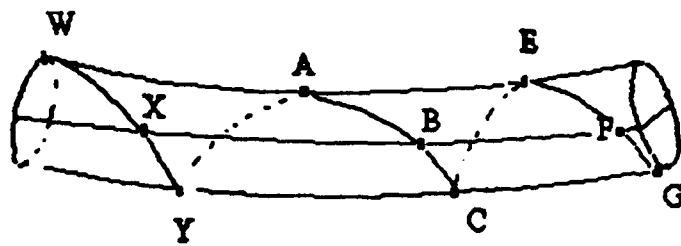
$$w_s = W_s(\alpha) \left[ \cos\left(\theta_s + \frac{s \sin \alpha}{R}\right) - \cos(\theta_s) \right] \quad (7.84)$$

$$W_s(\alpha) = \frac{R^2 C_B (\cos^2 \alpha - \nu \sin^2 \alpha)}{\sin \alpha} \operatorname{sinc}\left(\frac{b \cos \alpha}{R}\right)$$

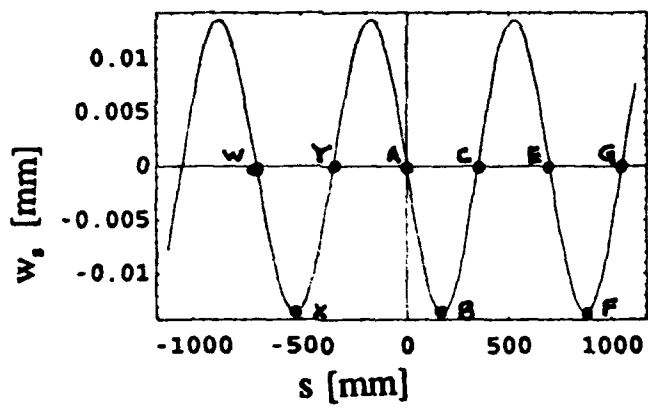
For  $\alpha=0$ ,  $w_s$  is defined in Equation (7.54). If alpha is nonzero,  $w_s$  is an oscillatory function with its maximum amplitude bounded by an envelope of width  $2W_s(\alpha)$ . The extrema of  $w_s$  occur when the strip crosses the neutral plane (i.e.,  $\theta=0$  or  $\theta=\pi$ ), and the zero crossings occur when the  $s$  coordinate crosses the top or bottom of the beam (i.e.,  $\theta= \pi/2$ ) (Figure 7.8). Because  $dw_s/ds$  is equal to the surface strain in the  $s$  direction, the surface strain attains its maximum magnitude at the top and bottom of the beam and is zero where the strip crosses the neutral plane.

If the barberpole damping strips are long enough to cross the beam neutral plane several times, the strains in the barberpole strips have characteristics similar to those in a damping treatment that has been periodically cut to improve performance, suggesting a "virtual segmentation" effect. For the unsegmented barberpole geometry, the "virtual segment" is defined as the portion of the unsegmented barberpole strip that lies between two crossings of the beam neutral plane. On a beam of radius  $R$  that is wrapped at pitch angle  $\alpha$ , the total length of the virtual segment is:

$$L_{\text{virtual}} = \frac{\pi R}{\sin \alpha} \quad (7.85)$$



7.8a. Barberpole Strip ( $\theta_0 = \pi/2$ )



7.8b. Substrate Displacement  $w_s$

Figure 7.8. Surface Displacement of Barberpole in Bending

The similarities between a virtual segment and an actual segment can be illustrated by comparing the nature of their solutions. In Figures 7.10 through 7.17, a portion of the barberpole solution for a long unsegmented strip is compared with similar solutions for a segment with its centerline running parallel to the beam generator located at the top of the beam furthest from the neutral axis, i.e., with  $\alpha = 0$  and  $\theta_0 = \pi/2$ . The two geometries that are compared are shown in Figure 7.9. The portion of the barberpole solution plotted represents the "virtual segment", i.e., the length of the barberpole strip between the crossings of the neutral axis. The actual segment is the same length as the virtual segment.

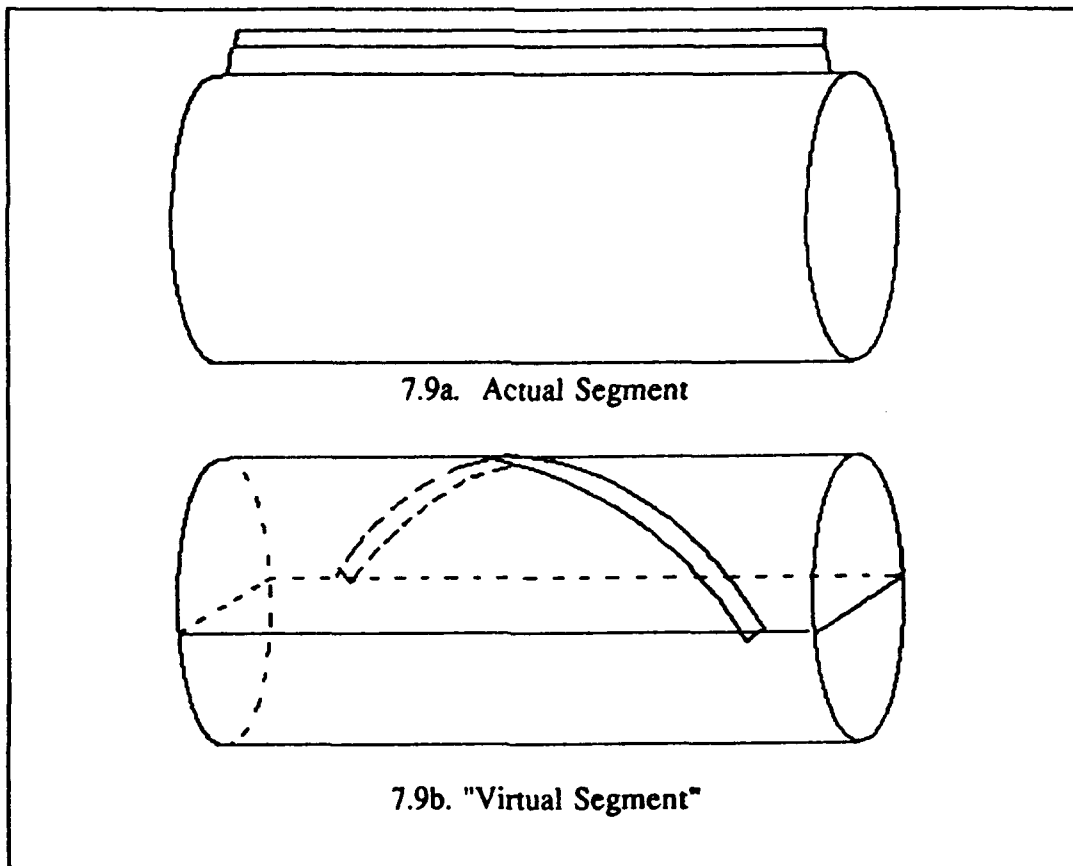


Figure 7.9 Actual and Virtual Segment Configurations

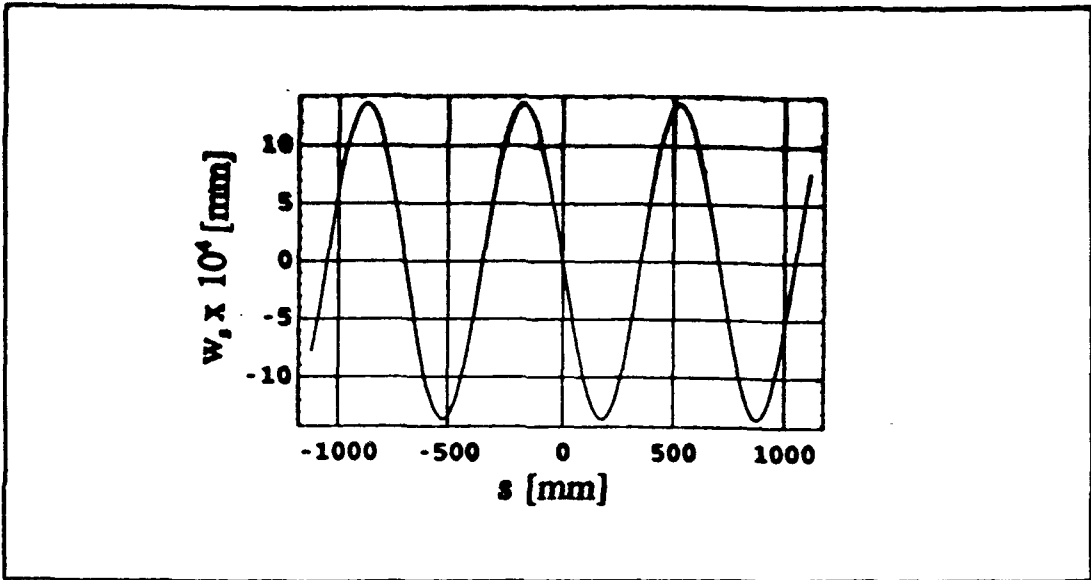


Figure 7.10. Barberpole Surface Displacement in  $s$  Direction ( $w_s$ )

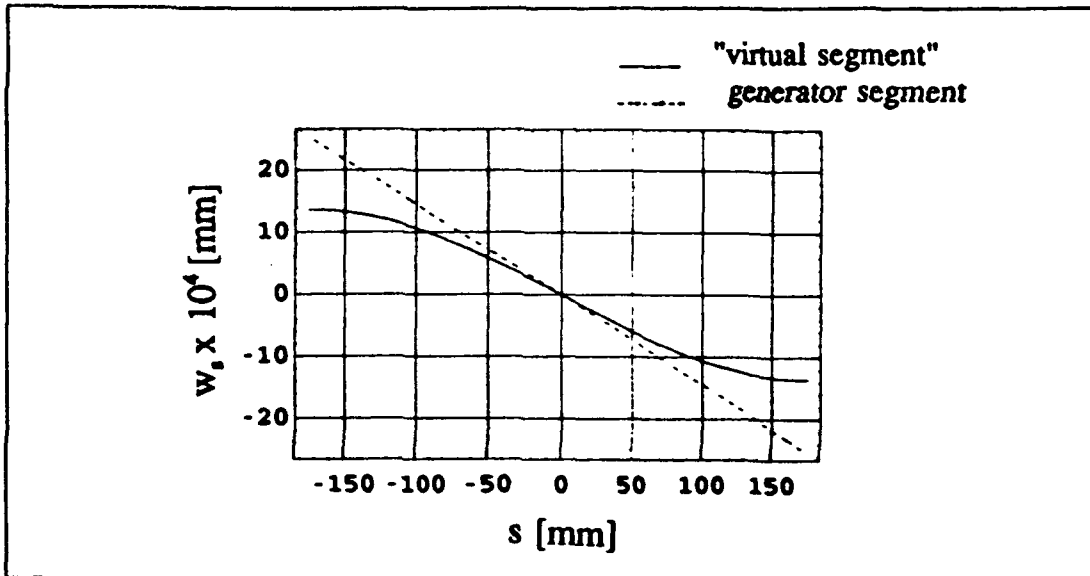


Figure 7.11 Surface Displacement for Virtual Segment Compared to Surface Displacement for Generator Segment at  $\pi/2$

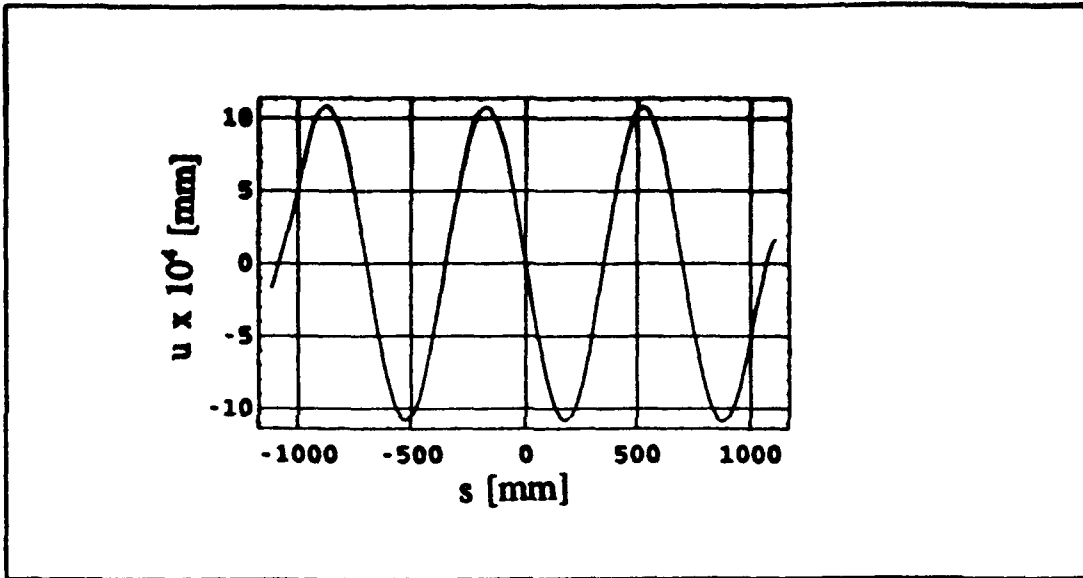


Figure 7.12. Unsegmented Barberpole Solution for Displacement  $u$

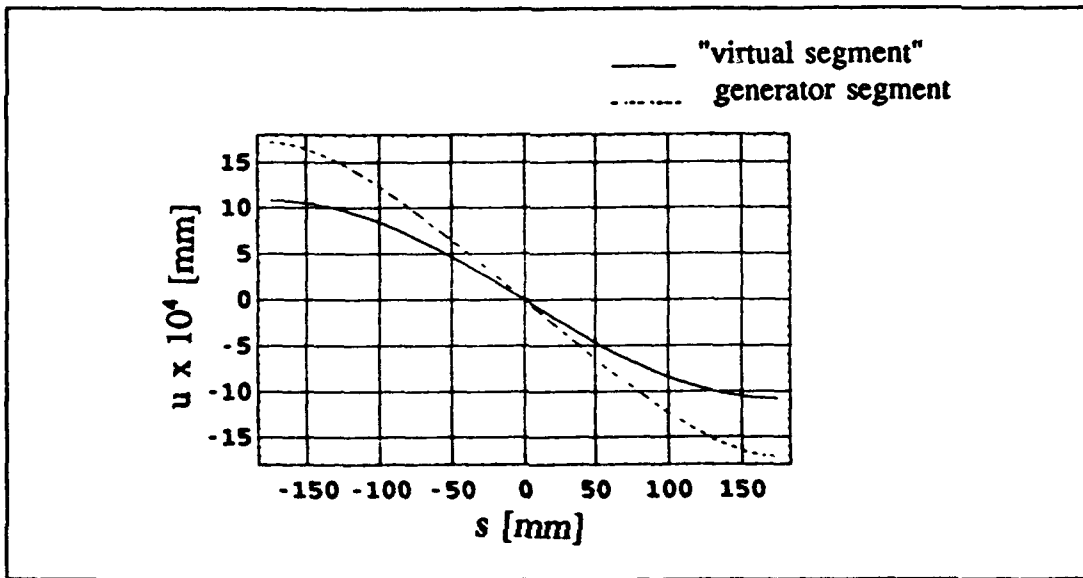


Figure 7.13. Displacement  $u$  for Virtual Segment Compared to Displacement  $u$  for Generator Segment at  $\pi/2$

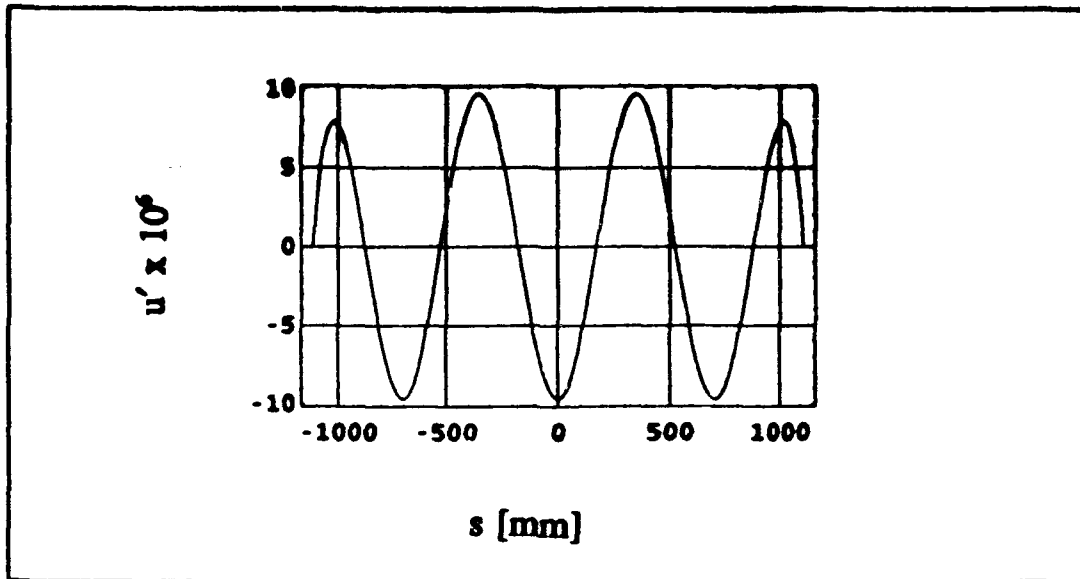


Figure 7.14. Unsegmented Barberpole Solution for Strain  $u'$

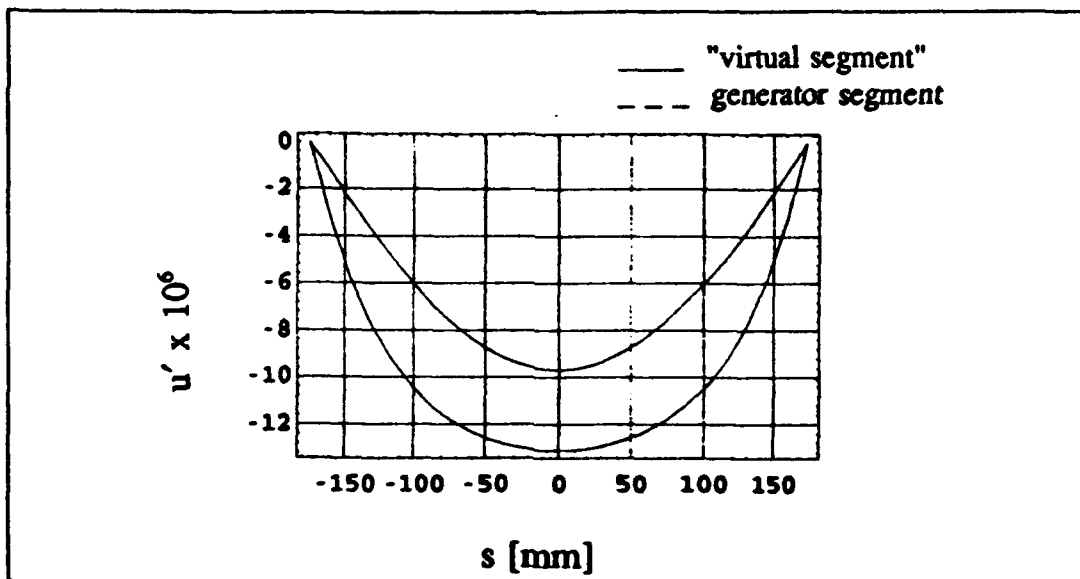


Figure 7.15. Strain  $u'$  for Virtual Segment Compared to Strain  $u'$  for Generator Segment at  $\pi/2$

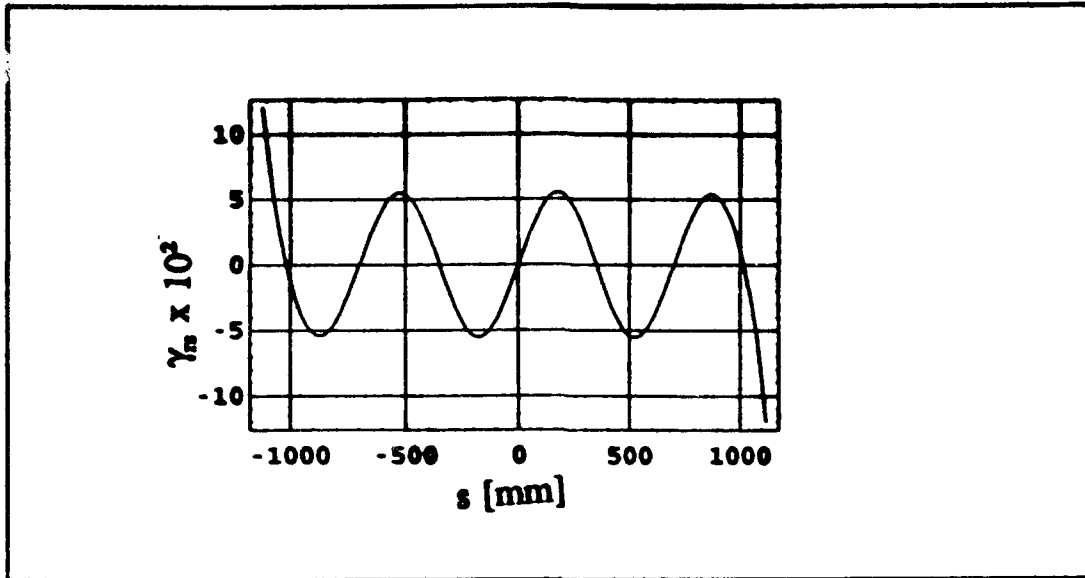


Figure 7.16. Unsegmented Barberpole Solution for Shear Strain  $\gamma_n$

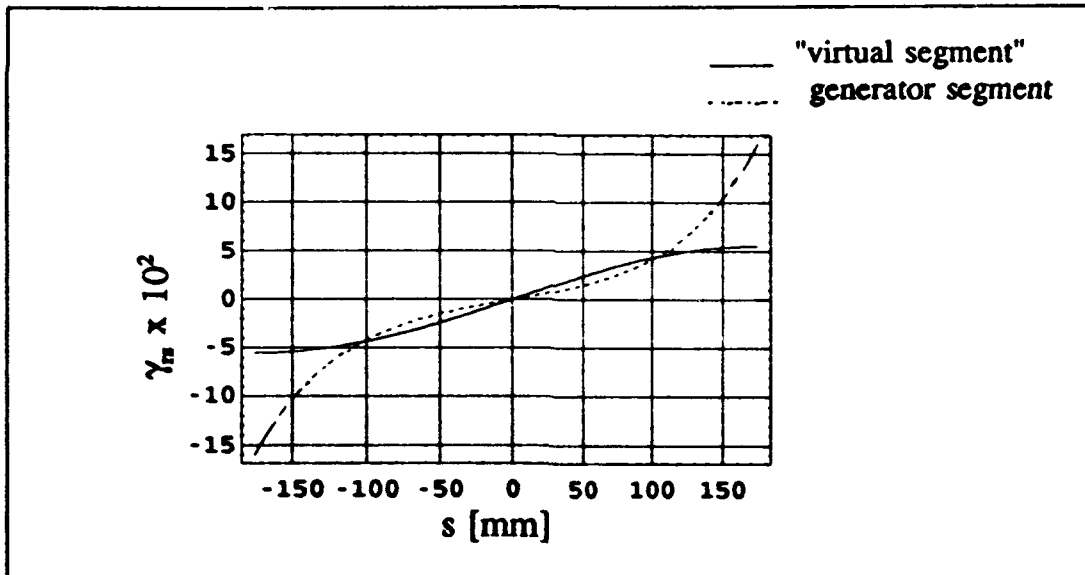


Figure 7.17. Shear Strain  $\gamma_n$  for Virtual Segment Compared to Shear Strain  $\gamma_n$  for Generator Segment at  $\pi/2$

Although there are similarities in the nature of the solutions, there are some very important differences that make the unsegmented barberpole solution with virtual segments less effective than optimally segmented generator strips. For a beam in a state of pure bending, a state of uniform surface strain exists under the generator segment, and most of the viscoelastic shear strain occurs at the ends of the strip. Viscoelastic shear strain in an unsegmented barberpole strip with nonzero pitch angle is driven by a non-uniform surface strain which drops to zero at the ends of the virtual segment (i.e., the neutral axis). As a result, there is less viscoelastic shear strain at the ends of the virtual segment, so the virtual segments provide less damping. The relative effectiveness of the barberpole geometry will be discussed in a later section.

*Choice of Pitch Angle for the Unsegmented Barberpole in Bending.* There are two major factors which drive the choice of pitch angle in the unsegmented barberpole problem. One factor is that the length of the virtual segments are controlled by pitch angle, and the effectiveness of the damping treatment will improve if the length of the virtual segments is near the optimal length. The other factor is that the magnitude of the substrate strain in the direction of  $s$  will decrease as the pitch angle  $\alpha$  increases. Both the optimal length and the substrate strain issues must be considered to identify the best choice of pitch angle .

*Optimal Pitch Angle: Effects of Optimal Length.* For the moment, ignore the effect of substrate strain and consider the issue of optimal length of the virtual segments.

The surface displacement  $w_s$  under the virtual segment is plotted in Figure 7.11, and it can be seen that the best quadratic approximation to the displacement is a straight line. A linear variation in surface displacement corresponds to the uniform strain condition, so the optimal length issues associated with the virtual segment will be addressed by adapting the uniform substrate strain analysis developed by Plunkett and Lee. This work is described in Chapter 3.

For the uniform surface strain problem, Plunkett and Lee identified the optimal length of a constrained layer segment to be  $L_{\text{optimal}} \approx 3.28/\sqrt{g}$  for a broad range of values of  $\eta_v$ . By combining this expression with the length of the virtual segment defined in Equation (7.85), the following choice of pitch angle produces a virtual segment of optimal length:

$$\sin \alpha = \frac{\pi R \sqrt{g}}{3.28} \quad (7.86)$$

An earlier analysis by Parfitt (71:1) can also be used to predict an optimal pitch angle similar to that identified in Equation (7.86). Parfitt considered a rectangular beam of infinite length with sinusoidal mode shapes of wavelength  $\lambda$ . Parfitt reported that if the beam is covered by a constrained layer damping treatment of infinite length and the system is lightly damped, maximum damping is attained when the following relation holds:

$$\sqrt{g} \lambda = 2 \pi \quad (7.87)$$

The state of surface strain for the rectangular beam with a sinusoidal mode shape is similar to surface strain under the barberpole strip in the direction of strip length. The wavelength  $\lambda$  identifies the distance between two areas of maximum extension or compression for the rectangular beam. The equivalent distance on the barberpole strip is the arclength of the strip that is required to make one full revolution about the beam, which is identified as  $s$  in Figure 7.18. By using this analogy, the results from Parfitt's analysis may be applied directly to the barberpole problem. From the barberpole geometry,  $s_\lambda = 2L_{\text{virtual}} = 2\pi R / \sin\alpha$ , so the expression for optimal pitch angle is found by substituting  $s_\lambda$  into Equation (7.87):

$$\sin\alpha = \sqrt{g} R \quad (7.88)$$

Note that this result is nearly equal to the result derived from the Plunkett and Lee expression in Equation (7.86).

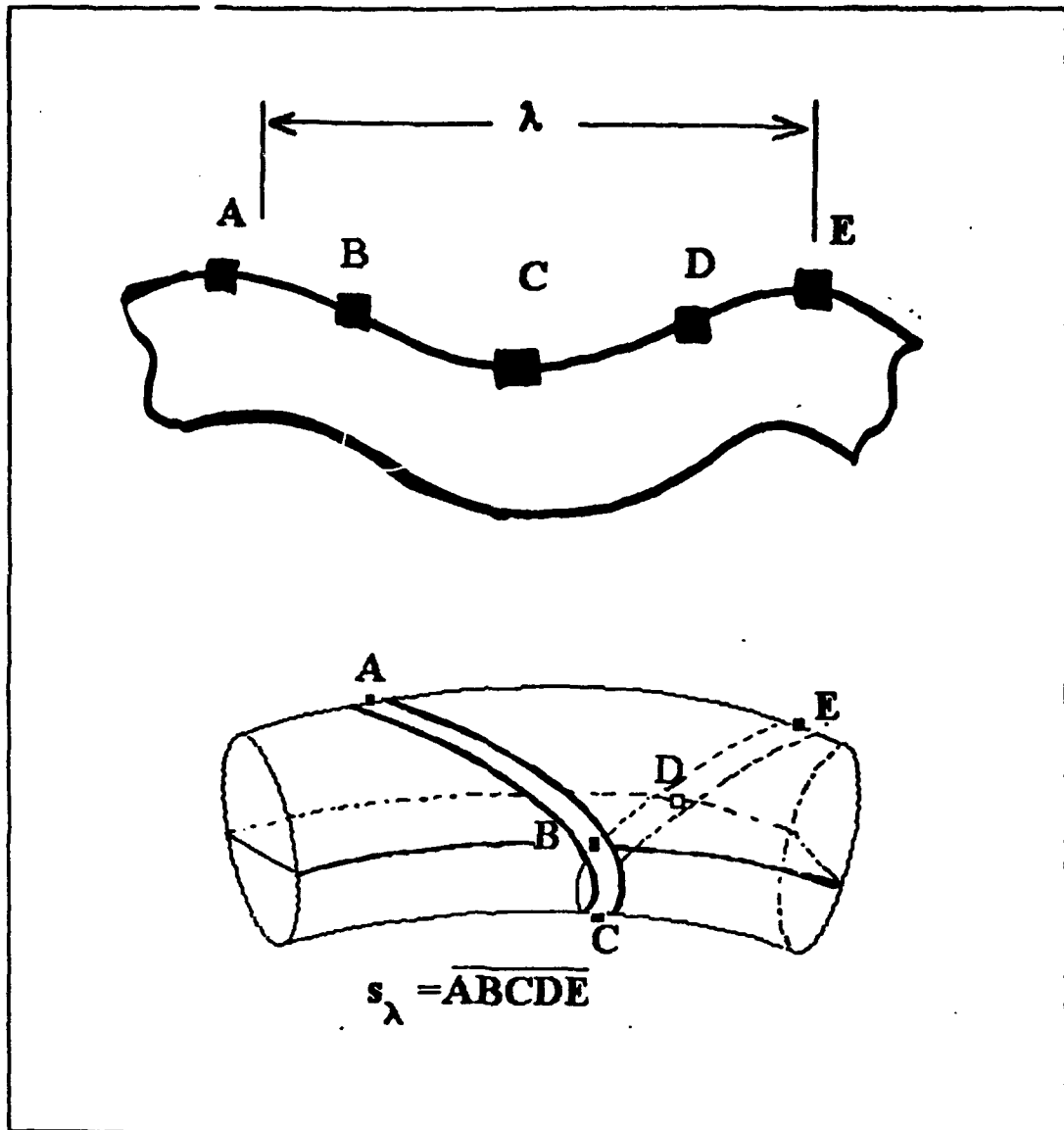


Figure 7.18. Analogy Between Barberpole Displacements and Parfit's Sinusoidal Displacements

The Plunkett and Lee loss coefficient  $H$  described in Chapter 3 may be adapted to quantify how the barberpole loss factor is affected by pitch angle. By substituting in the virtual segment length identified in Equation (7.85) into Equation (3.14), the loss coefficient becomes a function of  $\alpha$ :

$$H = \frac{4\pi}{\sqrt{g}L} \frac{\sinh A \sin \frac{\theta}{2} - \sin B \cos \frac{\theta}{2}}{\cosh A + \cos B} \quad (7.89)$$

where

$$A = \cos \frac{\theta}{2} \frac{\pi \sqrt{g} R}{\sin \alpha}, \quad B = \sin \frac{\theta}{2} \frac{\pi \sqrt{g} R}{\sin \alpha}, \quad \theta = \tan^{-1} \eta_v \quad (7.90)$$

In Equation (7.89), the dependence of the virtual segment length on pitch angle is unified with the effect of segment length on damping effectiveness. The expression will be used to quantify how the choice of pitch angle affects the barberpole loss factor through the effects of optimal length.

*Optimal Pitch Angle: Effects of Substrate Strain Amplitude.* Since the magnitude of the viscoelastic strain is proportional to the substrate strain, the effects of pitch angle on the substrate strain amplitude must also be considered. Consider the substrate strain in the  $s$  direction, which is found by taking the derivative of Equation (7.84 ):

$$e_s = \frac{dw_s}{ds} = RC_B \operatorname{sinc}\left(\frac{b \cos \alpha}{R}\right) (\cos^2 \alpha - \nu \sin^2 \alpha) \sin\left(\theta_o + \frac{s \sin \alpha}{R}\right) \quad (7.91)$$

Note that  $e_s$  is an oscillatory function with respect to  $s$  whose envelope is a function of  $\alpha$ . It is desirable to identify an expression that is a function of  $\alpha$ , but not a function of  $s$ , that may be used to identify the impact of the substrate strain on the barberpole loss factor. Viscoelastic shear strains are proportional to  $e_s$ , and the loss factor associated with the strip is proportional to the square of the shear strains integrated over the strip length. The magnitude of the loss factor is therefore proportional to the square of the function that defines the envelope:

$$E^2 = \left[ RC_B (\cos^2 \alpha - \nu \sin^2 \alpha) \operatorname{sinc}\left(\frac{b \cos \alpha}{R}\right) \right]^2 \quad (7.92)$$

$E^2$  and  $H$  are plotted as functions of  $\alpha$  in Figure 7.19 (both are multiplied by arbitrary scaling terms). The product of these two terms is plotted in Figure 7.20, and the loss factor as a function of  $\alpha$  is plotted in Figure 7.21. It can be seen that  $HE^2$  and the loss factor attain their maximum values near the same value of  $\alpha$ , which suggests the value of  $\alpha$  that maximizes  $HE^2$  would be a good estimate of the optimal pitch angle for the unsegmented barberpole configuration.

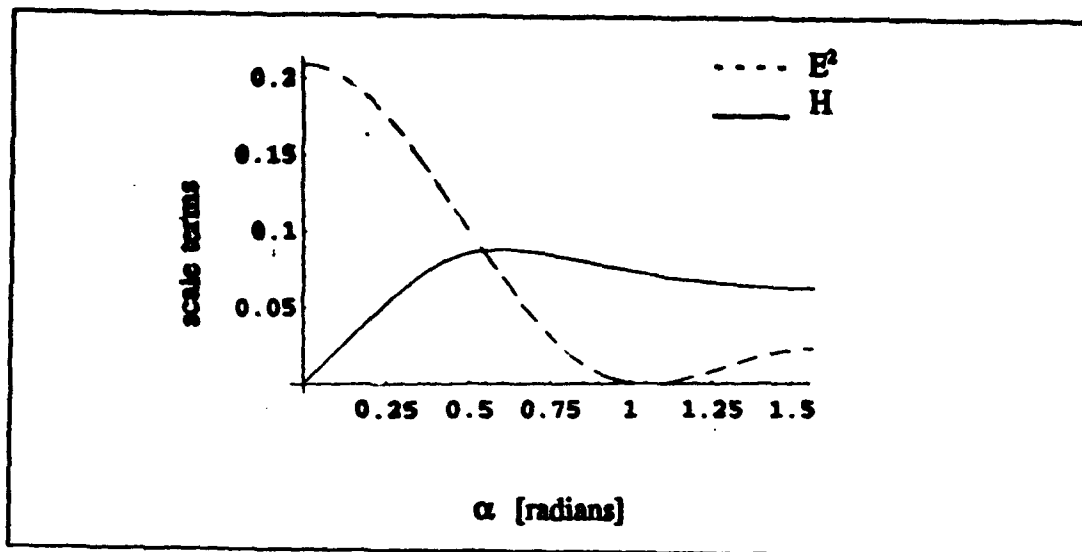


Figure 7.19. Effect of Pitch Angle on Substrate Strain ( $E^2$ ) and Virtual Segment Optimal Length ( $H$ ) ( $G_v = 100\text{KPa}$ )

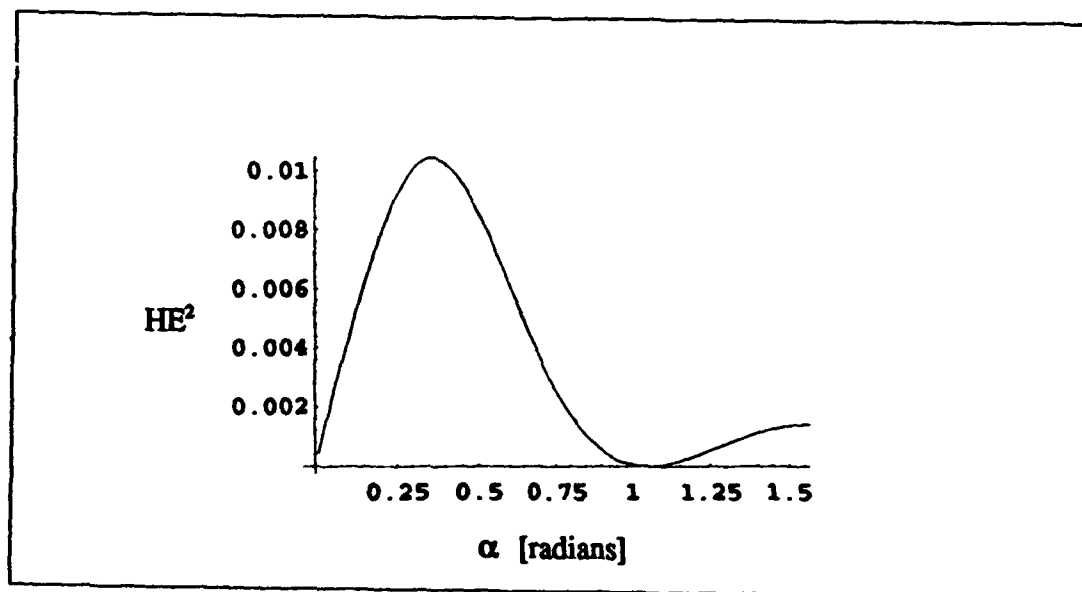


Figure 7.20. Combined Effect of Substrate Strain and Pitch Angle on Loss Factor ( $G_v = 100\text{KPa}$ )

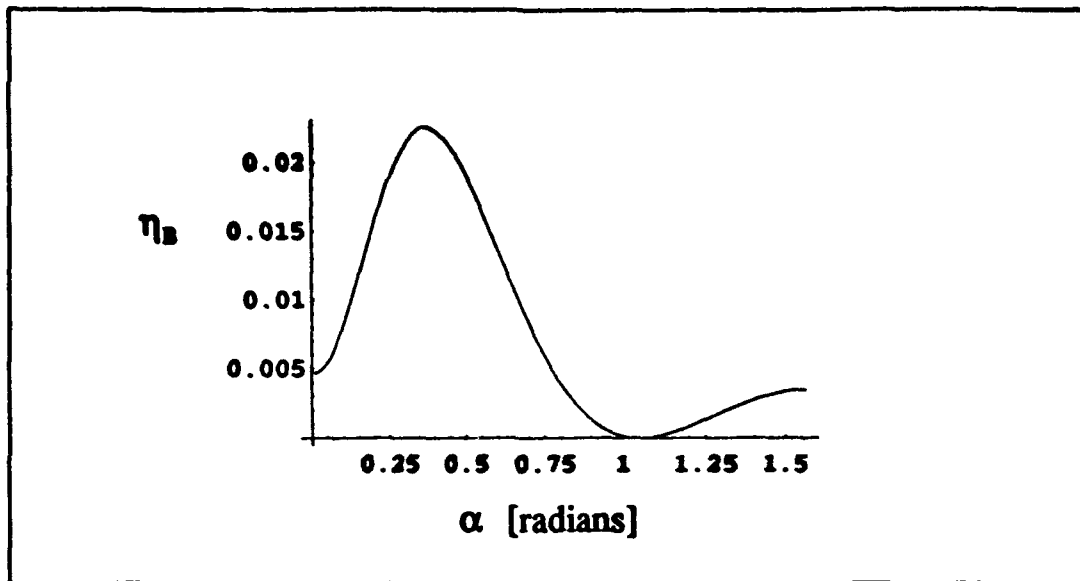


Figure 7.21. Effect of  $\alpha$  on Bending Loss Factor

In Table 7.1, the maximum bending loss factors for a fully covered barberpole ( $\eta_{\max}$ ) and the optimal pitch angles at which these loss factors occur ( $\alpha_{\text{optimal}}$ ) are identified for four different configurations. The values of alpha that maximize the function  $HE^2$  ( $\alpha_{\text{HE}}$ ) are also shown. In the four configurations the beam and damping strip geometries are identical, but the viscoelastic shear moduli have different values. The four values of shear modulus used in the figures are 70 KPa (10 lb/in<sup>2</sup>), 100 KPa (15 lb/in<sup>2</sup>), 140 KPa (20 lb/in<sup>2</sup>), and 331 KPa (48 lb/in<sup>2</sup>). From the table it can be seen that  $\alpha_{\text{HE}}$  provides a good approximation to  $\alpha_{\text{optimal}}$ , the pitch angle that provides the maximum damping for the unsegmented barberpole geometry. Also note that the maximum attainable loss factor for the unsegmented barberpole increases for damping treatments whose optimal pitch angle is small.

**Table 7.1 Unsegmented Barberpole Problem: Effect of Pitch Angle and Shear Modulus**

viscoelastic modulus $G_v$	70KPa	100KPa	140KPa	331KPa
$g$ [ $m^2$ ]	154	231	318	760
$3.28/\sqrt{g}$ [mm]	264	216	184	119
maximum attainable barberpole loss factor $\eta_{max}$	.026	.022	.020	.012
$\alpha_{optimal}$ [radians]	.34	.37	.39	.45
$\alpha$ at maximum $HE^2$ : $\alpha_{HE}$ [radians]	.33	.36	.38	.40

*Effectiveness of Unsegmented Barberpole Damping Treatment.* In this section the bending loss factor obtained from the unsegmented barberpole damping treatment is compared with two generator strip configurations (i.e.,  $\alpha=0$ ). One configuration consists of unsegmented generator strips running the full length of the beam, while the other configuration consists of generator strips cut to optimal length. Comparisons are performed for the four values of viscoelastic shear modulus identified in the previous section. The barberpole pitch angle for each case is  $\alpha_{\text{optimal}}$ , which provides the maximum possible damping from the barberpole configuration .

Loss factors for a beam length of 1.83m (72") and 3.66m (144") were calculated for both the barberpole and the generator strip configurations, and the results are shown in Table 7.2. Because the beam is in a state of uniform bending, the value of the loss factor for the segmented generator strip configuration is the same for any beam whose length is an integer multiple of the optimal segment length. The loss factor for the barberpole configuration is also relatively insensitive to the beam length. This is not the case for the unsegmented generator strip configuration. For this case, the longer beam has a loss factor one-half the value of the loss factor of the shorter beam. Because the constraining layer is much longer than optimal length, the viscoelastic shear strain is concentrated at the edges of the strip. Adding length to the beam and damping treatment only increases the amount of elastic structure that must be damped without adding to the shear strain in the viscoelastic layer.

**Table 7.2 Comparison of Unsegmented Barberpole Problem  
with the Generator Strip Configurations**

<b>DAMPING TREATMENT PROPERTIES</b>				
viscoelastic modulus $G_v$ g [m <sup>-2</sup> ]	70KPa	100KPa	140KPa	331KPa
	154	231	318	760
<b>OPTIMALLY CUT GENERATOR SEGMENTS</b>				
$L_{opt}=3.28/\sqrt{g}$ [mm]	264	216	184	119
$\eta_b$	.035	.035	.035	.035
<b>UNSEGMENTED BARBERPOLE</b>				
pitch angle $\alpha$	.34	.37	.39	.45
$\eta_b$ (1.83m beam)	.026	.023	.020	.012
$\eta_b$ (3.66m beam)	.026	.022	.020	.012
<b>UNSEGMENTED STRAIGHT STRIP</b>				
$\eta_b$ (1.83m beam)	.0074	.0057	.0050	.0032
$\eta_b$ (3.66m beam)	.0035	.0029	.0025	.0016

The data in Table 7.2 show that the loss factor for the unsegmented barberpole geometry lies between the values for the optimally cut straight strip and the unsegmented straight strip geometry. The best barberpole damping treatment is approximately three to four times better than the unsegmented straight strips on a 1.83m beam with a 76mm outer diameter. As the pitch angle decreases, the effectiveness of the barberpole configuration improves with respect to the optimally cut straight strip configuration.

The barberpole geometry provides better damping than the unsegmented straight strip because the shear strain in the viscoelastic layer is distributed more uniformly over the length of the strip. Figure 7.22 compares the viscoelastic shear strain of a full length

barberpole strip with a straight unsegmented strip. Proper choice of pitch angle maximizes the viscoelastic shear for each virtual segment.

Because the unsegmented barberpole geometry provides an improvement over the unsegmented problem without requiring segmentation cuts in the constraining layer, it may be considered a viable damping treatment for the pure bending problem if there are operational reasons to avoid segmentation. There may be situations where the additional cuts required for segmentation in the constraining layer could create maintenance problems in harsh operational environments. In space environments, problems can be caused by outgassing of some viscoelastic materials. It might be possible to develop a damping product that is fully encapsulated, yet takes advantage of the virtual segmentation effect. Because it is the pitch angle that determines the effective length of the segment, the same damping product could be used in different applications to generate virtual segments of different lengths. If such a treatment were designed without relying on the barberpole geometry for virtual segmentation, the encapsulated treatment would have to be available in a wide variety of segment lengths because the optimal length will depend on the frequency to be damped due to the frequency dependence of  $G_v$ .

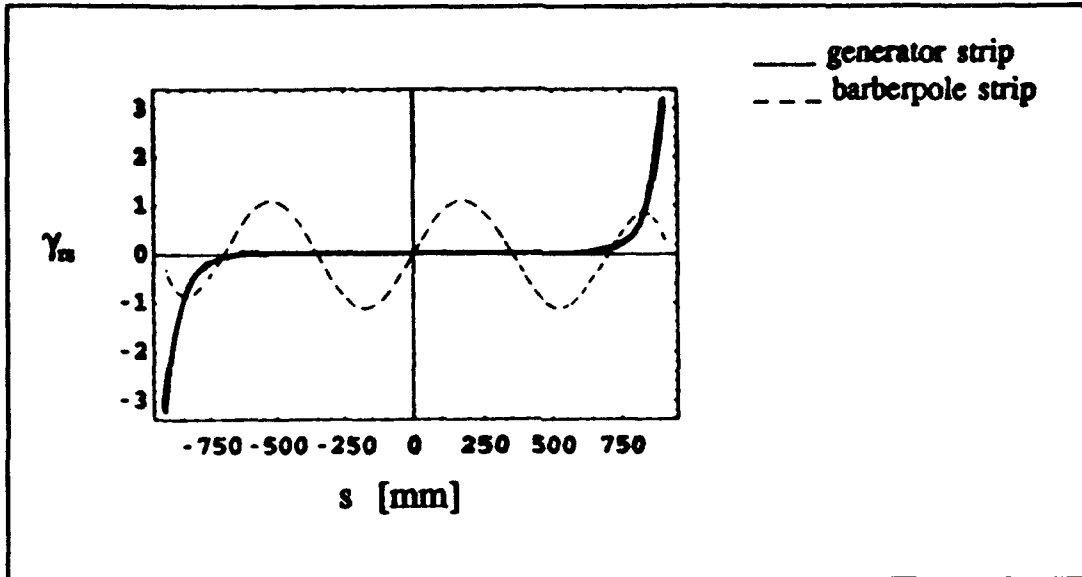


Figure 7.22. Viscoelastic Shear Strain in Unsegmented Generator and Barberpole Strips

### *Segmentation of the Barberpole Damping Strips*

In this section, barberpole design for the combined bending-torsion problem is examined. The segmented barberpole geometry considered in the parametric studies consists of a beam fully covered with strips at a common pitch angle which have periodically been cut along the circumference of the beam cross section, leaving bands of segments of equal length (Figure 7.1). One advantage of this configuration is that it is equally effective for bending in all planes and there is no preferred orientation of the beam. The cuts along the circumference of the beam are also easy to make without special cutting equipment. Another advantage of this configuration is that the spacing of the cuts can be varied along the  $z$  coordinate of the beam, which can be useful if damping of a higher mode is of particular concern. Bands of segments of optimal length for the higher frequency can be placed at areas of high strain for that particular mode shape.

A potential disadvantage of the banded configuration is that less viscoelastic shear strain will develop at the free ends of the cut constraining layer if the end of one of the bands is coincident with a beam nodal point. If the existence of nodal points is a problem that can not be alleviated by shifting the position of the bands, a second option for segmentation is to make spiral cuts into the constraining layer strips at a pitch angle equal to  $\pi/2 - \alpha$  radians, which produces rectangular damping segments (Figure 7.23). One advantage of this geometry is that the segment ends do not line up at a single  $z$  coordinate, so the position of the beam nodes for a given mode shape is relatively

insignificant. The geometry has the disadvantage of having some short segment lengths at either end of the beam which will not be as effective as segments of optimal length.

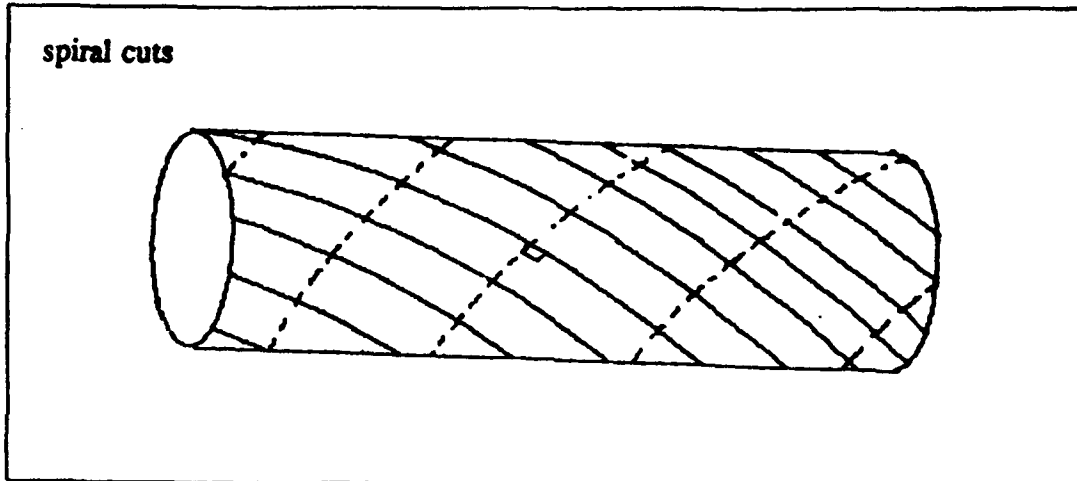


Figure 7.23. Alternative Segmentation Pattern: Spiral Cuts

### *The Barberpole in Torsion*

The torsional analysis of the barberpole yields solutions that have the same characteristics for both the segmented and unsegmented configurations. Earlier in the chapter it was noted that the torsional solutions for  $u'$  and  $\gamma_{xz}$  from Equations (7.39) and (7.40) have the same form as the uniform substrate strain problem discussed in Chapter 3. As a result, the shear strain in the viscoelastic layer is maximized when the effective strain,  $RC \cos\alpha \sin\alpha$ , is maximized, and the total length of the barberpole strips is equal to the optimal length identified by Plunkett and Lee. The optimal length can be achieved by either segmenting the strips to be of optimal length, or designing the unsegmented

geometry to be of optimal length. In these studies the segmentation approach is used because it allows the greatest flexibility in design, and can be used with several thin, commercially available constrained layer damping treatments that have an optimal length that is much shorter than the beam length (87).

The effects of geometry on torsional damping may be seen by calculating the loss factors for a range of torsional configurations, where both the pitch angle and the segment length are varied. In Figure 7.24, the effects of segment length on the torsional loss factor  $\eta_T$  are shown for pitch angles fixed at  $\alpha=.615$  and  $\alpha=\pi/4$  radians. For both cases, the peak loss factor occurs at a segment length  $L$  of 117 mm (4.6"), the length that maximizes the Plunkett and Lee loss coefficient for  $\eta_v=1$ . (The optimal length formula  $L_{\text{optimal}}=3.28/\sqrt{g}$ , which is independent of  $\eta_v$ , predicts an optimal length of 119mm.) At the optimal length, the loss factor for  $\alpha=\pi/4$  is  $\eta_T=.024$ , and for  $\alpha=.615$  the maximum loss factor is  $\eta_T=.021$ .

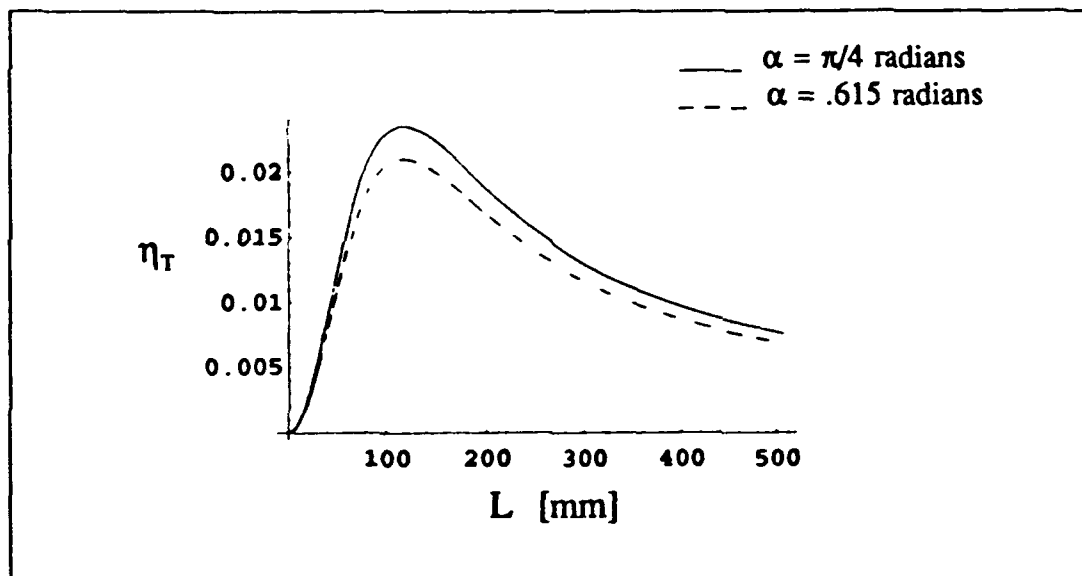


Figure 7.24. Effects of Segment Length on Torsional Loss Factor

In Figure 7.25, the effects of pitch angle on loss factor are shown for the torsion problem. Loss factors for two lengths of damping strips are identified; one configuration is an unsegmented damping treatment on a 1.83m beam at a pitch angle of .615 radians, and the other is the same damping treatment cut into segments of optimal length ( $L=119\text{mm}$ ). These two configurations, when wrapped at a pitch angle of .615 radians, correspond to the damping geometries used in the experiment described in the next chapter, before and after segmentation. The unsegmented barberpole loss factor is  $\eta_T=0.00155$  for  $\alpha=.615$ . For the segmented configuration, the loss factor increases to  $\eta_T=0.021$ , which is a 13 fold increase over the loss factor of the unsegmented configuration. Both curves show the  $\sin\alpha \cos\alpha$  dependence on pitch angle for the torsion problem. Similar studies for damping strips of different lengths would produce the same shape, with the only difference being the magnitudes of the loss factor.

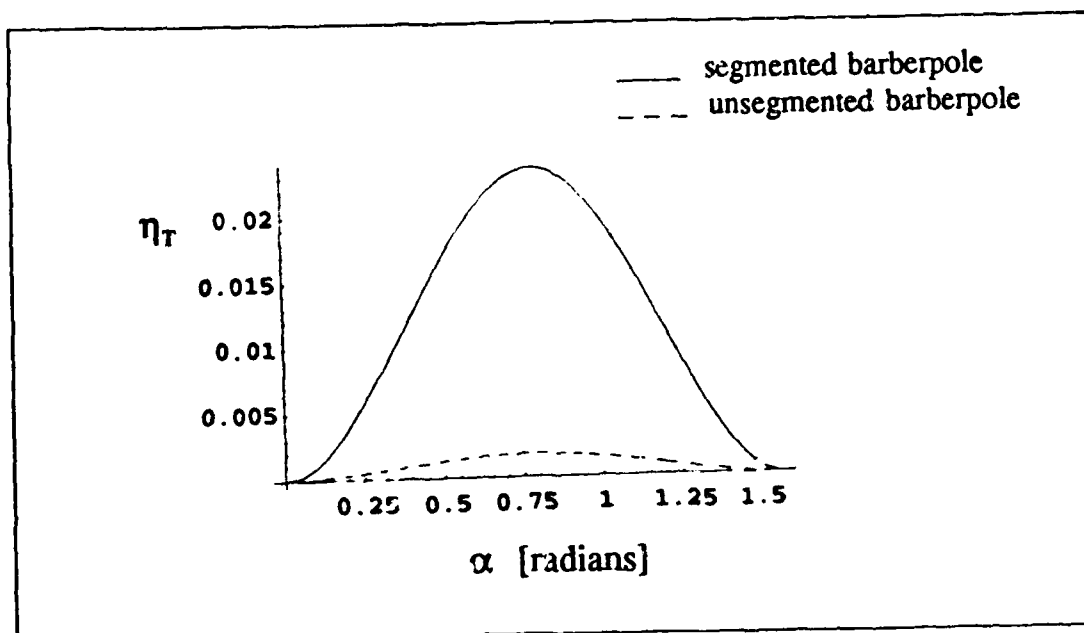


Figure 7.25. Effect of Pitch Angle on Torsional Loss Factor

### *The Segmented Barberpole in Bending*

The previous discussions provide a framework to understand the segmented barberpole problem in bending. In this section it is tacitly assumed that the optimal length of the damping treatment is relatively short compared to beam circumference, and that a strip of optimal length placed at an pitch angle of  $\pi/4$  radians or less will only cross the neutral axis once. Because of this assumption, virtual segmentation will not be an issue in the damping treatment design.

Because there is no need for neutral axis crossings to create virtual segments, the damping generated by a segmented barberpole configuration will decrease with increasing pitch angle. Figure 7.26 shows the dependence of bending loss factor  $\eta_B$  on  $\alpha$  for a segments of optimal length as defined by Plunkett and Lee. Note that the  $\alpha$  dependence is similar to  $E_s^2$ , the square of the envelope of the effective substrate strain  $\epsilon_s$ .  $E_s^2$  is plotted in Figure 7.16 and defined in Equation (7.67). The optimal damping for bending occurs when  $\alpha=0$ , and the only reason to have a nonzero pitch angle is to obtain damping for torsional vibrations. The best choice of  $\alpha$  will depend on the relative importance of the torsional vibration damping.

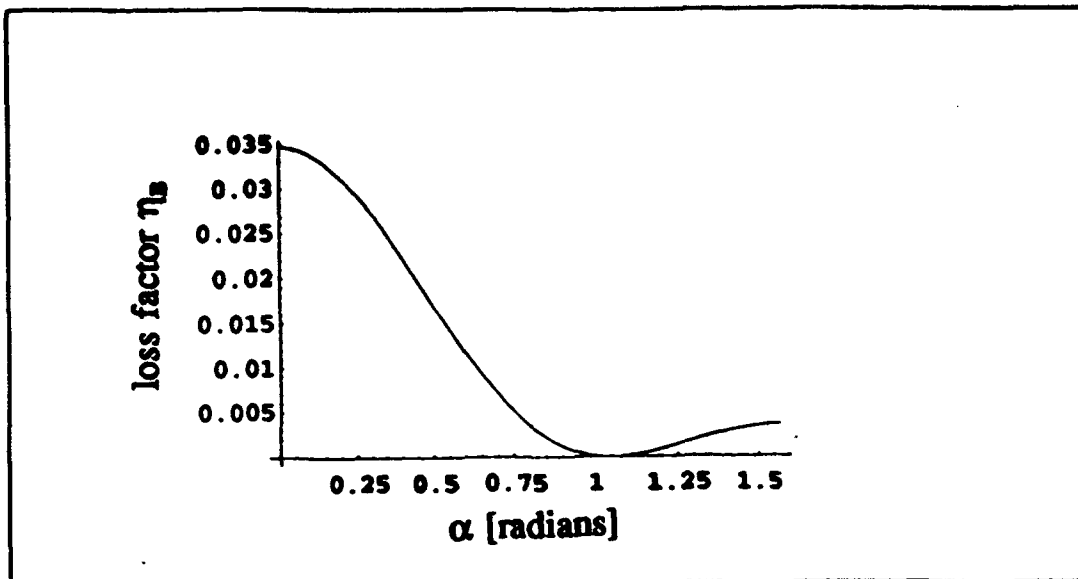


Figure 7.26. Effect of  $\alpha$  on Bending Loss Factor (  $L=193$  mm)

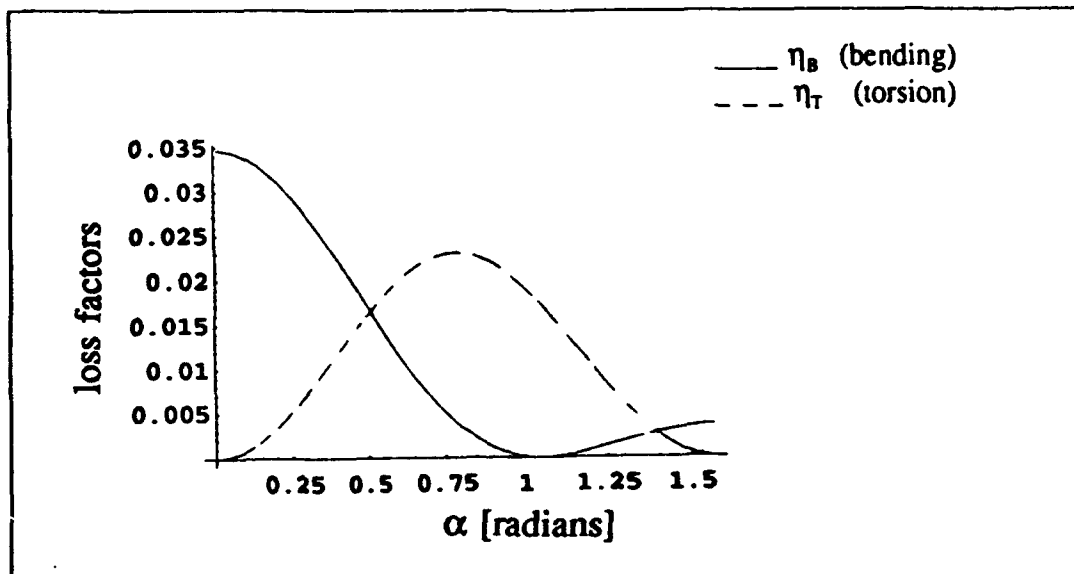


Figure 7.27. Effect of  $\alpha$  on Bending and Torsional Loss Factors

In Figure 7.27, the alpha dependence of the bending and torsional loss factors  $\eta_B$  and  $\eta_T$  are plotted for the beam geometry and damping treatment used in the experiment that is described in the next chapter. The figure illustrates how the choice of pitch angle is a trade-off between concerns over bending and torsional vibrations. For the figure, it is assumed that both the bending and torsional vibrations of concern are in same frequency range, approximately 20 hertz. Note that if a beam is part of a larger structure, often the global modes of the assembly are of concern, which usually occur at frequencies much lower than the fundamental frequencies of the beam itself.

Now suppose  $\alpha$  is fixed at some value which reflects the relative importance of the bending and torsional vibration. The optimal length analysis of Plunkett and Lee provides guidance on sizing the length of the damping strips in the problem. For the damping treatment used in the experiment, the Plunkett and Lee formula specifies  $L_{\text{optimal}} = 119$  mm for the case of uniform surface strain.

In Figure 7.28, the loss factor of the barberpole geometry in bending is plotted for pitch angles of .3, .5, and .615 radians. Note that the maximum attainable loss factors decrease with an increase in pitch angle, but each has a maximum value near that predicted by the Plunkett and Lee analysis. For a pitch angle of .615 radians, the loss factor of the beam is maximized for a length  $L$  of 123mm. This result is consistent with the findings in Chapter 3, which showed that if the surface strain under the constraining layer has a nonuniform strain, the optimal length of a segment tends to be longer than that predicted by the Plunkett and Lee formulation. The length  $L$  that maximizes  $\eta_T$  is

117mm (from Figure 7.24). The optimal lengths in bending and torsion are approximately equal because the viscoelastic properties at 20 hertz were used for both analyses. It is important to remember that a second trade-off between bending and torsion will occur in the choice of segment length if there is a large spread in the bending and torsional frequencies. Because the damping drops off sharply if the segment is chosen to be shorter than optimal length, the larger length should be chosen if the two optimal lengths are relatively close in value.

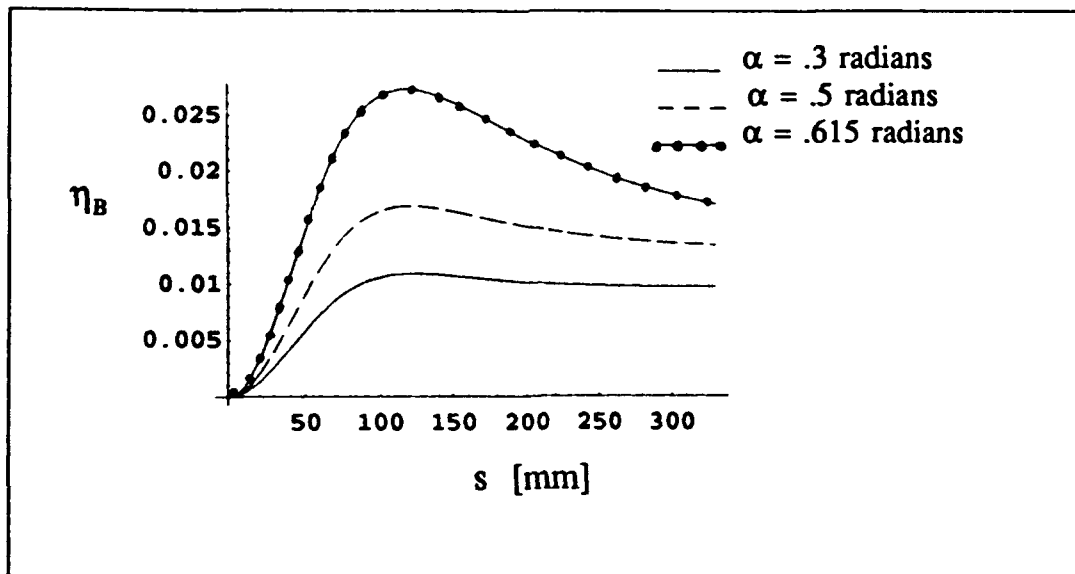


Figure 7.28 Effects of Strip Length on Bending Loss Factor.

### *Chapter Summary*

In Chapter 7, a new constrained layer configuration was proposed for the damping of beams of circular cross section that are subjected to both bending and torsional vibrations. The damping treatment consists of thin, narrow strips of constrained layer damping treatment oriented at a common pitch angle in a helical or "barberpole" configuration, then periodically segmented along their length. An analysis was developed that shows that the barberpole configuration has the capability to damp both bending and torsional vibrations. It was shown that for the pure bending problem, the unsegmented barberpole geometry provides more damping than unsegmented strips parallel to the generator lines. Although the unsegmented barberpole geometry is not as effective as the optimally cut generator strips for damping bending vibrations, it could be useful for applications where periodic segmentation along the beam length is undesirable due to environmental or operational reasons. It is also shown that the barberpole configuration may be used to provide damping for a beam subjected to both bending and torsional vibrations. The optimal geometry for damping torsion is a segmented barberpole configuration with a pitch angle of  $\pi/4$  radians, while the optimal geometry for damping bending vibrations has a zero pitch angle and segments of optimal length. The best barberpole design for a given configuration will depend on the relative importance of damping torsional and bending motion.

**Appendix 7A: Average Strain Energy in the Damping Strips  
for the Fully Coated Barberpole in Bending**

If the Modal Strain Energy Method is used to calculate loss factors, the value for the loss factor for N strips is identified in Equation 7.79:

$$\eta_{system} = \frac{\sum_{n=1}^W \eta_{v_n} U_{\gamma_n}}{U_b + \sum_{n=1}^W U_{\gamma_n} + \sum_{n=1}^W U_{c_n}} \quad (7A.1)$$

The strain energies for an individual strip have the following form:

$$U_c = \frac{1}{2} \int_{-l}^l E_c A_c u'^2 ds \quad (7A.2)$$

$$U_{\gamma} = \frac{1}{2} \int_{-l}^l G_v A_v \gamma_{rs}^2 ds$$

The constraining layer extensional strain  $u'$  is obtained from the derivative of Equation (7.71), while the viscoelastic shear strain is identified in Equation (7.73):

$$u' = W_s(\alpha) \left[ \frac{g \sin \alpha \sin \left( \theta_o + s \frac{\sin \alpha}{R} \right)}{R \left( g + \left( \frac{\sin \alpha}{R} \right)^2 \right)} + \sqrt{g} P \sinh(\sqrt{g} s) + \sqrt{g} Q \cosh(\sqrt{g} s) \right] \quad (7A.3)$$

$$\gamma_{rs} = -\frac{W_s(\alpha)}{2h_v} \left[ \left( 1 + \frac{g}{s + \left( \frac{\sin \alpha}{R} \right)^2} \right) \cos \left( \theta_o + s \frac{\sin \alpha}{R} \right) + P \cosh(\sqrt{g} s) + Q \sinh(\sqrt{g} s) \right] \quad (7A.4)$$

For the purposes of this proof, redefine  $u'$  and  $\gamma_{rs}$  by using the following properties:

$$\begin{aligned} 2 \sin(a+b) &= \sin(a)\cos(b) + \cos(a)\sin(b) \\ 2 \cos(a+b) &= \cos(a)\cos(b) - \sin(a)\sin(b) \end{aligned} \quad (7A.5)$$

The expression for  $u'$  may be written as:

$$\begin{aligned} u' &= A_1 \left[ \sin\theta_o \cos\left(s \frac{\sin\alpha}{R}\right) + \cos\theta_o \sin\left(s \frac{\sin\alpha}{R}\right) \right] \\ &\quad + P_1 \sinh(\sqrt{g} s) + Q_1 \cosh(\sqrt{g} s) \end{aligned} \quad (7A.6)$$

where

$$A_1 = W_s(\alpha) \frac{g \sin\alpha}{R \left( g + \left( \frac{\sin\alpha}{R} \right)^2 \right)}, \quad P_1 = \sqrt{g} P W_s(\alpha), \quad Q_1 = \sqrt{g} Q W_s(\alpha)$$

The expression for  $\gamma_{rs}$  may be written as:

$$\gamma_{rs} = A_2 \left[ \cos\theta_o \cos\left(s \frac{\sin\alpha}{R}\right) - \sin\theta_o \sin\left(s \frac{\sin\alpha}{R}\right) \right] + P_2 \cosh(\sqrt{g} s) + Q_2 \sinh(\sqrt{g} s) \quad (7A.7)$$

where

$$A_2 = -\frac{W_s(\alpha)}{2h_v} \left( 1 + \frac{g}{s \left( \frac{\sin\alpha}{R} \right)^2} \right), \quad P_2 = \frac{W_s(\alpha) P}{2h_v}, \quad Q_2 = \frac{W_s(\alpha) Q}{2h_v}$$

Rewrite  $u'$  and  $\gamma_{rs}$  as the sum of even and odd functions:

$$\begin{aligned} u' &= \sin\theta_o f_e(s) + \cos\theta_o f_o(s) \\ \gamma_{rs} &= \cos\theta_o g_e(s) + \sin\theta_o g_o(s) \end{aligned} \quad (7A.8)$$

where functions  $f_e$ ,  $f_o$ ,  $g_e$ , and  $g_o$  are functions of  $s$ , but are independent of theta:

$$f_e(s) = A_1 \cos \frac{s \sin \alpha}{R} + Q_1 \cosh \sqrt{g}s \quad (7A.9)$$

$$f_o(s) = A_1 \sin \frac{s \sin \alpha}{R} + P_1 \sinh \sqrt{g}s$$

$$g_e(s) = A_2 \cos \frac{s \sin \alpha}{R} + P_2 \cosh \sqrt{g}s \quad (7A.10)$$

$$g_o(s) = -A_2 \sin \frac{s \sin \alpha}{R} + Q_2 \sinh \sqrt{g}s$$

The product of an even and odd function is an odd function, and the integral of an odd function in  $s$  over the interval  $s \in [-1, 1]$  is zero. As a result, the strain energy terms have the following form:

$$\begin{aligned} U_c &= \frac{1}{2} \int_{-1}^1 E_c A_c [\sin \theta_o f_e(s) + \cos \theta_o f_o(s)]^2 ds \\ &= \frac{1}{2} \int_{-1}^1 E_c A_c [(\sin \theta_o f_e(s))^2 + (\cos \theta_o f_o(s))^2] ds \\ &= \sin^2 \theta_o F_E + \cos^2 \theta_o F_O \end{aligned} \quad (7A.11)$$

$$\begin{aligned} U_v &= \frac{1}{2} \int_{-1}^1 G_v A_v [\cos \theta_o g_e(s) + \sin \theta_o g_o(s)]^2 ds \\ &= \frac{1}{2} \int_{-1}^1 G_v A_v [(\cos \theta_o g_e(s))^2 + (\sin \theta_o g_o(s))^2] ds \\ &= \cos^2 \theta_o G_E + \sin^2 \theta_o G_O \end{aligned} \quad (7A.12)$$

where

$$F_E = \frac{1}{2} \int_{-l}^l E_c A_c f_e(s)^2 ds, \quad F_O = \frac{1}{2} \int_{-l}^l E_c A_c f_o(s)^2 ds$$

$$G_E = \frac{1}{2} \int_{-l}^l G_v A_v g_e(s)^2 ds, \quad G_O = \frac{1}{2} \int_{-l}^l G_v A_v g_o(s)^2 ds$$

$F_E$ ,  $F_O$ ,  $G_E$ , and  $G_O$  are independent of  $\theta_o$ , and therefore are the same for all strips with the same pitch angle, material properties, and cross section. Now consider the sum of these terms for the case where there are  $N$  total strips, which are arranged in sets of 4, where each strip of the set is  $\pi/2$  radians apart from each other (Figure 7.7).

$$\begin{aligned} \sum_{n=1}^N U_{Y_n} &= \sum_{n=1}^N [\cos^2 \theta_o G_E + \sin^2 \theta_o G_O] \\ &= 2 \sum_{n=1}^{N/2} [\cos^2 \theta_o G_E + \sin^2 \theta_o G_O] \\ &= 2 \sum_{n=1}^{N/4} [\cos^2 \theta_o G_E + \sin^2 \theta_o G_O + \sin^2 \theta_o G_E + \cos^2 \theta_o G_O] \\ &= \frac{N}{2} [G_E + G_O] \end{aligned} \tag{7A.13}$$

$$\begin{aligned} \sum_{n=1}^N U_{C_n} &= \sum_{n=1}^N [\sin^2 \theta_o F_E + \cos^2 \theta_o F_O] \\ &= 2 \sum_{n=1}^{N/2} [\sin^2 \theta_o F_E + \cos^2 \theta_o F_O] \\ &= 2 \sum_{n=1}^{N/4} [\sin^2 \theta_o F_E + \cos^2 \theta_o F_O + \cos^2 \theta_o F_E + \sin^2 \theta_o F_O] \\ &= \frac{N}{2} [F_E + F_O] \end{aligned} \tag{7A.14}$$

Now consider the configuration for the special case where  $\theta_o = \pi/4$ . From Equation 7A.11 and 7A.12, the strain energies are:

$$U_\gamma |_{\theta_o = \pi/4} = \frac{1}{2} [G_E + G_O] \quad (7A.15)$$
$$U_c |_{\theta_o = \pi/4} = \frac{1}{2} [F_E + F_O]$$

It can be seen that the strain energies of the damping strip at  $\theta_o = \pi/4$  are equal to the average value of the strain energies associated with the N strips on the fully coated barberpole.

### *VIII. The Barberpole in Bending: Comparison of Theory and Experiment*

The barberpole bending analysis presented in Chapter 7 characterized a geometry that is much more complicated than the rectangular beams customarily studied. Because it was desirable to obtain equations that could be solved in closed form, several higher order effects were neglected in modelling the constraining layer displacements. Due to these factors, a series of free vibration experiments was performed on a cantilever beam to insure that the bending analysis correctly captured the dominant effects of the barberpole configuration. The loss factors obtained from the experiments were compared with those predicted using the bending analysis of Chapter 7.

#### *Experimental Apparatus*

*Test Article.* The test article was a aluminum tube with a 76 mm (3") outer diameter. The tube had a .07 mm (.0028") wall thickness and was constructed from 6061 T-4 aluminum. The beam was mounted to an area of the floor that had been isolated from building vibrations. The tube had an overall length of 1.91 m (75"), but the effective length of the cantilever beam was 1.83 m (72") because 3" of the tubing was restrained in the mounting fixture and was considered part of the root of the beam.

Special care was taken in the design of the test article to minimize the damping of the bare beam and to simulate the idealized rigid root used in the cantilever analysis.

A bolted aluminum support was designed to mount the beam to the floor securely. The support consisted of a 3" long inner plug that extended into the tube, with a set of six thick support brackets that bolted into the tube and plug, then bolted into a base plate. All the mating surfaces were machined to very tight tolerances to minimize relative motion.

A loading fixture made of aluminum was bolted to the free end of the beam to allow the initial displacement to be applied without inducing deformations in the cross section. The loading fixture had a design similar to the root support, but was much less massive. It consisted of a thin aluminum ring that was held in place inside the tube by a set of six brackets. The total added tip mass was 254 grams.

*Instrumentation.* Accelerometer data from a Kistler 8528B5 Piezobeam accelerometer and a Kistler 2612A signal coupler were used to obtain the measure of damping. The accelerometer was mounted at the free end of the cantilever beam. A 8528B50 Piezobeam accelerometer was also mounted at the free end of the beam as a redundant data source. A Tektronix 2642 Fourier Analyzer was used to collect, store, and process the test data. The accelerometer calibration data from the vendor was verified at a single frequency near the beam resonance using a reference accelerometer.

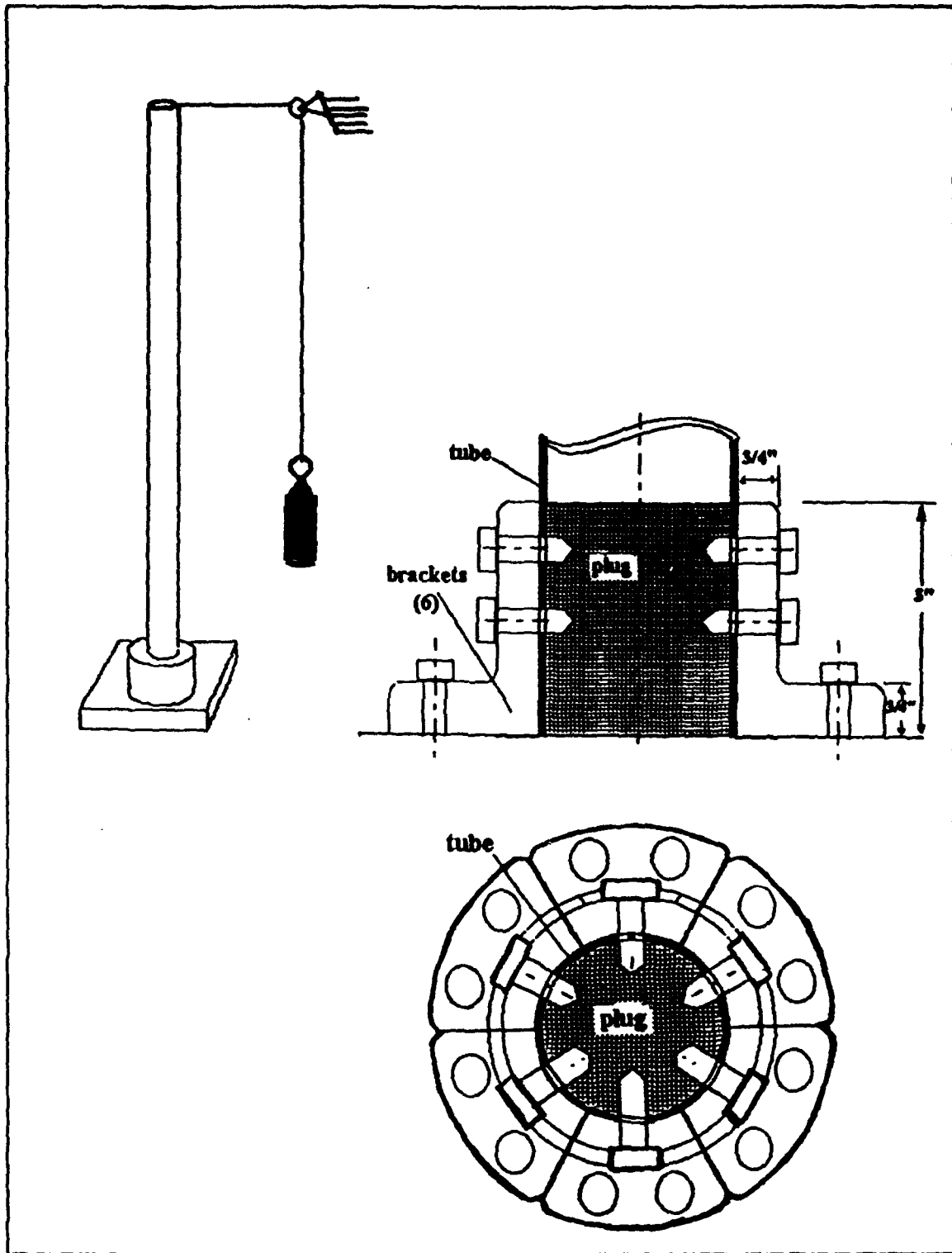


Figure 8.1 . Test Article and Root Support

*Damping Treatment.* A prepackaged constrained layer damping treatment manufactured by 3M was used to produce the damped configurations. The viscoelastic layer consisted of a .05 mm (.002") layer of ISD-112 affixed to a .13 mm (.005") layer of aluminum. Material properties for ISD-112 are located in Figure 8.2. The viscoelastic layer was self-adhesive and pressure activated. The damping treatment was acquired in continuous roll form, and was thin enough to be easily cut and applied to the cylindrical beam surface.

*Barberpole Damping Configurations.* To fabricate the barberpole damping treatment, 32 narrow strips were cut from the roll of damping material. Each strip was 2.23 m long and approximately 5.5 mm wide for the unsegmented damping treatment. The bare beam was cleaned with acetone prior to the application of the damping strips, which were wrapped at a pitch angle of  $-.61$  radians ( $-35$  degrees).

After the unsegmented barberpole configuration was tested, the damping strips on the beam were cut to form the segmented configuration. Nineteen bands of segments were produced by making 18 cuts around the beam circumference that were separated by a distance of 97 mm as measured along the z axis. The length between cuts was chosen to produce segments whose dimension in the s direction would be the optimal length identified by the Plunkett and Lee analysis for a frequency of vibration near 20 hertz. The cuts produced 18 bands of segments of optimal length (119 mm) and one band of segments near the free end of the beam with a length in the s direction equal to 80 mm.

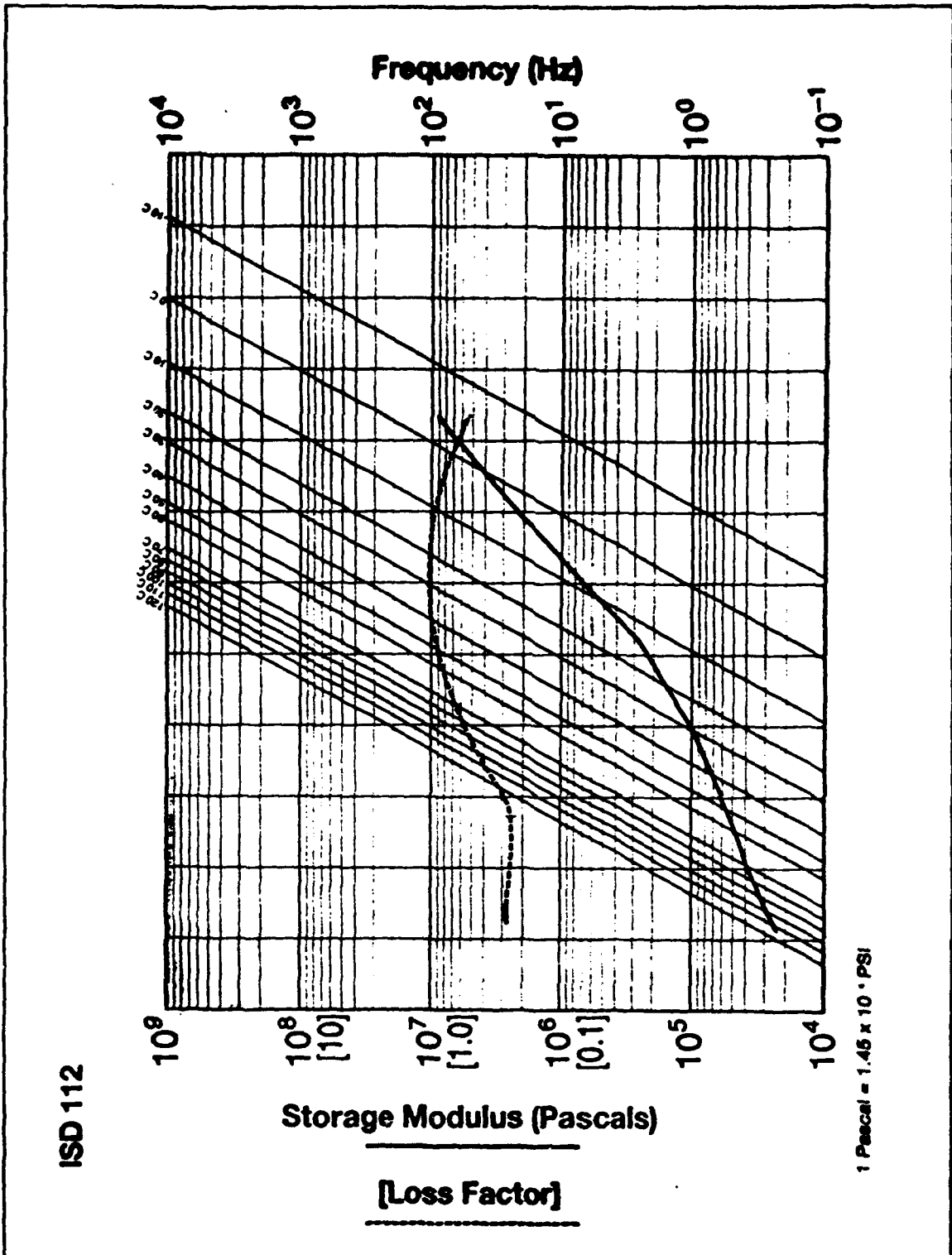


Figure 8.2. Properties of ISD-112

### *Experimental Procedure: Acquisition of Data*

The procedure used to collect and process the data was identical for all configurations tested. The data sets were collected using the sequence of activities described below.

*Record Temperature and Prepare Instrumentation:* Because the properties of the viscoelastic material were temperature dependent, the ambient temperature of the laboratory was recorded for each test series. The Tektronix IP software program was initialized, and a batch file containing the default settings for the data acquisition was loaded.

*Create Initial Tip Displacement:* An initial displacement of the tip of the cantilever beam was generated by the static force from a suspended one kilogram mass. A cord attached to the mass was routed through a pulley and attached to the load fixture at the free end of the beam (Figure 8.1).

*Initiate Test and Acquire Data:* Prior to each test, the Tektronix analyzer data acquisition system was activated and armed. Once armed, the acquisition of data would begin once the accelerometer experienced a offset equal to 6% of the expected full scale signal. The cord was then burned through near its attachment to the beam. This approach was simple to execute and provided a relatively clean release. The beam began to vibrate as soon as the cord was burned through, and its motion triggered the acquisition of data. After a test, the time history of the tip acceleration was stored in digital form for further analysis.

### *Determining Damping from the Experimental Data*

A measure of the damping was obtained from the raw data using the same method for all data sets. Because the loss factor  $\eta$  is used as a measure of damping in most of the constrained layer literature, the experimentally obtained percent critical damping ( $\zeta$ ) was converted into a loss factor by using the relation  $\eta=2\zeta$ . To find  $\zeta$ , it was assumed that the envelope of the oscillatory signal from the accelerometer was of the form  $\exp[-\zeta \omega_n t]$ , where  $\omega_n$  is the undamped natural frequency of the beam. The amplitudes  $A_1$  and  $A_2$  were defined as the peak to peak magnitudes of oscillation that correspond to times  $t_1$  and  $t_2$ . Using the relationship between  $\omega_d$  and  $\omega_n$  (the damped and undamped frequencies of the beam), an expression for zeta was obtained from terms collected from the graph:

$$A_2 = A_1 e^{-\zeta \omega_n (t_2 - t_1)}, \quad \omega_n = \frac{\omega_d}{\sqrt{1 - \zeta^2}} \quad (8.1)$$
$$\rightarrow \zeta = \frac{\zeta}{\sqrt{1 - \zeta^2}} = \frac{\text{Ln} \left( \frac{A_1}{A_2} \right)}{\omega_d (t_2 - t_1)}$$

It should be noted that this measure of damping is independent of the magnitude of the accelerometer calibration factor as long as the calibration factor does not change between times  $t_1$  and  $t_2$ . Because the method uses the natural logarithm of the ratio of two peak amplitudes, any constant multiplied by the amplitudes does not affect the predicted damping.

To assess the linearity of the value for zeta over the amplitudes tested, the logarithm of the accelerometer output magnitude was plotted versus time. On this type of "semi-log" plot, the envelope of the accelerometer signal has a linear envelope if the magnitude of the system damping does not vary with the amplitude of vibration.

#### *Obtaining Predictions from the Barberpole Analysis*

The loss factors obtained from the experimental data were compared with theoretical values obtained from the barberpole theory described in Chapter 7. Both the Modal Strain Energy and the Complex Rayleigh Quotient approaches were used to find the loss factors of each configuration. It was shown in Chapter 5 that for lightly damped systems, the Complex Rayleigh Quotient produced a loss factor similar in form to the Modal Strain Energy approach except the mode shapes used in the strain energy terms are complex.

In Chapter 7, the barberpole loss factor was defined in Equations (7.78) and (7.82) for the case where the damping of the beam was neglected. The bare cantilever beam in the experiment had some inherent damping, and the beam loss factor  $\eta_b$  was measured experimentally by testing the beam before the damping treatment was applied. Once the beam loss factor was obtained, it was used to modify Equations (7.78) and (7.82):

$$\eta_{MSE} = \frac{\eta_b U_b + N \eta_v U_v}{U_b + N U_v + N U_c} \quad (8.2)$$

$$\eta_{CRQ} = \frac{\eta_b U_b + N \eta_v U_{YCRQ}}{U_b + N U_{YCRQ} + N U_{cCRQ}} \quad (8.3)$$

The strain energy terms used in Equations (8.2) and (8.3) are defined in Equations (7.79), (7.81), and (7.83).

#### *Experimental Results: Bare Beam*

Free vibration tests were performed on the bare beam to identify  $\eta_b$ , the damping inherent in the beam and support assembly. A representative sample of the time histories used to calculate the damping is plotted in Figures 8.3 and 8.4. The envelope of the signal is linear when plotted on a semi-log scale, which indicates the loss factor is constant over the amplitudes tested (Figure 8.4). The fundamental frequency of the beam was 17.8 hertz.

Values for the loss factors obtained from the individual data sets are tabulated in Table 8.1, along with the amplitude range of the beam tip accelerations and root strains at which the beam loss factors were observed. The acceleration units are g's at peak value, and strain units are microstrains at peak value. The average loss factor from the data sets is  $\eta_b = .00146$ .

The first few seconds of many of the data sets for the bare beam had higher frequency components in the signal due to excitation of the second beam bending mode

at 115 hertz, but this effect died out quickly. For some data sets, the vibration in the second mode was significant enough to alter the shape of the envelope. In Figure 8.5, the effect of higher modes on the envelope of vibration is illustrated. Two envelopes associated with a frequency of 17.8 hertz and 115 hertz, when added and plotted on a semi-log scale, create a curve which has a steeper slope in the first few seconds of the time history. The amount of the change in slope will depend on both the relative damping and the relative amplitudes of the two modes.

Some of the data sets that were collected were discarded because of beating phenomena from out of plane vibration. This out of plane vibration was generated when the hanging weight was improperly aligned before the test. The oscillating envelope that is characteristic of beating was highly visible on the semi-log plots, even when it was hardly noticeable on the linear plots.

*Table 8.1 Undamped Beam Loss Factors.*

Set	$\eta$ [g's (peak)]	tip acceleration [microstrain (peak) ]	root strain
1	.00160	.20- .5	6 - 16
2	.00146	.30- .6	10 -20
3	.00164	.15- .4	5 - 13
4	.00168	.15- .4	5 - 13
5	.00142	.12- .3	4 - 10
6	.00170	.08- .2	1 - 6
7	.00156	.10- .2	3 - 6
8	.00152	.15- .3	5 - 10
9	.00160	.10- .2	3 - 6
Average Loss Factor:		.00154	

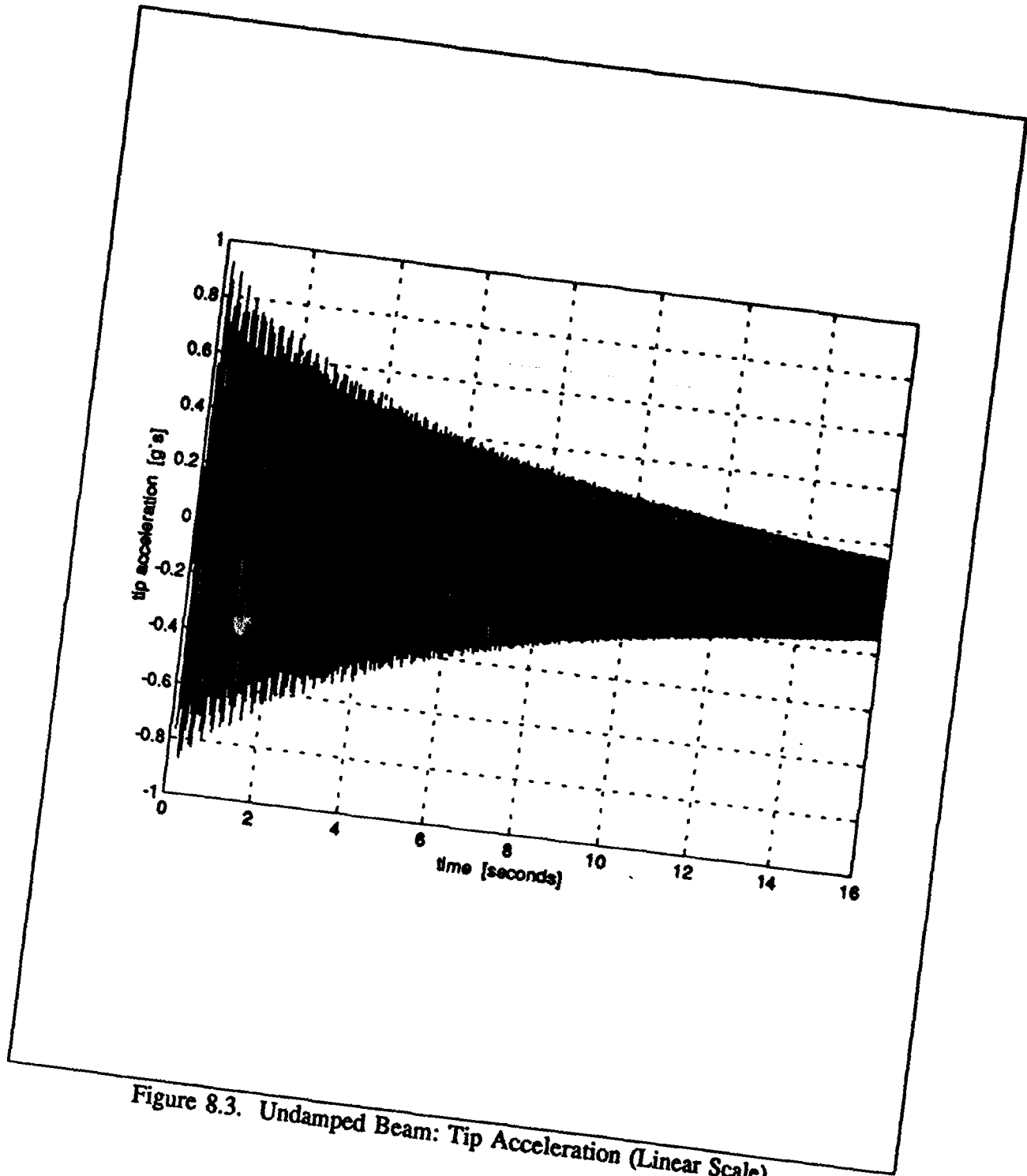


Figure 8.3. Undamped Beam: Tip Acceleration (Linear Scale)

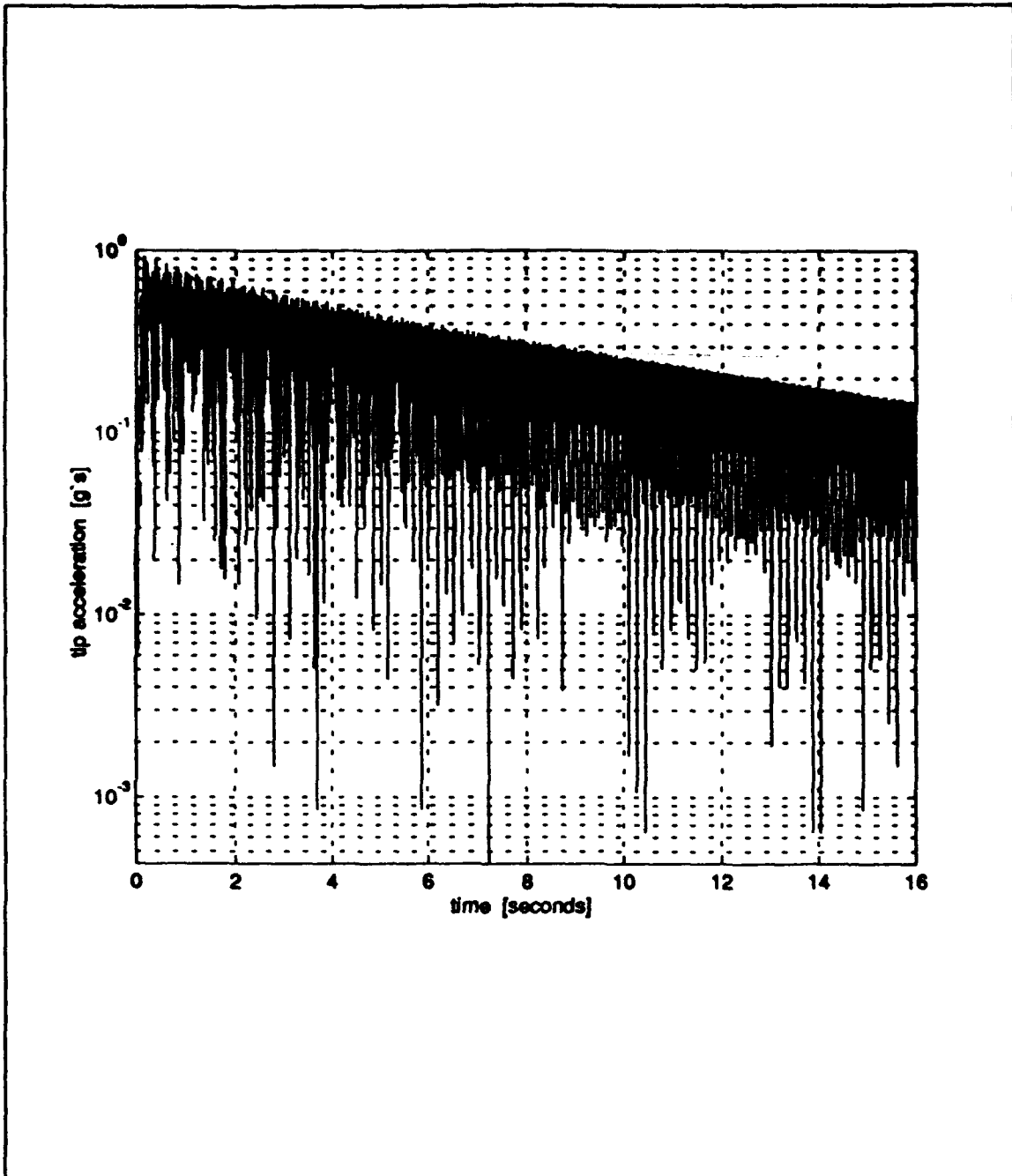


Figure 8.4. Undamped Beam: Tip Acceleration (Semi-Log Scale)

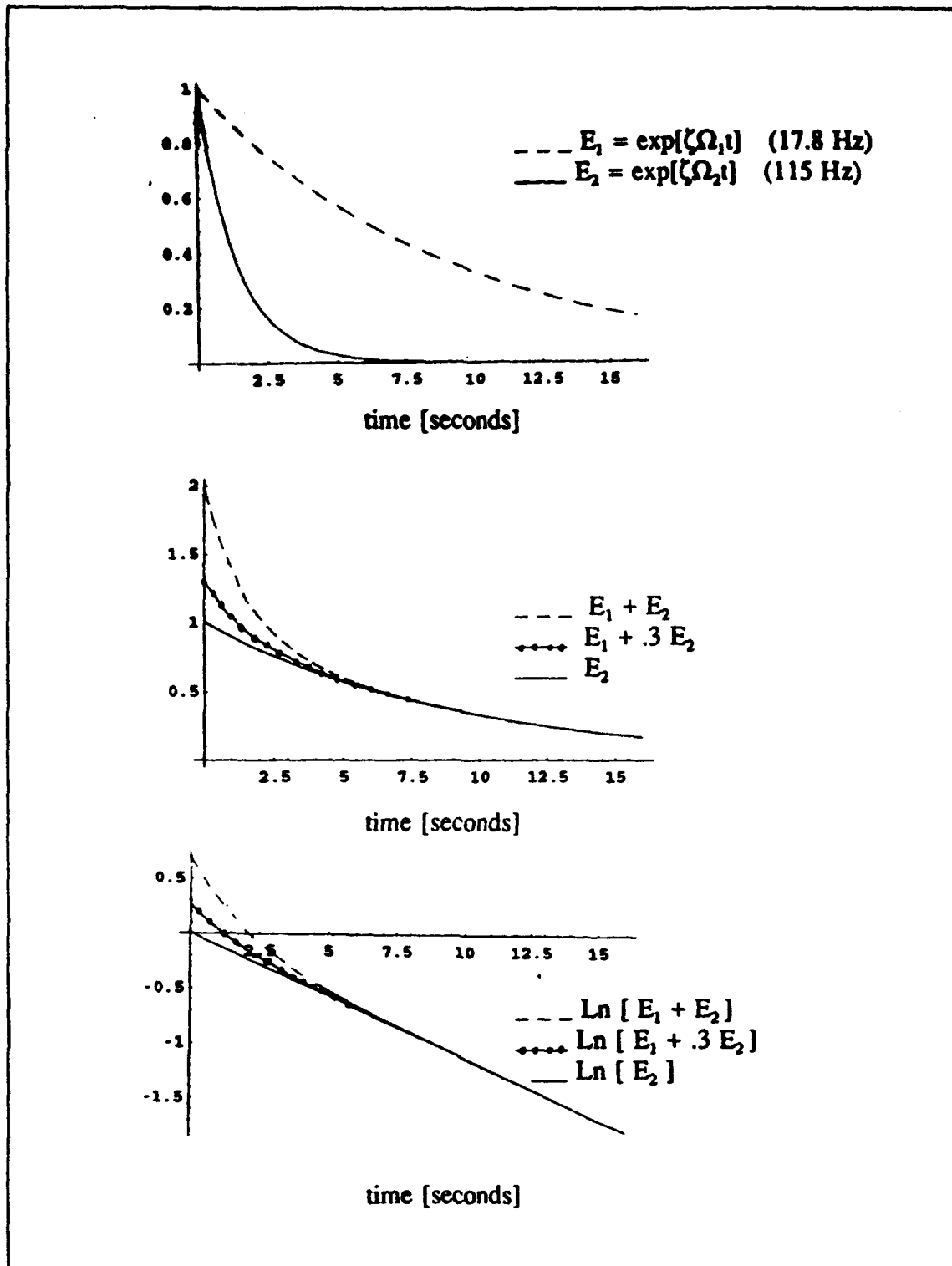


Figure 8.5 Effect of Second Mode on Envelope of Vibration

*Experimental Results: Unsegmented Barberpole.* The unsegmented barberpole geometry was tested at ambient temperatures of 19°C, 25°C, and 26°C. Over this range, the real part of the viscoelastic shear modulus ranges from 331 to 428 KPa (48 to 62 lbs/in<sup>2</sup>), but the viscoelastic loss factor is relatively unchanged ( $\eta_v=1$ ). A typical data set used to calculate the loss factors is shown in Figures 8.6 and 8.7. The data sets for this configuration had a linear range, but the magnitude of the signal decayed enough in 15 seconds to encounter noise in the last few seconds of the signal. There was also a small nonzero offset in some of the data sets that became noticeable in the last few seconds of the signal. For these reasons, the straight lines of the envelope tended to deteriorate after 9 seconds. In the first few seconds of some of the data sets, an increase in the magnitude of the slope was seen on the semi-log plots. It was not clear if this indicated vibration in the second mode of bending, transient effects due to an unclean release, or nonlinear effects, so this portion of the graphs was ignored, and the portion of the graph with a linear envelope was used to calculate the damping.

A list of the loss factors obtained from each data set is seen in Table 8.2, along with the amplitude range of the beam tip accelerations and root strains at which the beam loss factors were observed. The acceleration units are g's at peak value, and strain units are microstrains at peak value. The experimentally obtained loss factors ranged from .0070 to .0088, an increase of 4.5 to 5.7 times the loss factor of the undamped beam.

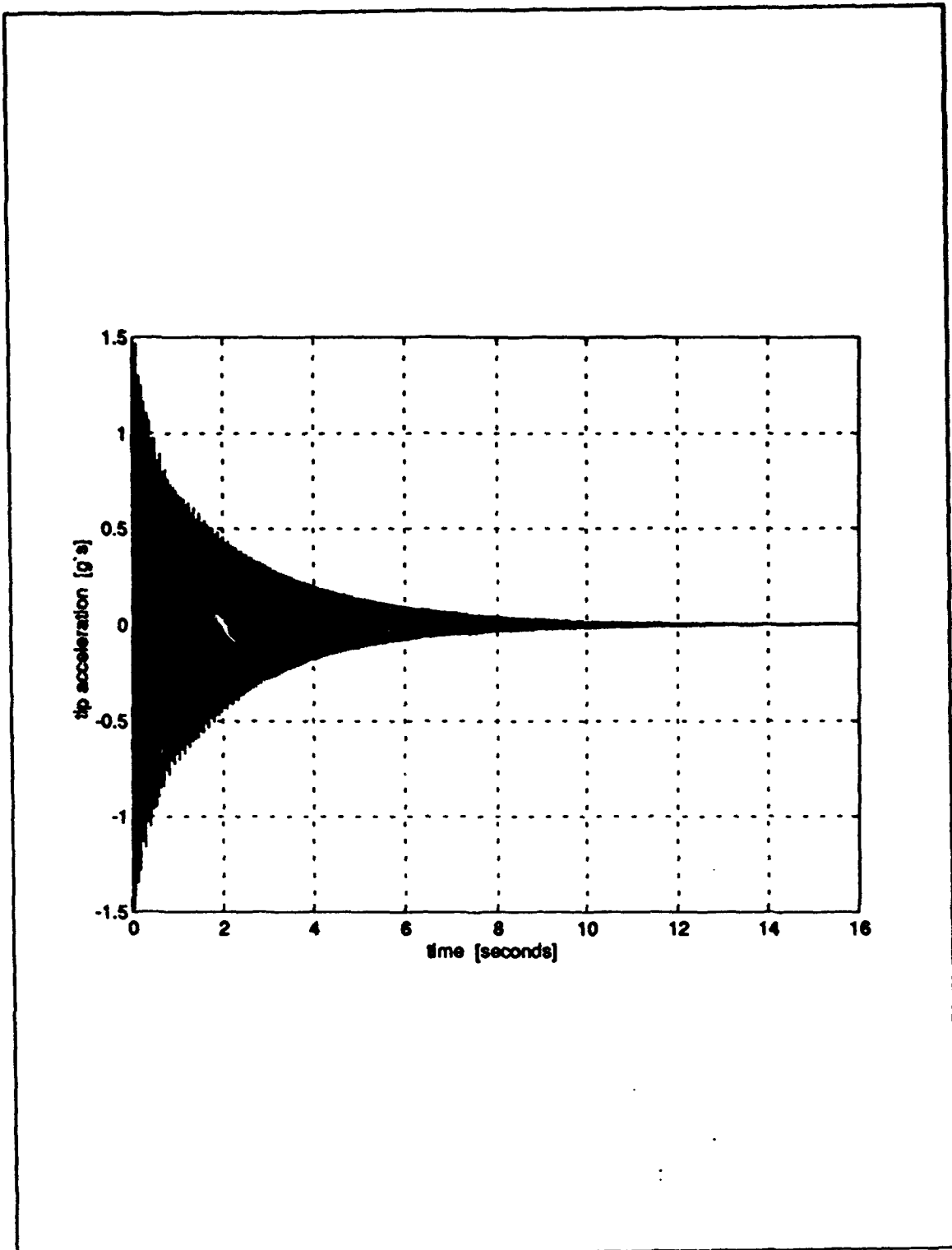


Figure 8.6. Unsegmented Barberpole: Tip Acceleration (Linear Scale)

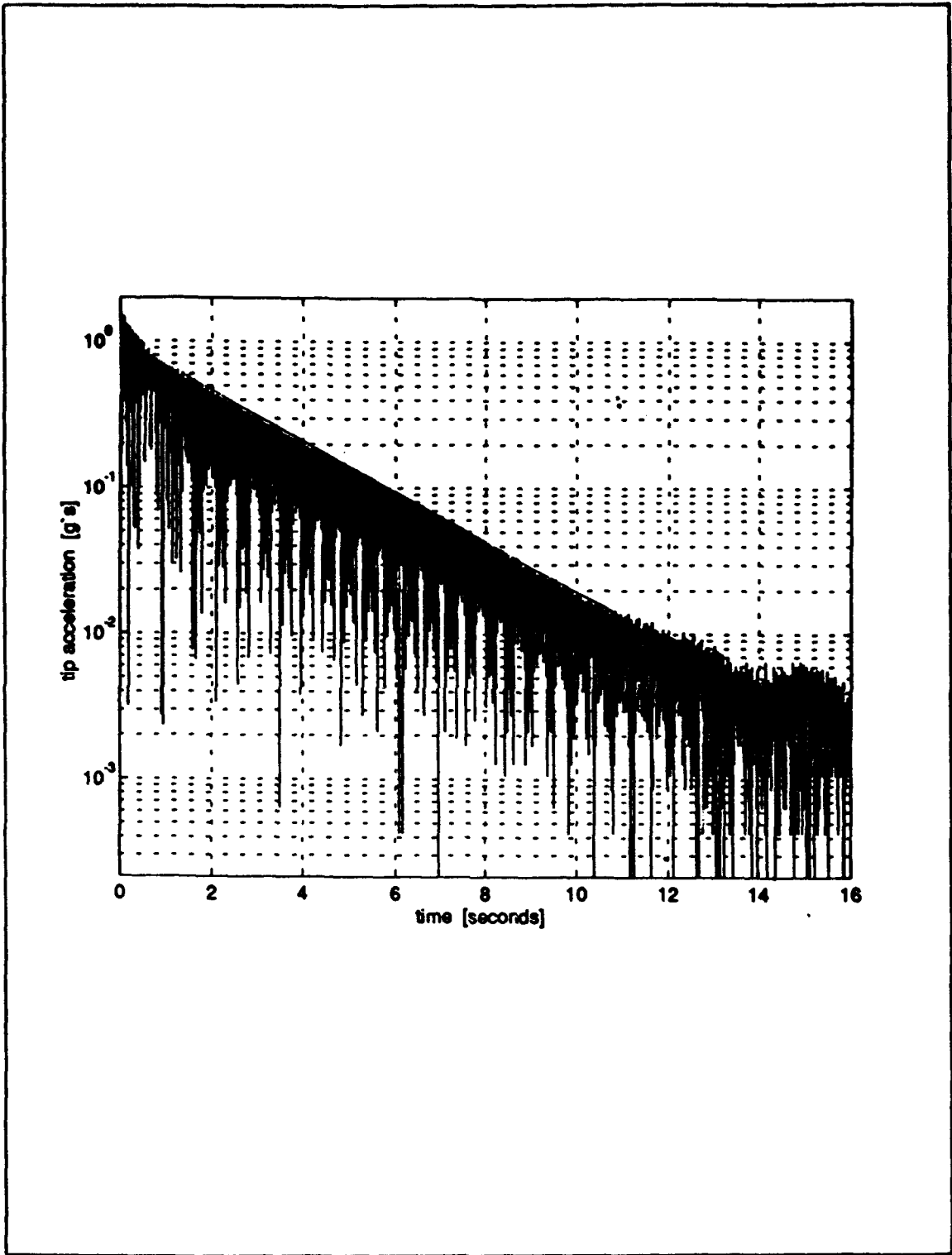


Figure 8.7. Unsegmented Barberpole: Tip Acceleration (Semi- Log Scale)

*Table 8.2. Unsegmented Barberpole Geometry: Loss Factors from Experiment*

---

*25 March Data Sets: 19 degrees C*

---

Set	$\eta$	tip acceleration [g's (peak)]	root strain [microstrain (peak) ]
1	.0068	.03 - .2	1 - 7
2	.0070	.02 - .6	1 - 20
3	.0072	.03- .6	1 - 20
4	.0070	.02- .7	1 - 23
Average Loss Factor:		.0070	

---



---

*28 March Data Sets: 25 degrees C*

---

Set	$\eta$	tip acceleration [g's (peak)]	root strain [microstrain (peak) ]
1	.0070	.03 - .3	1 - 10
2	.0072	.02 - .4	1 - 13
3	.0072	.02- .3	1 - 10
4	.0076	.02- .4	1 - 13
5	.0072	.03- .5	1 - 16
6	.0070	.05- .6	2 - 20
7	.0072	.02- .6	1 - 20
8	.0072	.04- .6	1 - 20
Average Loss Factor:		.0072	

---



---

*18 April Data Set : 26 degrees C*

---

Set	$\eta$	tip acceleration [g's (peak)]	root strain [microstrain (peak) ]
1	.0086	.03-.7	1 - 23
2	.0086	.03-.9	1 - 29
3	.0086	.10-.4	3 - 13
4	.0090	.05- 1.	2 - 33
5	.0092	.02-.4	1 - 13
6	.0090	.02-.7	1 - 23
7	.0092	.03-.7	1 - 23
Average Loss Factor:		.0088	

---

*Experimental Results: Segmented Barberpole Configuration.* A representative sample of the data used to calculate the loss factors in the segmented barberpole configuration is seen in Figure 8.8. In the semi-log plots of the segmented barberpole data, the magnitude of the envelope's slope increases with amplitude, which indicates the damping is amplitude dependent. In these data sets, a larger initial displacement is used in testing and two measures of damping at different amplitudes are obtained from each data set.

Values for the loss factors obtained from the individual data sets are tabulated in Table 8.3, along with the amplitude range of the beam tip accelerations and root strains at which the beam loss factors were observed. The acceleration units are g's at peak value, and the strain units are microstrains at peak value. The average values of the loss factor at lower and higher strain amplitudes are .0098 and .0118 respectively, which are values 6.4 and 7.7 times larger than the loss factor of the bare beam.

The viscoelastic material data used in the theoretical predictions of damping for the barberpole problem was obtained by tests performed by 3M at a strain amplitude of 8.42% peak to peak (87:2). When the beam is vibrating in its fundamental mode and the tip acceleration is 1g peak, the segmented barberpole viscoelastic layer has a maximum strain amplitude of 1.5% peak to peak, which is much less than the strain amplitude of the 3M test. (The unsegmented barberpole has an maximum viscoelastic strain amplitude of 1% peak to peak.) As a result, when considering the match between theory and experiment, the loss factors that were obtained at the higher strain amplitudes should be given more credence.

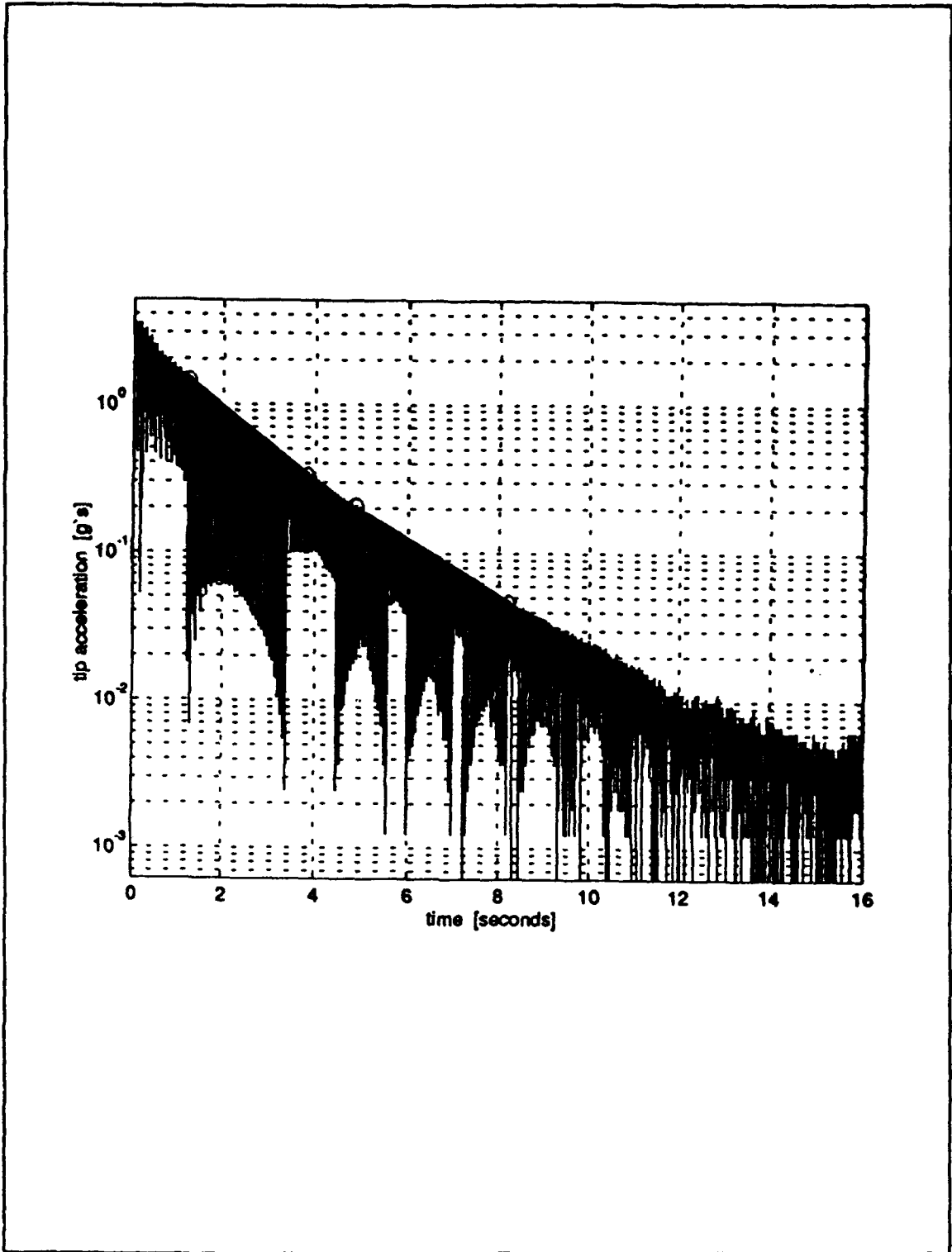


Figure 8.8. Segmented Barberpole: Tip Acceleration (Semi- Log Scale)

*Table 8.3 : Segmented Barberpole Experimental Data: 25.5 degrees C*

Low Strain Amplitude Data

Set	$\eta$	tip acceleration [g's (peak)]	root strain [microstrain (peak) ]
1	.0096	.03 - .15	1 - 5
2	.0100	.04- .20	1 - 6
3	.0100	.05- .15	2 - 5
4	.0100	.03- .10	1 - 3
5	.0092	.04- .13	1 - 4

Average Loss Factor: .0098

Higher Strain Amplitude Data

Set	$\eta$	tip acceleration [g's (peak)]	root strain [microstrain (peak) ]
1	.0118	.25- 0.8	8 - 26
2	.0118	.25- 1.0	8 - 32
3	.0116	.20- 1.2	7 - 39
4	.0124	.18- 0.7	6 - 23
5	.0114	.25- 0.9	8 - 29

Average Loss Factor: .0118

*Barberpole Loss Factors: Comparison of Theory and Experiment*

The average values for loss factor obtained from the experiments were compared with predictions from the barberpole theory using the Modal Strain Energy method and the Complex Rayleigh Quotient approaches. The results are listed below in Tables 8.4 and 8.5.

*Table 8.4 Unsegmented Barberpole Damping:  
Comparison of Experimental and Theoretical Values*

Temp[°C]	G <sub>v</sub> [KPa]	$\eta_{\text{experimental}}$	$\eta_{\text{MSE}}$	$\eta_{\text{CRQ}}$
19	428	.0070	.0092	.0062
25	331	.0072	.0104	.0072
26	331	.0088	.0104	.0072

*Table 8.5. Segmented Barberpole Damping:  
Comparison of Experimental and Theoretical Values ( 25°C)*

strain amplitude	$\eta_{\text{experimental}}$	$\eta_{\text{MSE}}$	$\eta_{\text{CRQ}}$
lower strain	.0098	.0119	.0100
higher strain	.0118	.0119	.0100

A measure of the discrepancy between theory and experiment can be defined using the following equation:

$$\% \text{ discrepancy} = \frac{\eta_{\text{approximation}} - \eta_{\text{experimental}}}{\eta_{\text{experimental}}} \times 100\%$$

Note that an approximate method that underpredicts the damping results in a negative value of the discrepancy. For the unsegmented barberpole configuration, the Complex Rayleigh Quotient consistently underpredicted the experimental results and provided better estimates of loss factor. The discrepancies associated with the Complex Rayleigh Quotient for the unsegmented configuration were -11% for the data taken at 19°C, 0% for the data taken at 25°C, and -18% for the data taken at 26°C. The corresponding discrepancies for the Modal Strain Energy method were 31%, 44%, and 18% respectively.

In the segmented barberpole tests, two experimental loss factors were obtained from each data set. One set of loss factors was at lower strain amplitudes, while the other set was obtained at higher amplitudes. The loss factors increased with amplitude. Both sets of strain amplitudes were lower than the amplitude at which the vendor data was obtained (87). The data was taken at 25°C. The Modal Strain Energy method predicted a loss factor of .0119, while the Complex Rayleigh Quotient method predicted a loss factor of .0100. The experimentally obtained loss factor for the lower strain amplitude strain was .0098, while the experimentally obtained loss factor at the higher strain amplitude was .0118. The discrepancy for the Modal Strain Energy method was 21% and the discrepancy using the Complex Rayleigh Quotient was 2%. For the higher

strain amplitude, the error associated with the Complex Rayleigh Quotient was -15%, while the error associated with Modal Strain Energy method was 1%.

*Chapter Summary:*

A series of free vibration tests was performed on a cantilever beam with a barberpole damping treatment to test the barberpole concept and to validate the barberpole bending analysis. The beam was first tested without an applied damping treatment to identify the baseline damping of the beam and its root support. Next, an unsegmented barberpole damping treatment was applied to the beam and the damping was measured. The unsegmented barberpole damping treatment was then modified by making periodic cuts around the circumference of the beam cross section, which created bands of segments of optimal length.

The addition of the unsegmented barberpole configuration to the bare beam increased the bending loss factor by approximately a factor of 5. The experimentally obtained loss factor for the segmented barberpole configuration was approximately 7 times larger than the loss factor for the bare beam. The Modal Strain Energy method and the Complex Rayleigh Quotient were used to obtain estimates for the beam loss factor. For most cases, the experimental data fell between the theoretical values defined by the two estimates. The barberpole concept was shown to add damping to the structure, and the theory was shown to be an effective tool in predicting the experimental damping from the barberpole configuration.

## *IX. Summary and Conclusions.*

There were two general goals of this research. One goal was to provide useful analytical tools to characterize the behavior of constrained layer damping treatments for beams of various geometries. The second goal was to suggest a new damping configuration for beams of circular cross section that are subjected to both bending and torsional vibrations. The first goal motivated the work in Chapters 3 through 6, while the second goal was addressed in Chapters 7 and 8. The main points of each chapter are discussed below.

### *Chapter 3*

In Chapter 3, issues regarding the optimal length of constrained layer damping treatments were described. The equilibrium equations were developed for a constraining layer mounted on a substrate with a specified surface displacement. Plunkett and Lee investigated this problem for the special case of uniform strain in the substrate, and identified an optimal length for the damping treatment (73:150). Their work was described, and an extension of their analysis for the case of linearly varying strain was provided.

Plunkett and Lee identified a system loss coefficient that depends only on a dimensionless parameter  $\sqrt{g}L$  and the viscoelastic loss factor  $\eta_v$ . The dimensionless

parameter provides a measure of the relative stiffnesses of the viscoelastic and constraining layers. They noted that for a wide range of values of the viscoelastic loss factor, the loss coefficient attained its maximum value when the dimensionless parameter was near the value 3.28. From this result, a simple formula that identifies the optimal length of the damping layer was produced. The authors did not discuss the effects of viscoelastic loss factor on the optimal length formula.

The Plunkett and Lee result was extended for the case of linearly varying substrate strain of the form  $ax+b$ , where  $a$  and  $b$  are arbitrary constants. It was shown that the loss coefficient for this case is a function of  $\eta_v$ , the dimensionless parameter  $\sqrt{gL}$ , plus another dimensionless parameter  $C_2=aL/b$  that provides a measure of the nonuniformity of the substrate strain. It was shown that an increase in  $C_2$  results in an increase in the length that provides optimal damping, but that the shift in optimal length is not rapid and the original analysis provides an error of less than 10% for configurations where  $C_2$  is less than two. The findings were presented in a series of charts and tables, and the effects of  $\eta_v$  on the optimal length were included. This extension of the Plunkett and Lee analysis for the case of linearly varying strain and the additional results on the effect of  $\eta_v$  on the optimal length for the uniform strain problem will assist designers of constrained layer damping treatments.

## *Chapter 4*

In Chapter 4, the equations of motion were developed for a rectangular beam with identical continuous constrained damping treatments applied to the top and bottom of the beam. This configuration is a symmetric five layer "sandwich" beam with alternating elastic and viscoelastic layers. These equations of motion have the same form as those developed by Mead and Markus (59:163) for a beam with a single constrained layer damping treatment, but with small differences in the geometric and material parameters of the problem.

The optimal length considerations described in Chapter 3 suggest that segmentation of the constraining layer would increase the damping if the beam to be damped is much longer than the damping treatment optimal length. This provides an incentive to consider the effects of segmentation on the equations developed for the continuous constraining layer configuration. The equations were modified for the case of a beam with  $M$  segments of equal length. Non-dimensional forms of the spatial and temporal variables were identified, and a form of the solution was proposed that simplified the problem into a  $6M \times 6M$  linear algebraic equation whose coefficient matrix was fabricated from identical submatrices corresponding to the boundary conditions of each segment. Exact solutions developed using this approach were used in Chapter 5 to assess the merit of a new approximation method.

## *Chapter 5*

In Chapter 5, approximate methods that are used in the analysis of damped systems were described, and a new method, the "Complex Rayleigh Quotient", was proposed. The idea of using a complex viscoelastic modulus in Rayleigh's Quotient to obtain a complex frequency was proposed by McIntyre and Woodhouse in their study of violin top plates (54:209), but they assumed the imaginary part of the viscoelastic modulus was much smaller than its real part, and they used real approximations of the system mode shapes in their formulation of strain energies. In this chapter it was shown that such an approach produces a loss factor equivalent to that found by the Modal Strain Energy method. Unlike the earlier approach, the Complex Rayleigh Quotient exploits the phase information contained in complex mode shapes to obtain an improved estimate of the complex natural frequency of the damped system. The complex mode shapes were developed from the Correspondence Principle. The form of the Complex Rayleigh Quotient was developed for both discrete and continuous systems. Information on the system damping may be obtained from the ratio of imaginary and real components of the complex frequency.

To illustrate the method, the Complex Rayleigh Quotient, the Modal Strain Energy method, and Rayleigh's Quotient were used to predict the natural frequency and damping of a cantilever beam with six damping segments applied to the top and bottom of the beam. The results were compared with the exact solutions developed from the formulation in Chapter 4. It was shown that the Complex Rayleigh Quotient provided

estimates of damping with approximately one-half to one-third the errors of the Modal Strain Energy method.

### *Chapter 6*

In Chapter 6, the system of equations was developed for a beam of circular cross section damped with strips parallel to the beam centerline. For the case of thin narrow strips, the equations collapse into equations similar in form to those derived for the rectangular sandwich beam in Chapter 4. The development in this section allows the well known results of the Mead and Markus sixth order theory (59:163) to be applied directly to beams of circular cross section. If the constraining layer strips on the cylindrical beam are segmented, the Chapter 6 results allow the exact equations developed in Chapter 4 for the segmented rectangular beam to be used.

### *Chapters 7 and 8*

The optimal constrained layer damping treatment for cylindrical beams in bending consists of narrow strips of optimal length that are parallel to the beam centerline. Unfortunately, this configuration is not an effective damping treatment for torsion. In Chapter 7, a new constrained layer configuration was proposed for the damping of beams of circular cross section that are subjected to both bending and torsional vibrations. The damping treatment consists of a complete coverage with thin, narrow strips of constrained layer damping treatment oriented at a common pitch angle in a helical or "barberpole"

configuration, then periodically segmented along their length. Analyses were developed which show that the barberpole configuration has the capability to damp both bending and torsional vibrations. The optimal barberpole geometry for torsion consists of optimally segmented strips with a pitch angle of  $\pi/4$  radians, while the optimal geometry for bending consists of optimally segmented strips at a zero pitch angle. The best barberpole design for a given configuration will depend on the relative importance of torsional damping.

It was also shown that for the pure bending problem, the unsegmented barberpole geometry provides more damping than unsegmented straight strips if the beam is much longer than the optimal length of the damping treatment. Though the unsegmented barberpole geometry in bending is not as effective as the optimally cut strips at zero pitch angle, it could be useful for applications where periodic segmentation along the beam length is undesirable due to environmental or operational reasons.

A series of free vibration tests was performed on a cantilever beam with a barberpole damping treatment to validate the barberpole bending analysis. The Modal Strain Energy and the Complex Rayleigh Quotient methods were used with the barberpole bending theory to obtain estimates for the beam loss factor for the fundamental mode of bending. The theory was shown to be an effective tool in predicting the experimental damping from the barberpole configurations.

### *Closing Remarks*

Several aspects of damped systems were investigated, and the use of constrained layer damping treatments was emphasized. The intent of the author was to illuminate certain aspects of the use of constrained layer damping treatments to suppress structural vibrations, to provide some additional design tools for their application to practical systems, and to suggest a new constrained layer configuration for bending and torsional vibrations in beams of circular cross section.

There was a recurring theme that surfaced in each chapter: constrained layer damping treatments may be used to add damping to structures, but their design is not trivial. A poorly designed constrained layer damping treatment may provide little or no damping while adding undesirable mass, while an effective design can provide significant damping. The author hopes that in some small way this research will help others to appreciate some of the subtleties in the design process, and thus design more effective damping treatments.

## BIBLIOGRAPHY

1. Abdulhadi, Fakhruddin. "Transverse Vibrations of Laminated Plates with Viscoelastic Layer Damping," *Sound and Vibration Bulletin*, 40 (5): 93-104 (December 1969).
2. Alam, N. and N.T. Asnani. "Vibration and Damping Analysis of a Multilayered Cylindrical Shell," *AIAA Journal*, 22: 803-810 (June 1984).
3. Alberts, T.E., Chen, Y., and Xia, H. "On the Effectiveness of Section Length Optimization for Constrained Viscoelastic Layer Damping Treatments," *Advances in Optical Structure Systems*, SPIE Vol 1303: 274-285 (1990).
4. Almy, C.R, and F.C. Nelson. "Damping of a Circular Ring Segment by a Constraining Layer," *Shock and Vibration Bulletin*, 42 (4): 121-124 (1972).
5. Barrett, D.J. "A Design for Improving the Structural Damping Properties of Axial Members," *Proceedings of Damping '89*, U.S. Air Force Wright Aeronautical Laboratories, Flight Dynamics Laboratory, WRDC-TR-89-3116, Paper HCB (November 1989).
6. Barrett, D.J. "An Anisotropic Laminated Damped Plate Theory," *Journal of Sound and Vibration*, 154 (3): 453-465 (1992).
7. Belknap, F.M. and J.B. Kosmatka. "Vibration Suppression of Thin Walled Composite Tubes Using Embedded Viscoelastic Layers," *Proceedings of Damping '91*, U.S. Air Force Wright Laboratory, Flight Dynamics Directorate, WL-TR-91-3078, Paper HAC, (1991).
8. Beer, F. and R. Johnson. *Mechanics of Materials*. New York: McGraw-Hill Book Company, 1981.
9. Bland, David R. *The Theory of Linear Viscoelasticity*. New York: Pergamon Press, 1960.

10. Bronowicki, A.J. and H.P. Diaz. "Analysis, Optimization, Fabrication and Test of Composite Shells with Embedded Viscoelastic Layers," *Proceedings of Damping '89*, U.S. Air Force Wright Aeronautical Laboratories, Flight Dynamics Laboratory, WRDC-TR-89-3116, Paper GCA, (November 1989).
11. Chandrasekharan, M.P. and A. Ghosh. "Damping Characteristics of Elastic-Viscoelastic Composite Shafts," *Journal of Sound and Vibration*, 37 (1): 1-15 (1974).
12. Chen, G-S., and B.P Dolgin. "Analysis of an Elastically Tailored Viscoelastic Damping Members," *Research in Structures, Structural Dynamics and Materials*, NASA, Langley Research Center, pp. 239-247 (1990) (also AIAA Paper N91-10319).
13. Chen, G-S, and B. K. Wada. "Passive Damping for Space Truss Structures," *AIAA SDM Issues of the International Space Station*, Williamsburg VA, April 21, 1988 pp.1-12 ( also AIAA Paper 88-2469).
14. Cottle, Eugene. *Damping of Layered Beams with Mixed Boundary Conditions*. Master's Thesis, Air Force Institute of Technology, 1990.
15. DiTaranto, R.A. "Free and Forced Response of a Laminated Ring," *Journal of the Acoustical Society of America*, 53:748-757 (1973).
16. DiTaranto, R.A. "Lateral Vibrations of a Damped Laminated Hollow Circular Cross-Section Beam," *Journal of Engineering for Industry*, pp. 845-852 (August 1974).
17. DiTaranto, R.A. "Theory of Vibratory Bending for Elastic and Viscoelastic Finite Length Beams," *Transactions of the ASME, Journal of Applied Mechanics*, 87: 881-886 (December 1965).
18. DiTaranto, R.A., and W. Blasingame. "Composite Damping of Vibrating Sandwich Beams," *Journal of Engineering for Industry* , pp. 633-638 (November 1967).

19. DiTaranto, R.A., Y.P. Lu, and B.E. Douglas. "Forced Response of a Discontinuously Constrained Damped Ring," *Journal of the Acoustical Society of America*, 54(1): 74-79 ( 1973).
20. DiTaranto, R.A., and J.R. McGraw, Jr. "Vibratory Bending of Damped Laminated Plates," *Journal of Engineering for Industry*, pp. 1081-1091 (November 1969).
21. Douglas, B.E. "Compressional Damping in Three-Layer Beams Incorporating Nearly Incompressible Viscoelastic Cores," *Journal of Sound and Vibration*, 104 (2): 343-347 (1986).
22. Douglas, B.E. and J.C.S. Yang. "Transverse Compressional Damping in the Vibratory Response of Elastic- Viscoelastic Beams," *AIAA Journal*, 16 (9): 925-930 (September 1978).
23. Durocher, L.L. and R. Solecki. "Harmonic Vibrations of Isotropic, Elastic and Elastic/Viscoelastic Three Layered Plates," *Journal of the Acoustical Society of America*, 60(1): 105-112 (July 1976).
24. El-Raheb, M. and P. Wagner. "Damped Response of Shells by a Constrained Viscoelastic Layer," *Journal of Applied Mechanics*, 53: 902-908 (December 1986).
25. Farkas, J. and K. Jarmai. "Structural Synthesis of Sandwich Beams with outer Layers of Box Section," *Journal of Sound and Vibration*, 84 (1): 47-56 (1982).
26. Fowler, B. et. al. "Passive Damping Techniques for Beam Control Structures," Air Force Weapons Laboratory Test Report, AFWL-TR-88-97 (April 1989).
27. Flugge, W. *Stresses in Shells*, Springer-Verlag, Berlin, 1960.
28. Grootenhuis, P. "The Control of Vibrations with Viscoelastic Materials," *Journal of Sound and Vibration*, 11(4 ): 421-433 (1970).
29. Hajela, P. and C-Y Lin. "Optimal Design of Viscoelastically Damped Beam Structures," *Applied Mechanics Review*, 44 (11): S96-S102 (November 1991).

30. He, J-F. and B-A. Ma. "Analysis of Flexural Vibration of Viscoelastically Damped Sandwich Plates," *Journal of Sound and Vibration*, 126 (1) : 237-47 (1988).
31. Hedgepeth, J.M. and M. Mobrem. "Investigation of Passive Damping of Large Space Truss Structures" *Proceedings of Damping '86*, U.S. Air Force Wright Aeronautical Laboratories, Flight Dynamics Laboratory, (1986).
32. Holman, R.E. and J.M Tanner. "Finite Element Modelling Techniques for Constrained Layer Damping," *AIAA Journal*, 21(5): 792-794 (May 1983).
33. Ioannides, E., and P. Grootenhuis. "A Finite Element Analysis of the Harmonic Response of Damped Three-Layer Plates," *Journal of Sound and Vibration*, 67 (2): 203-218 (1979).
34. Johnson, C.D., D.A. Kienholz, and L.C. Rogers. "Finite Element Design in Beams with Constrained Viscoelastic Layers," *Shock and Vibration Bulletin*, 51: 71-81 (May 1981).
35. Johnson, C.D. and D.A. Kienholz. "Finite Element Prediction of Damping in Structures with Constrained Viscoelastic Layers," *AIAA Journal*, 20(9): 1284-1290 (1980).
36. Kerwin, Jr., Edward M. "Damping of Flexural Waves by a Constrained Viscoelastic Layer," *Journal of the Acoustical Society of America*, 7 (31): 952-962 (July 1959).
37. Kerwin, Jr., Edward M. "Macromechanisms of Damping in Composite Structures," *Internal Friction, Damping and Cyclic Plasticity*, ASTM STP 378, American Society for Testing and Materials ( 1965).
38. Kerwin, Jr., Edward M. and P.W. Smith, Jr. "Segmenting and Mechanical Attachment of Constrained Viscoelastic Layer Damping Treatments for Flexural and Extensional Waves," *Proceedings of the U.S. Air Force Flight Dynamics Laboratory Vibration Damping Workshop*, Long Beach, CA. AFWAL TR-84-3064 , paper KK:1-24 (November 1984).
39. Khatua, T.P. and Y. K. Cheung. "Bending and Vibration of Multilayer Sandwich Beams and Plates," *International Journal of Numerical Methods in Engineering*, 6: 11-24 (1973).

40. Kishore, N. Nanda and A. Ghosh. "Damping Characteristics of Elastic-Viscoelastic Composite Curved Bars and Helical Springs," *Journal of Sound and Vibration*, 43(4): 621-632 (1975).
41. Kodiyalam, S. and J. Molnar. "Optimization of Constrained Viscoelastic Damping Treatments for Passive Vibration Control" AIAA Paper Number AIAA-92-2269-CP ( 1992).
42. Kress, G. "Improving Single-Constrained Layer Damping Treatment by Sectioning the Constraining Layer," *The Role of Damping in Vibration and Noise Control*, ASME DE-Vol.5: 41-48 (1987).
43. Lall, A.K., N.T. Asnani, and B.C. Nakra. "Damping Analysis of Partially Covered Sandwich Beams," *Journal of Sound and Vibration*, 123(2): 247-259 (1988).
44. Lifshitz J.M and M. Leibowitz. "Optimal Sandwich Beam design for Maximum Viscoelastic Damping," *International Journal of Solids and Structures*, 23(7): 1027-1034 (1987).
45. Lu, Y.P. "Forced Vibrations of Damped Cylindrical Shells filled with Pressurized Liquid," *AIAA Journal*, 15: 1242-1249 (September 1977).
46. Lu, Y.P. and B.E. Douglas. "On the Forced Vibration of Three Layer Damped Sandwich Beams," *Journal of Sound and Vibration*, 32(4): 513-516 (April 1974).
47. Lu, Y.P. and G.C. Everstine. "More on Finite Element Modelling of Damped Composite Systems" *Journal of Sound and Vibration*, 69(2): 199-205 ( 1980).
48. Lu, Y.P., J.W. Killian, and G.C. Everstine. "Vibration of Three Layer Damped Sandwich Plate Composites," *Journal of Sound and Vibration*, 64(1): 63-71 (1979).
49. Lu, Y.P, A.J. Roscoe III, and B.E. Douglas. "Analysis of the Response of Damped Cylindrical Shells Carrying Discontinuously Constrained Beam Elements," *Journal of Sound and Vibration*, 150(3): 395-403 (1991).

50. Lu, Y.P, A.J. Roscoe III, and H.C. Neilson. "Vibration Responses of a Composite Shell made of a Metallic Material with Damping Treatments," *1993 Damping Vibration Workshop*, San Diego, (February 1993).
51. Mantena, P. J., Ronald F. Gibson, and S. J. Hwang. "Optimal Constrained Viscoelastic Tape Lengths for Maximizing Damping in Laminated Composites," *AIAA Journal*, 29(10): 1678-1685 (1990).
52. Markus, S. "Shear Damping Reduction Effects in Sandwich Beams," *Journal of Sound and Vibration*, 55(4): 591-593 (December 1977).
53. Matlab. Version 3.1, VMS.. Computer Software. The MathWorks, Sherborn, ST, October 1987.
54. McIntyre, M.E. and J. Woodhouse. "The Influence of Geometry on Linear Damping," *Acustica*, 39(4): 209- 224 (1978).
55. McIntyre, M.E. and J. Woodhouse, "On Measuring the Elastic and Damping Constants of Orthotropic Sheet Materials," *Acta Metallurgica*, 36 (6): 1397-1416 (1988).
56. Mead, D. J. "A Comparison of Some Equations for the Flexural Vibration of Damped Sandwich Beams," *Journal of Sound and Vibration*, 83(3): 363-377 ( 1982).
57. Mead, D.J. and N.S. Bardell. "Free Vibration of a thin Cylindrical Shell with Periodic Circumferential Stiffeners," *Journal of Sound and Vibration*, 115(3): 499-520 ( 1987).
58. Mead, D.J. and R.A. DiTaranto. "Resonance Response Criteria of a Damped Three-Layered Beam," *Journal of Engineering for Industry*, 94B: 174-180 (February 1972).
59. Mead, D.J. and S. Markus. "Forced Vibration of a Three-Layer Damped Sandwich Beam with Arbitrary Boundary Conditions," *Journal of Sound and Vibration*, 10(2): 163-175, (1969).
60. Mead, D.J. and S. Markus. "Loss Factors and Resonant Frequencies of Encastre Damped Sandwich Beams," *Journal of Sound and Vibration*, 12(1): 99-112 (1970).

61. Meirovitch, Leonard. *Analytical Methods in Vibrations*. Macmillan Publishing Co, New York, 1967.
62. Meir, A.J., M.D. Gunzburger, and R.T. Schumacher. "Normal Modes of Orthotropic Plates," *Proceedings of the 12th International Congress on Acoustics*, Volume 3: Paper K3-3 (July 1986).
63. Miles, R.N. and P.G. Reinhall. "An Analytical Model for the Vibration of Laminated Beams Including the Effects of both Shear and Thickness Deformation in the Adhesive Layer," *Journal of Vibration, Acoustics, Stress, and Reliability in Design*, 108: 56-64 (1986).
64. Mukhopadhyay, A.K. and H.B. Kingsbury. "On the Dynamic Response of a Rectangular Sandwich Plate with Viscoelastic Core and Generally Orthotropic Facings," *Journal of Sound and Vibration*, 47(3): 347-358 (1976).
65. Nakra, B.C. "Vibration Control with Viscoelastic Materials," *Shock and Vibration Digest*, 8(6): 3-12 ( June 1975) .
66. Nakra, B.C. "Vibration Control with Viscoelastic Materials II," *Shock and Vibration Digest*, 13(1): 17-20 (June 1981) .
67. Nakra, B.C, and P. Grootenhuis. "Extensional Effects in Constrained Viscoelastic Layer Damping," *Aeronautical Quarterly*, 25: 225-231 (1974).
68. Nashif, A.D., D.I.G. Jones, and J.P. Henderson. *Vibration Damping*, Wiley-Interscience, New York, 1985.
69. Nelson, F.C. "Techniques for the Design of Highly Damped Structures," *Shock and Vibration Digest*, 9(7): 3-12 (July 1977).
70. Nokes, David. S. and Frederick C. Nelson. "Constrained Layer Damping with Partial Coverage," *Shock and Vibration Bulletin*, 38(3): 5-12 (November 1968).
71. Parfitt, G.G. "The Effect of Cuts in Damping Tapes," *Proceedings: Fourth International Congress on Acoustics, Copenhagen*, Paper P2: 1-4 (August 1962).

72. Plass, H.J. "Damping of Vibrations in Elastic Rods and Sandwich Structures by Incorporation of Additional Viscoelastic Materials," *Proceeding of the 3rd Midwest Conference of Solid Mechanics*, p.48 ( 1957).
73. Plunkett, R. and C.T. Lee, "Length Optimization for Constrained Layer Damping," *Journal of the Acoustical Society of America*, 48(1): 150-161 (1970).
74. Pulgrano, Louis. "Effectiveness of Partial Coverage for Constrained-Layer Damping Treatments," *Proceedings of the 64th Meeting of the Acoustical Society of America*, F-5:1976 (1962).
75. Rao, D.K. "Vibration of Short Sandwich Beams," *Journal of Sound and Vibration*, 52(2): 253-263 (1977).
76. Rao, D.K. "Frequency and Loss Factors of Sandwich Beams under Various Boundary Conditions," *Journal of Mechanical Engineering Science*, 20(5): 271-282 (1978).
77. Rao, Y.V.K.S. and Nakra, B.C. "Vibrations of Unsymmetrical Sandwich Beams and Plates with Viscoelastic Cores," *Journal of Sound and Vibration*, 34(3): 309-326 (1974).
78. Reddy, C.V.R., N. Ganesan, and B.V.A. Rao. "Dynamic Analysis of Viscoelastic Layered Beams and Plates By Finite Element Methods," *Proceedings of the Third International Conference in Australia on Finite Element Methods*, pp.467-482 (July 1979).
79. Ross, D., E.E. Ungar, and Kerwin, E. M. "Damping of Plate Flexural Vibrations by Means of Viscoelastic Laminaes," in *Structural Damping*, edited by J.E. Ruzicka, published by the ASME, pp. 49-87, (1959).
80. Saada, Adel S. *Elasticity: Theory and Applications*. Malabar, Florida: Robert E. Krieger Publishers, 1974.
81. Saito, H. and H. Tani. "Vibration of Bonded Beams with a Single Lap Adhesive Joint," *Journal of Sound and Vibration*, 92(2): 299-309 (1984).

82. Sandman, B.E. "Flexural Vibrations of Segmented Elastic-Viscoelastic Sandwich Beams," *Journal of Applied Mechanics*, 42(4): 897-900 ( December 1975).
83. Sattinger, S. S. "Constrained Layer Damping of Global Bending Vibration Modes of Thin Walled Beams," *Proceedings: Winter Annual Meeting of the ASME*, Dallas Texas, pp. 41-53 (November 1990).
84. Sattinger, S. S. "Directional Damping of the Global Vibration Modes of Tubular Structures by Constrained-Layer Treatments," *Proceedings: Damping '91*, U.S. Air Force Wright Laboratory, Flight Dynamics Directorate, WL-TR-91-3078, Paper HBA (August 1991).
85. Sattinger, S. S. "A Study of Extensional Damping Performance Discrepancies in Certain Constrained-Layer Treatments", *The Role of Damping in Vibration and Noise Control*, DE-Vol.5, ASME: 33-40 (1987).
86. Sattinger, S.S. and Z.N. Sanjana. "Damping Thin-Walled Composite Structures with Embedded Constraining Layers," *1993 Damping Workshop*, San Diego (February 1993).
87. "Scotchdamp Vibration Control Systems: Product Informaton and Performance Data," publication by 3M Industrial Tape And Specialties Division, 3M Center Bldg. 220-7E-01. St Paul, MN 55144-1000.
88. Segalman, D.J. and Philip Reamy. "Prediction and Measurement of Damping of a Laminated Beam with a Constrained Viscoelastic Layer," Report DE89-009002, SAND-888-2551 Sandia National Labs, Contract DE-AC04-76DP-00789 (February 1989).
89. Silverman, Richard. *Introductory Complex Analysis*. New York: Dover Publications, Inc. 1972.
90. Stevens, K.K., C.H. Kung, and S.E. Dunn. "Damping of Plates by Partial Viscoelastic Coatings: Part I: Analysis," NOISE-CON 81: Proceedings; National Conference of Noise Control Engineering; North Carolina State University, Raliegh, North Carolina: 445-452 (1981).
91. Sylwan, O. "Calculation of Partially Covering Damping Layers of Sandwich Structures with

some Practical Results," *Proceedings from Inter-noise-78*: 219-224 (1978).

92. Sylwan, O. "Shear and Compressional Damping Effects of Constrained Layered Beams," *Journal of Sound and Vibration*, 118 (1): 35-45 (1987).

93. Swallow, W. "An Improved Method of Damping Panel Vibrations," British Patent Specification 513, 171 (1939).

94. Torvik, Peter J. "The Analysis and Design of Constrained Layer Damping Treatments," *Damping Applications in Vibration Control*, Torvik, Peter J., editor, New York: ASME AMD Vol. 38: 85-112 (1980).

95. Torvik, P.J. and D.Z. Strickland. "Damping Additions for Plates Using Constrained Viscoelastic Layers," *Journal of the Acoustical Society of America*, 51(3): 985-991 (1972).

96. Ungar, E.E. "Loss Factors of Viscoelastically Damped Beam Structures," *Journal of the Acoustical Society of America*, 34(8): 1082-1089 (August 1962).

97. Ungar, E.E. and E.M. Kerwin, Jr., "Loss Factors of Viscoelastic Systems in Terms of Energy Concepts," *Journal of the Acoustical Society of America*, 34 (7): 954-957 (July 1962).

98. Vinogradov, B.D. and V.V. Chernoberevskii. "Damping of Tubes by a Constrained Coating," *Soviet Physics Acoustics*, 26(4): 328-330 ( July-August 1980).

99. Whittier, James S. "The Effect of Configurational Additions Using Viscoelastic Interfaces on the Damping of a Cantilever Beam," WADC Technical Report 58-568, Wright Air Development Center (May 1959).

100. Yadagiri, S., C. Papi Reddy, and T. Sanjeeva Reddy. "Viscoelastic Analysis of Adhesively Bonded Joints," *Computers and Structures*, 27(4): 445-454 (1987).

101. Yan, M-J, and E.H. Dowell, "Governing Equations for Vibrating Constrained Layer Damping of Sandwich Beams and Plates," *Journal of Engineering for Industry* 89:1041-1047 (December 1972).

102. Yildiz, A. and K. Stevens. "Optimum Thickness Distribution of Unconstrained Viscoelastic Damping Layer Treatment for Plates," *Journal of Sound and Vibration*, 103(2): 183-199 (1985).
103. Yin, T. P., T. J. Kelly and J. E. Barry. "A Quantitative Evaluation of Constrained-Layer Damping," *Journal of Engineering for Industry* : 773-784 (November 1967).
104. Yoos, Jr., T. R. and F. C. Nelson. "Damping of Low-Frequency Vibraton by Constrained Viscoelastic Layers," *American Society of Mechanical Engineers*, ASME Paper ASME-Vibr-62, (March 1967).
105. Yu, Y.Y. "Damping of Flexural Vibrations in Sandwich Plates," *Journal of the Aerospace Sciences*, 29: 790-803 ( July 1962).
106. Yu, Y.Y. "Dynamics and Vibration of Layered Plates and Shells- A Perspective from Sandwiches to Laminated Composites", AIAA Paper 89-1419-CP, 1989.
107. Zeinetdinova, R. Z, N. I. Naumkina, and B. D. Tartakovskii. "Effectiveness of a Vibration-Absorbing Coating with a Cut Constraining Layer," *Soviet Physics Acoustics*, 24 (4): 347-348, (July-August 1978).

## *Vita*

Kimberly J. Balkema was born in Green Cove Springs, Florida on September 18th, 1963. At the age of twelve she moved with her family from Miami, Florida to Jeddah, Saudi Arabia, where she attended the Parent's Cooperative School. Two years later she enrolled in Marymount International School, a boarding school in Rome, Italy. Though she never graduated from high school or obtained a General Equivalency Document, she talked her way past the Admissions Department of the University of Miami, Florida in 1980. At the age of twenty she graduated with a Bachelor of Science degree in Mechanical Engineering at the University of Colorado, Boulder in May 1984. That month she was commissioned as an officer in the United States Air Force and was assigned as a Space Shuttle Systems Engineer to Vandenberg Air Force Base, California where she worked on the activation of several launch support systems. Six months before the scheduled first launch of the Vandenberg site, the Shuttle Challenger exploded on launch from Kennedy Space Center on January 28, 1986, and the Vandenberg shuttle facility was deactivated. Capt Balkema was then transferred to Arizona State University, where she received a Master of Science degree in 1988. At Arnold Engineering Development Center, Tennessee, she was involved in both the daily operations and long term planning for a series of wind tunnels, hypervelocity ranges, and space chambers. She was transferred to the Air Force Institute of Technology in 1991, and received her Doctoral Degree in 1994. She is currently a Technical Manager at Wright Laboratory, Flight Dynamics Directorate.